Individualised Non-Invasive Brain Stimulation for Post-Stroke Motor Rehabilitation.

Jenny Lee

University College London (UCL)

Department of Clinical and Movement Neurosciences

UCL Queen Square Institute of Neurology

A thesis submitted for the degree of

Doctor of Philosophy

January 2023

DECLARATION PAGE

I, Jenny Lee, confirm that the work presented in my thesis is my own. Where information has been derived from other sources, I confirm that this has been indicated in the thesis.

ABSTRACT

Physical therapy improves upper limb rehabilitation after stroke, however access to high-dose training is often limited. Innovation is greatly needed to increase efficiency and accessibility of post-stroke rehabilitation. Transcranial direct current stimulation (tDCS) is a candidate tool to support neuroplasticity for rehabilitation. Exciting developments and potentially clinically relevant applications of tDCS are however subject to high outcome variability across studies, suggesting a need for further improvement of the technique. The work presented in this thesis aims to identify and minimise sources of tDCS outcome variability when applied in stroke.

Advances in current flow modelling (CFM) software now allow greater control over where, and in what manner exogenous fields encounter neuronal populations of interest, and improved mechanistic understanding of tDCS-induced excitability changes allows researchers to consider the potential neurophysiological impact of DC fields. However, increased control of tDCS application has not yet translated to improved outcomes. While modulation of motor evoked potential (MEP) amplitude by tDCS has been reported, the magnitude of the effect has steadily decreased since the turn of the century (Horvath et al., 2015), and optimal study conditions remain unknown. Here, a candidate computationally individualised tDCS protocol is described, including in-depth discussion of its methodological rationale and potential barriers to optimisation. This protocol was not found to significantly alter cortical excitability, probed using transcranial magnetic stimulation (TMS), in stroke survivors and neurotypical participants.

Meanwhile, reduced intra-cortical inhibition is here reported in sub-acute stroke survivors compared to neurotypical participants, and persistently increased variability in TMS-assessed excitability is reported in survivors up to 12 months post-stroke. The known state-dependent properties of tDCS suggest that individualised application may be required to further optimise the intervention in the heterogenous stroke population. Finally, a large computational study demonstrates the significant impact of stroke lesions on simulated tDCS electric field (E-field) delivered to the hand representation of the primary motor cortex, compared to neurotypical controls. This suggests that stroke-induced changes to

brain anatomy may significantly impact E-field properties at a cortical target, which has recently been shown to correlate with neurophysiological outcomes.

Taken together, heterogeneity in cortical anatomy and function in stroke survivors may contribute to variable tDCS outcomes and explain why computational approaches have not yet translated into larger effect sizes. Consequently, an individualised approach to protocol design is recommended to innovate tDCS application in stroke.

IMPACT STATEMENT

This work will impact progress within and outside the academic sphere. It has been reported that a 240% increase in training dose would be required to improve stroke outcomes (Schneider et al., 2016), and the majority of research into motor rehabilitation after stroke, the topic of interest in this thesis, has focussed on one-to-one training with a practitioner (Stewart et al., 2017). Under these conditions, an unsustainable increase in time and staff would be required to meaningfully improve outcomes for every stroke survivor (Dorsch & Elkins, 2020); innovation is greatly needed to increase the efficiency and accessibility of post-stroke rehabilitation.

This thesis therefore focussed on optimising a non-invasive neuromodulation technique, tDCS, in the context of stroke. TDCS-induced changes in cortical excitability have promise to maximise neuroplastic potential, to improve efficiency of motor rehabilitation. However, tDCS outcomes are subject to high variability and vulnerable to differences in underlying cortical excitability before stimulation is applied. The findings of this thesis suggest first that optimal timing of tDCS after stroke may be best-informed by individual assessment of the brain's functional state. This is contrary to a prevailing hypothesis that tDCS optimisation would be partly determined by time since stroke onset, as a hypothesised window of enhanced excitability was expected to occur in the sub-acute phase (1 week – 6 months post-stroke). I report that predictions of brain state by time post-stroke are too coarse to adequately optimise tDCS for a heterogeneous population of stroke survivors. Instead, individual assessment of cortical excitability is required to identify survivors best suited to benefit from the intervention.

Second, the findings of this thesis suggest that stroke-induced changes in brain anatomy have a significant impact on tDCS-induced electric field (E-field): conductive lesions are shown to draw current towards them even if small in size, altering E-field intensity in an ROI which may be in- or out-of-line with the path of current flow. Furthermore, network re-organisation may result in alteration of the optimal cortical target to modulate motor function, particularly in cases where the primary motor cortex is occluded by a lesion. Optimisation of tDCS in stroke may require individual identification of brain regions

supporting movement, instead of targeting the neurotypically-defined primary motor cortex.

Candidate methods to account for stroke-induced changes in brain anatomy and function include development of biophysically realistic current flow models (Aberra et al., 2020; Bonaiuto et al., 2016; Bonaiuto & Bestmann, 2015; Clusella et al., 2022; Galan-Gadea et al., 2022; Jansen & Rit, 1995; Lopez-Sola et al., 2022; Sanchez-Todo et al., 2022; Wang et al., 2018). In the research sphere, development of current flow models is recommended to implement advances in the mechanisms of tDCS and the physics of current flow to innovate tDCS protocol design. TDCS maintains its promise to improve public service by increasing efficiency of motor rehabilitation to improve quality of life after stroke. Further development of current flow models paired with research to improve accessibility of computational models in clinical settings is likely required for further progress, with a focus on minimising the time, expertise and costs required to implement them.

RESEARCH PAPER DECLARATION FORM

1. For a research manuscript that has already been published (if not yet published, please skip to section 2)**:**		
a) Where was the work published? (e.g. journal name)	Current Behavioral Neuroscience Reports	
b) Who published the work? (e.g. Elsevier/Oxford University Press):	Springer Nature	
c) When was the work published?	16/11/2021	
d) Was the work subject to academic peer review?	Yes	
e) Have you retained the copyright for the work?	Yes, the work is under creative commons	
[If no, please seek permission from the relevant publisher and check the box next to the below statement]: ☐ *I acknowledge permission of the publisher named under 1b to include in this thesis portions of the publication named as included in 1a.*		
2. For a research manuscript prepared for publication but that has not yet been published (if already published, please skip to section 3)**:**		
a) Has the manuscript been uploaded to a preprint server? (e.g. medRxiv):	Please select.	**If yes, which server?** Click or tap here to enter text.

b) Where is the work intended to be published? (e.g. names of journals that you are planning to submit to)	Click or tap here to enter text.
c) List the manuscript's authors in the intended authorship order:	Click or tap here to enter text.
d) Stage of publication	Please select.

3. For multi-authored work, please give a statement of contribution covering all authors (if single-author, please skip to section 4**):**

I contributed to conceptualisation, writing of the original draft, reviewing, editing of the article, visualisation, and project administration. Dr. Evans. Contributed to conceptualisation, writing and editing of the article, visualisation, and supervision. Prof. Bestmann contributed to conceptualisation, reviewing, editing of the article and supervision.

4. In which Chapter(s) of your thesis can this material be found?

Chapter 1: Introduction

Chapter 3: Re-opening the sensitive period after stroke with dose- and direction-controlled tDCS

Chapter 4: The impact of stroke lesions on tDCS electric field

Chapter 5: General discussion

5. e-Signatures confirming that the information above is accurate (this form should be co-signed by the supervisor/ senior author unless this is not appropriate, e.g. if the paper was a single-author work):

Candidate:	Jenny Lee	**Date:**	14/11/2022
Supervisor/ Senior Author (where appropriate)**:**	Carys Evans	**Date:**	14/11/2022

ACKNOWLEDGEMENTS

A heartfelt thank you to every person who took part in experimental sessions or volunteered their brain scans to research, especially through the pandemic. None of this would have been possible without your generosity. Thanks also to my wonderful family, Denis, Sharon and Robin, who support me in every way you can imagine, who made me enjoy learning in the first place and who gave me the sense of humour I've found is essential to get through a PhD. Thank you Jack, my partner and best friend, for your support and optimism through thick and thin. This PhD 'journey' has been yours as well as mine.

Particular thanks to Dr. Carys Evans, my mentor and friend, who offered level-headed advice when needed and a glass of wine when essential. Thanks to the rest of the fourth-floor gang for all the funny and interesting conversations over lunch, the advice, and the occasional rescue from death-by-MATLAB. A number of "beautiful people" (a favourite phrase of Alex Galvez Pol) have supported me beyond what I could repay in the last few years, and this is a great opportunity to say thank you so much to my colleagues-turned-friends: Will DeDoncker, Lydia Mardell, Catharina Zich, Eve Gregoriou, Ainslie Johnstone, Seb Sporn, India Walford, Lisa Tedesco Triccas, Will Kistler, Mireia Coll i Omaña, Massimo Bertoli, Silvia Salvalaggio, Anna Stroe, Clarissa Bachmann, Andy Watson, Sofia Loizou, Eddie Kane, João Teixeira Santos, Kirsten Thomas, Haya Akkad, Ben Beare, Ang Dawson, Alejandro Galvez Pol, Sasha Ondobaka, Jane Rondina, Danny Spampinato, Daniel Bates, Clive Negus and Megan Creasey.

Thanks also to Dr. Anna Kuppuswamy, Prof. James Kilner and Prof. John Rothwell for the friendly and constructive guidance. Thanks to Imran Sayed and Linda Taib who not only make the department tick, but have been kind and helpful without exception despite my countless emails and queries. Thank you to our lab manager, Paul Hammond, without whom things simply wouldn't work, and whose door was always open for a chat. Thanks especially Paul for getting us back up and running despite multiple lockdowns.

Thank you to my supervisors, Prof. Sven Bestmann and Prof. Nick Ward, for the guidance, support, insight, positivity, encouragement and for the opportunity. Thanks for the trips to

the pub, the picnics in the park and later, for the lockdown quizzes that made normality feel not so far away. Thanks Nick for teaching me to never lose sight of the bigger picture and to always be positive about my own work! Thanks Sven for the weekly one-on-ones (at least!), the always-quick feedback, the flexibility and unwavering support in tough moments, for making me laugh through meetings and for teaching me to turn uncertainties into questions. You have both encouraged me to grow as a person and a scientist in what have been four formative and wonderful years. Thanks for everything.

A sincere thank you to Brain Research UK not only for funding this work, but for your unyielding support through uncertain times. Thank you for your commitment to not only this project but the researchers behind it; it's been a pleasure.

Finally, thanks to the friends who were always behind the scenes: to Dunc and Kane for making London home, to Paulina, Sarah D., Dec, Martin, Pip, Flo, Tab, Hannah, James, Carys G., Jim, Claire, Henry, Jackson, Ellie, Dan, Alex, Sarah S., Miles, Ben, Georgia, Cam, Collum, Lauren, Dom, Kate, Whitney, George, Rachel, Yas and Meg, for the walks, dinners, debates, pints, advice, laughter and everything else for which I am so grateful.

CONTRIBUTORS

A breakdown of contributors for each empirical study is provided here.

In Chapter 2, titled A Longitudinal Comparison of Cortical Excitatory-Inhibitory Balance in Stroke and Neurotypical Populations, data were collected by Dr. Brenton Hordacre and colleagues at the Neuromotor Plasticity and Development TMS laboratory at the University of Adelaide in Australia, between September 2014 and April 2017. Dr. Hordacre generously shared raw EMG data for RMT, SICI, and pre-post cTBS measures. I developed study aims, processed the raw EMG data using MATLAB (*MATLAB*, 2018), planned and executed statistical analyses in R Studio (R Core Team, 2021), and interpreted and wrote up the findings.

Data presented in Chapter 3, titled Encouraging an Excitable Brain State after Stroke with Dose- and Direction-controlled tDCS, were collected by myself and my colleague, Dr. Carys Evans. I completed the ethical approval process including setting up multiple NHS data collection sites, completing paperwork, and communicating with the Joint Research Office, the Research Ethics Committee and the Stroke Research Team. Dr. Evans and myself completed study piloting, participant screening, project management and data collection responsibilities. Ms. Kirsten Thomas assisted with participant recruitment for 6 months on a part-time basis during the pandemic. I independently completed raw data processing and statistical analyses in MATLAB (*MATLAB*, 2018) and R Studio (R Core Team, 2021), and interpreted and wrote up the findings presented in Chapter 3.

Chapter 4, titled The Impact of Stroke Lesions on tDCS-induced Electric Field, includes data provided by the ENIGMA stroke recovery working group, chaired by Dr. Sook-Lei Liew (Liew et al., 2020; Liew et al., 2018, 2022; https://enigma.ini.usc.edu/ongoing/enigma-stroke-recovery/). This extensive database includes structural MRI data for >1000 stroke survivors and neurotypical participants, and manually segmented masks of stroke lesions. I presented planned work to an international panel of contributors for approval, and completed the secondary proposal process required to access these data. I discussed study ideas with my colleagues, Dr. Evans, Dr. Catharina Zich, Dr. Ainslie Johnstone and Prof. Sven Bestmann. I

independently completed 315 computational simulations using ROAST (Dmochowski et al., 2011, 2013; Huang, Thomas, et al., 2018; Huang, Datta, et al., 2018; Huang et al., 2019, retrieved from: https://www.parralab.org/roast/) and ROAST-lesion (Johnstone et al., in review) via MATLAB (*MATLAB*, 2018), and adapted code for ROAST-lesion to accept 'real' lesion data instead of computational insertion of synthetic lesions. I manually reviewed data quality for all simulations to identify poor tissue segmentation, electrode placement, or image resolution. I designed and executed the data analysis pipeline, including testing multiple methods to quantify 3-dimensional irregularly shaped lesions and their impact on E-field intensity in $M1_{hand}$. I extracted lesion characteristics (size, location, distance to target) for each participant using a custom MATLAB (*MATLAB*, 2018) script, and completed statistical analyses in R studio (R Core Team, 2021).

Appendix A includes an additional chapter, titled "Does Deviation of TMS Coil from Hotspot Predict MEP Amplitude?" This study was conceived by myself. I conducted the study design, piloting, and data collection, and independently completed data processing, analysis, interpretation and write-up. I processed EMG and NeuroNavigated TMS data in MATLAB (*MATLAB*, 2018), and planned and executed statistical analyses in R Studio (R Core Team, 2021). The study was conducted due to an interest in any source of variability associated with tDCS outcomes, yet as the PhD progressed I focussed my attention on characterising tDCS outcome variability in the context of stroke specifically. The work presented in appendix A, conducted with neurotypical volunteers, contributed value in characterising some of the variability associated with MEPs, a primary outcome measure in this thesis. It also boosted my own skillset as I improved precision of TMS application, learned to process data using MATLAB and to conduct analyses in RStudio. The study therefore represents a significant learning curve, and though its findings do not directly address the thesis objective, to interrogate optimisation targets for individualised non-invasive brain stimulation in stroke, it is included in appendices due to its relevance to the wider PhD endeavour.

TABLE OF CONTENTS

LIST OF FIGURES

LIST OF TABLES

KEY TERMS

Acute phase	1 – 7 days after stroke
Anatomical brain state	Morphology of brain tissue, including stroke lesions
CFM	Current flow modelling / Current flow model
Chronic phase	≥ 6 months after stroke
CSE	Cortico-spinal excitability
CSF	Cerebrospinal fluid
CST	Cortico-spinal tract
Early sub-acute phase	1 week – 3 months after stroke
E-field	Electric field
EMG	Electromyography
ENIGMA	Enhancing NeuroImaging Genetics through Meta‐Analysis
Functional brain state	Underlying brain activity, neurochemistry or excitability
GABA	gamma-aminobutyric acid
Hemiparesis	weakness or the inability to move on one side of the body
Hyper-acute phase	0 – 24 hours after stroke
IO curve	Input-output curve
Late sub-acute phase	3 – 6 months after stroke
M1	Primary motor cortex
$M1_{hand}$	Hand representation of the primary motor cortex.
mA	Milliampere, unit of tDCS current injected into scalp electrodes
MEP	Motor evoked potential
MRI	Magnetic Resonance Imaging
NHNN	National Hospital for Neurology and Neurosurgery
RMT	Resting motor threshold
ROI	Region of interest
S/m	Siemens per meter, unit for electrical conductivity
S1	Primary sensory cortex
tDCS	Transcranial direct current stimulation
TMS	Transcranial magnetic stimulation
UL	Upper limb
V/m	Volts per meter, the intensity of electric field in an electro-magnetic field.

CHAPTER 1. INTRODUCTION

1.1 The burden of stroke.

In 2015 approximately 117,600 people experienced a stroke in the United Kingdom (UK), bringing the estimated number of stroke survivors to 950,000. By 2035, stroke prevalence is expected to rise to 2,119,400, with an estimated societal cost of £75 billion (King et al., 2020).

This worsening projection is in part due to an ageing population and advances in acute care which have dramatically reduced mortality rates (Lackland et al., 2014); stroke survivors now live with chronic symptoms and there is a great need to improve long-term outcomes. The work presented in this thesis explores the potential of non-invasive brain stimulation to augment rehabilitation of the impaired upper limb after stroke, a symptom experienced by up to 80% of survivors (Langhorne et al., 2009). I will first describe current understanding of stroke recovery patterns and the neurobiology which might underpin them. I will then consider non-invasive brain stimulation methods to support the neuroplasticity required for rehabilitation at key time points after stroke.

1.2 A temporal framework for post-stroke recovery.

Four distinct epochs are recognised in stroke recovery, informed by preclinical and human research (Bernhardt et al., 2017). These distinct phases are identified by time since stroke onset: hyper-acute (0–24 hours), acute (1–7 days), early subacute (1 week–3 months) late subacute (3–6 months), and chronic (more than 6 months post-stroke) (Bernhardt et al., 2017). It is hypothesised that functional recovery, modulated by the brain's capacity for plasticity, might be understood within this framework. The work of Bernhardt and colleagues (Bernhardt et al., 2017), Joy and Carmichael (Joy & Carmichael, 2020), and Krakauer and Carmichael (Krakauer & Carmichael, 2017) comprise excellent summaries of post-stroke neurorehabilitative mechanisms which I will also outline here.

Within minutes of stroke onset, cell death occurs in the infarct core, a brain area characterised by extremely low cerebral blood flow (CBF) and metabolic oxygen rate. The

next 24 hours are termed the **hyper-acute phase** of stroke, characterised by a cascade of cellular processes which mediate excitotoxicity. During this time, clinicians aim to rescue penumbral tissue adjacent to the stroke core, characterised by reduced blood flow, which will progress to infarction without intervention (Fernández-Klett & Priller, 2014; Rosso & Samson, 2014).

The **acute phase** is defined as the week following stroke, characterised by delayed neuronal cell death caused by radial propagation of inflammation extending from the infarct core to adjacent and functionally connected regions (Sharp et al., 2000). Spreading inflammation causes parts of the penumbra to die; rodent models suggest this will occur within the first 2 days following stroke (Davis & Donnan, 2014). Human imaging studies have shown that extent and temporal trajectory of infarct growth in this stage is subject to high heterogeneity regardless of intervention (Moustafa & Baron, 2008). In fact, Rosso and Samson (Rosso & Samson, 2014) note that the thrombolysis window may vary between patients.

Within the acute phase, surviving penumbral tissue forms the peri-lesional zone, separated from the core by a thin layer of scar tissue (Fernández-Klett & Priller, 2014). During this phase, the brain is sensitive to processes that might potentiate further injury, such as elevated temperature, infection, altered physical activity levels, or increased cortical excitability. The unstable acute phase is not a target for interventions described in this thesis (Carmichael, 2012; Clarkson et al., 2011; Dromerick et al., 2009; The AVERT Trial Collaboration group, 2015).

The **sub-acute phase** occurs between 1 week and 6 months of stroke onset, though the period before 3 months, identified as the **early sub-acute phase**, is of particular interest (Bernhardt et al., 2017)**.** During the early sub-acute stroke period, accelerated recovery of function relative to gains achieved later in the timeline has been widely reported (Duncan et al., 1992; Krakauer et al., 2012; Kwakkel et al., 2003; Nishimura et al., 2007; Ward, 2017). Interestingly, these gains often occur irrespective of medical intervention. That is, they occur in a period of **spontaneous biological recovery** (Biernaskie, 2004; Nudo & Milliken, 1996; Zeiler et al., 2016).

1.2.1 Spontaneous biological recovery.

The concept was explored in a study by Nudo and Milliken (Nudo & Milliken, 1996), which demonstrated that squirrel monkeys' performance on a pellet retrieval task returned to pre-stroke levels within two months, in the absence of training. In a control group of monkeys that did receive training in the subacute phase (commencing from 5 days after stroke), the same performance level was reached within one month of induced stroke. This early finding highlighted both an endogenous process by which subjects might spontaneously regain function in the absence of training, and further demonstrated that at least the speed of this process might be modulated by intervention. Krakauer and Carmichael however point out some controversy over the description of "spontaneous" recovery, since daily movements outside of training sessions were not prohibited (Krakauer & Carmichael, 2017b).

While spontaneous biological recovery has been shown to result in near-complete functional recovery in some cases, others have reported that intervention might not only speed up the recovery process (Nudo & Milliken, 1996) but also improve functional outcomes (Murata et al., 2008; Ogden & Franz, 1917). Murata and colleagues demonstrated that macaques with large lesions encompassing all digit representations in the primary motor cortex (M1) were able to recover pre-stroke performance in a precision grip task within 1 or 2 months when training was delivered for 1 hour a day, 5 days a week. By contrast, monkeys in the spontaneous recovery group (no intervention) did regain the ability to flex and extend the thumb and index finger, but not to pre-operative levels required to consistently perform on the precision grip task. Taken together, early animal models indicated a time window in which recovery from stroke was spontaneously heightened, and open to modulation by training.

1.2.2 A sensitive period for recovery.

Stroke-induced spontaneous biological recovery and heightened sensitivity to training are time-limited. Biernaskie and colleagues (Biernaskie, 2004) for example demonstrated that enriched rehabilitation initiated 5 days after focal ischemia in 40 Sprague Dawley rats resulted in marked improvement in forearm reaching, narrow beam-walking and ladder tasks, and reduced dependence on the unaffected paw. By contrast, intervention delivered

at 14 days resulted in lesser improvement, and training delivered at 30 days resulted in functional gains comparable to rats given no training at all.

One might consider the contribution of loss of peripheral input to Biernaskie and colleagues' findings; perhaps muscle atrophy or preference for compensatory movements had set in after a month without intervention. The notion of a sensitive period of heightened endogenous plasticity induced by the stroke itself was tested by Zeiler and colleagues (Zeiler et al., 2016), who hypothesised that a second stroke might re-open the sensitive window and counter-intuitively improve functional outcomes. Mice were first trained in a reach-to-grasp task before the first stroke was induced. From 7 days post-stroke, mice were either trained for 19 days or trained to asymptote on the same task. In the latter group, a second stroke was induced and training re-commenced after only 48 hours. Mice in the single-stroke group experienced only mild performance gains which did not return to pre-stroke levels. In contrast, performance initially worsened in mice after a second stroke, before dramatically improving to levels comparable to pre-stroke levels. An additional control group underwent a second stroke in an area outside the functional network, the occipital cortex, which did not result in significant functional improvement. These findings supported hypotheses of a stroke-induced, time-limited window of heightened recovery potential in animal models of stroke, which has not yet been robustly translated to human stroke survivors, though research is ongoing (Dromerick et al., 2015, 2021; Hordacre et al., 2021; Rubio Ballester et al., 2018; reviewed in Cramer, 2020).

While it is recognised that stroke survivors have the capacity for significant functional improvement in all stages after stroke, including many years into the chronic phase with intensive training (Ward et al., 2019), it is also clear that a period of rapid spontaneous functional improvement, which may be open to modulation by intervention, occurs in the months following human stroke (Twitchell, 1951), now defined as the "sub-acute" phase of recovery (Bernhardt et al., 2017). Notably, this universal timeline may not apply to all human stroke survivors; the interaction between spontaneous biological recovery, the impact of training, and end-point recovery potential is likely moderated by stroke severity, which itself is determined by several factors including lesion size, remaining neural

substrates, ability to participate in functional training and comorbidity. I consider the difficulties of translation between animal and human models further in the discussion.

Understanding the molecular and cellular triggers which might open the sensitive period after stroke (and indeed, close it) is a focus for therapeutic research: could the critical window, during which rapid recovery is observed, be extended or supported non-invasively? In the next section, I will consider the brain environment which might support heightened sub-acute recovery.

1.3 Neurophysiological mechanisms of sub-acute stroke recovery.

Cortical excitability is here defined as the strength of response of cortical neurons to afferent input. In the sub-acute phase of stroke, a prevailing hypothesis based on pre-clinical work posits that increased sub-acute cortical excitability might underpin accelerated functional gains which are also observed in the sub-acute phase of stroke (Bernhardt et al., 2017; Carmichael, 2006; Cramer, 2008; Joy & Carmichael, 2020).

Notably, the trajectory of cortical excitatory-inhibitory shift after stroke is not linear. In the hyper-acute and acute phases, excitotoxicity prevails, and hyperexcitability is instead associated with cell death. Neuromodulatory research is focussed on the sub-acute phase not only because the steepest functional gains are observed 1 week to 6 months post-stroke, but because stroke-induced excitotoxicity occurs in the unstable acute phase which is generally not a target for neuromodulatory intervention (Carmichael, 2012; Clarkson et al., 2011; Dromerick et al., 2009; The AVERT Trial Collaboration group, 2015), though I note recent rodent work investigating the efficacy of tDCS to limit acute infarct expansion (Liu et al., 2017; Notturno et al., 2014; Peruzzotti-Jametti et al., 2013; Pruvost-Robieux et al., 2018).

Briefly, excitotoxicity after stroke is characterised by a positive feedback loop in which hypoxia results in neuronal polarisation, followed by glutamate release and binding to N-methyl-D-aspartate (NMDA) and α-amino-3-hydroxy-5-methyl-4-isoxazolepropionic acid (AMPA) receptors. Subsequent calcium and sodium influx in affected cells results in further neuronal depolarisation: an excitotoxic cycle associated with irreversible calcium-mediated

cell death (Jayaraj et al., 2019; Krakauer & Carmichael, 2017c; Lai et al., 2014; Shen et al., 2022).

Excitotoxic damage is countered by an increase in GABAergic signalling (Clarkson et al., 2010; Prabhakaran et al., 2008), as GABA accumulates at extrasynaptic $GABA_A$ receptors in peri-lesional tissue following stroke, via downregulation of the GABA transporter GAT3 (Clarkson et al., 2010). Increased GABAergic tone results in increased shunt current, which in turn increases the action potential threshold of affected neurons; persistent tonic inhibition reduces activity of neurons in the stroke-damaged circuit (Carmichael, 2012; Glykys & Mody, 2007).

1.3.1 Persisting GABAergic tone impedes functional recovery in sub-acute stroke.

However, the neuroprotective effect of GABAergic inhibition can be detrimental to stroke recovery if GABAergic tone persists into the sub-acute phase of stroke. In a seminal study, Clarkson and colleagues (Clarkson et al., 2010), confirmed that disinhibitory intervention, via pharmacological reduction of GABA in peri-lesional tissue, improved functional outcomes in mice when applied after the excitotoxic window had closed. The same intervention applied during the excitotoxic window was associated with poor functional outcomes. Recent work corroborates Clarkson and colleagues' finding that cortical recovery might be supported by alleviation of inhibitory signalling in brain regions affected by the stroke (Clarkson et al., 2010; Lake et al., 2015; Orfila et al., 2019). In humans, $GABA_A$ receptor availability has been shown to correlate with motor recovery after stroke in a PET study, where elevated $GABA_A$ receptor availability was recorded up to 1 month before returning to neurotypical group levels by 3 months post-stroke (Kim et al., 2014).

While alleviation of persistent inhibitory signalling is a therapeutic target in the human sub-acute phase, it is acknowledged that inhibitory systems do not respond uniformly to stroke. Enhanced long-term potentiation (LTP) and diminished response to paired-pulse inhibitory TMS protocols have also been reported in sub-acute stroke (Buchkremer-Ratzmann & Witte, 1997; Hagemann et al., 1998; Krakauer & Carmichael, 2017c; Qü et al., 1998; Schiene et al., 1996), thought to be underpinned by reduced phasic synaptic GABAergic inhibition in peri-lesional tissue. In fact, enhancement of phasic (instead of tonic) GABA with the agonist

zolpidem has been shown to improve functional recovery when applied days to months after rodent stroke (Hiu et al., 2016). Therapeutic interventions must therefore target selective inhibitory systems (Johnstone et al., 2018; Joy & Carmichael, 2020; Krakauer & Carmichael, 2017c).

1.3.2 Reducing inhibition and increasing excitability promotes sub-acute recovery.

Taken together, a recovery-promoting profile of excitatory-inhibitory balance after stroke may include reduced inhibition and increased excitation in brain areas adjacent to, or functionally connected with, remaining substrates in peri-lesional tissue. Though functional recovery and responsiveness to training continue in chronic stroke, spontaneous biological recovery and a sensitive period for training appear to be temporally coupled with a sub-acute 6-month window of atypical excitatory-inhibitory balance. This observation has given rise to the hypothesis that supporting an excitable brain environment may promote recovery after stroke (Carmichael, 2006; Cramer, 2008; Di Pino, Pellegrino, Capone, et al., 2014; Joy & Carmichael, 2020).

The temporal framework for post-stroke recovery outlined earlier in this Chapter was proposed by The Stroke Roundtable Consortium (Bernhardt et al., 2017), with the aim of creating a unified vision in stroke rehabilitation research by streamlining common language and definitions used. Four phases of the post-stroke timeline were defined by time since stroke onset (hyper-acute: 24 hours, acute: 1 day – 1 week, sub-acute: 1 week – 6 months, chronic: > 6 months). The rationale for these temporal divisions was grounded in observations that recovery-related processes after stroke are time-dependent (Biernaskie, 2004; Carmichael, 2016; Dobkin & Carmichael, 2016; Zeiler et al., 2016), and that the trajectory of functional recovery, particularly motor recovery, follows a relatively homogenous pattern whereby the most significant improvements are observed in the weeks and months following stroke, stabilising to chronic deficit by 6 months (Bernhardt et al., 2017; Buma et al., 2013; Cramer, 2008; Dobkin & Carmichael, 2016; Kwakkel et al., 2003, 2004). A hypothesis emerges, that functional gains and neurophysiological changes following stroke are temporally coupled. This concept is summarised in Figure 1.1. In Chapter 2 of this thesis, I interrogate TMS-assessed longitudinal excitability changes up to 12 months post-stroke, to determine whether a similar coupled trajectory of functional

gains and neurophysiological change occurs in human stroke survivors. Clearer characterisation of the human post-stroke timeline may reveal critical windows of time in which brain activity maximally supports potentiation of training, or conversely, periods of inhibition where neuromodulatory intervention may be best applied to support physical therapy.

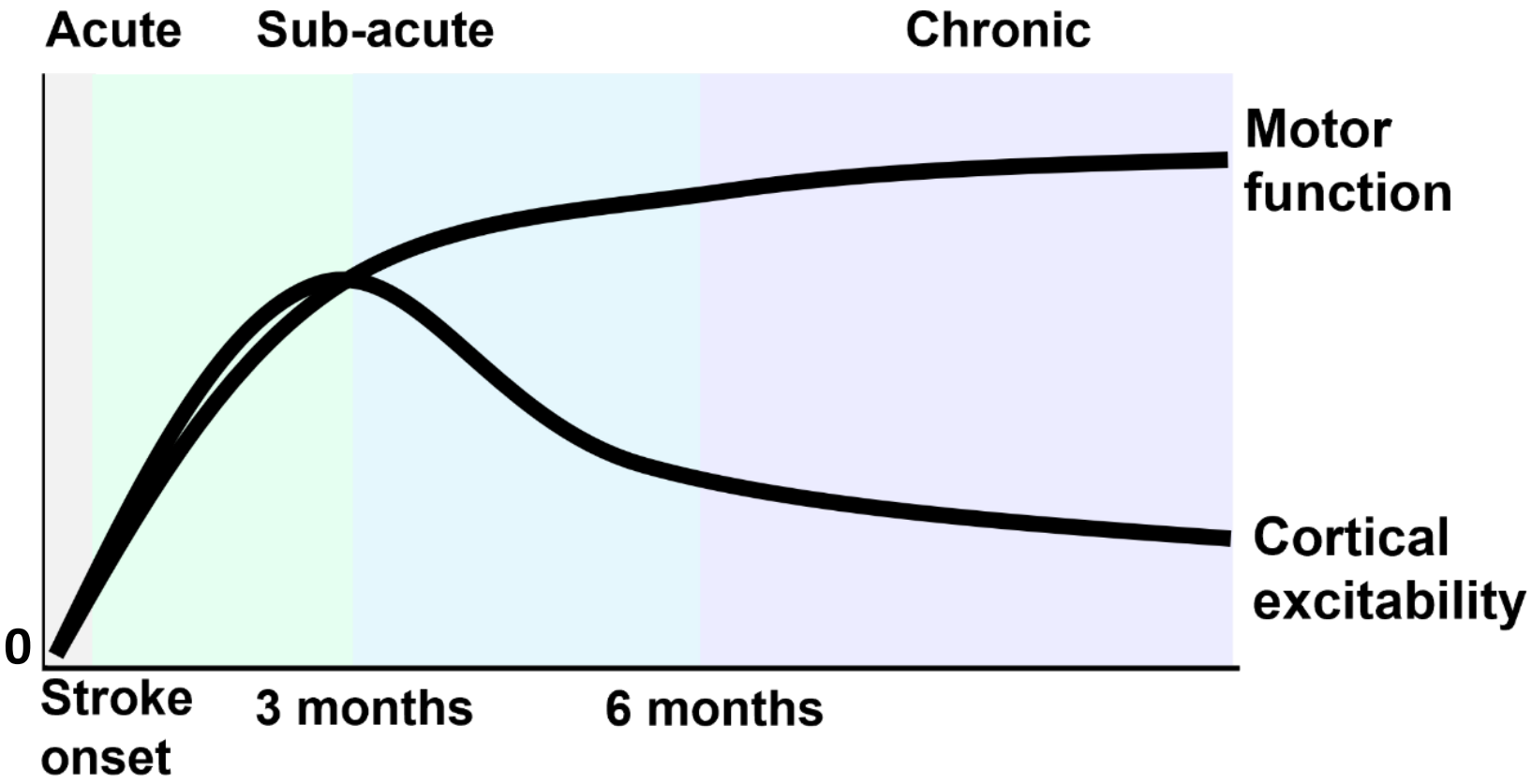

Figure 1.1. Schematic of the hypothesised coupled trajectories of cortical excitability change and functional gains after human stroke. Based on the work of Bernhardt and colleagues (Bernhardt et al., 2017). On the y-axis, 'zero' simultaneously represents neurotypical cortical excitability and minimum motor function. Time post-stroke is shown on the x-axis. Shaded areas represent each phase of stroke recovery (grey = acute, green = early sub-acute, blue = late sub-acute, purple = chronic) with labels included above shaded segments. A sub-acute peak in capacity for endogenous neuroplasticity may be underpinned by a stroke-induced increase in cortical excitability and disinhibition, giving rise to acceleration of functional gains in sub-acute stroke. In chronic stroke, cortical excitability is hypothesised to return to neurotypical levels, coupled with slowing of motor gains.

1.3.3 Sub-acute reduction in excitability due to lost connectivity.

In addition to alleviation of inhibitory signalling, promotion of excitatory activity in regions functionally connected with damaged networks is hypothesised to support recovery after stroke. Enhanced Brain-Derived Neurotrophic Factor (BDNF) signalling in the peri-lesional cortex has been linked with improved motor function after stroke (Clarkson et al., 2011, 2015), and treatment with AMPAkines has been shown to support binding of glutamate to AMPA-type glutamate receptors (AMPARs), leading to increased expression of BNDF and enhancement of peri-infarct brain re-organisation in sub-acute stroke (Wang et al., 2018).

Similarly to the pattern of persisting inhibition limiting recovery described above, decreased sub-acute neuronal excitability has been recorded in preclinical and human studies. Lim and colleagues (Lim et al., 2014) for example recorded widespread depression of optogenetically evoked activity 1 week after stroke. Though activity recovered to pre-stroke levels by 8 weeks, network strength remained impaired due to loss of key nodes in the functional circuit. The authors recommended intervention to support earlier network re-organisation, in cases where recovery-promoting excitation is dampened in the months following human stroke.

Reduced neuronal response to sensory stimuli in brain regions within a damaged network may be characteristic of an early sub-acute response to stroke (Brown et al., 2009; Di Lazzaro et al., 2010; Lim et al., 2014; McDonnell & Stinear, 2017). This is considered a direct result of lost connectivity within the network, as dendritic spines become unstable and the excitability of neurons adjacent to, or connected with, stroke-damaged neurons is reduced. This effect is network-specific: little network activity change is recorded in non-motor networks after motor stroke, such as the occipital cortex (Lindau et al., 2014). Alleviating reduced network signalling in sub-acute stroke, after the excitotoxic window has closed, is a therapeutic target for intervention, particularly in light of work reporting chronic network dysfunction after stroke, which may contribute to limited functional outcomes (Grefkes & Fink, 2012; Guggisberg et al., 2019; Siegel et al., 2016).

1.4 Why does increased cortical excitability support recovery?

Krakauer and Carmichael (Krakauer & Carmichael, 2017a) assert that motor recovery after stroke requires 3 components: (partially) in-tact neural substrates (i.e. remaining structures in motor or sensory networks), tissue re-organisation, and physical activity to train newly reorganised networks. The former is best addressed by acute stroke care with a focus on limiting expansion of the infarction (Rosso & Samson, 2014), and is beyond the scope of this thesis. The latter processes are discussed below.

1.4.1 Cortical excitability supports synaptic plasticity.

The primary events of tissue reorganisation after stroke include axonal sprouting and dendritic spine morphogenesis (Carmichael et al., 2017; Cramer, 2008), as damaged networks begin to re-establish connectivity. There is robust evidence for tissue re-organisation after stroke, though it is not always causally linked with functional recovery. Carmichael and colleagues (Carmichael et al., 2017) distinguish between reactive and reparative axonal sprouting, the former being part of the early 'clean up' response of the brain. **Reactive axonal sprouting** occurs in the peri-infarct zone, and is part of the cell turnover necessary for scar formation after infarction. It is not associated with functional improvement. **Reparative axonal sprouting** occurs not only in peri-lesional tissue but in distant, functionally connected brain regions. Increased network excitability can support recovery via growth of new connections after stroke. For example, optogenetically-increased synchronous firing of a population of neurons has been linked to improved post-stroke motor function (Cheng et al., 2014), which in turn is associated with growth of dendritic spines (Tennant et al., 2017) and axons (Wahl et al., 2017) in brain areas affected by stroke, both in peri-lesional tissue and distant, functionally connected regions (Li et al., 2010, 2015; Omura et al., 2016; Overman et al., 2012). Meanwhile, increasing excitability in non-relevant networks can impair motor recovery (Blomstedt & Hariz, 2006); encouraging network-specific excitability is a therapeutic target for stroke recovery.

1.4.2 Cortical excitability supports restoration of lost connectivity.

1.4.2.1 Increased cortical excitability supports motor engram formation.

Re-building damaged functional networks requires co-activation of neurons that are excitable enough to fire together. An engram, a term more commonly used in memory

neuroscience, is a physical trace of a memory in the brain (Josselyn et al., 2015; Tonegawa et al., 2015). The term has been adopted in stroke recovery, where a motor engram might be represented by co-activated neurons in the motor cortex which control upper limb movement. Allocation of neurons to a motor engram depends on their activity in response to a shared stimulus of interest (Biane et al., 2015; Costa et al., 2004; Ohashi et al., 2019). Neurons are competitively allocated to an engram based on their state of excitability; a cell that is more likely to respond to a given stimulus will be preferentially allocated to a network that prioritises efficiency (Tang et al., 2019). Therefore, promoting cortical excitability is a candidate method to support restoration of functional networks after stroke (Joy & Carmichael, 2020). Evidence has already emerged demonstrating that rehabilitative training (Clark et al., 2019) and artificial activation (Roy et al., 2016, 2017) of engram neurons strengthens synaptic contacts within the network, by supporting dendritic spine plasticity (Frank et al., 2018; Fu et al., 2012; Hayashi-Takagi et al., 2015; Huang, Li, et al., 2018; Sargin et al., 2013). Later in this thesis I will describe the potential of transcranial direct current stimulation (tDCS), a non-invasive technique and candidate method to artificially activate neurons in a target network.

1.4.2.2 Increased cortical excitability supports Creb induction.

Enhancement of neuronal activity following stroke is also moderated by the transcription factor CAMP response element binding protein (*Creb*). *Creb* enhances neuronal excitability and facilitates LTP (Wu et al., 2007) by altering the action potential threshold of affected neurons (Dong et al., 2006; Kim et al., 2013). *Creb* is powerfully induced in a very small number of motor cortical neurons following stroke (Gouty-Colomer et al., 2016; Han et al., 2007; Zhou et al., 2009). Notably, the number of *Creb*-induced neurons is similar to the number of neurons that are allocated to motor engrams described in the previous paragraph (Caracciolo et al., 2018; Joy & Carmichael, 2020). Animal studies have shown that induction of *Creb* in motor and premotor neurons facilitates full motor recovery following stroke, while blocking *Creb* signaling prevented recovery (Caracciolo et al., 2018). Indeed, *Creb* is suggested to have the capacity to turn stroke recovery "on and off" (Joy & Carmichael, 2020, p.9; Krakauer & Carmichael, 2017, p.149). Enhancement of neuronal activity via *Creb* induction is a therapeutic target in stroke, and the intervention of interest in this thesis, tDCS, has been associated with *Creb* induction (see section 1.5.2) via

modulation of intracellular calcium concentration (Kornhauser et al., 2002; Podda et al., 2016).

1.5 Non-invasive brain stimulation alters cortical excitability.

Transcranial direct current stimulation (tDCS) is a non-invasive brain stimulation technique that modulates neuronal activity via sustained low-intensity direct current (DC). The practical use and mechanisms of tDCS are described in the following sections, and a comprehensive commentary can be found in the work of Bikson and colleagues (Bikson et al., 2019). Briefly, the appeal of tDCS lies in its status as a cheap, portable, effective, and easy-to-use non-invasive neuromodulation technique which is well-tolerated by human participants (Chhatbar et al., 2017; Minhas et al., 2010; Pilloni et al., 2022; Reckow et al., 2018). In the context of stroke, tDCS is considered a promising tool with the potential to augment rehabilitation, under the hypothesis that exogenous electrical current may boost neuronal excitability, and in turn support potentiation of post-stroke training (Joy & Carmichael, 2020; Krakauer et al., 2012; Kronberg et al., 2017, 2019; Ward, 2016, 2017). However, evidence has accumulated to show high tDCS outcome variability, a barrier to its adoption in clinical settings. A core aim of this thesis is to identify and reduce sources of tDCS outcome variability particularly in the context of stroke, and to investigate whether optimised tDCS might reliably alter human cortical excitability to support recovery.

1.5.1 TDCS mechanisms of action.

During tDCS application, low-intensity electric field (E-field) is directed into the body via at least one anode electrode, and exits the body through at least one cathode electrode (herein referred to simply as “anode” and “cathode”). When applied to the head, the majority of electrical current is shunted across scalp and cerebrospinal fluid (CSF) tissue (Ciechanski et al., 2018; Kessler et al., 2013; Opitz et al., 2015), while a low dose of E-field penetrates to stimulate the brain; peak tDCS E-field in the brain is typically ~0.3 V/m when 1 mA tDCS is applied (Datta et al., 2009; Huang et al., 2017).

The physiological mechanisms by which tDCS modulates neuronal activity are not yet fully determined, though extensive research indicates that application of DC E-field over a timescale of minutes will result in polarisation of neuronal membranes (reviewed in Bikson

et al., 2019; Jackson et al., 2016; Stagg et al., 2018). Altered membrane potential can change neuronal excitability (Bindman et al., 1964) via tDCS-induced alteration of responsiveness to synaptic input (Rahman et al., 2013), modulation of individual neuron firing rate (Miranda et al., 2006; Wagner et al., 2007), and altered cellular (Huang et al., 2017b) and network (Reato et al., 2013) processing of information. Importantly, tDCS does not induce action potentials but modulates sub-threshold neuronal activity in a polarity-specific manner (Bikson et al., 2004; Chan et al., 1988).

In the seminal work which gave rise to contemporary tDCS use at the turn of the 21st century (Nitsche et al., 2003; Nitsche & Paulus, 2000; Priori et al., 1998), a motor-targeting bipolar tDCS montage was used whereby an anode was placed on the scalp above the motor cortex, and a cathode over the contralateral supra-orbital ridge (M1-SO, herein referred to as the "conventional montage") to modulate the amplitude of motor evoked potentials (MEPs) induced by transcranial magnetic stimulation (TMS; see section 1.8.2). This classic tDCS protocol did contribute to a seminal jump to contemporary low-intensity non-invasive brain stimulation use, and included important concepts such as the polarity-specific effects of stimulation (detailed in section 1.5.1.2). However, the emergence of current flow modelling (CFM) software (Dannhauer et al., 2012; Dmochowski et al., 2011, 2012, 2013; Huang, Datta, et al., 2018; Lee et al., 2017; Ruffini et al., 2014; Saturnino et al., 2015; Thielscher et al., 2015) and progress in pre-clinical work (Bikson et al., 2004; Jackson et al., 2016; Lafon et al., 2017; Radman et al., 2007, 2009b; Rahman et al., 2013) now enables researchers to consider the pattern of exogenous current in the human brain in detail. In the following, I will consider potential sources of the high variability associated with tDCS from the perspective of proposed mechanisms of action.

1.5.1.1 TDCS outcomes are variable.

Neurophysiological and behavioural outcomes associated with tDCS are subject to persistent high variability, which has been attributed to a number of factors including inter-individual differences in *anatomical brain state*, defined broadly as the morphology of brain tissue including stroke lesions; *functional brain state*, defined as underlying brain activity, neurochemistry or excitability; genetic neurotransmitter expression; sex; and age (Chew et al., 2015; Laakso et al., 2015; Polanía et al., 2018; Vergallito et al., 2022; Wiethoff et al.,

2014; Wörsching et al., 2016). Lack of protocol standardisation is also striking, limiting the reproducibility of findings. This has stunted progress in the field, and there is a great need to resolve confounding sources of variability to realise the therapeutic potential of the technique.

Wiethoff and colleagues (Wiethoff et al., 2014) investigated tDCS outcome variability in a group of 53 adults, who underwent 10 minutes of 2 milliamp (mA) motor-targeted tDCS with a conventional bipolar montage (electrodes positioned over the TMS-identified motor hotspot and the contralateral supra-orbital ridge). The authors reported that when "anodal" tDCS was applied, a 75:25 ratio of facilitation:inhibition was recorded across participants, while a 60:40 ratio was reported after the electrode positions were reversed ("cathodal" tDCS). A two-step cluster analysis identified 'responders' who demonstrated a significant motor evoked potential (MEP, see section 1.8.2) amplitude change following tDCS, and 'non-responders', who showed no mean overall effect.

Findings such as these do not suggest subsequent research should always stratify subjects into 'responder' and 'non-responder' groups. Rather, this is evidence of outcome variability, and is it important to consider what might underly it. Research has also emerged showing significant intra-individual variability in tDCS outcomes between tDCS sessions in the same subjects, spaced 6 to 12 months apart (Chew et al., 2015; López-Alonso et al., 2015). There is an urgent need for mechanistically-informed tDCS protocol development, because optimised tDCS has promise to support recovery in a number of disorders including stroke.

TDCS has already been applied in the stroke population, with mixed results. A recent Cochrane review for example reported very low efficacy of tDCS used as an adjunct to post-stroke therapy (Elsner et al., 2020) while another meta-analysis found a positive impact of tDCS (Shen et al., 2022). I note that meta-analyses of tDCS studies are at present problematic because un-standardised stimulation protocols and outcome measures, recorded at different time points (e.g. during or post-tDCS) do not allow for robust comparison of findings between studies. In the next section, I consider the mechanisms underlying neuromodulation by tDCS and discuss recent developments in mechanistically-informed stimulation protocol. I then consider the generalisability of tDCS optimisation methods to the stroke population.

1.5.1.2 Direction of current flow dictates neuronal membrane polarisation.

Maximal membrane polarisation of pyramidal neurons by DC fields occurs when current flows parallel to the somato-dendritic axis. The strength of somatic polarisation by exogenous current is related to the morphology of the cell (Radman et al., 2009; Svirskis et al., 1997); large layer 5 pyramidal neurons are particularly sensitive to DC stimulation (Radman et al., 2009). Pyramidal cells are typically oriented with apical dendrites pointing towards the cortical surface, and so current flowing radial-inward with respect to the surface of the cortex predominantly flows parallel to pyramidal neurons towards the somatic compartment of the cell (Figure 1.2). Radial-inward current flow relative to the cortical surface is associated with somatic depolarisation of pyramidal neurons, while radial-outward current flow towards apical dendrites is associated with somatic hyper-polarsation. Current flowing along the cortical surface, predominantly tangential to pyramidal cell somato-dendritic axes, does not significantly polarise the somatic compartment of pyramidal neurons (Berzhanskaya et al., 2013; Bikson et al., 2004; Chan et al., 1988; Farahani et al., 2021; Radman et al., 2009; Rahman et al., 2013). Due to cortical folding, tDCS will produce mixed somatic polarisation of cells underneath and between electrodes (Lafon et al., 2017; Rahman et al., 2013; Figure 1.2), and inter-individual morphological differences result in varied E-field direction produced in a cortical target between participants (Evans et al., 2022). In this way, the predominant direction of E-field in a cortical region of interest (ROI) significantly differs between subjects when the same stimulation protocol is used (Evans et al., 2022). It appeals to intuition that variable E-field delivery may contribute to variability in behavioural outcomes of stimulation.

Importantly, this description of the determinant effect of tDCS current direction on neuronal polarisation includes only the somatic compartment of the cell. The so-called 'somatic doctrine' focuses on the impact of E-field on the soma because of its critical contribution in eliciting action potentials, and in turn its determinant effect on excitability changes caused by DC fields (Bikson et al., 2004; Bindman et al., 1964; Purpura & McMurtry, 1965; Radman et al., 2007). However, increased understanding of the mechanisms of tDCS highlights the impact of exogenous E-field on all cellular compartments including dendrites and axons (Kabakov et al., 2012; Kronberg et al., 2017; Rahman et al., 2013), for example, radial-inward current will result in both hyperpolarisation of apical dendrites and depolarisation of

the somatic compartment of the same cell (Figure 1.2; Bikson et al., 2004; Chan et al., 1988; Radman et al., 2009). Meanwhile, CA1 pyramidal neurons are oppositely polarised to layer II/IV and layer 5 pyramidal neurons due to their inverted orientation (Kronberg et al., 2017), and a significant impact of DC field on inter-neuronal excitability has been shown in animal work (Purpura & McMurtry, 1965). Taken together, the impact of transcranial DC field in humans has not yet been fully elucidated, and may explain difficulties in predicting outcomes in human studies even when the direction of current flow is controlled (Hannah et al., 2019; Rawji et al., 2018).

Achieving radial-inward current relative to the cortical surface in a target ROI remains a key aim in tDCS optimisation, and is prioritised in the work presented in Chapter 3. However, I note that this approach does not account for complexities of the impact of exogeneous E-field in the brain beyond the 'somatic doctrine'; for example tangential current flow may have a greater impact on tDCS outcomes than previously thought (Rahman et al., 2013). In section 1.6.2, I discuss how current flow modelling (CFM) software is utilised to control the direction of tDCS current flow within the bounds of current understanding and modelling capabilities. Optimising direction of current flow may be important to reduce variability in tDCS outcomes, which in turn may improve the efficacy of tDCS in the context of stroke rehabilitation.

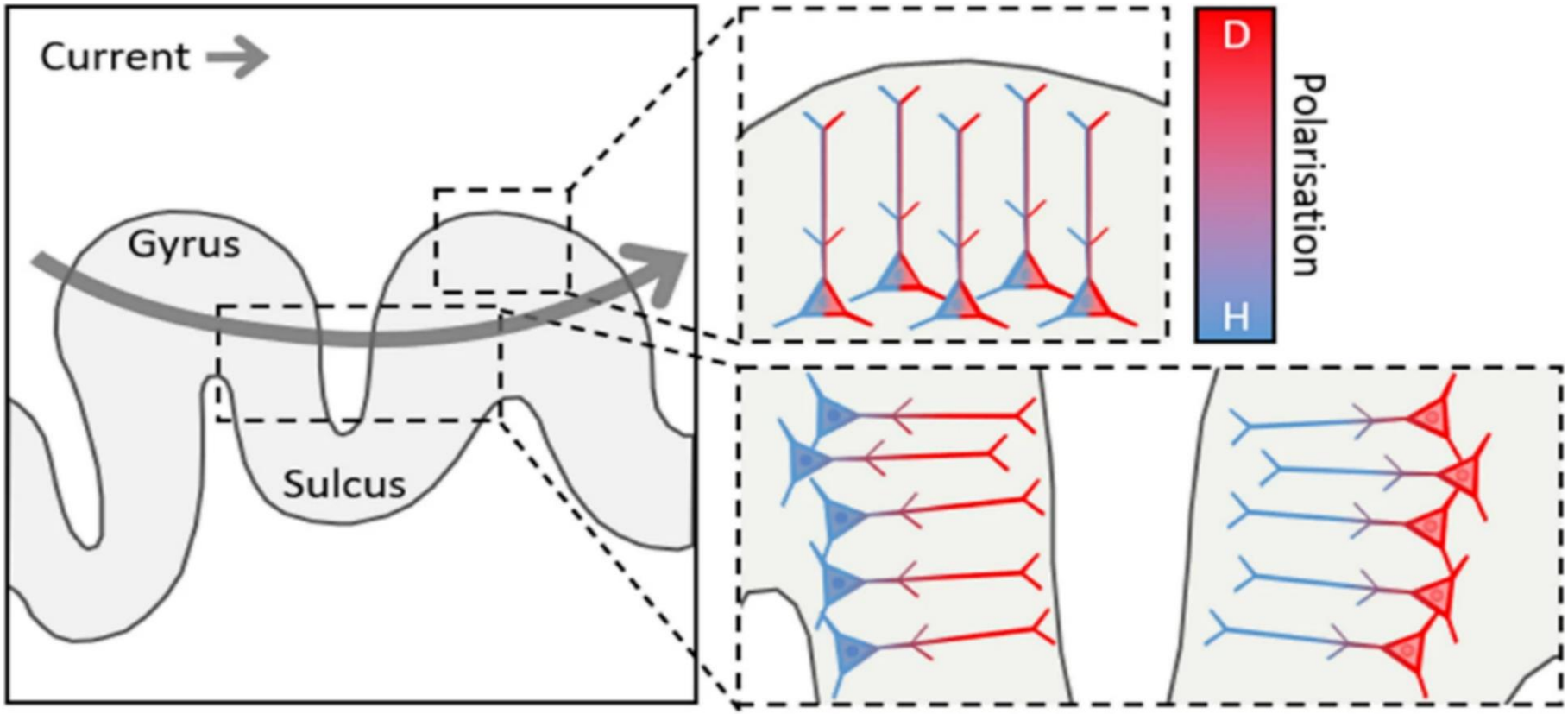

Figure 1.2. Polarisation of cortical pyramidal neurons by exogenous DC fields. Cells are predominantly oriented with apical dendrites pointing to the cortical surface. Radial-inward current flow relative to the surface of the cortex is associated with somatic de-polarisation (D, depicted in red). Radial-outward current flow is associated with somatic hyper-polarisation (H, in blue), and tangential current flow causes little to no polarisation effect of the somatic compartment of layer II/IV and layer 5 pyramidal neurons. Figure from Lee and colleagues (2021), under creative commons.

1.5.1.3 The intensity of tDCS required for behaviourally significant neuromodulation is unknown.

Computational models of tDCS-induced fields in the human head have estimated that peak E-field intensity achieved in grey matter is ~0.3 V/m when 1 mA tDCS is applied to scalp electrodes (Datta et al., 2009; Huang et al., 2017). However, the optimal intensity of stimulation required for behaviourally meaningful modulation of neuronal activity is unknown. *In vitro* work has demonstrated a statistically significant change in neuronal spike timing when ~0.5 V/m uniform DC field was applied to rodent hippocampal slices (Radman et al., 2007). Importantly, translation from *in vitro* animal work to predicting outcomes in human transcranial stimulation studies is not straightforward for two primary reasons, detailed in the paragraphs below.

1.5.1.3.1 The extent of neuronal polarisation by DC fields is moderated by cellular morphology.

First, the relationship between somatic polarisation and extra-cellular DC fields is moderated by neuronal morphology, which differs between humans and the animals involved in reported studies (Bikson et al., 2004; Chan et al., 1988; Jefferys, 1981; Joucla & Yvert, 2009; Reato et al., 2013). The impact of neuronal morphology on sensitivity to extracellular E-field is described mathematically by the coupling constant (units: mm), which is used to describe the change in somatic voltage (in mV) of a cell per V/M of applied E-field, giving the formula:

$$\Delta V = c_E(M)E$$

Where ΔV (in mV) denotes change in somatic voltage, c_E represents the coupling constant, derived from a complex function for neuronal morphology (M), and E denotes the intensity of uniform DC E-field oriented parallel to the somato-dendritic axis (Bikson et al., 2004; Chan et al., 1988; Jefferys, 1981). Bikson and colleagues (Bikson et al., 2004) estimated a coupling constant of 0.1–0.2 mV/V/m for rodent pyramidal cortical neurons, a value later confirmed by an *in vitro* study in ferret slices (Fröhlich & McCormick, 2010) and in CA3 pyramidal neurons in the rodent hippocampus (Deans et al., 2007). In humans, neuronal length is typically longer (Joucla & Yvert, 2009). Reato and colleagues (Reato et al., 2019) point out that this difference in neuronal morphology may produce a higher coupling

constant for humans compared to rodents, suggesting that greater somatic polarisation might be achieved per V/m of applied current, though this has not been directly confirmed.

1.5.1.3.2 The dose-response relationship of tDCS is non-monotonic.

A second key reason why translation of findings from *in vitro* animal research to predict the dose-response relationship in humans is not straightforward, is because a linear relationship between applied current and somatic polarisation does not translate to a linear brain-wide response to increasing E-field. In fact, the dose-response relationship for tDCS in humans is likely non-monotonic (Esmaeilpour et al., 2018). This is because DC field delivered to the brain will impact not only isolated neurons but wider active networks. Network response to E-field will likely depend on the profile of endogenous activity, i.e. the *functional state* of the brain before stimulation is applied (Reato et al., 2013; Schmidt et al., 2014), and on the modulatory effects of distributed current in structures which are functionally connected to an ROI, though spatially distinct (Nitsche et al., 2005).

1.5.1.3.3 Sub-threshold tDCS modulates on-going network activity.

As discussed above, extracellular E-field will modulate membrane potential of single neurons directly during tDCS. An indirect impact of applied DC field is however also likely, as a tDCS-induced change in neuronal activity elsewhere in the network impacts the whole population (Reato et al., 2010). To add complexity, the polarity of direct and indirect effects may differ. The network impact of DC field acting on non-quiescent cells does however explain how sub-threshold modulation of neuronal activity might produce a detectable physiological change in brain activity. While the action potential (AP) threshold for a neuron is typically 10-20 mV above resting potential, E-fields produced by tDCS are expected to alter membrane potential by only 0.2 – 0.5 mV (Opitz et al., 2016; Radman et al., 2009). TDCS is therefore expected to have maximal impact on already-active neurons (Terzuolo & Bullock, 1956), as membrane potential is brought closer-to or further-from AP threshold. In the context of network activity, a feed-forward impact of DC field may also apply, whereby neurons pushed over AP threshold by tDCS may in turn trigger activity elsewhere in the neuronal population (Polanía et al., 2010; Reato et al., 2010). Taken together, DC fields applied trans-cranially to the human cortex produce direct and indirect modulation of single-cell and network activity; the complex relationship between the intensity of current

applied to scalp electrodes, E-field magnitude at cortical ROIs, and behavioural response to stimulation has not yet been elucidated.

1.5.1.3.4 Reverse-calculation is used to probe tDCS dose-response relationship.

Retrospective investigation into tDCS E-field intensities associated with a measurable change in cortico-spinal excitability (CSE) has been conducted to identify contributing factors to the dose-response relationship in human tDCS studies. While the optimal tDCS dose remains unknown, Evans and colleagues (Evans et al., 2020) demonstrated that average E-field intensity in an M1 ROI was ~ 0.185 V/m in a group of 50 healthy adults when a 1 mA conventional tDCS montage was simulated. The dose-response relationship of tDCS was also probed in the work of Laakso and collgeagues (Laakso et al., 2018, 2019) which reported a significant relationship between estimated E-field intensity in M1 and MEP size in response to transcranial magnetic stimulation (TMS; see section 1.8.2). Opposite changes in MEP-assessed excitability were found in participants with the lowest and highest modelled E-field in M1 (Laakso et al., 2019). Furthermore, a significant association has been reported between GABA concentration in ipsilesional M1 and behavioural gains following tDCS in stroke survivors (O'Shea et al., 2014). Finally, the mechanisms underlying neuromodulation by tDCS were probed in a recent study which reported a significant negative correlation between intra-cortical E-field intensity and tDCS-induced GABA concentration in MRS data from 5 human participants (Nandi et al., 2022). Though these findings offer insight into the neurophysiological effects of tDCS in humans, significant correlation does not imply causality.

1.5.1.4 TDCS is inherently non-focal.

In addition to the direction- and intensity-dependent nature of tDCS effects, the impact of E-field focality, or lack thereof, must be considered when planning or interpreting studies. Conventional tDCS application can produce current flow across 30-70% of the brain (DaSilva et al., 2012), far beyond common anatomical targets such as the hand representation of the motor cortex ($M1_{hand}$, anatomical characteristics described in Caulo et al., 2007; Dechent & Frahm, 2003; Yousry, 1997). The potential effects of neuromodulation beyond an ROI cannot be ignored, and are likely subject to inter-individual variability due to anatomical differences and varied endogenous activity of affected networks. However, by virtue of

modulating only sub-threshold neuronal activity, inherent focality may be achieved with tDCS where functionally active networks are maximally affected by DC fields despite a lack of spatial specificity – a concept referred to as "functional selectivity" (Bestmann et al., 2015; Bikson & Rahman, 2013; Ranieri et al., 2012). In keeping with Ohm's law, a core assumption on which the physics of tDCS current flow is based (Miranda, 2013), increasing tDCS stimulator output will result in a linear increase in spatial distribution of E-field above a given value. The impact of distributed fields moderated by endogenous activity is not yet fully understood. Multi-electrode montages can be used to improve tDCS focality (Datta et al., 2008) though improved focality comes at the cost of E-field intensity, as current is increasingly shunted between scalp electrodes instead of penetrating to reach the brain (Datta et al., 2008; Mikkonen et al., 2020). At present it is difficult to balance the intensity, direction and distribution of current simultaneously during tDCS to optimally stimulate a given ROI (see Figure 1.4). Researchers are left with the un-resolved multi-variate dilemma of prioritising different E-field properties over others with a 'best guess' of the impact on a function of interest (Lee et al., 2021)

1.5.2 Optimised tDCS may increase neuroplastic potential to support stroke recovery.

As discussed, tDCS mechanisms of action are not yet fully understood despite extensive research, and are likely to interact with endogenous activity on a cellular and network scale. Nevertheless, the concept of neuronal polarisation by extra-cellular DC field is well-established (Bikson et al., 2004; Chan et al., 1988; Jefferys, 1981), and reports of variable outcomes include evidence for a significant impact of tDCS alongside null effects. The factors giving rise to variable tDCS effects have been difficult to identify amongst a lack of protocol standardization; even in cases where the conventional montage is applied, stimulation duration, intensity, and electrode size have varied, and relatively few studies report or individualise estimated E-field intensity, direction, or focality of applied current, often due to lack of access to individualised MRI scans required for detailed current flow modeling.

The appeal of tDCS as a tool to support stroke rehabilitation persists because it is grounded in research suggesting tDCS may increase potential for neuroplasticity. This includes tDCS-induced activation of N-methyl-Daspartate (NMDA) receptors and L-type voltage-gated

calcium channels (L-VGCC; (Nitsche et al., 2003; Nitsche & Paulus, 2011; Stagg et al., 2011, 2018) modulating the degree of calcium influx into affected cells. In this way, tDCS may alter long-term depression (LTD) and long-term potentiation-like plasticity (LTP), since a low increase in intra-cellular calcium concentration has been linked to LTD, high calcium influx is associated with LTP, and the intermediary zone is not associated with modulation of plastic potential (Lisman, 2001; Stagg et al., 2018). This mechanism for cortical excitability modulation by DC field may partly explain the non-linear relationship between applied current and neuronal response: in addition to an intermediary zone described above, long stimulation duration may be linked to a homeostatic switch from LTP to LTD (Monte-Silva et al., 2013).

TDCS may also impact neuronal activity via alteration of GABAergic activity (Amadi et al., 2015; Antonenko et al., 2017; Bachtiar et al., 2015; Johnstone et al., 2018; Kim et al., 2014; Nandi et al., 2022; O'Shea et al., 2014), which mediates glutamatergic plasticity (Castro-Alamancos et al., 1995). In the context of stroke, alteration of GABergic activity is also suggested as a mechanism underlying sub-acute rehabilitation (Blicher et al., 2015, 2015; Clarkson et al., 2010; Hiu et al., 2016; Kim et al., 2014), and so tDCS is a candidate intervention to 'boost' or extend the brain environment underlying sub-acute accelerated recovery (discussed earlier in this Chapter).

Also of particular relevance to stroke rehabilitation, tDCS has been found to induce the transcription factor *Creb* via modulation of intracellular calcium concentration (Kornhauser et al., 2002; Podda et al., 2016). As previously discussed, *Creb* has been shown to increase neuronal excitability and facilitate LTP (Wu et al., 2007; Dong et al., 2006; Kim et al., 2013), and was shown to facilitate full motor recovery in animal models of stroke (Caracciolo et al., 2012). In addition, Podda and colleagues (Podda et al., 2016) found that *Creb* levels were significantly higher in mouse hippocampal slices exposed to tDCS compared to control slices, suggesting tDCS-induced epigenetic changes. Caracciolo and colleagues (Caracciolo et al., 2018) conducted a viral gene delivery study in the rodent stroke model, which showed induced *Creb* in peri-lesional neurons was associated with fewer faults in foot placement compared to a neurotypical group of mice without *Creb* induction. Interestingly, when the *Creb*-activating drug washed out, impairment recordings were worse than baseline, leading

to the substantial suggestion that inhibiting or releasing *Creb*-induced neurons may be akin to turning stroke recovery "on and off" (Joy & Carmichael, 2020, p. 9; Krakauer & Carmichael, 2017, p.149). Taken together, the potential for tDCS-induced changes in *Creb* induction, glutamatergic plasticity mediated by GABAergic activity, and modulation of calcium influx suggest tDCS is a promising candidate to facilitate rehabilitation after stroke in humans. However, the technique is currently stunted by high outcome variability and lack of protocol standardisation. In the following section I will discuss how CFM software may be implemented to quantify and minimise tDCS-induced E-field variability, with the aim of improving reliability of tDCS outcomes.

1.6 Current flow models estimate tDCS E-field in the brain.

The following text describing CFM applications and considerations has been published in an article written by myself and my colleagues, Dr. Carys Evans and Prof. Sven Bestmann (Lee et al., 2021). The original open-access article is under a creative commons licence which permits unrestricted use, distribution, and reproduction of the work in any medium, provided the original work is properly cited. I was not required to obtain permission to include content from the article in this thesis.

1.6.1 Modelling assumptions.

Lee and colleagues (Lee et al., 2021) describe that CFMs simulate tDCS application and provide estimates of the magnitude, distribution, and direction of E-fields that a given protocol will deliver to the brain. This is achieved through the classification of different tissue types, based on MRI scans (Huang et al., 2013), and the assignment of conductivity values to the segmented tissue compartments (e.g., skin, scalp, CSF, grey matter, white matter). This allows for predicting the properties of endogenous current flow throughout the head (Miranda et al., 2007; Wagner et al., 2004).

Previously modelled on concentric spheres (Datta et al., 2008; Miranda et al., 2006; Rush & Driscoll, 1968) or standard model heads (Dmochowski et al., 2012), CFMs today use individual structural MRIs to inform researchers of where and how much current is likely to reach different parts of the brain, given a specific electrode montage and stimulation intensity (Dannhauer et al., 2012; Dmochowski et al., 2011, 2013; Huang, Thomas, et al.,

2018; Huang, Datta, et al., 2018; Huang et al., 2019; Lee et al., 2017; Saturnino, Puonti, et al., 2019).

CFMs have now been validated in a range of studies, including comparison with *in vivo* human and non-human primate recordings during application of tDCS (Datta et al., 2009; Huang et al., 2017, 2019a; Koessler et al., 2016; Opitz et al., 2016). While nuanced differences distinguish between different CFM approaches, they generally provide accurate, gyri-precise estimates of E-fields in the brain. CFMs are based on the quasi-uniform assumption, which states that the extent of polarisation of a target region is proportional to the strength of local E-field, without taking regional differences in functional activity, biophysics, or cellular morphology into account (Bikson et al., 2013). Therefore, CFMs are inherently agnostic to the physiological impact of exogenous fields and are taken as a reasonable first approximation of areas more- or less-exposed to applied fields, without predicting the outcomes of stimulation.

1.6.2 CFM functionality.

Lee and colleagues (Lee et al., 2021) point out that E-field estimates provided by CFMs cannot be obtained non-invasively by other means. The functionality of CFMs is two-fold: to estimate current flow induced by a given tDCS montage, or to guide tDCS montage selection given a set of criteria, such as desired magnitude or direction of E-field in a cortical region of interest. The studies presented in this thesis will utilise the former functionality: estimating E-field properties given a user-defined tDCS protocol. The Realistic vOlumetric-Approach-based Simulator For tDCS (ROAST) current flow modelling package created by Yu (Andy) Huang and colleagues (Dmochowski et al., 2013; Huang, Thomas, et al., 2018; Huang, Liu, et al., 2018; Huang, Datta, et al., 2018; Huang et al., 2019; available from: https://www.parralab.org/roast/) was used for all modelling work presented in this thesis (Chapter 3 and Chapter 4). The ROAST current flow modelling pipeline and data extraction methods used are detailed in section 1.8.1.

While CFMs provide estimates of the physical properties of applied current, they do not extend to recommending a tDCS protocol which might give rise to a desired physiological effect. Researchers are instead able to use CFMs to standardise E-field delivery to an ROI across a group of individuals, or to maximise a given property of applied current. For

example, a researcher may use CFM to ensure maximum E-field intensity is delivered to a cortical ROI, though modelling software will not provide suggestions of the optimal profile of electrical current: should one prioritise high intensity, or radial-inward direction of current flow in an ROI (Lee et al., 2021)?

1.6.2.1 CFM is used to dose-control tDCS E-field intensity.

In a recent CFM study, Evans and colleagues (Evans et al., 2020) demonstrated poor consistency in E-field intensity in an M1 cortical target when 1mA fixed dose (instead of individualised dose) tDCS application was simulated. The authors showed that applying a fixed dose to variable sizes of participant samples could contribute to variable tDCS study outcomes. In 50 participants (aged 22- 35 years), 1mA tDCS yielded a mean E-field intensity in the cortical target of 0.185V/m. In small samples (N=15), 52% of 1000 bootstrapped resamples produced an E-field intensity <0.185 V/m in the cortical target. For larger samples (N=30), 48% of 1000 resamples produced a mean <0.185 V/m in the cortical target. In the sample with the lowest mean, E-field intensity in left M1 was <0.185 V/m for 80% of subjects. In samples with the highest mean, the majority of individuals had intensities higher than 0.185 V/m. These data demonstrate that application of fixed-dose tDCS, as is the norm across tDCS literature to date, can yield vastly different E-field strength delivered to a cortical ROI across individuals. Use of CFM to standardise E-field intensity in an ROI across individuals holds promise as a method to reduce tDCS outcome variability. Assuming that the E-field intensity in the ROI is a determining factor of tDCS on neural processing, tDCS optimisation efforts have included adjustment of tDCS dose applied to the scalp to achieve low variance in E-field delivered to a cortical ROI between individuals (Caulfield et al., 2020; Evans et al., 2020). It appeals to intuition that minimising variance in E-field should also reduce variance in physiological effects of stimulation. The work presented in Chapter 3 of this thesis investigates the impact of CFM-informed tDCS on physiological outcomes in stroke and neurotypical populations.

Dose-controlled tDCS can be achieved using current flow models, simulated with a fixed dose of injected current (e.g. 1mA) to scalp electrodes. By exploiting Ohm's law, a researcher can use the predictions of CFM to adjust stimulator output for each subject such that the dose in a cortical target area is matched across all subjects. *Individualised dose* can

be calculated by working backwards from modelled *actual E-field* achieved in the cortical ROI with a *fixed dose*, using the formula:

$$Individualised\ dose = \left(\frac{Target\ E\text{-}Field}{Actual\ E\text{-}Field}\right) \times Fixed\ dose$$

In keeping with the methods used by Evans and colleagues (Evans et al., 2020), *Target E-field* represents researcher-defined target E-field intensity, *Actual E-field* is the E-field intensity estimated in an ROI in each subject when a fixed dose of tDCS is applied, and *Fixed Dose* is the injected current (in mA) delivered to scalp electrodes in the original model. For example, if a modelled 1mA *Fixed Dose* protocol is found to deliver 0.14 V/m *Actual E-Field* to a cortical target, and the *Target E-Field* is 0.185V/m, the *Individualised Dose* of tDCS required for the participant would be: (.185V/m/.14V/m) x 1mA) = 1.32mA tDCS stimulator output. Note that many tDCS stimulator devices, including the NeuroConn device used in the presented studies (DC-Stimulator Plus; NeuroConn, Ilmenau, Germany), are limited by parameter constraints of the equipment, for example dosage options increase in increments of 0.25mA. In the case described above, the *Individualised Dose* of 1.32mA would be rounded to 1.50mA to meet equipment constraints. Although this re-introduces some variance, rounded *Individualised Dose* was found to produce lower E-field variability in the cortical ROI compared to a *Fixed Dose* protocol (Evans et al., 2020).

1.6.2.2 Direction of E-field can be controlled by CFM-informed electrode placement.

In addition to controlling E-field intensity delivered to an ROI, CFMs can be used to measure and control the direction of current flow through an ROI. This is of import given the direction-dependent impact of extra-cellular fields on neuronal membrane polarisation, previously discussed in section 1.5.1.2. Directional control of current flow can be achieved by electrode placement (Bikson, Rahman, Datta, et al., 2012; Datta et al., 2008; Evans et al., 2022; Faria et al., 2009; Galletta et al., 2015; Laakso et al., 2017; Nikolin et al., 2015; Rush & Driscoll, 1968; Salvador et al., 2015; Saturnino et al., 2015) and so alteration of electrode montage is a candidate method to optimise current direction in tDCS study design.

CFM-informed alternatives to the conventional montage have emerged, which might better exploit the directional component of applied field. Rawji and colleagues (Rawji et al., 2018) for example found more consistent direction of current flow through $M1_{hand}$ when electrodes were placed either side of the ROI, compared to directly over it (as with the conventional montage). Furthermore, Evans and colleagues (Evans et al., 2022) reported that when the anode is positioned posteriorly and the cathode anteriorly to the ROI (a PA-tDCS montage, Figure 1.3), the most consistent radial-inward E-field was recorded in $M1_{hand}$, and higher E-field intensities were achieved compared to alternative montages. Notably, though the PA-tDCS montage is CFM-informed, it can be achieved in the absence of a high-quality MRI scan and CFM expertise, since the location and orientation of the motor strip can be approximated using TMS (Evans et al., 2022).

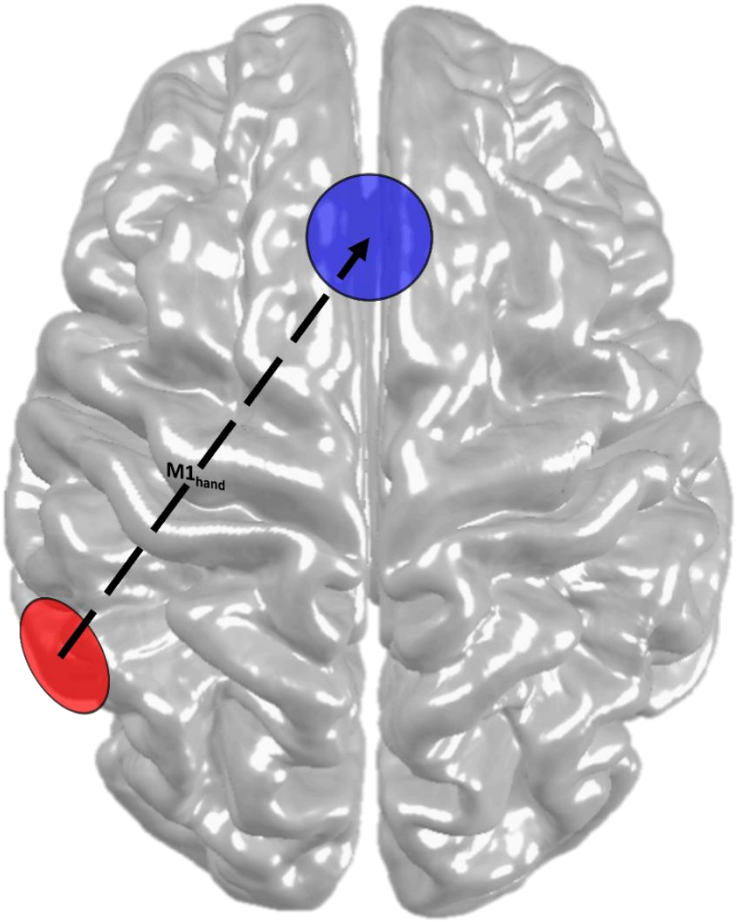

Figure 1.3. Schematic of the PA-tDCS montage. Direction of current flow (black arrow) through $M1_{hand}$ is approximated by scalp electrode placement. An anode (red) is placed posteriorly and a cathode (blue) anteriorly to $M1_{hand}$, to produce predominantly radial-inward current flow relative to the cortical surface at $M1_{hand}$.

1.6.2.3 CFMs estimate the spatial distribution of tDCS-induced current.

Finally, CFMs can be used to control E-field focality. Lee and colleagues (Lee et al., 2021) point out that the physiological implications of diffuse current are unclear, though it appeals to intuition that inter-individual differences in the spatial distribution of current may contribute to variability in the physiological outcomes of tDCS. Two approaches can be used to limit the spatial extent of E-field throughout the brain. First, one can simply reduce stimulator output intensity, resulting in exposure of fewer brain regions to current above a certain threshold. Second, the use of multi-electrode tDCS montages can constrain diffuse currents (Datta et al., 2009; Dmochowski et al., 2011; Edwards et al., 2013; Saturnino et al., 2015). An example of this approach is the so-called 4x1 montage, also referred to as high-definition (HD) tDCS, where an electrode (e.g. an anode) is placed on the scalp over a cortical region of interest and encircled by a ring of electrodes (e.g. cathodes). Such a montage constrains the spread of current radiating from the central anode to within the electrode ring (Datta et al., 2008, 2009).

However, controlling for intensity and focality of current simultaneously poses a complex optimisation problem that cannot be solved by CFM. The potential benefits of increased focality must be balanced against reduced E-field intensity, as increased shunting of current occurs between electrodes placed proximally on the scalp and leads to lower penetration of E-field to the brain (Dmochowski et al., 2011; Faria et al., 2011). Moreover, Lee and colleagues (Lee et al., 2021) note that use of HD-tDCS results in poorer control of E-field direction in a cortical ROI compared to bipolar tDCS, as current exits the body via multiple electrodes instead of flowing in a relatively uniform direction between anode and cathode. In fact, Mikkonen and colleagues (Mikkonen et al., 2020) recently reported that HD-tDCS is associated with increased E-field variability compared to a bipolar conventional montage with the same stimulator dose. Meanwhile, bipolar montages prioritise E-field direction at the cost of focality (Figure 1.4).

Current understanding suggests a computationally optimised tDCS protocol should account for the impact of E-field intensity, focality, and direction on target neuronal populations. This multi-variate issue presents a barrier to protocol optimisation: the CFM user must decide which parameters to prioritise. This may be possible when sufficient precedence

exists in the literature for the expected effects of a given tDCS protocol. However, it is often unclear which E-field characteristics should be prioritised to target a given brain region or function. Indeed, the importance of focality is yet to be confirmed, the optimal E-field intensity required to alter behaviour in humans is unknown, and variable E-field direction relative to cellular orientation is expected under and between stimulation electrodes.

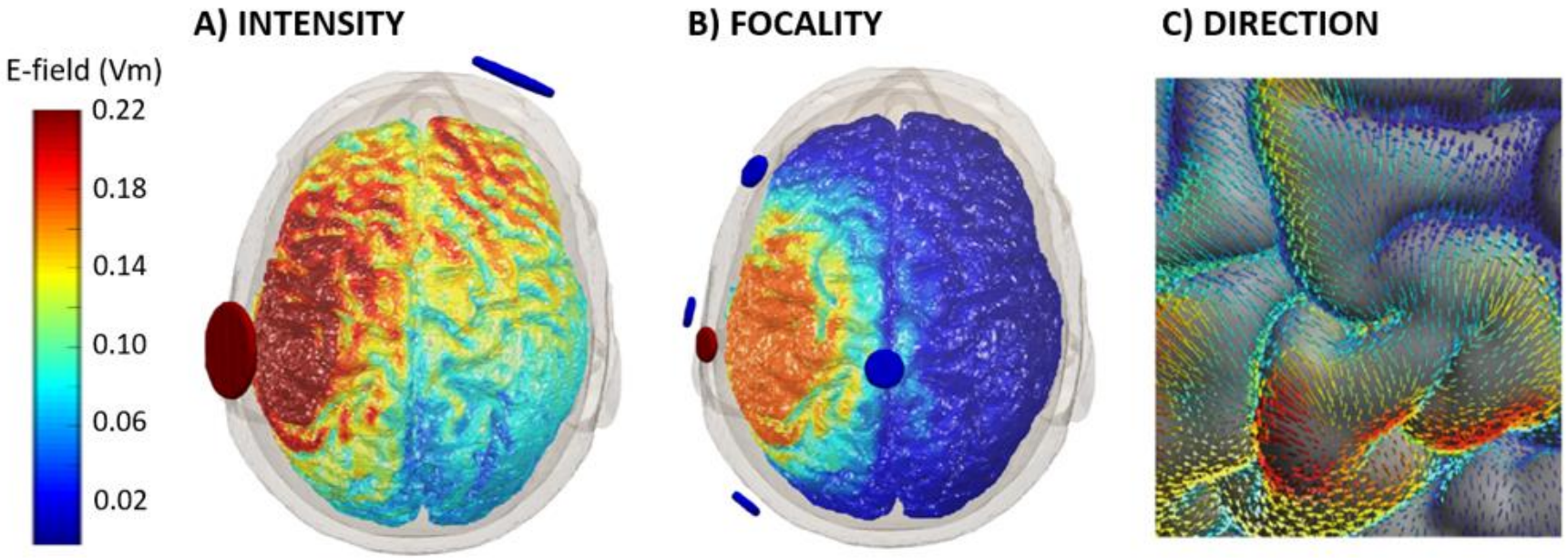

Figure 1.4. The multi-variate tDCS optimisation problem. Image is taken from Lee et al., 2021, and includes an image taken from Saturnino et al., 2019 (far right). (A) CFM estimate of tDCS-induced E-field when the conventional tDCS montage is applied at 1mA to one example subject. Higher E-field intensities are observed at the cost of spatial focality of current. (B) Estimated E-field when a HD (4 × 1) electrode montage is simulated. Increased focality is achieved at the cost of E-field intensity and direction. (C) Example of exogenous current direction around the central sulcus, which can be controlled by varying electrode montage.

1.7 Can current flow models reduce tDCS outcome variability in stroke?

CFMs have succeeded in describing the properties of tDCS-induced E-field, and researchers with access to individual structural MR scans can use them to standardise prioritised tDCS parameters across individuals. While the impact of E-field standardisation has not yet been fully described, and optimal stimulation parameters remain unknown, CFMs constitute a relative leap in progress for tDCS study design, with promise to reduce variability and standarise research to promote further progress.

However, translation of CFM-informed protocol to stroke survivors may not be straightforward, as CFMs are not designed to account for the *functional* or *anatomical state* of the pathological brain. For example, tDCS applied to a stroke survivor with altered excitatory-inhibitory balance may produce different neuromodulatory outcomes to a neurotypical participant. In Chapter 3 of this thesis, I use CFM to control E-field intensity and direction of current flow in $M1_{hand}$, and compare the physiological response to this individualised tDCS protocol in chronic stroke survivors and neurotypical individuals.

Furthermore, anatomical changes associated with stroke such as brain lesions may impact the distribution of induced current such that application of optimal protocols, should they emerge, to a stroke population may not result in comparable stimulation to a neurotypical group. To add complexity, CFMs at present do not account for pathological tissue properties; lesions are often assigned the same conductivity value as cerebrospinal fluid (CSF) for example, though histological research suggests lesion conductivity may vary substantially from CSF (McCann et al., 2019). In Chapter 4 of this thesis, I use an adapted version of ROAST (Johnstone et al., in review) to investigate the impact of stroke lesions on tDCS-induced E-field, and compare findings to tDCS simulated in neurotypical participants.

1.8 Notable techniques.

Here I outline two techniques of note, which recur in the following Chapters. The first is the processing pipeline and data extraction steps required for CFM using ROAST (Huang, Datta, et al., 2018). The second section includes the basic principles of transcranial magnetic stimulation, which was used to probe brain activity both after stroke and in response to tDCS intervention.

1.8.1 TDCS modelling and data extraction pipeline.

ROAST (Dmochowski et al., 2011, 2013; Huang, Thomas, et al., 2018; Huang, Datta, et al., 2018; Huang et al., 2019, retrieved from: https://www.parralab.org/roast/) is a fully automated, open-source tool which runs on MATLAB (*MATLAB*, 2018). ROAST requires an isotropic MR structural image, and estimates current flow by segmenting the MRI into 6 tissues (grey matter, white matter, CSF, bone, skin, air) using SPM12 (http://www.fil.ion.ucl.ac.uk/spm/), placing virtual electrodes on the scalp, generating a finite element model (FEM) mesh using *Iso2Mesh* (Fang & Boas, 2009), retrieved from http://Iso2Mesh.sourceforge.net/cgi-bin/index.cgi) and numerically solving the FEM using *getDP* (Dular et al., 1998, retrieved from: https://*getDP*.info/). All software packages called by ROAST are open-source. Simulations for a given montage complete in approximately 20 minutes (Huang, Datta, et al., 2018). The ROAST modelling pipeline used in the work presented in this thesis is depicted in Figure 1.5. I note that it does not depict all ROAST functionalities available.

Default conductivity values assigned to each tissue type in ROAST are as follows (in S/m): air: $2.5x10^{-14}$; electrode gel: 0.3; electrode: $5.9x10^{7}$; skin: 0.465; bone: 0.01; grey matter: 0.276; white matter: 0.126; CSF: 1.65. ROAST completes automatic touch-up of segmented images to remove holes using simple heuristics (for detail see Huang et al., 2013, 2018). ROAST produces structural MRI and E-field results images which are here processed in SPM12 (http://www.fil.ion.ucl.ac.uk/spm/) to obtain E-field data in researcher-defined regions of interest (ROI) using the MarsBaR toolbox (Brett et al., 2002, retrieved from: https://marsbar-toolbox.github.io/).

Data extraction is achieved by normalising ROAST results images (2x2x2mm resampled) into Montreal Neurological Institute (MNI) space, and smoothing to increase signal-to-noise ratio with a 4 mm full-width at half-maximum Gaussian kernel. Separate grey and white matter tissue masks are then created from the non-binary tissue masks produced by ROAST, with a binary inclusion threshold of >0.2 intensity. Binary masks are combined, and subsequent extraction of E-field data is limited to voxels in grey and white matter.

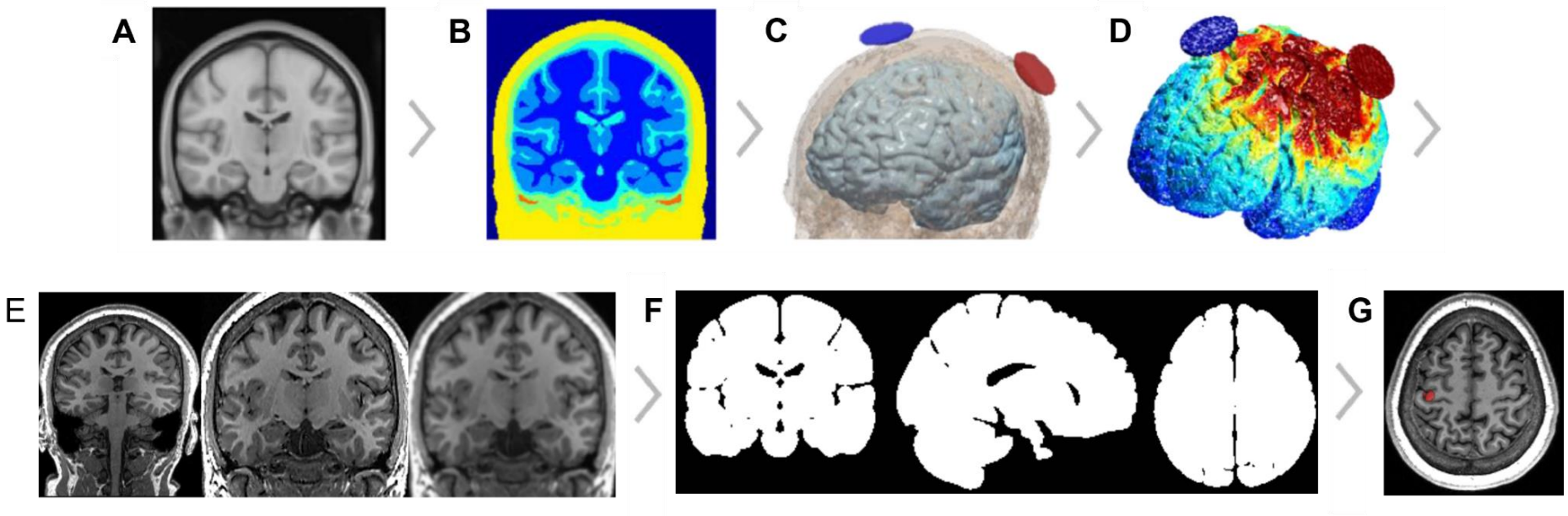

Figure 1.5. ROAST current flow modelling pipeline. Steps A-D are automated in ROAST and steps E-G are completed by the user during data extraction. A) a structural MR image of an individual participant's head, B) head tissue is segmented into 8 tissue types, calling SPM12, C) simulated tDCS electrodes are applied and using Iso2Mesh *(Fang & Boas, 2009), D) the FEM is solved using getDP (Dular et al., 1998), E) in SPM12, the MR image is normalised and smoothed, F) A binary mask of grey and white matter is created , G) ROAST results data are extracted from the* $M1_{hand}$ *region of interest using MarsBaR (Brett et al., 2002). Image is adapted from Lee et al., 2021.*

1.8.2 TMS is used to probe CSE.

In Chapter 2 and Chapter 3 of this thesis, Transcranial Magnetic Stimulation (TMS) is used to probe excitatory-inhibitory balance in stroke survivors and neurotypical participants. During TMS, electrical currents are induced in the brain via magnetic induction (Faraday, 1832). An electrical pulse is sent through copper wiring encased in a TMS coil, in this case shaped in a figure-of-eight. The short-duration (<1ms) electrical pulse produces a magnetic field of up to 2.5 Tesla perpendicular to the centre of the coil, which is placed flush with the scalp directly over $M1_{hand}$, the cortical ROI for all studies presented in this thesis. The magnetic pulse passes unimpeded through skull and scalp tissue, and induces electrical current in the brain which flows parallel to the TMS coil (Hallett, 2000). Single-pulse TMS is an established technique used to probe the human motor system, applied at intensities which evoke action potentials in affected neurons to elicit an involuntary muscle twitch in the contra-lateral hand (a motor evoked potential, MEP). Depolarisation of neurons by TMS-induced electric field can occur directly, through the axon hillock, or indirectly via depolarisation of interneurons. The amplitude of the MEP, measured with electromyography (EMG) electrodes placed on the skin over the first dorsal interosseous (FDI) muscle, is correlated to the number of neurons which responded to stimulation and is subject to change as a function of CSE. For example, a TMS pulse of a given intensity may evoke an MEP of larger amplitude if the target neuronal population is in a state of relative excitability.

Importantly, the TMS-evoked MEP does not solely represent cortical excitability, but a combination of complex cortico-spinal projections, and is influenced by several physiological components including excitability of cortical and spinal circuits (Bestmann & Krakauer, 2015). The compound nature of the MEP measure gives rise to high trial-to-trial variability (Corp et al., 2021), necessitating measurement via average scores taken from a number of pulses to reflect excitatory tone. In Chapters 2 and 3 I describe distinct measures which can be derived from single-pulse TMS, including the intensity of stimulator output required to reliably evoke an MEP of 50 microvolts (µV) in amplitude, and the recruitment curve, which reflects gain in the input-output function of a neuronal population as stimulator intensity is increased.

1.8.3 Linear Mixed Models

Linear mixed models (LMM) were used throughout this thesis to analyse repeated measures data collected from the same participants at different timepoints, or under different conditions. They include fixed and random effects; fixed effects reflect the relationship between predictor variables and the dependent variable, while random effects account for individual differences between participants or other factors known to contribute to variability. In this way, LMMs are able to model variability both within and between subjects, compared to repeated measures analysis of variance (rm-ANOVA) which only accounts for variability within-subjects. LMMs were selected for use in this thesis because they provide greater flexibility, model fit, and statistical power compared to rm-ANOVAs, though interpretation of the results produced by LMMs in slightly more complex.

The flexibility of LMMs was also particularly important in cases where study design was unbalanced or data was missing. In Chapter 2, for example, data were available at 3 timepoints for the neurotypical group and 4 timepoints for the stroke survivor group. Here, LMMs allowed inclusion of participants with missing data in the analysis, increasing statistical power and generalisability of findings compared to the rm-ANOVA.

LMMs also allow the researcher to account for individual variability via inclusion of random effects. For example, inclusion of a random intercept per participant (notation: + 1|PT) accounts for inter-individual variability in MEP amplitude (Pitcher et al., 2003) which may confound variables of interest. By comparison, the rm-ANOVA assumes the same mean and variance for all participants, reducing accuracy of results. Furthermore, LMMs are able to account for clustering of data which rm-ANOVA is not equipped to deal with, for example by accounting for systematic variations in image quality between MR images collected at different data collection sites (notation: 1|site), which may have impacted the quality of tissue segmentations required for current flow modelling in Chapter 4.

Model comparison was carried out using two alternative methods in this thesis. Candidate models described in Chapter 2 were compared using the Likelihood ratio test (LRT), which compares the likelihood of increasingly complex models to simpler nested models with fewer fixed or random effects. In this case, models with and without a variable describing lesion size were compared. The LRT compares the -2 log likelihood of two candidate models,

where the test statistics follow a chi-squared distribution with degrees of freedom equal to the difference in the number of parameters between the models. The chi-squared test was then used to determine if the difference in log-likelihoods between models was significant ($p<.05$).

Later in Chapter 4, the goodness of fit of seventeen viable models of increasing complexity, which included a variety of candidate fixed effects to describe the location, position and size of a stroke lesion, were compared. First, the variance inflation factor (VIF) was calculated to identify colinear predictors. The VIF is a measure of the degree of multicollinearity present between predictors in a model. Multicollinearity causes difficulty in determining the separate effects of each predictor on the outcome variable, as the variance for the estimated coefficient for a given predictor can be inflated. The VIF was calculated using the *vif* function in R's *car* package (Fox & Weisberg, 2019), which divides the variance of the coefficient in the full model by the variance of the coefficient in a model with only that predictor variable (equation: $VIF = 1 / (1 - R^2)$, where R^2 is the coefficient of determination obtained from a regression of the predictor of interest on all the other predictors in the model. Models including predictors with a VIF value of 5 or higher were excluded from model comparison, as this is considered to indicate significant multicollinearity between predictors.

Further research into the optimal method for LMM comparison suggested that Akaike's information criterion (AIC; Akaike, 1974) and the Bayesian information criterion (BIC; Schwarz, 1978) were appropriate instead of the LRT method described above when comparing both nested and un-nested LMMs (Speekenbrink, 2022), since the LRT evaluates model fit without providing a measure of the relative complexity of un-nested models. AIC and BIC were therefore used for model comparison in Chapter 4 instead of the LRT method.

Briefly, the AIC and BIC are both statistical methods used to compare models with the same outcome variable. the AIC provides a relative measure of model fit given a set of data and the number of parameters used to describe the relationship between predictors and outcome variables. The AIC balances model fit with model complexity by adjusting the maximised likelihood function of the model for the number of parameters used (equation:

AIC = -2log(L) + 2k, where L is the maximised likelihood function of the model, and k is the number of parameters).

Meanwhile, the BIC differs from the AIC because it places a stronger penalty on the number of parameters in the model. It is also calculated by adjusting the maximised likelihood function for the model, though it differs from the AIC as it solves for the bayes solution, and accounts for the size of the sample in the calculation (equation: BIC = -2log(L) + klog(n), where L is the maximised likelihood function of the model, k is the number of parameters in the model, and n is the sample size).

AIC and BIC take both accuracy and complexity into account when assessing the quality of model fit for a given dataset. BIC penalises models with multiple predictors more heavily than the AIC; the AIC tends to select more complex models while the BIC can sacrifice model fit for parsimony. AIC is based on information theory and better-suited to smaller sample sizes, while the BIC is based on Bayesian statistics and is considered more appropriate for larger sample sizes (Burnham & Anderson, 2004).

AIC and BIC were both calculated and compared for each candidate model in Chapter 4, with smaller values indicating better model fit. Where AIC and BIC results conflicted, model fit was further interrogated by calculating marginal R^2 ($R^2_{LMM(m)}$) and conditional R^2 for each model, which describe the proportion of variance explained by the fixed factor(s) in the model, or the variance explained by both fixed and random factors respectively (Nakagawa & Schielzeth, 2013). This process was favoured compared to the LRT method used in Chapter 2 since multiple measures of model fit and comparison allowed for more transparent model selection.

1.9 Thesis overview

High-dose physical training is a gold standard for rehabilitation in both sub-acute and chronic stroke (Lohse et al., 2014; Ward, 2017; Ward et al., 2019) however stroke survivors with severe upper limb deficits are less able to access, and show less reliable outcomes from, interventions which require a baseline ability to complete repetitive movements (Byblow et al., 2015; Wuwei et al., 2015; Buch et al., 2016; Guggisberg et al., 2017). Neuromodulation is a candidate method to improve outcomes, to non-invasively “boost”

brain activity to get the most out of training sessions where dose or accessibility are sub-optimal. The over-arching aim of this thesis is to identify and develop methods to minimise variability in tDCS outcomes in the context of stroke.

1.9.1 Study 1: A longitudinal comparison of cortical excitatory-inhibitory balance in stroke and neurotypical populations.

Chapter 2 of this thesis investigates the trajectory of changes to excitatory-inhibitory balance over 12 months post-stroke, and compares longitudinal data collected from stroke survivors and neurotypical volunteers. The primary aim of this study was to determine whether there are distinct windows of time in which neuromodulatory interventions may be best applied in stroke survivors. I hypothesised that a heightened neuroplastic potential would occur in the sub-acute phase (1 week- 6 months) of human stroke, before returning to neurotypical levels in the chronic phase (>6 months), indicating a time window in which response to intervention may be maximal in human stroke survivors. In addition, I hypothesised that longitudinal changes in excitatory-inhibitory balance would positively correlate with functional gains, in keeping with the framework outlined in The Stroke Roundtable Consortium (Bernhardt et al., 2017).

1.9.2 Study 2: Encouraging an excitable brain state after stroke with intensity- and direction-controlled tDCS.

In Chapter 3, I present data from neurotypical participants and chronic stroke survivors who underwent CFM-informed tDCS, individualised to ensure a standard E-field intensity and current direction was achieved in $M1_{hand}$. Single-pulse TMS was used to probe cortical excitability before, during, and after tDCS application. The primary aim of this study was to compare responses to plasticity-promoting tDCS between groups, to ascertain whether an optimised tDCS protocol might translate between neurotypical and stroke populations. I hypothesised first that TMS-assessed CSE at baseline would be subject to higher variability in stroke survivors, in light of reported chronic network dysfunction and variable integrity of efferent pathways. Second, I hypothesised that response to tDCS would differ between groups, possibly due to stroke-related differences in the *functional* and *anatomical state* of the brain.

1.9.3 Study 3: The impact of stroke lesions on tDCS-induced electric field.

Finally, in Chapter 4 I investigate the impact of real (as opposed to synthetic) stroke lesions on simulated tDCS-induced electric field in a large sample of stroke survivors and neurotypical participants, using MR data provided by the ENIGMA Stroke Recovery Working Group (Liew et al., 2020; Liew et al., 2018, 2022; https://enigma.ini.usc.edu/ongoing/enigma-stroke-recovery/). The primary aim was to compare current delivery to M1 in neurotypical participants and stroke survivors when a fixed conventional tDCS protocol was simulated. I hypothesised that tDCS-induced E-field intensity in $M1_{hand}$ would be more variable in stroke survivors. Second, I hypothesised that E-field intensity in $M1_{hand}$ would correlate to lesion size, location, and distance to the ROI, in keeping with work previously conducted by our group to investigate the impact of synthetic lesions on tDCS-induced fields (Johnstone et al., in review).

1.9.4 Appendix : Does deviation of TMS coil from hotspot predict MEP amplitude?

This chapter is presented in appendix A. Data were collected while ethical approval was obtained for the empirical work described in Chapter 3. The primary aim of this study was to assess variance in MEP amplitude which might be attributed to TMS coil position error. MEPs are a hallmark measure of corticospinal excitability used to assess neurophysiological outcome in M1-targeted tDCS studies (Bastani & Jaberzadeh, 2012; Horvath et al., 2015). However, the peak-to-peak amplitude of MEPs are subject to high trial-to-trial variability because the measure results from a combination of cortical and spinal projections of varied origin (Bestmann & Krakauer, 2015; Burke et al., 1995; Kukke et al., 2014). Since the focus of this thesis was minimisation of tDCS outcome variability, assessment of variance explained by the outcome measure, MEPs themselves, was of interest. However, as the work progressed the focus shifted to optimising tDCS after stroke, by characterising variability which may be associated with stroke-induced *anatomical* and *functional brain state* during tDCS application. While characterisation of variability associated with TMS remains highly relevant, it does not meet the core aim of this thesis: to optimise tDCS application in the context of stroke. The study is therefore included in appendices.

This study found that small movements of the TMS coil away from the hotspot position significantly predicted some of the variance in MEP amplitude, though the percentage of

variance explained, measured by conditional and marginal R^2, was low. Though a significant impact of TMS coil position on MEP amplitude was detected, a large proportion of the the high trial-to-trial variability of MEPs was not explained by deviation of coil position when experienced coil operators applied TMS.

1.10 Impact of the Coronavirus pandemic

Data collection was impacted by the coronavirus pandemic. The study described in Chapter 3 of this thesis, which required close contact with participants to apply non-invasive brain stimulation techniques, was paused on 23rd March 2020 and re-commenced in October 2020. However, a second national lockdown began on the 5th November 2020. In response to the uncertainty associated with lockdowns, I explored computational avenues of research (Chapter 4), and collaborated with Dr. Brenton Hordacre, who generously provided the data presented in Chapter 2.

Recruitment of patients from hospital wards during the acute and early-subacute phases of stroke was particularly affected by the pandemic, as hospital operational changes included restricted access and limited contact with patients. Potential participants at all stages after stroke, and neurotypical volunteers, expressed concern over attending study sessions on hospital premises citing risk of exposure to COVID-19; inclination to take part in research decreased.

Brain Research UK (BRUK, 2017), who funded this project, responded generously to pandemic limitations by extending project funding by one year. Mitigation measures included remote recruitment (via telephone or email) of chronic stroke patients and neurotypical participants during lockdowns. The remote process was limited to carrying out screening and providing study information. Eligible participants could then be invited to participate once restrictions were lifted. This process was greatly aided by a dedicated study recruiter in the research team, Ms. Kirsten Thomas. Project management and data collection responsibilities were shared between myself and Dr. Carys Evans. Empirical findings are presented in Chapter 3 of this thesis.

CHAPTER 2. A LONGITUDINAL COMPARISON OF CORTICAL EXCITABILITY IN STROKE AND NEUROTYPICAL POPULATIONS

2.1 Data sharing

The data presented in this Chapter were collected by Dr. Brenton Hordacre and colleagues at the Neuromotor Plasticity and Development TMS laboratory at the University of Adelaide in Australia, between September 2014 and April 2017. Ethical approval was given by the Central Adelaide Local Health Network Human Research Ethics Committee. A partial dataset has already been published (Hordacre, Austin, et al., 2021). Here, I present unpublished data generously shared by Dr. Hordacre to mitigate the impact of the coronavirus pandemic, which limited my own access to data collection facilities.

2.2 Introduction

Preclinical work suggests that spontaneous biological recovery observed in sub-acute stroke may be accompanied by a sensitive period in which the effects of intervention are maximised (Biernaskie, 2004; Zeiler et al., 2016). Both events are thought to be underpinned by a brain environment of increased excitability and reduced inhibition in tissue adjacent to and functionally connected with the infarct core (Bernhardt et al., 2017; Caracciolo et al., 2018; Carmichael, 2006; Cheng et al., 2014; Clarkson et al., 2010, 2011, 2015; Cramer, 2008; Di Pino, Pellegrino, Assenza, et al., 2014; Gouty-Colomer et al., 2016; Han et al., 2007; Hiu et al., 2016; Joy & Carmichael, 2020; Kim et al., 2014; Krakauer & Carmichael, 2017b; Kwakkel et al., 2003; Lake et al., 2015; Nishimura et al., 2007; Orfila et al., 2019; Overman et al., 2012; Schiene et al., 1996; Zhou et al., 2009). In this Chapter, cortico-spinal excitability (CSE) and intra-cortical inhibition (ICI) are probed in the 12 months following stroke, using single- and paired-pulse TMS protocols respectively. The effects of a neuromodulatory TMS intervention, continuous theta burst stimulation (cTBS) are also investigated, to determine whether response to a plasticity-altering intervention differed between post-stroke phases. The core aim of this work was to determine whether there are distinct windows of time in which neuromodulatory interventions, such as tDCS, might be best applied after human stroke.

As discussed in the introduction (section 1.5), the effects of tDCS likely depend on the *functional state* of the brain before stimulation is applied (Esmaeilpour et al., 2018; Polanía et al., 2010; Reato et al., 2010, 2013; Schmidt et al., 2014; Terzuolo & Bullock, 1956). Briefly, sub-threshold membrane polarisation by tDCS-induced E-field is thought to give rise to detectable neurophysiological change because non-quiescent cells in an active network are pushed further towards, or away from, the action potential (AP) threshold (Reato et al., 2013; Terzuolo & Bullock, 1956). Furthermore, altered activity of structures within a given network may have an indirect influence on activity elsewhere (Polanía et al., 2010; Reato et al., 2010; Schmidt et al., 2014). In the context of stroke, where preclinical work suggests that GABAergic inhibition (Blicher et al., 2015; Clarkson et al., 2010; Hiu et al., 2016; Kim et al., 2014; Lake et al., 2015; Orfila et al., 2019) and neuronal excitability (Caracciolo et al., 2018; Carmichael, 2006; Cheng et al., 2014; Clarkson et al., 2011, 2015; Gouty-Colomer et al., 2016; Han et al., 2007; Kwakkel et al., 2003; Nishimura et al., 2007; Overman et al., 2012) may differ in 'phases' defined by time since stroke onset (Bernhardt et al., 2017; Biernaskie, 2004; Cramer, 2008; Dobkin & Carmichael, 2016; Zeiler et al., 2016), it is hypothesised that the effects of tDCS may differ depending on the post-stroke phase in which stimulation is applied.

In the following I describe TMS-assessed changes in excitatory-inhibitory balance and capacity for neuromodulation over 1 year post-stroke, and compare findings with data collected from a group of neurotypical participants. Longitudinal changes in symptom severity are represented by the Action Research Arm Test (ARAT) and Functional Independence Measure (FIM), and global impairment on admission to hospital is quantified using the National Institute of Health Stroke Scale (NIHSS). These clinical scores are correlated with TMS-assessed excitatory-inhibitory balance, to ascertain whether a window of spontaneous recovery might align with a window in which the *functional state* of the brain is primed to maximise efficiency of rehabilitative interventions.

2.2.1 Continuous theta burst stimulation probes LTD-like plasticity.

CTBS is a repetitive transcranial magnetic stimulation (rTMS) technique used to probe long-term depression (LTD)-like plasticity in humans (see Corp et al., 2020; Suppa et al., 2016 for comprehensive reviews). Theta-burst stimulation (TBS) was originally conceived as a neuromodulatory technique because burst discharges within the theta range (3-8 Hz) were

recorded from the rat hippocampus during exploratory behaviour (Diamond et al., 1988). Subsequently, Theta burst stimulation was used to induce plasticity in animal brain slice studies (Capocchi et al., 1992; Larson & Lynch, 1986, 1989). In humans, stimulation parameters have been adjusted to meet the capabilities of rTMS equipment, for example in the presented study, each cTBS train consisted of 600 pulses delivered in triplets at 50Hz, repeated at 5Hz for 40 seconds. In comparison animal work often includes pulses delivered at 100Hz repeated at 5Hz (Suppa et al., 2016). While short intermittent bouts of stimulation are associated with enhancement of LTP-like plasticity (intermittent theta-burst stimulation, iTBS), continuous stimulation has been found to support LTD (Heusler et al., 2000; Larson et al., 1986; Takita et al., 1999).

The proposed mechanism of action for cTBS is repetitive activation of synaptic connections in targeted tissue; early synaptic plasticity processes are modulated via activation of NMDA receptors (Lenz et al., 2015). This is supported by evidence that inhibitory cTBS effects are blocked by NMDAR antagonists (Huang et al., 2007; Wankerl et al., 2010), and voltage-gated calcium channel blocker drugs have been shown to modulate cTBS effects in a dose-dependent manner (Wankerl et al., 2010).

In the presented study, an inhibitory cTBS protocol was selected not for its promise as a potential treatment, but to probe capacity for synaptic plasticity (Hordacre et al., 2021). An inhibitory protocol was preferred because data collection began 1 week after stroke when excitotoxic processes may still have been active; Hordacre and colleagues avoided use of excitatory neuromodulation protocols to account for elevated seizure risk in acute stroke (Hordacre, Austin, et al., 2021). The magnitude of response to cTBS is here taken to reflect neuroplastic potential at different timepoints after stroke onset. The impact of cTBS is quantified as change in single-pulse TMS-MEP amplitude recorded before and after cTBS intervention. A greater reduction in MEP amplitude after cTBS intervention would be associated with heightened responsiveness to neuromodulation.

2.2.2 TMS resting motor threshold probes CSE.

Two TMS measures of *functional brain state*, resting motor threshold (RMT) and short-interval intra-cortical inhibition (SICI) were assessed longitudinally in stroke and neurotypical groups. According to the International Federation of Clinical Neurophysiology

(IFCN), resting motor threshold (RMT) is defined as the intensity of TMS stimulator output (in per cent) required to elicit MEPs of a given amplitude in a relaxed target muscle in 5 of 10 trials (Rossini et al., 1994, 2015). Protocol used in the following studies was based on recently updated IFCN guidelines (Groppa et al., 2012).

Recent work has shown that higher RMT, indicative of reduced CSE, in stroke survivors relative to a neurotypical population is associated with greater motor impairment of the hand (Veldema et al., 2021). In neurotypical populations, RMT variability is moderate within studies (ICC = 0.50) though relatively consistent between studies (CV = 19.67) (Corp et al., 2021). RMT is reportedly stable in the absence of cortical activity changes, and so changes in RMT over time are thought to reflect substantial changes in brain state (Danner et al., 2008; Engelhardt et al., 2019, 2019; Kimiskidis et al., 2005; ter Braack et al., 2019).

Previous work tracking RMT after stroke includes a longitudinal study of patients with lesions involving the cortico-spinal tract (CST) (Swayne et al., 2008). Swayne and colleagues recorded reduced CSE (higher RMT) in the affected hemisphere compared to the unaffected hemisphere and a neurotypical group. This effect was strongest in acute stroke, declining to neurotypical levels over 6 months. RMT was also found to correlate with Action Research Arm Test (ARAT) scores, a clinical measure of upper limb performance, with the strongest association found in acute stroke and correlations growing weaker over 6 months (Swayne et al., 2008). Correlation between decreasing ipsilesional RMT and improved hand movement has also been reported in recent work (McDonnell & Stinear, 2017; Rosso & Lamy, 2018; Stinear et al., 2015). For example, Stinear and colleagues (Stinear et al., 2015) demonstrated changes in RMT as a function of both time post-stroke and severity of symptoms, whereby the highest RMTs are expected in early, severe stroke, and the lowest in mild, chronic stroke. These findings are in keeping with the hypothesis of a coupled trajectory of CSE and motor recovery after stroke (Bernhardt et al., 2017).

2.2.3 Paired-pulse TMS probes GABA-mediated intra-cortical inhibition.

Lastly, paired-pulse TMS data are presented to interrogate changes to intra-cortical inhibition following stroke, in keeping with preclinical work suggesting alleviation of GABAergic inhibition promotes stroke recovery particularly in the sub-acute phase (Clarkson et al., 2010; Lake et al., 2015; Orfila et al., 2019).

Paired-pulse TMS paradigms can be used to measure specific neurochemical systems via a sub-threshold conditioning pulse, which stimulates interneurons, and a supra-threshold test pulse which generates an action potential in pyramidal neurons with a higher threshold for activation (Kujirai et al., 1993; Ziemann, Rothwell, et al., 1996). The influence of inter-neuronal activity on pyramidal cell output is time-dependent, as the time course of signalling with distinct post-synaptic receptors differs (Di Lazzaro et al., 1998, 2006; Kujirai et al., 1993). Short interval intra-cortical inhibition (SICI) is a TMS paradigm used here to measure GABA-mediated intra-cortical inhibition.

Sub- and supra-threshold TMS pulses applied with a short inter-stimulus interval (1-5ms) are associated with reduced MEP amplitude. SICI is thought to be mediated by $GABA_A$ receptor activation (Di Lazzaro et al., 2007; Ziemann, Lönnecker, et al., 1996), and so greater MEP suppression by a SICI TMS protocol is interpreted as greater GABAergic inhibition in the stimulated brain area. The size of test MEPs compared to those elicited with single-pulse TMS at the same stimulator output (here, 120% RMT) is proportional to the activity of the targeted neurotransmitter system (Di Lazzaro et al., 1998; Kujirai et al., 1993).

In stroke, functional recovery has been shown to correlate with reduced tonic GABA (Blicher et al., 2015; Kim et al., 2014; Krakauer & Carmichael, 2017b), and reversing tonic GABA pharmacologically has been linked with improved motor function in mice (Clarkson et al., 2010; Di Lazzaro et al., 1998; Orfila et al., 2019)**.** Beyond the stroke literature, motor learning is associated with reduced GABA in the motor cortex (Kolasinski et al., 2019; Sampaio-Baptista et al., 2015; Stagg et al., 2011). Therefore, tracking GABAergic inhibition after stroke is a target for research as it may provide insight into the mechanisms underlying motor recovery during each post-stroke phase. For example, sub-acute reduction in SICI after stroke may be a mechanism supporting cellular reorganisation and recovery (Murphy & Corbett, 2009).

2.2.4 TMS measures of CSE may be impacted by brain anatomy.

In addition to TMS measuring CSE, it is also noted that lesions may confound findings due to stroke-induced damage to efferent motor pathways such as the cortico-spinal tract (CST). It is difficult to disentangle the contribution of cortico-spinal tissue damage and excitability of cortical regions where motor signals are generated when interpreting RMT measures in

particular (Potter-Baker et al., 2016, 2018). Lesion size data were collected for the majority of stroke survivors involved in this study, and are included in statistical analyses to determine whether lesion characteristics impact TMS measures of excitatory-inhibitory balance after stroke.

2.2.5 Hypotheses.

Previous findings on RMT- and SICI-probed excitability changes following stroke are neatly demonstrated in the meta-analysis by McDonnell and Stinear (McDonnell & Stinear, 2017), which showed higher RMT in both early and chronic stroke compared to neurotypical participants, and lower SICI in early stroke only, compared to neurotypical participants. Here, lesion size data are added to analyses to determine whether the *anatomical state* of the brain after stroke might impact TMS-assessed *functional state*. First, it is hypothesised that longitudinal changes in excitatory-inhibitory balance will positively correlate with functional gains, in keeping with the framework outlined in The Stroke Roundtable Consortium (Bernhardt et al., 2017). In addition, heightened excitability is expected to occur in the sub-acute phase (1 week- 6 months) of human stroke, before returning to neurotypical levels in the chronic phase (>6 months). This may indicate a time window in which response to intervention could be maximal in human stroke survivors. Finally, lesion size is taken to represent one aspect of *anatomical brain state,* and is here expected to interact with TMS-assessments of *functional brain state.*

2.3 Methods.

2.3.1 Participants.

Thirty-one stroke survivors (mean age = 66.58 ± 17.75, 11 females) and 28 neurotypical participants (age = 64.90 ± 11.46, 8 females) took part. Stroke survivors attended 8 experimental sessions, at 1, 2, and 3 weeks, and 1, 2, 3, 6, and 12 months post-stroke. Neurotypical participant data were collected at three time points separated by 6-month intervals (i.e., 0, 6, and 12-month time points).

Four post-stroke time points of interest were selected for analysis. Timepoint 1 (T1) describes data collected in the first of 3 sessions attended by neurotypical participants, and at 3 weeks post-stroke. Data collected 3 weeks after stroke was inspected because it is

within the hypothesised window of sub-acute hyperexcitability in humans (1 week – 6 months) and also falls within the subacute period defined in animal models, which follows a shorter timeline (up to approximately 1 month; Biernaskie, 2004; Zeiler et al., 2016).

Timepoint 2 (T2) describes data collected 3 months post-stroke, in the stroke survivor group only (data were not collected from neurotypical participants at T2). A second timepoint in the human sub-acute window was selected to ensure representation of functional brain state in both the early and late sub-acute phases of human stroke (1 week – 3 months, and 3 months – 6 months respectively; Bernhardt et al., 2017). Timepoint 3 (T3) represents the second session attended by neurotypical participants, after a 6-month interval. In the stroke survivor group, T3 describes data collected 6 months after stroke, at the beginning of the chronic phase (≥6 months; Bernhardt et al., 2017). Finally, Timepoint 4 (T4) represents data collected during chronic stroke, 12 months after infarction, and the final session attended by neurotypical participants after a 6-month interval (Figure 2.1). At each timepoint, 3 TMS assessments of corticospinal excitability were collected, namely TMS-assessed response cTBS, SICI, and RMT, herein referred to as *TMS measures of interest*.

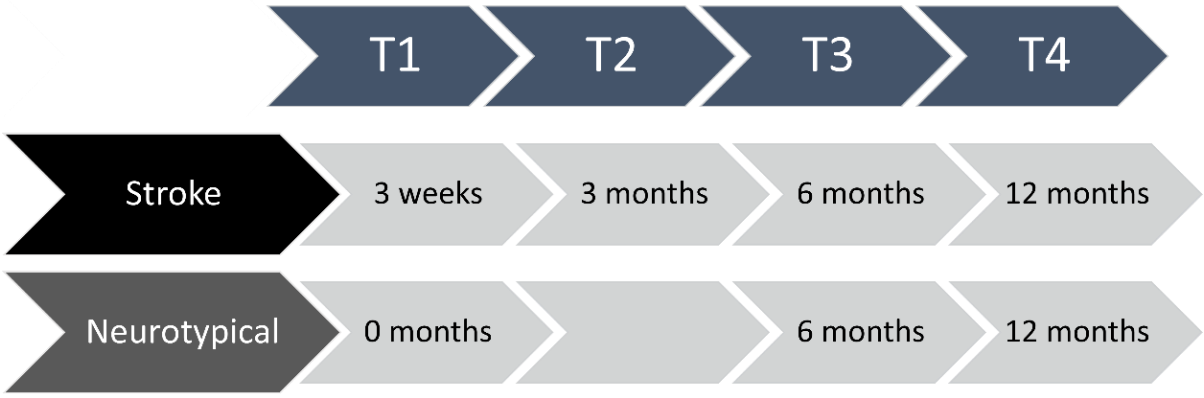

Figure 2.1. Longitudinal study design. Data from 4 time points were included in analyses. Data in Timepoint 1 (T1) were collected 3 weeks post-stroke (early sub-acute phase), and in the first session attended by neurotypical participants. Data were not collected from neurotypical participants at timepoint 2 (T2). Stroke survivor data at T2 were collected 3 months post-stroke (late sub-acute phase). Data in Timepoint 3 (T3) were collected 6 months post-stroke (chronic phase), and six months after the first session attended by neurotypical volunteers. Timepoint 4 (T4) data were collected 12 months post-stroke (chronic phase) and 12 months after the first session attended by neurotypical participants.

2.3.2 Inclusion criteria.

An experienced neuroradiologist confirmed stroke diagnosis using either computed tomography (CT) or MRI scans. Participants were recruited if they were >18 years old, had experienced first-ever ischemic stroke with upper limb motor impairment, were medically stable, and had a recordable MEP amplitude of at least 50 microvolts (μV). Exclusion criteria were history of other neurological disease, craniotomy or other neurosurgery, inability to give informed consent, taking medication known to modify seizure threshold or other contraindications to TMS such as metallic implants in the skull, implanted pacemaker or a history of seizures.

2.3.3 Clinical scores.

The National Institute of Health Stroke Scale (NIHSS) was used to quantify stroke severity on admission, and the Action Research Arm Test (ARAT) and Functional Independence Measure (FIM) were recorded at each timepoint in the longitudinal dataset. The NIHSS is a measure of stroke-related neurological deficit consisting of 15 items that evaluate consciousness, language, visual-field loss, neglect, extra-ocular movement, motor strength, dysarthria, ataxia, and sensory loss. Each item is rated out of 4, where a score of 0 reflects normal function and higher scores indicate greater impairment. Scores for each element are added

to give a final NIHSS score out of 42. Symptoms are categorised as mild for scores less than 5, moderate between 5 and 14, severe between 15 and 24, and scores above 25 reflected very severe symptoms.

The action research arm test (ARAT) was administered at each timepoint of data collection. The ARAT is a measure of upper limb function consisting of 19 items divided into 4 subscales: grasp, grip, pinch, and gross movement. Each item is scored from 0 to 3, where higher scores represent arm activity closer to normal performance. Sub-score measures were not available in this dataset, and so scores are presented out of a maximum possible 57.

The functional independence measure (FIM) was also administered during each session in this longitudinal dataset. The FIM is a measure of functional status, based on the level of assistance required to complete a task. The assessment consists of 18 items divided into 2 subscales: motor and cognitive function. Here, sub-scores were not available so motor and cognitive data are combined. The total score is presented as a value between 18-126 (standard practice involves scoring no lower than 1 for each item). A score of 1 is given when an observed task requires total assistance or is it not testable due to risk. Maximum motor score is 92, and the cognitive subscale is scored out of 35.

2.3.4 Transcranial magnetic stimulation.

Single- and paired-pulse TMS were applied to either the ipsilesional (stroke group) or dominant (neurotypical group) motor cortex using a 70 mm internal diameter Alpha coil (The Magstim Co. Ltd), which was held at approximately 45° relative to the sagittal plane of each participant's head. Coil position was marked on the scalp using a waterproof marker pen.

Skin overlaying the first dorsal interosseous (FDI) muscle of the target hand was prepared with alcohol and NuPrep abrasive gel, and a ground strap was placed on the wrist. Surface electromyographic (EMG) recordings were taken from the FDI muscle of the hand using Ag–AgCl electrodes (Ambu, Ballerup, Denmark) in a belly tendon montage. The raw signals were sampled at 5 kHz (CED 1401, Cambridge Electronic Design), amplified 1000× (CED 1902,

Cambridge Electronic Design, or Digitimer D360), and bandpass filtered (20-1000 Hz), then stored for analysis offline (Signal Software, Cambridge Electronic Design).

Raw data from each MEP trial were processed using a custom MATLAB script, in which a 100ms window was inspected for muscle contraction preceding TMS pulse onset. Root mean square (RMS) of muscle activity up to 100ms preceding the TMS pulse was calculated for all trials in a given block, then averaged. Single trials were excluded if RMS muscle activity up to 100ms preceding the TMS pulse exceeded average RMS muscle activity plus 2 standard deviations for the whole block. Trials were also discarded if the MEP was indistinguishable from background noise (MEP amplitude ≤ RMS pre-contraction per trial), or if the TMS pulse failed to fire (TMS artifact amplitude ≤ RMS pre-contraction per trial, and MEP amplitude ≤ RMS pre-contraction per trial). In R Studio, *ggstatsplot* (Patil, 2021) was used to identify and exclude outliers in stroke and neurotypical data separately. Peak-to-peak MEP amplitude was averaged per block for single-pulse measures (pre- and post-cTBS), or per condition in paired-pulse TMS blocks (SICI).

2.3.4.1 RMT.

Single-pulse TMS was delivered at 0.2 Hz ± 10% frequency. Optimal coil position was identified and marked on the scalp with a water-soluble marker pen, and RMT was identified as the minimum TMS stimulus intensity required to evoke a peak-to-peak MEP amplitude of 50 µV in 5 of 10 trials in the relaxed FDI muscle of the contralateral hand.

2.3.4.2 SICI.

Paired-pulse TMS blocks were delivered using two Magstim 2002 stimulators, which were connected to a single coil through a BISTIM module (The Magstim Co. Ltd). Unconditioned MEP amplitude elicited by 120% RMT test pulses was compared to conditioned MEP amplitude, where test pulses (120% RMT) were preceded by a conditioning pulse, delivered at 70% RMT. The inter-stimulus interval (ISI) between conditioning and test pulses was either 2ms or 3ms. Each block of SICI comprised 50 pulses, 17 unconditioned trials (120% RMT), 16 2ms ISI conditioned trials and 17 3ms ISI conditioned trials (70% RMT). SICI ratio was calculated using the equation: (conditioned MEP amplitude / unconditioned MEP amplitude) × 100, where a value < 100% represented MEP suppression; smaller values reflect greater intra-cortical inhibition.

2.3.4.3 CTBS.

A Magstim Rapid stimulator was used to deliver cTBS with a biphasic pulse waveform to the target motor cortex at 70% RMT. Two trains of cTBS were delivered, separated by a 10-minute break in which participants were asked to keep muscles relaxed. Each cTBS train consisted of 600 pulses delivered in triplets at 50Hz, repeated at 5Hz for 40 seconds. Single pulse MEPs at 120% RMT were recorded before and after cTBS intervention, delivered at a frequency of 0.2 Hz ± 10%. Prior to cTBS, 2 blocks of 20 single-pulse MEPs separated by a 2-minute interval were recorded to assess baseline CSE. MEP blocks were also recorded 5, 15, 30, and 45 minutes post-cTBS intervention. Blocks at 5 and 15 minutes only were included in analyses, in keeping with the findings of a recent meta-analysis showing cTBS effects outlast stimulation for up to 10 minutes (Corp et al., 2020). CTBS response was quantified as conditioned MEP amplitude (i.e. recorded after cTBS) normalised to baseline MEP amplitude (pre-cTBS): (conditioned MEP amplitude/baseline MEP amplitude) x 100. A value of 100% represents no change following cTBS and values <100% reflect suppressed MEP amplitude.

2.4 Statistical analyses.

2.4.1 Linear mixed effects models.

Analyses are presented in sub-sections for 3 *TMS measures of interest*: cTBS response, SICI, and RMT. Linear mixed effects models (LMMs) were used to account for the non-independence of observations in this repeated measures study design. LMMs achieve this by positively correlating observations within each subject, down-weighting repeated measures adjusting statistical power downwards for detection trends over time. Consequently, timepoint-by-group interactions will be appropriately conservative with a significance level of $p < 0.05$.

LMMs were also selected for their capacity to cope with unbalanced time points (Cnaan et al., 1997), allowing inclusion of four time points in the stroke survivor group and three time points in the neurotypical group. In order to account for unbalanced designs, LMMs calculate approximate F-statistics and degrees of freedom for fixed effects. Estimation and testing are based on restricted maximum likelihood (REML), which can handle unequal sample size, and p-values for tests of fixed effects are conservatively adjusted to account for unbalanced designs.

LMMs were constructed in Rstudio using *lme4* (Bates et al., 2020) and the *lmertest* package (Kuznetsova et al., 2017) was used to obtain p-values. Model fit was assessed using marginal R^2 ($R^2_{LMM(m)}$), which describes the proportion of variance explained by only the fixed factor(s) in the model, and conditional R^2 ($R^2_{LMM(c)}$), which reflects the proportion of variance explained by both fixed and random factors (Nakagawa & Schielzeth, 2013).

Addition of clinical scores, lesion location, and lesion size were considered for each model, and the Akaike's Information Criterion (AIC) and Bayesian information criterion (BIC) were calculated for model comparison using the *AICcmodavg* R package (Mazerolle, 2020). AIC and BIC values were compared for candidate models, and those with delta-AIC or delta-BIC (difference in AIC scores, or BIC scores between models, respectively) values of more than -2 were selected as the best available fit for the data. Chi-squared values were also inspected to assess significance of differences in model fit. Figures were created using ggplot2 (Wickham, 2016).

2.4.1.1 CTBS analysis.

For cTBS data, separate LMMs for stroke and neurotypical groups were first constructed to compare MEP amplitude before and after cTBS application at each timepoint. *Block* and *Timepoint* were included as fixed effects, and a random intercept per *participant* was included (notation: (1|Participant)) to account for non-independence of repeated measures within subjects. If an effect of cTBS was detected, stroke and neurotypical data would be combined, and the effect of cTBS between populations over time would be compared using a linear mixed model with an added fixed effect of *Group*, giving the formula:

$$MEP\ amplitude \sim Block \times Timepoint \times Group + (1|Participant)$$

2.4.1.2 SICI analysis.

The same analysis process was followed to interrogate SICI data, whereby separate LMMs for each group were first used to assess the efficacy of the technique. First, data from each SICI *condition* (2ms and 3ms ISI) were combined, after confirmation of no statistically significant difference between conditions. This is in concurrence with a recent meta-analysis that reported no difference in conditioned MEP amplitude under 2ms or 3ms SICI protocols in neurotypical participants (Corp et al., 2021). Models were then constructed with fixed

effects of *Trial Type* (conditioned or un-conditioned MEP) and *Timepoint*, with a random intercept per *Participant*.

After the efficacy of the paired-pulse TMS protocol was confirmed, SICI ratio was calculated ((conditioned MEP amplitude / unconditioned MEP amplitude) × 100) and data from both groups were combined to compare SICI between groups over time, using an LMM with *Timepoint* and *Group* as a fixed effects, and *participant* as a random intercept:

$$SICI\ ratio \sim Timepoint \times Group + (1|Participant)$$

2.4.1.3 RMT analysis.

To compare RMT over time in stroke and neurotypical groups, an LMM was constructed with *Timepoint* and *Group* as fixed effects, and a random intercept per *Participant*, giving the formula:

$$RMT \sim Timepoint \times Group + (1|Participant)$$

2.4.1.4 Analysing the relationship between TMS-assessed excitability, clinical scores, and lesion size.

Data collected from stroke survivors were then inspected to assess interactions between ARAT and FIM scores (collectively referred to as clinical scores of interest) over time on each TMS measure of interest. Clinical scores were added as interacting fixed effects to each LMM, with the template formula:

$$TMS\ measure\ of\ interest \sim Timepoint \times clinical\ score\ of\ interest + (1|Participant)$$

Since *Lesion volume* data were collected at one timepoint only and may impact longitudinal measures of interest, *lesion volume* was converted to a categorical variable. Stratification was based on the median lesion volume reported in a larger study, where Sperber and Karnath (Sperber & Karnath, 2016) found normalized lesion size was 31.9 cm^3 in a sample of 439 MRI scans (25%-quantile = 9.4 cm^3, 75%-quantile = 72.9 cm^3). Nineteen participant's lesions in the presented study were smaller than the 25th per centile (9.4cm^3) reported by Sperber and Karnath (Sperber & Karnath, 2016), 9 were between the 25th and 75th per centiles (9.41 -72.9cm^3) and just 1 participant's lesion was larger than the 75th per centile.

Stroke survivor data were stratified by *Lesion Size* smaller or larger than the 25th per centile (9.4cm^3) and labelled as *small* or *mid-sized*. An LMM was constructed to assess the interaction between *Timepoint* and categorical *Lesion Size, with* the formula:

$$Measure\ of\ interest \sim Timepoint \times Lesion\ Size + (1|Participant)$$

2.5 Results.

2.5.1 Clinical scores reflect mild stroke symptom severity.

Admission NIHSS reflected mild-moderate stroke symptoms in the group (mean = 6.74, SD = 4.86, where scores <5 are considered mild, and scores >25 represent very severe symptoms). A ceiling effect in ARAT scores was recognised at all time points, as all participants received a mild score from the earliest timepoint onwards (mean at 3 weeks = 55.85, max. possible score = 57, SD = 3.92). Levene's test showed there was no significant change in the variance of ARAT scores between time points, p> .05.

FIM scores were also at ceiling from the earliest timepoint onwards (mean at 3 weeks = 121.82 of a possible 126, SD = 5.43). Levene's test showed no change in variance of FIM scores between time points (p>.05). Due to increased likelihood of inflated type 1 error with measures involving a ceiling effect (Austin & Brunner, 2003), FIM and ARAT scores were not included in subsequent models as planned. Descriptive data are instead displayed in Table 2.1.

2.5.2 Lesion characteristics.

Lesions were identified in 7 vascular territories (Left ACA/MCA, n = 2; Left MCA, n = 11, Left PCA, n= 1; Right ACA, n = 1; Right ACA/MCA, n = 1; Right MCA, n = 14; Right PCA, n = 1). Median lesion size was 5.16cm^3 (range = 0.19-87.65cm^3, 25%-quantile = 2.28 cm^3, 75%-quantile = 12.8 cm^3). Clinical scores, lesion location, and lesion size information for each participant are included in Table 2.1.

Table 2.1. Stroke survivors' individual clinical scores and lesion information. Abbreviations: M, mean; SD, standard deviation; ACA, anterior cerebral artery; MCA, middle cerebral artery; PCA, posterior cerebral artery; PICA, posterior inferior cerebellar artery; NIHSS, National Institutes of Health Stroke Scale; FIM, Functional Independence Measure; ARAT, Action Research Arm Test.

ID	Admission NIHSS (normal function = 0)	FIM (normal function = 126)		ARAT (normal function = 57)		Lesion location	Lesion volume (cm^3)	Lesion Size
		M	SD	M	SD			
1	7	123.75	0.46	57.00	0.00	Left MCA	11.83	Mid-sized
2	2	125.17	0.41	57.00	0.00	Right MCA	5.16	Small
3	1	125.00	0.76	56.50	0.93	Right MCA	2.92	Small
4	14	125.00	0.00	42.00	0.00	Left ACA/MCA	9.65	Mid-sized
5	16	108.25	2.76	57.00	0.00	Right ACA	6.01	Small
6	3	118.25	1.58	45.00	3.93	Right MCA	4.16	Small
7	13	120.25	3.58	56.00	0.76	Right MCA	87.65	Large
8	4	125.00	0.76	57.00	0.00	Left MCA	8.91	Small
9	3	125.50	0.93	57.00	0.00	Right MCA	2.28	Small
10	13	110.75	5.47	57.00	0.00	Right MCA	39.87	Mid-sized
11	13	123.00	1.85	56.75	0.46	Left ACA/MCA	1.36	Small
12	6	120.50	3.51	56.75	0.46	Left MCA	24.34	Mid-sized
13	4	113.00	5.90	57.00	0.00	Left MCA	0.74	Small
14	5	109.00	5.61	56.00	1.85	Left MCA	NA	NA
15	13	116.75	2.05	57.00	0.00	Right MCA	NA	NA
16	11	123.50	0.58	57.00	0.00	Left MCA	6.15	Small
17	3	124.00	3.70	56.25	1.39	Right MCA	2.11	Small
18	4	125.00	0.00	57.00	0.00	Left MCA	24.91	Mid-sized
19	17	122.33	1.03	57.00	0.00	Right MCA	3.07	Small
20	2	125.50	0.53	57.00	0.00	Right MCA	7.63	Small

21	4	124.75	0.46	57.00	0.00	Right MCA	0.3	Small
22	3	125.00	0.89	57.00	0.00	Left MCA	2.66	Small
23	5	124.33	1.03	57.00	0.00	Left PCA	0.91	Small
24	6	122.86	1.35	57.00	0.00	Left MCA	19.5	Mid-sized
25	3	121.71	3.90	56.71	0.49	Left MCA	2.67	Small
26	2	124.75	0.46	57.00	0.00	Right MCA	31.26	Mid-sized
27	3	123.75	1.75	54.75	2.66	Left MCA	4.83	Small
28	4	117.86	8.11	47.29	11.27	Right PICA	0.19	Small
29	4	123.00	1.63	56.71	0.76	Right ACA/MCA	12.85	Mid-sized
30	14	125.75	0.46	57.00	0.00	Right MCA	29.9	Mid-sized
31	7	123.20	1.79	57.00	0.00	Right MCA	1.31	Small

NA = information not available.

2.5.3 CTBS did not significantly alter MEP amplitude.

An unpaired t-test demonstrated no difference in MEP amplitude in blocks collected 5- and 15- minutes post-cTBS, in the stroke survivor group, t(197) = -.34, p = .74, and the neurotypical group(t(145) = .53 , p = .60). Therefore data collected in blocks post-cTBS were combined. LMMs were constructed to compare MEP amplitude data in each *block* (pre- and post-cTBS) at each *timepoint* separately for each *group*, with the formula: MEP amplitude ~ Block×Timepoint+(1|Participant). No difference in MEP amplitude was found between *blocks* in the neurotypical group, F(1,112) = .26, p = .61, and there was no significant interaction with *timepoint*, F(2, 112) = 1.27, p = .20. The same was found in the stroke group, with no detectable difference in MEP amplitude detected after cTBS intervention, F(1, 177) = .65, p = .42, and no significant interaction with *timepoint*, F(3, 177) = .18, p = .91. Due to ineffectiveness of the cTBS intervention, analyses were not expanded on.

2.5.4 SICI was significantly suppressed 3 weeks post-stroke, returning to neurotypical levels by 6 months.

Two-way ANOVAs constructed for each group showed no significant difference in SICI ratio under 2ms and 3ms ISI protocols at each timepoint (stroke: F(3,42) = 1.70, p = .18; neurotypical: F(2,40) = .34, p = .71). SICI data under each ISI were therefore combined to increase statistical power. The efficacy of paired-pulse protocol was first assessed using LMMs to compare MEP amplitude under each *condition* (conditioned or unconditioned trials) at each *timepoint* in the stroke survivor and neurotypical groups separately (formula: MEP amplitude ~ Timepoint x condition + (1|Participant)). A significant difference in conditioned MEP size compared to unconditioned MEP size was detected in the neurotypical group (F(1, 120) = 299.22, p<.01) and the stroke survivor group (F(1,172) = 485.75, p<.01). The efficacy of paired-pulse SICI protocol did not change over time in either group (p>.05).

After the effectiveness of paired-pulse TMS was established, SICI ratio was compared between groups over time (formula: SICI ratio ~ Timepoint × Group + (1|Participant)). Coefficients of variation (CV) showed high variance in SICI ratio in the stroke (CV = 52.66) and neurotypical (CV = 58.71) groups, indicating a poor ratio of standard deviation to the

mean. Levene's test showed no significant difference in variance of SICI ratio between time points or groups, or their interaction (p>.05).

The model converged successfully, with fixed factors alone accounting for 4% variance, and 65% variance explained by both and fixed and random factors ($R^2_{LLM(m)}$ = .04, $R^2_{LMM(c)}$ = .65). A *Timepoint×Group* interaction revealed a significant difference in SICI ratio between groups at T1 only (3 weeks post-stroke), whereby SICI was significantly suppressed (19% lower) in the stroke compared to the neurotypical group at T1 (β = -18.91, CI=-36.29—1.53, p = .03).

Within the stroke group, a significant 13% difference in SICI was detected between T1 and T3 (3 weeks and 6 months post-stroke; β = -12.81, CI= -23.73—1.89, p = .02). No difference in SICI was detected between the other time points in the stroke group, including no significant difference between SICI at T1 and T4 (3 weeks compared to 12 months post-stroke; β = -3.03, CI= -15.93 – 9.21, p = .60). Addition of categorical *Lesion Size* improved the model, resulting in lower AIC and BIC values, though model comparison with chi-squared was non-significant, χ^2 (4, N = 29) = 1.7, p > .05. *Lesion size* did not significantly predict SICI ratio, F(1,25) = .01, p = .94, and *Lesion Size* did not significantly interact with *Timepoint,* F(3,62) = .53, p = .66. *Lesion volume* was also included as a continuous variable (formula: SICI ratio ~ Timepoint × lesion volume + (1|Participant)), and model comparison showed no improvement relative to the model without lesion volume included, χ^2 (4) = 2.68, p > .05, $R^2_{LLM(m)}$ = .03, $R^2_{LMM(c)}$ = .63. *Lesion volume* did not significantly predict S*ICI ratio* (F(1, 23) = .003, p = .95) and did not significantly interact with *Timepoint* (F(3,60) = .83, p = .48).

Group comparison revealed a significantly larger difference in SICI ratio between T1 and T3 in the stroke group, compared to the difference between T1 and T3 in the neurotypical group (3 weeks and 6 months post-stroke; β = 16.11, CI=0.75-31.47, p = .04; Figure 2.2). No significant difference was found between groups at T3 (6 months; β = -2.8, CI= -20.37 – 14.77, p = .75) or T4 (12 months; β = -5.88, CI=-24.13 – 12.37, p = .53). Results are summarised in Figure 2.2.

To check whether results were distorted by missing data, group comparisons were repeated after omitting T2 (3 months), where neurotypical data were not collected. In concurrence with the model including all time points reported above, SICI was significantly suppressed in

the stroke group at T1 compared to T3 (β = -13.4, CI=-24.01 - -2.79, p = .01), and a significant difference was found between groups at T1 (3 weeks post-stroke), β = -19.87, CI=-36.99 - -2.76, p = .02. A significant interaction was also in concurrence with the previously reported results, showing a significantly larger difference in SICI ratio at T1 and T3 in the stroke group, compared to the difference between T1 and T3 in the neurotypical group (β = 16.72, CI= 1.86-31.58, p = .03).

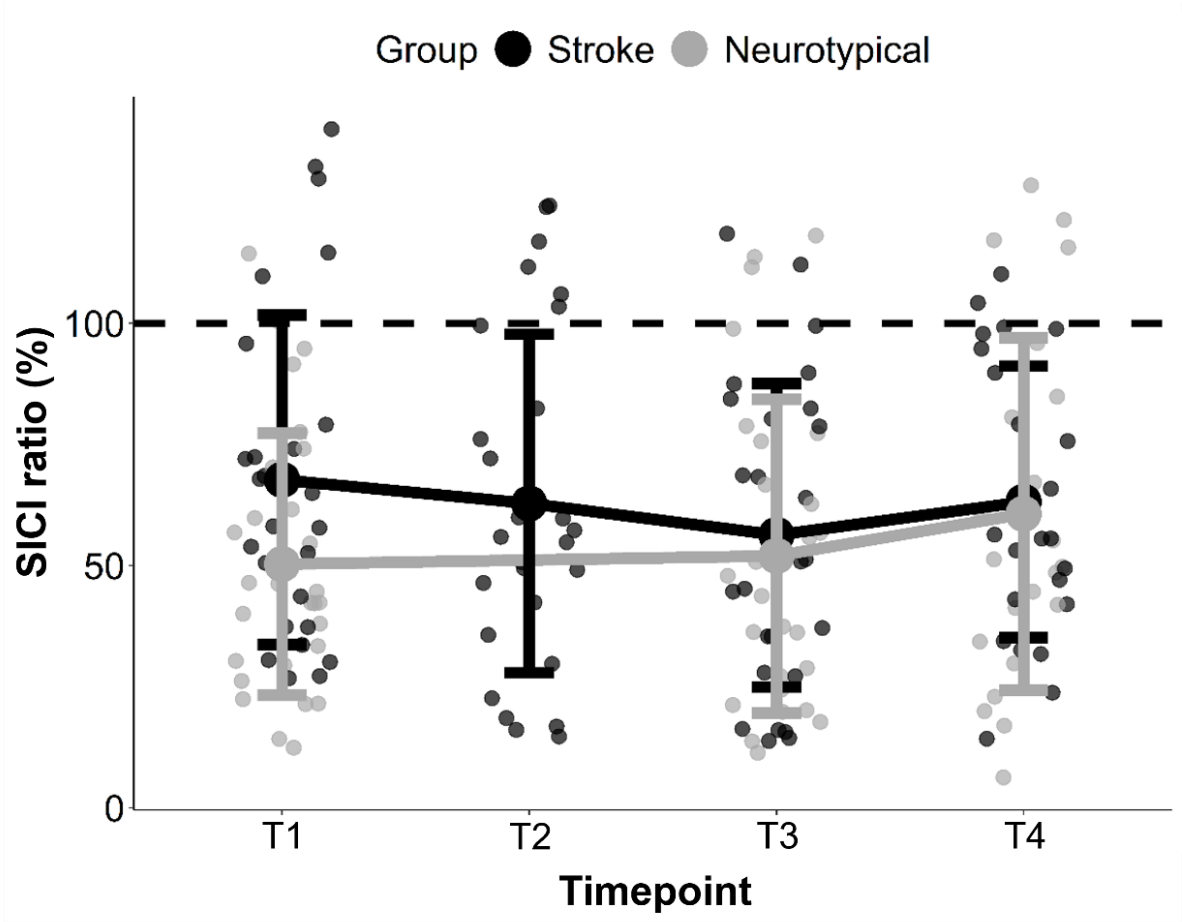

Figure 2.2. Intra-cortical inhibition in stroke survivors and neurotypical participants over 12 months. Stroke survivor data are shown in black, neurotypical data in grey. SICI ratio (y-axis) is conditioned MEP amplitude expressed as a per centage of unconditioned MEP amplitude. Time points reflect time post-stroke for stroke survivor data (T1 = 3 weeks, T2 = 3 months, T3 = 6 months, T4 = 12 months, while neurotypical data were collected at 6-month intervals (T1, T3, T4; x-axis). Error bars show standard deviation. SICI is suppressed (-19%) at T1 in stroke survivors compared to neurotypical participants (β = -18.91, CI=-36.29—1.53, p = .03).

2.5.5 Persistently increased variability in RMT after stroke compared to (neurotypical participants.

Significantly higher variance in RMT was detected in the stroke (CV = 21.78) compared to neurotypical (CV = 12.70) group (Levene's test: $F(1,174) = 23.06$, $p<.001$). Levene's test showed no significant difference in variance between time points within groups (stroke: $F(3,111) = .59$, $p = .62$; neurotypical: $F(2,58) = .19$, $p = .83$; Figure 2.3).

A linear mixed effects model with a random intercept per participant was used to assess differences in RMT between groups over time, with the formula: RMT ~ Timepoint × Group + (1|Participant). The model converged successfully with 87% variance explained by fixed and random effects, and 1% variance explained by fixed effects alone ($R^2_{LMM(c)} = .87$, $R^2_{LLM(m)} = .01$,). No significant difference in RMT over time was detected in the stroke group ($F(3,82) = .62$, $p =.60$) or the neurotypical group ($F(2,38) = 1.14$, $p = .33$). No significant interaction between Group and Timepoint was detected, $F(2, 120) = .63$, $p = .50$.

To investigate the influence of varying lesion size on RMT over time, *Lesion Size* was added to the model as a categorical fixed effect interacting with *Timepoint*. Addition of *Lesion Size* did not alter model fit (χ^2 (4, N = 29) = 8.33, p = .08). The model converged with 11% variance explained by the fixed effects alone and 89% variance explained by fixed and random effects combined ($R^2_{LLM(m)} = .11$, $R^2_{LMM(c)} = .89$). A trend in lesion size predicting RMT was detected, $F(1,27) = 3.67$, $p = .07$, whereby larger lesions were associated with lower RMT. No significant interaction with *Timepoint* was detected, $F(3,73) = 1.44$, $p = .24$ (Figure 2.3). *Lesion volume* was also included in the model as a continuous variable (formula: RMT ~ Timepoint × lesion volume + (1|Participant)), which significantly improved model fit compared to the model without lesion volume included, χ^2 (4) =11.37, $p > .02$, $R^2_{LLM(m)} = .22$, $R^2_{LMM(c)} = .89$. Results of the model showed that *Lesion volume* significantly predicted RMT ($F(1,27) = 8.35$, $p = .01$), whereby with each $1cm^3$ increase in lesion volume, the expected value of RMT decreased by 0.33 on average ($\beta = -.33$, CI= -0.54 -0.13, $p = .003$). *Lesion volume* was not found to significantly interact with *Timepoint* ($F(3,72) = 1.12$, $p = .35$).

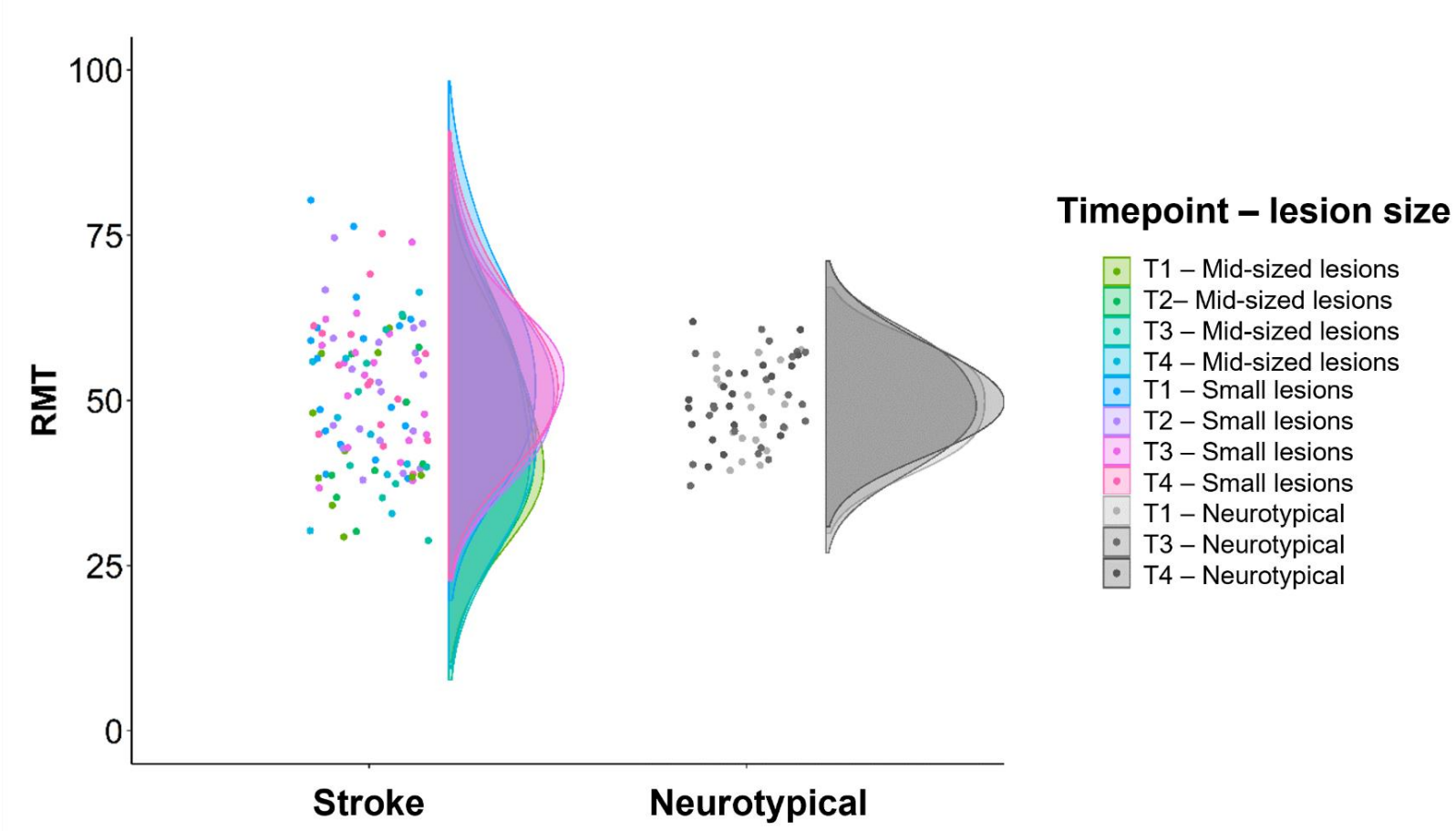

Figure 2.3. RMT of stroke survivors and neurotypical participants at time points 1-4. Distribution curves represent RMT per group, per timepoint. Datapoints show RMT per participant, at each timepoint. Colours reflect lesion size in the stroke survivor group. Higher variance in RMT was found in stroke survivors compared to neurotypical participants across all time points (Levene's test: $F(1,174) = 23.06$, $p<.001$). No change in RMT was detected over time in stroke or neurotypical groups ($F(2, 120) = .63$, $p = .50$). In the stroke group, a trend was detected whereby larger lesions were associated with lower RMT ($F(1,27) = 3.67$, $p = .07$).

2.6 Discussion.

In this Chapter I compared longitudinal data collected from stroke survivors and neurotypical volunteers. The primary aim was to determine whether there are distinct windows of time in which neuromodulatory interventions may be best applied in stroke survivors, in keeping with a temporal framework that suggests heightened cortical excitability underpins accelerated recovery in sub-acute stroke (Bernhardt et al., 2017; concept in Figure 1.1).

To interrogate whether the trajectories of functional and neurophysiological change are coupled after human stroke (Bernhardt et al., 2017; Buma et al., 2013; Dobkin & Carmichael, 2016; Kwakkel et al., 2004), I aimed to examine longitudinal changes in TMS-assessed cortical excitatory-inhibitory balance and clinical scores (ARAT and FIM) recorded up to 12 months post-stroke. In concurrence with previous research (Liepert et al., 2000; Manganotti et al., 2002; McDonnell & Stinear, 2017; Swayne et al., 2008), I found that intra-cortical inhibition was significantly weaker in the early sub-acute phase (3 weeks post-stroke) before returning to neurotypical levels in chronic stroke (from 6 months). However, stroke symptom severity was at ceiling across all time points, preventing longitudinal comparison of functional and neurophysiological change due to inflation of type 1 errors (Austin & Brunner, 2003).

Instead, clinical data here reflect a well-recovered sub-group of the wider stroke survivor population, whose functional recovery trajectory was static and at ceiling from the earliest timepoint onwards. The finding of decreased intra-cortical inhibition early after stroke in a well-recovered cohort is contextualised by evidence that disinhibition of ipsilesional M1 in human subacute and chronic stroke (Cicinelli et al., 2003; Hummel et al., 2009; Liepert et al., 2000), may support functional recovery (Clarkson et al., 2010; Lake et al., 2015; Orfila et al., 2019; Blicher et al., 2015; Kim et al., 2014). The presented data align with the hypothesis that an early reduction in GABA-mediated intra-cortical inhibition may facilitate good motor recovery after human stroke. However, they do not evidence a coupled trajectory of functional and physiological change; clinical scores remained static while SICI in $M1_{hand}$ differed significantly between 3 weeks and 6 months post-stroke.

2.6.1 Functional gains are not temporally coupled with neurophysiological change in mild stroke.

The longitudinal relationship between SICI and functional stroke outcomes has been investigated previously. In the notable work of Swayne and colleagues (Swayne et al., 2008) data from a relatively heterogeneous group of 10 stroke survivors were presented, with ARAT scores ranging from 0-100% (Mean = ~60%) within 1 month of stroke. Correlation of SICI and ARAT scores was non-significant ≤ 1 month post-stroke, with significance only detected at the 3-month timepoint when ARAT scores had reached ceiling. These findings remain inconclusive due to ceiling effects producing inflated type 1 errors at the 3-month timepoint, and the authors noted reduced power of statistical analysis of data at ≤ 1 month, due to high variability of ARAT scores in the relatively small sample.

In addition, Manganotti and colleagues (Manganotti et al., 2008) reported longitudinal data from 13 stroke survivors with varied impairment profiles. Ipsilesional SICI was lower ~1 week post-stroke compared to 1-month and 3-month time points in all survivors. Between 1 and 3 months, SICI returned to neurotypical levels in 5 participants with mild impairment (defined as Barthel Index score >60 at 1-week post-stroke), and atypical SICI persisted in 8 survivors with moderate-severe impairment (Barthel Index score <60 at 1-week post-stroke). Longitudinal comparison of hand and arm functionality (measured by the Lindmark scale; Lindmark & Hamrin, 1988) with ipsilesional SICI did not yield significant results. I maintain that these studies do not offer reliable evidence of a coupled trajectory of functional gains and neurophysiological change after human stroke, as variable findings in small samples of participants produce low-powered results.

More recently, Honaga and colleagues (Honaga et al., 2013) attempted to address bias towards mild impairment and small sample size in a study of intra-cortical inhibition in 72 chronic stroke survivors (average time since stroke onset = 28.2 months, range = 6-104 months), whom each attended one session in contrast to the longitudinal design of the studies described above. Participants were moderately or severely impaired, assessed by the upper limb section of the Fugl-Meyer (FM-UL; Fugl-Meyer et al., 1975). Just 24 of 72 participants had recordable MEPs after TMS was applied to the ipsilesional hemisphere,

highlighting the difficulties of using TMS biomarkers to investigate neurophysiology after stroke.

Honaga and colleagues (Honaga et al., 2013) reported greater intra-cortical inhibition in participants with less upper limb impairment, in contrast to pre-clinical work which suggests reduced inhibition might support recovery (Clarkson et al., 2010; Lake et al., 2015; Orfila et al., 2019; Blicher et al., 2015; Kim et al., 2014). In addition SICI was significantly stronger in survivors with greater time since stroke onset, and FM-UL did not correlate with time since stroke onset. This not only indicates a de-coupling of neurophysiological and recovery timelines, but demonstrates changeable excitatory-inhibitory balance persisting into chronic stroke in moderately impaired survivors. This contends the hypothesis that brain excitability will return to neurotypical levels in chronic stroke, and may point to an opportunity to exploit a pro-plastic brain environment beyond the sub-acute phase.

The mixed findings reported in this Chapter, and in previous work outlined above, describe heterogeneity in post-stroke intra-cortical inhibition and functional gains which do not align with the homogenous, coupled timelines proposed in The Stroke Roundtable Consortium (Bernhardt et al., 2017).

2.6.2 Functional and neurophysiological trajectories may differ depending on stroke severity.

Lack of representation of stroke survivors with moderate and severe symptoms limits the impact of findings from the data presented in this Chapter. One could argue that future work with a large sample of survivors and heterogeneous symptom severity may yet demonstrate the accuracy of the temporal framework described by The Stroke Roundtable Consortium (Bernhardt et al., 2017). However, growing evidence suggests that functional recovery does not match the homogenous trajectory proposed; recovery from stroke may instead differ depending on symptom severity. Van der Vliet and colleagues (van der Vliet et al., 2020) recently reported a longitudinal mixture model of FM-UL scores of 412 stroke survivors with motor impairment, collected at a minimum of 2 time points spaced 12 weeks apart. I briefly note that the majority of survivors included in the study received rehabilitative treatment in keeping with Dutch guidelines (Duncan et al., 2005; Quinn et al.,

2009), though the intervention is not significantly associated with a change in FM-UL scores (Kundert et al., 2019).

Five sub-groups of survivors were identified with differing speed, trajectory, and outcome of motor function by 8 months post-stroke: mildly impaired survivors reached 90% recovery potential in the first weeks after stroke, while survivors with moderate impairment regained good function over a much longer time frame, an initial indicator of heterogeneous recovery trajectories. This was further quantified by an exponential term representing the predicted recovery rate for survivors in each sub-group. This value was derived by a time constant (units = weeks), which signified the timepoint at which exponential recovery reached 63.2% of total recovery. This functional 'peak' (though notably lower than maximum outcome) occurred ≤ 3 weeks post-stroke in two sub-groups of mildly impaired participants, and at ~10 weeks post-stroke in 2 sub-groups of moderately impaired survivors. Interestingly, severely impaired participants reached 63.2% total recovery ~5 weeks post-stroke, earlier than the moderately impaired group, though overall functional outcome was poorer. In addition, a recent modeling study implemented advanced Bayesian statistics with FM-UL data of 489 stroke survivors (Bonkhoff et al., 2022) and found greater improvement in FM-UL scores by 3-6 months in survivors with non-severe symptoms and greater initial impairment, while severely affected survivors recovered more if their initial impairment was lower.

These findings suggest that temporally-defined, homogenous post-stroke 'phases' set out by The Stroke Roundtable Consortium (Bernhardt et al., 2017) are an over-simplification of the human post-stroke recovery trajectory. Instead, the timeline of functional gains likely differs depending on stroke severity, and may or may not be coupled with neurophysiological changes in brain activity. While the work presented in this Chapter does not rule out coupling of physiology and function in moderate and severely impaired groups of stroke survivors, it does indicate that the mechanisms of post-stroke recovery in humans are subject to greater complexity than those observed in animal models of stroke. In a recent review Grekes and Fink (Grefkes & Fink, 2020) underscore the point, by suggesting that recovery-associated processes at 10-and 80-days post-stroke will likely differ substantially between human stroke survivors, yet both time points fall in the so-called 'sub-acute' phase.

Continued use of language such as “sub-acute” and “chronic” stroke to simultaneously describe time-since-stroke and neurophysiological capacity for recovery may prevent development of optimised rehabilitation interventions tailored to individual stroke survivors with heterogeneous recovery trajectories.

2.6.3 Higher variance in RMT after stroke reflects heterogeneous post-stroke anatomy and cortico-spinal excitability.

In this study, alongside a time-dependent change in SICI after stroke, I found no significant change in RMT over time. RMT values were however persistently more variable in stroke survivors compared to the neurotypical group. This variability is likely reflective of the compound nature of the RMT measure, which is influenced by the excitability of spinal motor neurons (Brouwer & Schryburt-Brown, 2006; Groppa et al., 2012) and cortico-cortical projections to M1 (Borich et al., 2015) in addition to variations in age (Corp et al., 2021), time post-stroke (Rosso & Lamy, 2018; Stinear & Byblow, 2017), variable tone in hand muscles producing MEPs (Darling et al., 2006; Kiers et al., 1993), and cortico-spinal tract integrity (Kemlin, Moulton, Lamy, et al., 2019; Potter-Baker et al., 2018); the relationship between RMT and M1 excitability is non-linear. Meanwhile, consensus has not been reached on the relationship between RMT and functional gains after stroke, with some work suggesting the two are highly correlated (Kemlin, Moulton, Lamy, et al., 2019; Rosso & Lamy, 2018) while no relationship is reported elsewhere (Freundlieb et al., 2015). In this study, high variance in RMT data is not reflected in functional scores, though I note again the issue is not directly interrogated due to ceiling effects. These data do not provide conclusive evidence of the relationship (or lack thereof) been cortical excitability and functional recovery trajectory after stroke, though they do evidence greater variability in TMS-measures of cortico-spinal excitability in stroke survivors.

Lesion size was identified as a contributing factor to RMT variability, as lower RMT (i.e. higher CSE) was associated with larger lesion volume. However, I note that large lesions were not well-represented; just one participant’s lesion volume was higher than the 75th per centile of a larger sample of 439 stroke survivors (Sperber & Karnath, 2016). Though seemingly counter-intuitive, small, subcortical lesions reportedly have a greater impact on efferent motor pathways (Freundlieb et al., 2015), which may be because descending white

matter tracts are more densely occluded by sub-cortical lesions than larger cortical ones. In this sample of survivors with relatively small lesions, smaller lesions appear to be associated with higher RMT, possibly due to greater CST damage (Kemlin, Moulton, Lamy, et al., 2019). Due to small sample size and limited lesion information in this study, the potential relationship between lesion characteristics and RMT is non-conclusive; a target for further investigation which might explain high variability in TMS measures of cortical excitability in the stroke population.

In addition to the possible impact of lesions on RMT variability, secondary stroke-induced structural changes including enlarged ventricles and cortical atrophy may impact the amplitude of TMS-evoked MEPs (Minjoli et al., 2017; Skriver et al., 1990). In a recent study that modelled TMS current flow in 2 stroke survivors (Minjoli et al., 2017) increased atrophy and lesioned tissue near the cortical target were associated with a lower volume of grey matter affected by TMS-induced E-field. In the context of the findings reported here, I suggest that stroke-induced anatomical changes may contribute to the observation of higher RMT variability in stroke compared to neurotypical groups. Future work may be improved by individualised modelling of TMS E-field, to account for variance in outcome measures attributed to pathological anatomy.

2.6.4 Limitations.

In this study, I aimed not only to measure changes in the balance of cortical excitation and inhibition using RMT and SICI measures, but to also investigate whether stroke survivors' potential for plasticity changed as a function of time since stroke. After all, alterations to excitatory-inhibitory balance in the brain are of interest because they may modulate neuroplastic potential. To this end, an inhibitory TBS protocol was used to modulate excitability in the motor cortex of stroke survivors and neurotypical participants, though it was found to be ineffective; no difference in MEP amplitude was found before and after cTBS intervention in both the neurotypical and stroke survivor groups. This finding is in concurrence with a recent large-scale meta-analysis of data from 430 neurotypical participants (mean age = 42) which found that reliability of cTBS response was "almost non-existent" within studies (Corp et al., 2020, p. 1480). However, increased variability in MEPs collected during TBS studies was reported when TMS pulses were delivered at 120% RMT, as

they were in this study, compared to an alternative method where the intensity of TMS pulse was prescribed by the minimum dose required to evoke 1mV amplitude MEPs (Corp et al., 2021). Future work may benefit from this minor protocol alteration.

In addition to potential sources of variability in TMS measures described above, the functional scores reported may not optimally reflect the post-stroke trajectory of motor recovery. ARAT scores reflect cognitive, personal, and environmental factors as well as motor function (Schepers et al., 2007), while the FIM and NIHSS are generalised measures not limited to motor symptoms after stroke. The FM-UL, which quantifies impairment instead of function, may be better suited to assess the trajectory of motor recovery after stroke, as incremental reductions in motor impairment which may not yet result in detectable change in a given function, may produce a more fine-grained assessment of recovery which is less susceptible to ceiling effects. To capture the full picture of the post-stroke recovery timeline, multiple measures of function and impairment should be reported.

Finally, I note that SICI and RMT are indirect measures of excitatory and inhibitory brain function which will not fully capture the complex and changeable post-stroke brain environment. In fact, Grigoras and colleagues (Grigoras & Stagg, 2021) point out that reported change in excitatory-inhibitory balance after stroke tends to differ between modalities used. For example, a positron emission tomography (PET) study found increased ipsilesional $GABA_A$ receptor availability at 1 and 3 months post-stroke in 10 participants, while a recent magnetic resonance spectroscopy (MRS) study showed no significant difference in ipsilesional GABA between sub-acute stroke survivors and age-matched neurotypical participants (Cirillo et al., 2020). Further multi-modal investigation is required to elucidate the physiological mechanisms which might underlie individualised motor recovery after human stroke.

2.6.5 Conclusion.

Here, I investigated whether post-stroke functional gains and TMS-assessed changes in excitatory-inhibitory balance follow temporally coupled trajectories. I also considered whether the homogenous timeline set out in the Stroke Roundtable Consortium (Bernhardt et al., 2017) accurately describes human recovery after stroke. I report that TMS-assessed

CSE is persistently more variable in stroke survivors than neurotypical participants, which may be due in part to the impact of pathological anatomy on TMS-induced E-fields (Minjoli et al., 2017; Scrivener et al., 2012).

Further, I found that the timeline of motor functional recovery was temporally de-coupled from GABA-mediated intra-cortical inhibition in survivors with mild stroke symptoms. In light of recent work evidencing varied stroke recovery trajectories in survivors with different symptom severity (Bonkhoff et al., 2022; van der Vliet et al., 2020), I suggest that temporally-defined, group-wide 'phases' of recovery do not adequately describe the human post-stroke trajectory. Stroke-induced periods of an enhanced propensity for neuroplasticity are well evidenced in the animal literature (Biernaskie, 2004; Zeiler et al., 2016) and may well be underpinned by reduced inhibition and enhanced excitation (reviewed in Di Pino et al., 2014); I suggest that these periods may occur at different times, and for different durations, in stroke survivors with varying symptom severity.

Though stroke rehabilitation research has already moved beyond the outdated notion that significant recovery is not achievable after the sub-acute window has closed (Ward et al., 2019), the next step should be towards individualised identification of 'pro-plastic periods' after stroke when interventions may be most effective. Optimal timing of neuromodulatory interventions such as tDCS may for example benefit from individual assessment of functional brain state, which cannot be accurately predicted by recovery "phase" defined time since stroke onset.

CHAPTER 3. ENCOURAGING AN EXCITABLE BRAIN STATE AFTER STROKE WITH DOSE- AND DIRECTION-CONTROLLED TDCS.

3.1 Introduction

The work presented in this thesis interrogates how neuromodulation might be best applied to augment motor rehabilitation after stroke. In this Chapter, I investigate the impact of dose- and direction-controlled tDCS targeting $M1_{hand}$, in neurotypical participants and stroke survivors in the chronic phase of recovery. TMS-MEPs are used to probe neurophysiological changes during- and post-tDCS application. While CFM-informed tDCS is hypothesised to increase the reliability of stimulation outcomes, I expected to find higher variability in stroke survivors' response to tDCS due to stroke-induced changes in *functional* and *anatomical brain state* (discussed previously in section 1.5.1).

3.1.1 Re-opening the sensitive period after stroke.

The majority of recovery after stroke is observed within the first month in rodent models (Biernaskie, 2004; Krakauer et al., 2012; Murphy & Corbett, 2009) and within the first 6 months following human stroke (Buma et al., 2013; Cramer, 2008; Duncan et al., 1992; Hankey et al., 2007; Jorgensen et al., 1999; Kwakkel et al., 2004; Prabhakaran et al., 2008; Skilbeck et al., 1983; Ward, 2017). During this time, spontaneous biological recovery is observed (Cramer, 2008; Krakauer & Carmichael, 2017b; Nudo & Milliken, 1996) alongside heightened responsiveness to training (Biernaskie, 2004; Zeiler et al., 2016). In animal models of stroke, a sensitive period is recognised where endogenous recovery and heightened responsiveness to training are thought to be underpinned by a time-limited window of increased neuroplastic potential, the mechanisms of which are not yet fully understood (Zeiler et al., 2016; Zeiler & Krakauer, 2013).

Identification of a sensitive period after stroke necessitates two interesting lines of research. First, to maximise training interventions within the sensitive period: promising avenues of research include enriched rehabilitation environments for experience-dependent learning

(Aberra et al., 2020; Baroncelli et al., 2010; Bavelier et al., 2010; McDonald et al., 2018; Zeiler & Krakauer, 2013), and increased training dose (Birkenmeier et al., 2010; Lohse et al., 2014; Scrivener et al., 2012; Waddell et al., 2014; Winstein et al., 2019).

Second, promoting a brain environment that might support the sensitive period is a promising therapeutic target. Converging evidence suggests that accelerated sub-acute recovery is underpinned by enhanced endogenous plasticity (for reviews, see (Joy & Carmichael, 2020; Krakauer & Carmichael, 2017b). Increasing cortical excitability pharmacologically (Abe et al., 2019, 2019; Chollet et al., 2011; Clarkson et al., 2010; Liu et al., 2021; Liu et al., 2018; Lundström et al., 2021; Mead et al., 2013), or using non-invasive brain stimulation (Bai et al., 2022; Cheng et al., 2014; Chhatbar et al., 2016; Dmochowski et al., 2013; Elsner et al., 2018; Figlewski et al., 2017; Hamoudi et al., 2018; Hordacre, McCambridge, et al., 2021; Hummel & Cohen, 2006; Hummel & Cohen, 2005; Kubis, 2016; Levy et al., 2008; Malcolm et al., 2014; Marquez et al., 2015; Stinear et al., 2015; Yoon et al., 2012) are among candidate therapeutic interventions to promote neuroplasticity after stroke, intended for use alongside physical training.

A key unanswered question is when plasticity-promoting interventions might be best applied in humans: during the hypothesised sensitive period or after it? In other words, should researchers aim to support, extend or re-open the hypothesised critical window for recovery in humans? Notably, since tDCS modulates ongoing neuronal activity (Reato et al., 2013; Terzuolo & Bullock, 1956) and effects are state-dependent (Esmaeilpour et al., 2018; Polanía et al., 2010; Reato et al., 2010, 2013; Schmidt et al., 2014; Terzuolo & Bullock, 1956), response to tDCS will likely differ as a function of brain activity changes throughout the recovery timeline. In rodents, for example, tDCS applied 5-10 days after stroke has been linked to greater functional recovery compared to rats with tDCS administered within 1-5 days, or not at all after stroke (Yoon et al., 2012).

In humans, a recent study found improved performance on the Jebsen–Taylor hand function test after anodal tDCS was applied in the subacute compared to chronic stages after stroke (Pavlova et al., 2020). In a recent review, Lefaucheur and colleagues attempted to summarise the impact of tDCS on human motor performance during different post-stroke phases (Lefaucheur et al., 2017). The report accurately reflects a literature without

consensus; Lefaucher and colleagues describe studies where tDCS application in the sub-acute (Chang et al., 2015; Khedr et al., 2013) and chronic (Allman et al., 2016) post-stroke phases is associated with improved motor performance, while no functional impact of tDCS applied in the sub-acute (Hesse et al., 2011) and chronic phases (Geroin et al., 2011; Viana et al., 2014) is reported elsewhere. Importantly, meta-analyses such as these do not account for variability in tDCS protocols or outcome measures used between studies, reducing the power of findings.

3.1.2 TDCS optimisation.

Differences in tDCS protocols between studies include varying stimulation intensity, duration, electrode montage, and sham condition used. Outcomes also vary within protocols however, between individuals in the same study (Laakso et al., 2015; Polanía et al., 2018; Vergallito et al., 2022; Wiethoff et al., 2014). The emergence of open-access current flow modelling (CFM) software (Dannhauer et al., 2012; Dmochowski et al., 2011, 2013; Huang, Thomas, et al., 2018; Huang, Datta, et al., 2018; Huang et al., 2019; Lee et al., 2017; Saturnino, Puonti, et al., 2019) has enabled researchers to interrogate where, and how much current is flowing through ROIs in the brain during a simulated tDCS protocol, and subsequent work utilising CFMs has shown that E-field intensity in a cortical ROI can vary greatly between individuals when an identical protocol is applied (Bikson, Rahman, & Datta, 2012; Bikson, Rahman, Datta, et al., 2012; Caulfield et al., 2020; Datta et al., 2012; Dmochowski et al., 2011; Evans et al., 2020). Individual differences in E-field delivered to an ROI partially explain regional changes in neurotransmitter concentration (Nandi et al., 2022) and MEP amplitude change following stimulation (Laakso et al., 2019). Minimising variance in E-field delivered to an ROI across participants may in turn reduce variability in outcomes and improve tDCS efficacy.

3.1.2.1 Individualised tDCS dose.

Previous work undertaken by our group (Evans et al., 2020) utilised ROAST CFM software (Huang, Datta, et al., 2018; Huang et al., 2019) to simulate a conventional bipolar motor-targeted tDCS protocol in 50 structural MRI scans of neurotypical individuals. When simulated tDCS stimulator output was fixed at 1mA, the average E-field intensity recorded in the cortical target, $M1_{hand,}$ was 0.185V/m. A reverse calculation method was then used to ascertain the

tDCS stimulator output required to achieve uniform 0.185 V/m E-field intensity in $M1_{hand}$ in each participant, using the formula:

$$Individualised\ dose = \left(\frac{Target\ E\text{-}Field}{Actual\ E\text{-}Field}\right) \times Fixed\ dose$$

Where *Target E-field* was the target E-field intensity, set as 0.185V/m to match the group average. *Actual E-field* was the E-field intensity recorded in $M1_{hand}$ in each individual when fixed dose 1mA tDCS was simulated, and *Fixed Dose* was the injected current (1 mA) delivered to scalp electrodes in the original model. Methodology for reverse-calculated tDCS dose control has also been reported by Caulfield and colleagues (Caulfield et al., 2020), and recent iterations of current flow modelling software allow users to specify target E-field at coordinates denoting a target cortical ROI (Dmochowski et al., 2011, 2013; Huang, Thomas, et al., 2018). Dose-control methods which do not require CFMs are also emerging, a notable example being individualised tDCS stimulator output calculated as a function of head circumference (Antonenko et al., 2021). In the presented study, the reverse calculation method described by Evans and colleagues (Evans et al., 2020) was used to individualise stimulator output for each participant.

3.1.2.2 Optimised tDCS direction.

The direction of current relative to the somato-denditic axes of pyramidal neurons dictates polarisation effects (Bikson et al., 2004; Farahani et al., 2021; Lafon et al., 2017; Rahman et al., 2013, 2015; Seo & Jun, 2019). As previously discussed, the cortical surface of an ROI is taken as a proxy for the predominant orientation of pyramidal neurons in grey matter, typically oriented with apical dendrites close to the surface. Current flowing radial-inward relative to the surface of the cortex is associated with somatic depolarisation and heightened neuronal excitability, and was therefore the target for current direction optimisation in this study. In contrast, current flowing radial-outward is associated with somatic hyperpolarisation and decreased excitability, and current flow orthogonal to somato-dendritic axes (parallel to the cortical surface) is not associated with significant tDCS-induced somatic polarization (Bikson et al., 2004; Chan et al., 1988). This concept is summarised in Figure 1.2 in Chapter 1 of this thesis.

In humans, the direction-dependency of tDCS effects has long been evidenced by reports of electrode polarity determining outcomes (Nitsche & Paulus, 2000). Recent advances in the field

have given rise to CFM-informed montages, including the PA-tDCS montage described in Figure 1.3, where an anode is placed posteriorly and a cathode anteriorly to the cortical target, $M1_{hand}$, to produce predominantly radial-inward current flow relative to the cortical surface of the ROI. Greater consistency in current direction in $M1_{hand}$ has been shown when a PA-tDCS montage was used, compared to the conventional tDCS montage where the anode is placed directly above an ROI (Datta et al., 2009; Hannah et al., 2019; Rampersad et al., 2014; Rawji et al., 2018). Recent work by our group (Evans et al., 2022) confirmed that PA-tDCS produces predominantly radial-inward current in $M1_{hand}$ across participants, and the highest estimated E-field intensity in $M1_{hand}$ was found using PA-tDCS compared to alternative montages.

While current direction and E-field intensity are not correlated (Evans et al., 2022), both are likely to impact tDCS effects. Here, PA-tDCS is applied with reverse-calculated dose control, to minimise variance in tDCS-induced E-field intensity and current direction in $M1_{hand}$ across neurotypical participants and stroke survivors.

3.1.3 TMS recruitment curves quantify neurophysiological response to tDCS

Single-pulse TMS was used to assess changes in CSE during and post-tDCS application compared to baseline. MEPs were recorded from the FDI muscle of the hand when TMS pulses of varying intensities were applied to the motor hotspot on the scalp. Typically, stronger TMS pulses result in a sigmoidal increase in muscle response: MEP amplitude increases with TMS intensity before reaching a plateau (Devanne et al., 1997; Hess et al., 1987). The sigmoid describing the relationship between TMS intensity and evoked response is herein referred to as a recruitment curve (RC), synonymous with “stimulus-response curve” or “input-output curve”. It has been suggested that redundancy exists among parameters which can be extracted from RCs to measure CSE, for example, the gradient of the maximal slope of the sigmoid and the area under the curve tend be positively correlated (Kemlin, Moulton, Leder, et al., 2019).

This study aimed to compare response to a CFM-informed tDCS protocol in neurotypical individuals and stroke survivors in the chronic phase of recovery. While cortical excitability is hypothesised to return to pre-stroke levels in the chronic phase, approximately 6 months post-stroke (Bernhardt et al., 2017), it was hypothesised that TMS-assessed CSE at baseline would be more variable in the stroke survivor group, due to stroke-induced changes in

functional and *anatomical brain state*. Chronic network dysfunction (Grefkes & Fink, 2012; Guggisberg et al., 2019; Lim et al., 2014; Siegel et al., 2016), variable muscle tone at rest (Darling et al., 2006; Kiers et al., 1993), and individual differences in integrity of the cortico-spinal tract (CST; Potter-Baker et al., 2018) may also result in differing TMS-assessed response to optimised-tDCS in stroke survivors compared to neurotypical participants, as stroke-induced changes to *functional* and *anatomical brain state* may alter the distribution of, and response to, tDCS-induced E-fields (this concept is discussed at length in section 1.5.1). It was therefore hypothesised that dose- and direction-controlled tDCS would increase $M1_{hand}$ excitability in neurotypical participants, while greater variability and lower predictability of outcomes were expected in the chronic stroke survivor group.

3.2 Methods.

3.2.1 Overview.

Individual structural MRI scans were used for current flow modelling (Figure 3.1A), to determine the tDCS stimulator output required to deliver 0.185 V/m E-field to $M1_{hand}$ in each participant. Participants then attended two sessions in which real and sham tDCS were applied in a pseudo-randomised order. TMS recruitment curves were collected before, during and after tDCS intervention, and a wildlife documentary was played throughout sessions to counter participant fatigue (Figure 3.1B). The project was approved by the UCL Research Ethics Committee (project ID: 18/0441).

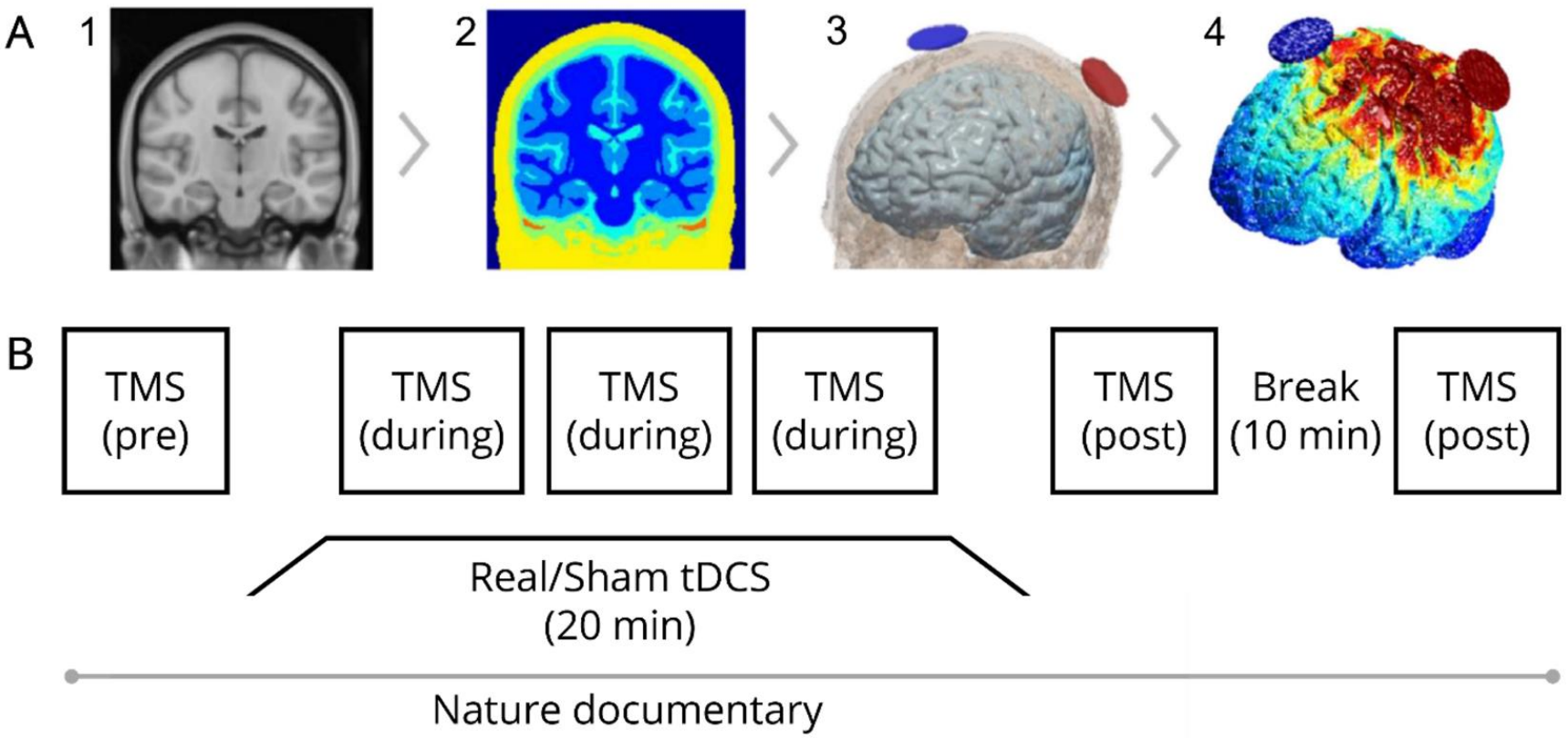

Figure 3.1. Study design. A) Current flow model simulation pipeline using ROASTV2.7: structural MRI scans (A1) were segmented into 8 tissues (A2) electrodes were applied (A3) and the FEM was solved (A4) to simulate current flow during PA-tDCS in each participant. B) Experimental design. TMS recruitment curves were collected before, during, and after 20 minutes of real or sham tDCS application. A nature documentary was played throughout the experiment to counter participant fatigue.

3.2.2 Inclusion criteria.

Inclusion criteria for stroke survivors were: first-time hemiparetic stroke, upper limb motor impairment, presence of voluntary flickers of finger extension on the affected hand, > 18 years old, no history of neurological disease, no history of craniotomy or other neurosurgery, able to give informed consent, no medication known to modify seizure threshold or other contraindications to TMS or tDCS such as metallic implants in the skull, implanted pacemaker or a history of seizures, no contra-indications to MRI, and able to access 2 experimental sessions of approximately 3-hour duration. Pre-pandemic criteria included stroke survivors any time since stroke, revised to recruitment of chronic stroke survivors only as hospital access was limited by coronavirus safety restrictions. Examples of safety screening forms, participant information sheets and consent forms are included in Appendices A-D. Stroke survivors were screened over the phone, via email, or in person in the Hyper-Acute Stroke Unit (HASU) at the National Hospital for Neurology and Neurosurgery (NHNN).

3.2.3 Participants.

Four hundred and thirty-three stroke survivors, and 120 neurotypical participants were screened for inclusion in this study. Of these, 18 chronic stroke survivors (age = 58.9 ± 8.46, 5 females) and 21 neurotypical participants (age = 56.2 ± 14.6, 10 females) completed participation. The high exclusion rate was due primarily to a previously planned version of the study, before access restrictions due to the pandemic, which included recruitment of stroke survivors in the acute stage of stroke to facilitate data collection in the sub-acute phase. Stroke survivors in the acute stage of stroke were therefore routinely screened and approached for consent to take part in the study, with researchers requesting they return within months of discharge from hospital to take part. Primary reasons for exclusion in these cases were lack of capacity to consent, inaccessibility of the study which required 2 experimental sessions of approximately 3-hour duration and an MRI scan, and loss of contact as patients returned home, were moved to alternative facilities, or ceased responding over the pandemic period. Other reasons for exclusion included severity of motor deficit (absence of voluntary flickers of finger extension was taken as a predictor of MEP-negative status), previous history of stroke, and contraindications to MRI at the Wellcome Centre for Human Neuroimaging (WCHN). In the neurotypical group, primary

reasons for exclusion included the distance between potential participants' homes and the research facilities located in London, contraindication to MRI, and loss of contact over the pandemic period.

3.2.4 Clinical information.

Stroke survivors' motor impairment was measured during one experimental session using the Fugl-Meyer assessment of the upper limb (FM-UL; Fugl-Meyer et al., 1975), which was administered by researchers. A video of the assessment was recorded, with consent, for accurate scoring after study sessions.

3.2.5 MRI scans

Individual structural MRI scans were obtained before tDCS was applied. Where possible, existing MRI scans are used. Participants who did not already have a $1mm^3$ resolution T1 or T2-weighted MPRAGE MRI scan of sufficient quality for tDCS current flow modelling were scanned at the Wellcome Centre for Human Neuroimaging, on a 3T scanner (SIEMENS, Trio) with a 32-channel head coil. MRI scans were anonymised by removal of the header using MRIcroN software (NITRC: MRIcron: Tool/Resource Info), since anonymisation by defacing would alter tissue segmentations necessary for current flow modelling.

3.2.6 TDCS simulation.

ROAST v2.7.1 (Huang, Datta, et al., 2018; Huang et al., 2019) was used for tDCS current flow modelling. A PA-tDCS montage was simulated on the ipsilesional hemisphere of stroke survivors and the dominant hemisphere of neurotypical participants. Disc electrodes (3cm diameter, 2mm height) were simulated over 10-10 coordinates CP5/CP6 (anode) and F1/F2 (cathode), to target $M1_{hand}$. Thirty voxels of zero-padding were added to ensure tissue did not extend beyond image boundaries. Default conductivity values for each tissue type were used, defined in ROAST as (in S/m): grey matter: 0.276; white matter: 0.126; CSF: 1.65; bone: 0.01; skin: 0.465; air: 2.5×10^{14}; gel: 0.3; electrode: 5.9×10^{7}.

3.2.7 TDCS application.

Participants attended 2 experimental sessions after obtaining a structural MR scan, in which real and sham tDCS are applied in a pseudo-randomised order. During real stimulation, the *individualised dose* of tDCS required to deliver 0.185V/m E-field intensity to $M1_{hand}$ for each

participant was applied for 20 minutes with a 15-second ramp-up and -down to minimise detectable sensation of stimulation on the skin. Sham stimulation comprised of a 15-second ramp up, before stimulation was turned off for the duration of the 20-minute block. MRI scans could not be obtained for 2 stroke survivors and two neurotypical participants during a period of uncertainty associated with the coronavirus pandemic, where study duration was minimised to limit person-to-person contact. In these cases, the group average of *individualised dose* was applied, with tDCS electrodes positioned 7cm anteriorly and posteriorly to the TMS-identified motor hotspot, in the orientation of the TMS coil.

Where MRI scans were available, accurate scalp electrode placement was achieved during study sessions by uploading the segmented tissue masks of skin, electrodes and electrode gel generated by ROAST to Brainsight® TMS Navigation software (Brainbox Ltd.). Each subject's head was calibrated to its virtual counterpart using the Brainsight® Subject Glasses and Pointer in keeping with the manufacturer's instructions, and the pointer was used to locate the centre of each simulated electrode on the participant's scalp. A chinagraph pencil was used to mark anode and cathode positions. Hair was parted in an 'X' shape over electrode positions and skin was prepped using alcohol and NuPrep abraisive gel to minimise impedance, before tDCS electrodes were applied to the scalp. Electrodes were adhered using ~2mm of Ten20 EEG conductive and adhesive paste. Impendence was kept below 5 kΩ in keeping with practical guidelines (DaSilva et al., 2011).

3.2.8 Transcranial magnetic stimulation.

Electromyographic (EMG) Ag/AgCl electrodes were used to record MEPs from the first dorsal interosseous (FDI) muscle of the target hand. An active electrode was placed over the belly of the FDI muscle, a reference electrode on the proximal inter-phalangeal joint of the index finger of the same hand, and a ground electrode on the head of the ulna bone on the wrist. Cushions were used for participant comfort and to stabilise the upper limb during data collection. EMG signals were amplified (1000x), band-pass filtered (3-2500 Hz; D360, Digitimer, Welwyn Garden City, UK), digitised at 5 kHz (CED Power 1401, Cambridge Electronic Design Ltd, UK) and viewed online then saved via Signal software (Version 6.0, Cambridge Electronic Design Ltd).

The hotspot for each participant was determined as the TMS coil position which elicited 50 microvolt (μV) MEPs in 5 of 10 trials. The TMS stimulator output required to achieve this response was recorded as the resting motor threshold (RMT). The hotspot location was marked on each participant's head using a Chinagraph Pencil.

Each TMS block consisted of 48 pulses applied at 6 different TMS stimulator intensities ranging from 90 to 140% RMT in increments of 10%. Eight complete recruitment curves were obtained per block. One TMS block was applied before, 3 blocks during and 2 blocks after stimulation. TMS blocks during stimulation were applied 2, 8 and 14 minutes post-tDCS stimulator ramp up, with a 2-minute break between each block. One block of TMS was applied immediately post-tDCS, and the final block of TMS was recorded after a 10-minute break (Figure 3.1).

3.3 Analysis.

3.3.1 Current flow model data extraction.

Data were extracted from current flow models produced by ROAST using MATLAB (*MATLAB*, 2018). First, individualised ROIs were identified using structural MR scans viewed in MRIcroN software (Rorden & Brett, 2000, retrieved from: www.nitrc.org/projects/mricron). $M1_{hand}$ was visually identified for each participant in keeping with anatomical descriptions in the literature (Caulo et al., 2007; Dechent & Frahm, 2003; Yousry, 1997). MRIcroN's drawing tool (www.nitrc.org/projects/mricron) was then used to create a 1cm diameter spherical ROI, extending outwards from the voxel identified as the centre of individualised $M1_{hand}$. Next, explicit binary masks of grey and white matter tissue masks produced by ROAST were created using SPM12 (0.2 intensity threshold; http://www.fil.ion.ucl.ac.uk/spm/) and combined. Each subject's binary grey and white matter mask was applied to the ROI sphere, to create individualised ROIs for $M1_{hand}$. Finally, E-field data were extracted from individualised ROIs using Matlab's *MarsBaR* toolbox (Brett et al., 2002, retrieved from: https://marsbar-toolbox.github.io/), to derive estimated mean E-field intensity (V/m) in grey and white matter of $M1_{hand}$ when fixed-dose (1 mA) PA-tDCS was simulated in each participant. *Individualised tDCS dose* was reverse-calculated using the formula described above.

3.3.2 MEP processing.

MEP data were pre-processed in MATLAB (*MATLAB*, 2018). Trials were removed if atypical muscle contraction was detected before TMS pulse onset in each trial. Since some stroke survivors experienced mild resting muscle tone in the impaired upper limb, a cut-off value for muscle activity was not appropriate for use across participants. Instead, the average of the root mean square (RMS) of muscle activity up to 100ms before the TMS pulse was calculated for all trials in a given block. Single trials were excluded if RMS muscle activity in the 100ms preceding the TMS pulse exceeded RMS muscle activity for the whole block plus 2 standard deviations. Trials were also discarded if the MEP was indistinguishable from background noise (MEP amplitude ≤ RMS pre-contraction per trial). Or if the TMS pulse failed to fire (TMS artefact amplitude ≤ RMS pre-contraction per trial and MEP amplitude ≤ RMS pre-contraction per trial). All trials of EMG data were then overlayed onto two plots per participant, one depicting data before pre-processing and one after pre-processing, to visually identify unusual inclusion or exclusion of trials. Grubbs' test (Grubbs, 1969) was then used to identify and exclude outliers in stroke and neurotypical data separately.

3.3.2.1 Recruitment curve construction and data extraction.

To construct recruitment curves from MEP data, MEP amplitude at each increment of RMT (90-140%) was averaged per participant, per block. MATLAB's curve fitting tool (https://www.mathworks.com/products/curvefitting.html) was then used to fit a sigmoidal curve to the data. The modified Boltzmann equation (Carroll et al., 2001; Devanne et al., 1997; Iyer & Madhavan, 2019) was used for sigmoidal fit, with the formula:

$$\frac{MEP_{max}}{1 + e^{m(S50-s)}}$$

Where MEP_{max} is the maximum estimated MEP amplitude, S50 is the stimulus intensity at which MEP amplitude is 50% of MEP_{max}, *m* is the slope parameter of the function, and *s* represents TMS stimulator output as a per centage of RMT (90-140%).

In some cases, fitted MEP_{max} values for sigmoidal recruitment curves extended beyond neurophysiologically plausible values. For example, in the data presented in this Chapter, fitted MEP_{max} values exceeded the maximum recorded MEP by ≥1mV in 87 of 467 fitted sigmoidal recruitment curves (18.63% TMS blocks), with adjusted R^2 values counter-

intuitively implying good fit in these cases (M = .89, SD = .16). To avoid inclusion of misleading fitted values, data were constrained to values which reflected experimental conditions (TMS intensities between 90-140% RMT). Linear and exponential curve fits were compared to sigmoidal fit, since the sigmoidal pattern commonly used to describe RCs (Carroll et al., 2001; Carson et al., 2013; Iyer & Madhavan, 2019) may not have optimally represented stroke survivor data constrained to 90-140% RMT in this study (Figure 3.2).

Recruitment curve outcome measures of interest include the gradient of the curve at half-maximum of fitted MEP values (RC_{slope}), the area under the curve (RC_{AUC}) and fitted MEP amplitude at a fixed per centage of RMT (here, 120% of RMT, denoted as $RC_{120\%}$). RC_{slope} was calculated using MATLAB's *gradient* function (https://uk.mathworks.com/help/matlab/ref/gradient.html) and RC_{AUC} was calculated within the range of applied TMS pulses (90-140% RMT) using MATLAB's *trapz* function (https://uk.mathworks.com/help/matlab/ref/trapz.html), which computes the approximate integral of MEP amplitude via the trapezoidal method.

To account for the potentially misleading value of RC_{slope} where a full sigmoidal curve was not represented within 90-100% RMT, $RC_{120\%}$ and RC_{AUC} values are reported. RC_{slope}, RC_{AUC}, and $RC_{120\%}$ are herein collectively referred to as *RC measures of interest*. Larger values of *RC measures of interest* indicate greater excitability of neural structures stimulated by TMS, as they reflect corticomotor output across 90-140% of RMT (Boroojerdi et al., 2001; Carson et al., 2013; Devanne et al., 1997; Iyer & Madhavan, 2019; Potter-Baker et al., 2016; Ridding & Rothwell, 1997; Siebner et al., 2022).

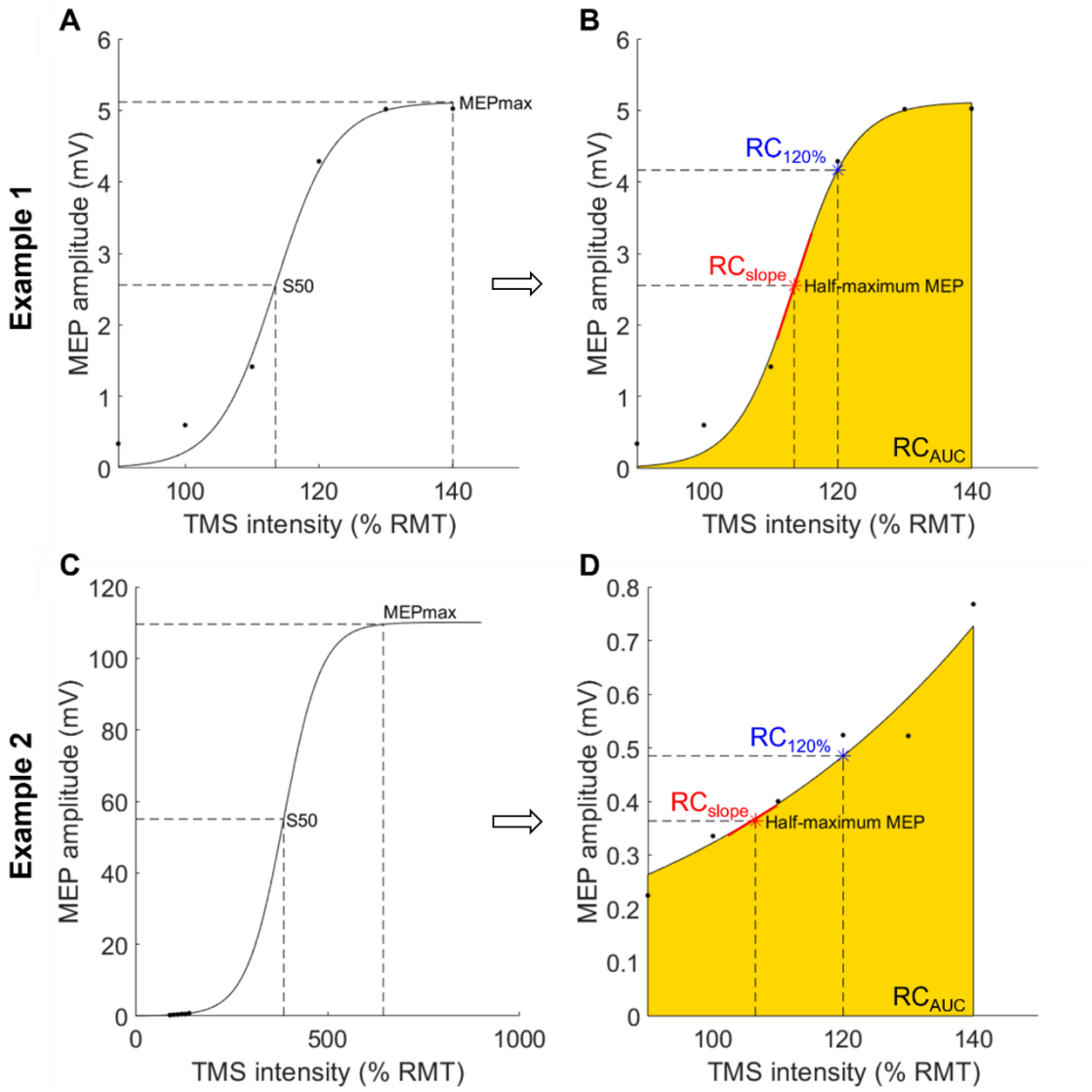

Figure 3.2. Fitted sigmoidal recruitment curve with neurophysiologically plausible values (Example 1: A, B) and implausible values (Example 2: C, D). Black data points represent average MEP amplitude per TMS intensity for one RC block, and black lines are fitted sigmoidal curves. On the left (A, C) are full fitted sigmoids and black data points for examples 1 and 2. On the right (B, D) the same curves are shown, constrained to TMS intensities used in experimental sessions (90-140% RMT). RC_{slope} is shown in red, reflecting the tangent of the recruitment curve slope at half MEP_{max} within 90-140% RMT range. RC_{AUC} within TMS intensities 90-140% RMT is shown in yellow. $RC_{120\%}$ is depicted by a blue star. ***Example 1.*** *A) Averaged MEP values are well-fitted to the full sigmoidal recruitment curve. Fitted S50 and MEP_{max} values are neurophysiologically plausible. B) Fitted data extracted from A. RC_{slope} is representative of gain in the centre of the full sigmoid, fitted $RC_{120\%}$ is similar to the recorded value, and RC_{AUC} reflects the area under the full recruitment curve.* ***Example 2.*** *C) Averaged MEP values fall at the base of the fitted recruitment curve, with implausible S50 and MEP_{max} fitted values. Fitted TMS intensities extend beyond experimental protocol (TMS intensity >140% RMT). D) Fitted data extracted from C, constrained to values which reflected experimental protocol (TMS intensities between 90-140% RMT). RC_{slope} does not represent the maximum gain of the sigmoid, fitted $RC_{120\%}$ is similar to the recorded value, and RC_{AUC} reflects the area under available data well, but not the area under the full recruitment curve.*

3.3.3 Statistical analyses.

First-order polynomial (linear), one-term exponential, and sigmoidal curves were compared for fit with recruitment curve data, with the coefficient of determination (R^2) provided by MATLAB's fitting function used to measure of goodness of fit (Iyer & Madhavan, 2019).

Values for *RC measures of interest* above the 75th, or below the 25th per centile plus three times the inter-quartile range were identified as extreme outliers and removed from analyses. Separate linear mixed effects models for stroke and neurotypical groups were first constructed to compare *RC measures of interest* collected during- and post-tDCS to baseline, to determine whether the tDCS intervention was effective. *Block* (pre-, during-, and post-tDCS) and *condition* (real- or sham-tDCS) were included as fixed effects, with a random intercept per *participant* to account for non-independence of data between sessions, using the formula:

$$RC\ measure\ of\ interest \sim Block \times Condition + (1|Participant)$$

If an effect of tDCS was detected, data collected during- and post-tDCS was normalised to baseline using the following template formula:

$$100 \times \frac{RC\ post\text{-}tDCS}{RC\ pre\text{-}tDCS}$$

Normalised stroke and neurotypical data would then be combined to compare the impact of tDCS between groups and tDCS conditions, using the formula:

$$Normalised\ RC\ measure\ of\ interest \sim Group \times Block \times Condition + (1|Participant)$$

3.4 Results.

3.4.1 Descriptive statistics.

Slightly higher tDCS *individualised dose* was required in the stroke group (M = 1.20, SD = 0.27mA) compared to the neurotypical group (M = 1.08, SD = 0.22 mA), to deliver *target E-field (0.185 V/m)* to $M1_{hand}$. In the stroke survivor group, 12 participants had mildly impaired upper limb movement, 2 were moderately impaired and 2 were severely impaired (FM-UL: Mean = 60, SD = 13.96). Fugl-Meyer data were not collected for 2 participants due to

session time constraints (anecdotal notes taken imply these participants experienced mild upper limb impairment, evidenced by a broad range of voluntary movement). Average time post-stroke was 49.81 months (Range = 5.62 – 136.60 months, SD = 39.95 months). TDCS *actual E-field* and *individualised dose* data are presented in Table 3.1, along with FM-UL scores and time post-stroke for each participant, where applicable.

Table 3.1. CFM and clinical data for stroke survivors (S) and neurotypical (N) participants. Actual E-field recorded in $M1_{hand}$ when a fixed-dose tDCS protocol was simulated, individualised dose required to achieve target E-field (0.185 V/m) in $M1_{hand}$, days post-stroke, and FM-UL scores reflecting upper-limb impairment are shown where applicable. A FM-UL score of 66 represents no upper limb impairment.

ID	TDCS *Actual E-field* in $M1_{hand}$, pre-individualisation (V/m)	TDCS *individualised dose* (mA)	Days post-stroke	FM-UL (no impairment = 66)
S1	0.18	1.05	984	59
S2	0.15	1.25	406	55
S3	0.18	1.05	2361	44
S4	0.16	1.18	851	60
S5	0.19	0.98	2038	56
S6	0.18	1.03	764	31
S7	0.2	0.9	243	49
S8	0.17	1.07	363	53
S9	NA	1.06*	221	NA
S10	0.09	1.98	3541	43
S11	NA	1.17*	2508	15
S12	0.16	1.18	1039	18
S13	0.11	1.62	2236	57
S14	0.12	1.55	3135	58
S15	0.19	0.98	883	30
S16	0.13	1.4	4155	50
S17	0.17	1.1	171	47
S18	0.16	1.18	999	NA
N1	0.15	1.2	-	-
N2	0.16	1.18	-	-
N3	0.18	1.03	-	-
N4	0.15	1.2	-	-
N5	0.17	1.12	-	-
N6	0.24	0.78	-	-
N7	0.13	1.43	-	-
N8	0.13	1.45	-	-
N9	0.19	0.98	-	-
N10	0.12	1.5	-	-
N11	0.19	0.98	-	-
N12	0.2	0.92	-	-
N13	0.21	0.88	-	-
N14	0.21	0.88	-	-
N15	NA	1.11*	-	-
N16	0.14	1.28	-	-
N17	NA	1.12*	-	-
N18	0.23	0.83	-	-
N19	0.18	1.03	-	-
N20	0.24	0.78	-	-
N21	0.17	1.12	-	-

* Cumulative group average of tDCS *individualised dose* was used for participants where MRI scans were unavailable. NA = information not available

3.4.2 Cortico-spinal excitability pre-tDCS was lower in chronic stroke survivors than neurotypical participants.

3.4.2.1 Recruitment curves were shallower for chronic stroke survivors.

Sigmoidal fit was optimal for RCs, as demonstrated by grand mean r-squared values for stroke survivor data (Sigmoidal fit R^2 = .91, SD = .12; linear fit R^2 = .85, SD = .13; exponential fit R^2 = .84, SD = .15), and neurotypical data (Sigmoidal fit R^2 = .95, SD = .06; linear fit R^2 = .88, SD = .07.; exponential fit R^2 = .86, SD = .10). Poorly fitting RCs (R^2 <.4) were excluded from analyses (<2%).

Baseline RC data for both experimental sessions were combined after no difference was detected within groups (two-way ANOVA: RC_{AUC}, F(1,72) = .45, p = .50; RC_{slope}, F(1,71) = .02, p =.88; $RC_{120\%}$, F(1,71) = .05, p = .82). Data were non-normally distributed in the stroke group (Shapiro's test: RC_{AUC} = .85, p = .01; RC_{slope} = .76, p <.01; $RC_{120\%}$ = .84, p = .01) and the neurotypical group except for RC_{AUC} data (Shapiro's test: RC_{AUC}= .93, p = .15; RC_{slope}= .88, p = .01; RC_{120}% = .88, p = .01).

High variance was detected in both groups for all *RC measures of interest* (coefficient of variation (CV): RC_{AUC}, stroke = 101, neurotypical = 44; RC_{slope}, stroke = 131, neurotypical = 63.3; $RC_{120\%}$, stroke = 100, neurotypical = 46.6). Though CV values reflected greater variance in the stroke survivor group, the difference in variance between groups did not reach significance (Levene's test: RC_{AUC}, F(1,37) = 1.79, p = .10; RC_{slope}, F(1,37) = .92, p = .34; $RC_{120\%}$, F(1,37) = .93, p = .34).

Unpaired two-samples Wilcoxon tests were used to compare non-parametric baseline RC measures between groups. Group comparison was statistically significant (RC_{AUC}: z = -2.08, p = .02; RC_{slope}: z = -2.11, p = .02, $RC_{120\%}$: z = -2.25, p = .01), whereby significantly lower values for all *RC measures of interest* were detected in the stroke compared to neurotypical group pre-tDCS (median: RC_{AUC}, stroke = 21, neurotypical = 47.6; RC_{slope}, stroke = .02, neurotypical = .09; $RC_{120\%}$, stroke = .47, neurotypical = 1.00; Figure 3.3A-C).

3.4.2.2 RMTs were higher and more variable for chronic stroke survivors.

RMT did not differ significantly between sessions within participants (paired samples t-test: stroke, t(18) = .56, p=.58; neurotypical, t(21) = 1.01, p=.32) and so RMT data between

sessions were combined for each participant. RMT data were normally distributed in both groups (Shapira's test >.05). A significant difference in RMT variance was detected between groups (Levene's test = $F(1,76) = 9.24$, $p < .01$), whereby variance was higher in the stroke group (CV stroke = 25.99, CV neurotypical = 19.32). RMTs were significantly higher in the stroke group compared to the neurotypical group (Welch's test: $t(28) = 2.23$, $p = .03$; Figure 3.3D).

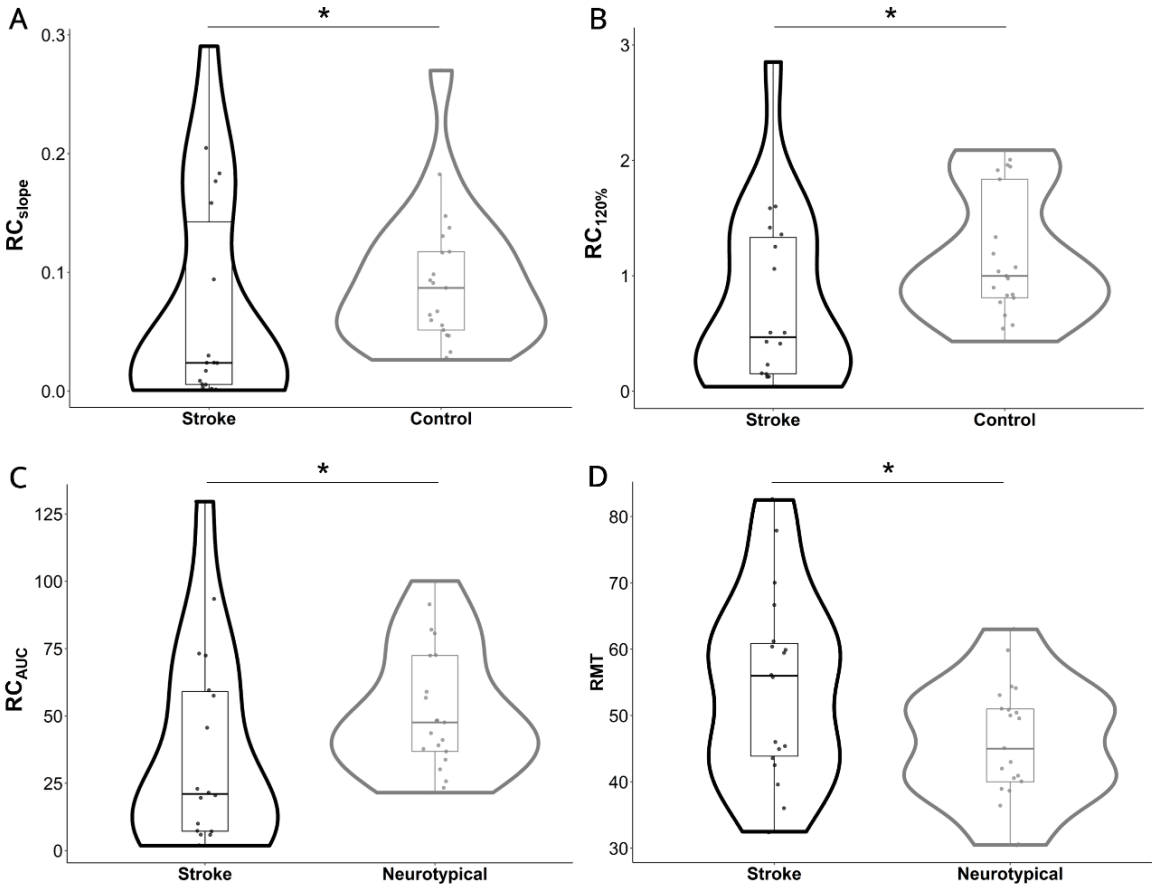

Figure 3.3. TMS-assessed CSE is lower pre-tDCS in stroke survivors than in neurotypical participants. A) RC_{slope}: The gradient of recruitment curves at half MEP_{max} was shallower for stroke survivors than neurotypical participants. Variance did not differ significantly between groups, B) $RC_{120\%}$: MEP amplitude at 120% RMT was smaller in stroke survivors than neurotypical participants, Variance did not differ significantly between groups, C) RC_{AUC}: area under the recruitment curve between 90-120% RMT was smaller for stroke survivors than neurotypical participants, and variance did not differ significantly between groups, D) RMT: resting motor thresholds were significantly higher, and significantly more variable in the stroke survivor group compared to the neurotypical group.

3.4.3 Dose- and direction-controlled tDCS did not significantly alter TMS-assessed CSE.

To interrogate the impact of tDCS, data from stroke and neurotypical groups were first analysed separately. Separate one-way ANOVAs were conducted for each RC measure of interest ($RC_{AU,}$ RC_{slope}, and $RC_{120\%}$). No significant difference in RC data collected during tDCS was found under real or sham conditions ($p>.05$). Blocks of data from 3 blocks collected during tDCS under each condition were therefore combined.

Separate LMMs were constructed for each *RC measure of interest* ($RC_{AU,}$ RC_{slope}, and $RC_{120\%}$). No significant difference in RC measures recorded in blocks pre-, during-, and post-tDCS under both tDCS conditions was found in the neurotypical group (RC_{AUC}, $F(3,135) = .52$, $p = .67$; RC_{slope}, $F(3,133) = .17$, $p = .91$; $RC_{120\%}$, $F(3,135) = .72$, $p = .54$) or the stroke survivor group, (RC_{AUC}, $F(3,111) = 1,13$, $p = .34$; RC_{slope}, $F(3,113) = .65$, $p = .58$; $RC_{120\%}$, $F(3,107) = .73$, $p = .58$; Figure 3.4). No significant interaction was detected between tDCS condition (real/sham) or block (pre-, during-, or post-tDCS) in the neurotypical group (RC_{AUC}, $F(3,135) = .14$, $p = .94$; RC_{slope}, $F(3,133) = .19$, $p = .90$; $RC_{120\%}$, $F(3,136) = .49$, $P = .69$) or the stroke survivor group (RC_{AUC}, $F(3,111) = .44$, $p = .72$; RC_{slope}, $F(3,113) = 1.28$, $p = .29$; $RC_{120\%}$, $F(3,107) = .66$, $p = .58$).

$RC_{120\%}$ values were persistently significantly higher in the neurotypical compared to stroke survivor group regardless of block or condition, while group comparison was non-significant for other *RC measures of interest* (RC_{AUC}, $F(1,37) = 3.62$, $p = .06$; RC_{slope}, $F(1,37) = 1.59$, $p = .22$; $RC_{120\%}$, $F(1,37) = 6.41$, $p = .02$; Figure 3.4A-C). Due to ineffectiveness of the tDCS intervention, analyses were not expanded on.

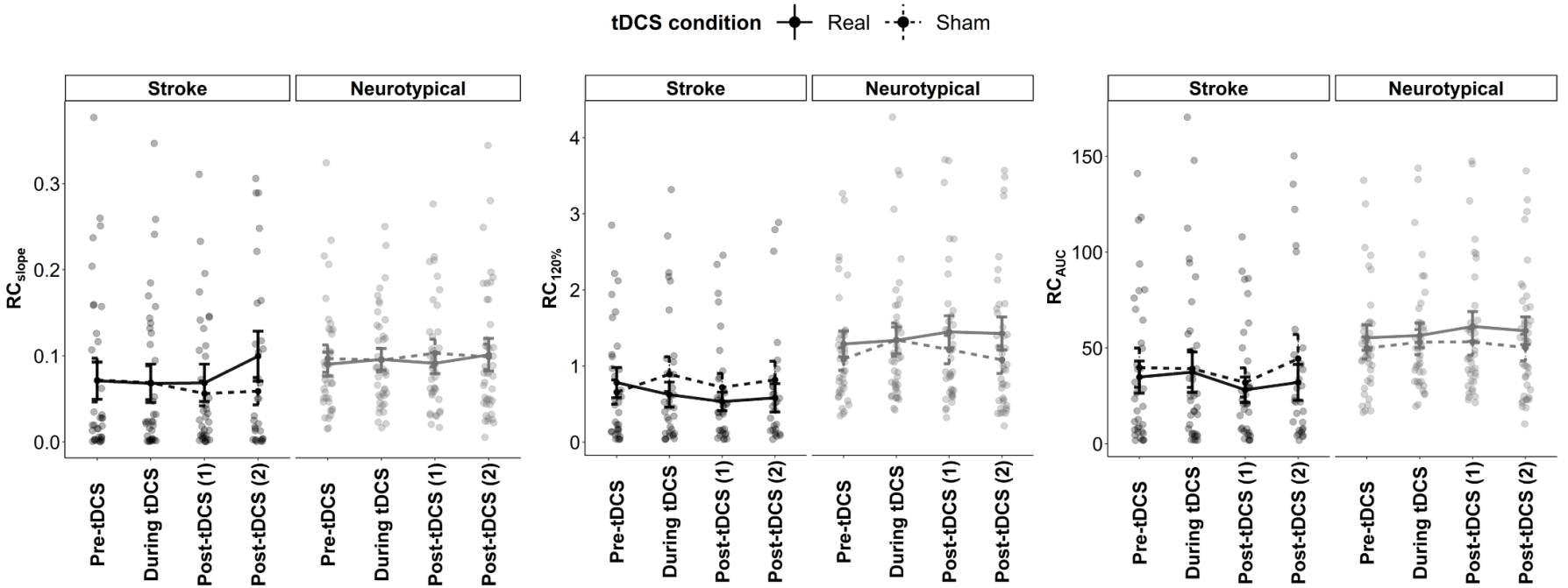

Figure 3.4. Recruitment curve measures of interest collected pre-, during, and post-tDCS show no significant impact of dose- and direction-controlled tDCS. Stroke survivor data are shown in black, and neurotypical data in grey. Solid lines depict data collected under the real-tDCS condition, dotted lines show sham-tDCS data. Error bars show standard error. A) RC_{slope}: no significant difference between blocks in the neurotypical group ($F(3,133) = .17$, $p = .91$) or the stroke survivor group, ($F(3,113) = .65$, $p = .58$). B) $RC_{120\%}$: No significant difference was detected in $RC_{120\%}$ between blocks in the neurotypical group ($F(3,135) = .72$, $p = .54$) or the stroke survivor group, ($F(3,107) = .73$, $p = .58$). Fitted MEP amplitude at 120% RMT is persistently lower in the stroke survivor group compared to the neurotypical group ($F(1,37) = 6.41$, $p = .02$). C) RC_{AUC}, no significant difference between blocks in the neurotypical group ($F(3,135) = .52$, $p = .67$) and stroke survivor group ($F(3,111) = 1,13$, $p = .34$).

3.5 Discussion.

In this Chapter, I compared TMS-assessed CSE in $M1_{hand}$ in chronic stroke survivors and neurotypical participants, before, during and after dose- and direction controlled tDCS. The central aim was to determine when plasticity-promoting interventions might be best applied in humans. To this end, tDCS was applied in chronic stroke survivors and neurotypical participants to investigate whether outcomes differed as a function of chronic stroke-induced changes to *functional* and *anatomical brain state*. I found lower CSE in chronic stroke survivors compared to neurotypical participants at baseline, and found no impact of CMF-informed tDCS on CSE in both participant groups. In concurrence with the data presented in Chapter 2, I also found higher variability in RMTs recorded in stroke survivors compared to neurotypical participants.

3.5.1 Functional brain state differed in chronic stroke survivors compared to neurotypical participants.

In this study, a difference in *functional brain state* was detected between groups, whereby TMS-assessed CSE at baseline was significantly lower in chronic stroke survivors than neurotypical participants. This finding concurs with a recent meta-analysis of data from 112 stroke survivors and 112 neurotypical participants from 9 studies (McDonnell & Stinear, 2017), which reported lower MEP amplitude and higher RMT in both sub-acute and chronic stroke. This persisting atypical excitatory-inhibitory balance is in contention with the temporal framework set out by The Stroke Round table consortium (Bernhardt et al., 2017) which posits that brain activity returns to neurotypical levels in the chronic phase of stroke. Since tDCS is state-dependent (Reato et al., 2010, 2013; Terzuolo & Bullock, 1956) it was hypothesised that application in different post-stroke phases characterised by fluctuations in brain state, may produce different effects. The findings presented here suggest that this approach is too coarse; categorising survivors into post-stroke "phases" may not adequately reflect the endogenous excitability of a target network. As discussed in Chapter 2 for example, the trajectory of brain state fluctuations after stroke may be as heterogeneous as the motor recovery timeline (Bonkhoff et al., 2022; van der Vliet et al., 2020), and so application of tDCS in one post-stroke phase over another may not constitute optimal timing of the intervention.

Since pre-clinical work converges to suggest that interventions which boost excitability and reduce inhibition are beneficial for post-stroke recovery (for reviews, see (Cramer, 2008; Di Pino, Pellegrino, Assenza, et al., 2014; Joy & Carmichael, 2020; Krakauer & Carmichael, 2017b), I suggest that individualised detection of periods of low CSE may be required for optimised timing of the tDCS intervention. A state-dependent approach to neuromodulatory intervention after stroke may be more effective than pursuing an answer to questions such as "in which post-stroke phase is tDCS best applied?".

3.5.2 TDCS individualisation does not equate to optimisation.

Interestingly, a detectable difference in functional brain state between groups did not equate to a detectable difference in response to tDCS, which produced no change in TMS-assessed CSE. I note that while CFMs may have successfully individualised the intensity and direction of current flow in $M1_{hand}$, individualisation does not equate to optimisation. The PA-tDCS montage was selected for use in this study because previous work has demonstrated the impact of the direction of estimated current flow across $M1_{hand}$, controlled by electrode montage, on MEP amplitude (Evans et al., 2022; Rawji et al., 2018). These studies built on preclinical work which demonstrated the determinant effect of E-field direction relative to the somato-dendritic axes of affected cells on neuronal membrane polarisation (Berzhanskaya et al., 2013; Bikson et al., 2004; Chan et al., 1988; Farahani et al., 2021; Radman et al., 2009; Rahman et al., 2013). While selection of the PA-montage used here is supported by this rationale, comparison of its efficacy relative to conventional tDCS (anode positioned on the scalp directly above a cortical target) was not interrogated and is recommended for future work. The aim of this study was only to interrogate the efficacy of tDCS applied in chronic stroke survivors compared to neurotypical participants.

Since no significant effect of PA-tDCS was detected in both the neurotypical and stroke survivor groups, in the following section I consider the intensity, direction and focality of E-fields induced with the PA-tDCS montage, and discuss why they did not result in significant neuromodulation in either group.

3.5.2.1 The optimal dose of tDCS remains unknown.

Despite use of an *individualised dose* of tDCS to ensure *target E-field* was achieved in $M1_{hand}$ across participants, TMS-assessed CSE was not significantly altered by tDCS. A *target E-field*

intensity of 0.185 V/m was selected because on average, 1 mA conventional tDCS produced 0.185 V/m E-field in $M1_{hand}$ in simulations previously conducted with MR scans of 50 neurotypical adults (Evans et al., 2020). However, the optimal E-field intensity required for behaviourally meaningful alteration of neuronal activity remains unknown. Importantly, there is no minimum tDCS-induced electric field which is inert, by virtue of the linear relationship between exogenous fields and transmembrane polarisation (Bikson et al., 2004). Bikson and colleagues (Bikson et al., 2004, 2019) point out that tightly controlled preclinical experiments which suggest fields as low as 0.2 V/m may alter cellular excitability (Reato et al., 2010) are easily misinterpreted, as minute yet statistically significant differences observed in a controlled experimental system do not represent the lowest E-field intensity required to meaningfully modulate neuroplasticity. Rather than identifying a single E-field intensity such as 0.185 V/m to optimally target an ROI, progress in optimising tDCS dose will depend on increased understanding of why applied fields produce a given effect, in a given brain environment. Optimal dose may itself require individualisation, instead of standardization, in humans. In other words, since more tDCS-induced E-field will not produce more neuroplasticity (Esmaeilpour et al., 2018), research efforts are best directed to understand why, and to facilitate informed tDCS use to manipulate parameters important for modulating plastic potential in each individual.

CFMs do not yet have the capacity to determine the *individualised dose* required to modulate neuroplasticity, as they are agnostic to the physiological outcomes of stimulation. While the intensity of E-field required to modulate activity remains unknown, so too does the optimal state of network activation required to alter potentiation of a motor task; researchers are not only blind to how much to “put in” to a target neuronal system, but also of how much one might hope to “get out”. The multivariate nature of the tDCS optimisation problem produces uncertainty when considering factors which might contribute to variable outcomes. In this study, for example, optimal current direction may have been achieved in $M1_{hand}$ without sufficient field strength to produce a detectable change in MEP amplitude. Standardisation of tDCS protocol across the literature is needed to mitigate this problem. In the absence of a detailed understanding of the cellular and network mechanisms of tDCS and their relationship with human behaviour, progress may be facilitated in the interim by

systematic prioritisation of controllable E-field characteristics via CFM use. This goal is presently within reach, and the parameter space has not yet been fully explored.

3.5.2.2 PA-tDCS may not sufficiently optimise current direction in $M1_{hand}$.

While the optimal intensity of E-field required for effective neuromodulation is unknown, the optimal direction of tDCS-induced E-field has been described. As discussed previously, maximal neuronal membrane polarisation by DC field occurs when the direction of current flow is parallel to the somato-dendritic axes of target pyramidal cells (Berzhanskaya et al., 2013; Bikson et al., 2004; Chan et al., 1988; Farahani et al., 2021; Radman et al., 2009; Rahman et al., 2013). Since it is impractical to attempt to control the direction of transcranially-applied current relative to all pyramidal neurons in $M1_{hand}$, the cortical surface is used as a proxy for the predominant orientation of pyramidal cells in grey matter (Lafon et al., 2017; Rahman et al., 2013). Achieving radial-inward current flow with respect to the surface of the cortex is expected to produce maximal somatic depolarisation of cortical pyramidal neurons, and in turn, shift the balance of the neuronal population towards excitability.

Here, a PA-tDCS montage was used to produce radial-inward current flow in $M1_{hand}$. In a recent study which compared tDCS montages, Evans and colleagues (Evans et al., 2022) reported that while PA-tDCS was associated with the most consistent direction of current in $M1_{hand}$ compared to other montages, high variability in current direction between participants did persist when PA-tDCS was applied. This may be due to individual differences in cortical folding; anatomical differences have been shown to cause local fluctuations in the path of current flow (Dmochowski et al., 2012; Gomez-Tames et al., 2020; Kashyap et al., 2022).

The impact of PA-tDCS on TMS-assessed CSE has been investigated previously. Rawji and colleagues (Rawji et al., 2018) not only reported greater consistency in current direction in $M1_{hand}$ when PA-tDCS was applied, but also found a consistent reduction in MEP amplitude after PA-tDCS application. This finding is contrary to predictions of increased cortical excitability associated with radial-inward current in $M1_{hand}$ (Berzhanskaya et al., 2013; Bikson et al., 2004; Chan et al., 1988; Farahani et al., 2021; Radman et al., 2009; Rahman et al., 2013), which is expected to result in increased MEP amplitude. Elsewhere, performance

on learning retention for a ballistic movement task was reportedly not altered by PA-tDCS, while AP-tDCS was significantly associated with impaired learning retention (Hannah et al., 2019). While I note that tDCS-induced E-field intensity was not individualised in either study, both support recent findings which suggest that polarity-specific polarisation of the somatic compartment of affected cells does not comprise a full description of the effects of DC field on neuronal polarisation. Bikson and colleagues (Bikson et al., 2019) point out that the "somatic doctrine" (Bikson et al., 2004; Bindman et al., 1964; Purpura & McMurtry, 1965; Radman et al., 2007) does not extend to describing the impact of DC fields on non-somatic neuronal compartments, other cell types, synaptic efficacy, network activity, or neuroplasticity. For example, DC fields have long been known to impact interneuron excitability (Kabakov et al., 2012; Purpura & McMurtry, 1965), and the network effects of tDCS may have an indirect influence on tDCS outcomes measured from a relatively small ROI, such as $M1_{hand}$ (Polanía et al., 2010; Reato et al., 2010). The macroscopic effects of applied current may explain the counter-intuitive and varied outcomes associated with PA-tDCS; even if radial-inward current flow is achieved in $M1_{hand}$, it may not reliably increase TMS-assessed CSE as predicted. While further research is required to elucidate the varied effects of DC fields in the brain, I note that the benefit of an increased understanding of the cellular mechanisms of tDCS is limited by the inherent non-focality of the technique. It is for example possible that the somatic doctrine optimally explains the impact of tDCS, but that using the cortical surface as a proxy for the direction of transcranially-applied current relative to single neurons is not sufficient to optimise current direction, to modulate complex human motor control.

3.5.2.3 The impact of spatially distributed tDCS-induced E-field is not accounted for.

While CFMs were used to individualise the intensity and direction of tDCS-induced E-field in this study, the spatial distribution of E-field was not constrained. The impact of focality on tDCS efficacy has not yet been established, and the concept that tDCS will have a maximal impact on brain networks which are already active (functional selectivity; Bestmann et al., 2015; Bikson & Rahman, 2013; Ranieri et al., 2012) implies that controlling for brain state may be more effective than controlling the spatial spread of induced fields. However, standardising E-field distribution between participants may be desirable to simplify interpretation of tDCS outcomes. Again, the multi-variate nature of the optimisation problem is highlighted here: in keeping with Ohm's law, individualisation of tDCS stimulator

output to achieve dose-control will exacerbate inter-individual differences in the spatial distribution of tDCS-induced E-fields. A higher *individualised dose* will result in greater spread of E-field above a given threshold, and vice versa for participants who require lower *individualised dose* to achieve standardised *target E-field* in $M1_{hand}$.

Furthermore, the neuromodulatory effects of distributed current in structures which are functionally connected to an ROI, though spatially distinct, could be non-trivial (Boros et al., 2008; Kirimoto et al., 2011; Lang et al., 2005). For example, while predominantly radial-inward current flow is produced in $M1_{hand}$ when a PA-tDCS montage is applied, radial-outward current flow is simultaneously produced in the primary sensory cortex (S1) positioned on the posterior bank of the central sulcus (Evans et al., 2022). M1 and S1 are intimately connected nodes within the sensorimotor network, evidenced in studies showing that peripheral sensory stimulation can modulate corticomotor excitability and in turn MEP size (Kaelin-Lang et al., 2002; Kojima et al., 2019; Ridding et al., 2000; Ridding & Taylor, 2001). The PA-tDCS montage used in this study may have oppositely polarised neurons in M1 and S1, confounding the TMS-assessed response to tDCS. I note however that this has not yet been formally investigated, and preclinical work suggests that opposite polarisation of neighbouring structures does not 'cancel out' stimulation effects, because the excitatory effect of radial-inward DC field is more robust than inhibition associated with radial-outward current flow (Lafon et al., 2017; Rahman et al., 2013; Reato et al., 2013).

Taken together, it cannot be ruled out that the inefficacy of tDCS reported in this study may be due to sub-optimal control of the intensity, direction, and focality of tDCS-induced fields, or variability in endogenous network activity between individuals. Neuron-specific control of these parameters is currently beyond the scope of available CFM software, though improved understanding of tDCS mechanisms may allow researchers to realise the full potential of CFMs, by virtue of informed decision-making when considering the parameter space for applied fields.

3.5.3 Higher tDCS intensity is required for individuals with stroke-induced anatomical changes.

Finally, I note that higher *individualised dose* of tDCS was required for stroke survivors compared to neurotypical participants. According to Ohm's law, this may produce a

systematic difference in the focality of stimulation between groups; as discussed above, higher *individualised dose* will result in greater distribution of fields above a given threshold throughout the brain. This is an intuitive example of difficulties associated with translating tDCS optimised for the neurotypical brain to clinical populations.

Differences in anatomical brain state between stroke survivors and neurotypical participants, such as the presence of lesions, grey matter atrophy and enlarged ventricles (Skriver et al., 1990), may explain the need for higher *individualised dose* in the stroke group. Higher variability in tDCS E-field has been reported in populations with increased CSF thickness associated with cortical atrophy (Antonenko et al., 2018; Laakso et al., 2015; Mahdavi & Towhidkhah, 2018; McCann & Beltrachini, 2021; Opitz et al., 2015), and converging evidence suggests that current can be canalised through brain structures with high CSF density, such as stroke lesions and ventricles, and away from grey matter in an ROI (Gomez-Tames et al., 2020; Johnstone et al., in review; Kashyap et al., 2022; Minjoli et al., 2017; Piastra et al., 2021). Diversion of tDCS-induced current flow away from $M1_{hand}$ and towards structures with higher CSF density may explain the requirement for higher tDCS *individualised dose* in stroke survivors compared to neurotypical participants. This theory is considered in detail in the following Chapter, where the impact of stroke-induced anatomy changes on tDCS-induced E-field is investigated.

3.5.4 Conclusion.

Previous work addressing variable tDCS outcomes has been limited by a lack of computationally-informed, standardised protocol design, which prevented interrogation of tDCS-induced E-field produced by a given protocol. Outcome variability in these cases may be mirrored, at least in part, by variability in applied current. The inefficacy of the CFM-informed tDCS protocol used in this Chapter does not negate the promise of the technique as a neuromodulatory tool with far-reaching applications. Rather, it constitutes a step towards transparent, mechanistically-informed tDCS study design which in turn allows better interrogation of factors which may contribute to variable tDCS effects.

Further preclinical work is needed to better understand the impact of DC fields on varied neuronal structures, and detailed reporting of estimated intensity, direction and focality of

tDCS-induced fields is needed when available, to bridge the gap between understanding of the physics of current flow and its impact on behaviour.

This work has begun, and research describing a relationship between E-field intensity in a cortical target and physiological outcomes suggests that we are on the right track (Antonenko et al., 2019; Laakso et al., 2019; Mosayebi-Samani et al., 2021; Nandi et al., 2022). A target for further research is identifying conditions under which tDCS has been effective, including positive results reported after conventional tDCS application, to develop methods for reliable replication. In the context of this thesis, this may involve interrogation of E-field properties including the intensity and direction of extra-cellular current which might give rise to MEP modulation by tDCS in humans. Horvath and colleagues (Horvath et al., 2015), for example, reported that MEP amplitude is sensitive to modulation by conventional tDCS, and research to understand the induced E-field properties underlying this effect is encouraged. However, Horvath and colleagues (Horvath et al., 2015) also noted that the effect has been decreasing significantly since the year 2000, and that more reliable TMS measures of CSE, believed to be underpinned by similar neural mechanisms (e.g. SICI) have shown no significant modulation by tDCS (Horvath et al., 2015). In order to address the issue, two lines of investigation are appropriate: interrogation of the E-field properties which might explain positive outcomes observed with conventional tDCS. Second, continued research into the mechanistic underpinnings of tDCS, and how they might best be integrated into innovative protocol design.

Importantly, it remains unclear how the outcomes of this research will translate to the stroke survivor community, where stroke-induced changes to *functional* and *anatomical brain state* must be directly accounted for, instead of translating neurotypically-informed protocol optimisation to the pathological brain.

CHAPTER 4. THE IMPACT OF STROKE LESIONS ON TDCS-INDUCED ELECTRIC FIELD

4.1 Introduction

In Chapters 2 and 3 of this thesis I considered how the *functional state* of the brain after stroke, quantified by TMS-assessed ICI and CSE, might be accounted for in tDCS study design. Here, I consider the impact of stroke-induced changes in *anatomical state* may impact tDCS-induced fields in the brain. Current flow modelling is used to investigate the impact of lesion size, location and distance from $M1_{hand}$ on exogenous E-field, and the findings are compared to a large neurotypical sample. The primary aim of this work was to consider stroke-specific anatomical factors which might contribute to tDCS outcome variability, to better understand how they might be accounted for in an optimised protocol.

4.1.1 The impact of 'real' brain lesions on tDCS-induced current flow is unknown.

Previous studies investigating the impact of stroke lesions on tDCS current flow have been limited by small sample size or the use of simulated lesions which may not reflect realistic morphology (Datta et al., 2011; Galletta et al., 2015; Handiru et al., 2021; Johnstone et al., in review; Minjoli et al., 2017; Piastra et al., 2021); it is not clear if the findings would generalise to the wider stroke survivor population. Simulated lesion work has however provided valuable insights into the systematic impact of lesion-like structures on tDCS E-field delivered to a cortical ROI. For example, Johnstone and colleagues (Johnstone et al., in review) revealed a systematic pattern whereby spherical synthetic lesions positioned in-line with the direction of current flow had the greatest impact on E-field intensity in an ROI. The sign of change in E-field intensity in the ROI was found to depend on the position of the lesion: lesions in the path of current flow between anode and ROI prevented delivery of current to the ROI, possibly due to current being drawn towards conductive lesion tissue instead. Meanwhile, lesions positioned between the ROI and cathode tended to result in increased E-field intensity, as current was drawn through the ROI towards conductive lesion tissue. This effect was significantly modulated by lesion size, distance to ROI, and conductivity. Overall, the presence of synthetic lesions was found to alter E-field intensity

delivered to the ROI by up to 30%, an effect which is not accounted for in CFM based on the neurotypical head.

Elsewhere, modelling work conducted in structural MR scans with real (as opposed to synthetic) brain lesions has reported consistently lower estimated E-field intensity in ROIs when tDCS is simulated in stroke survivors compared to neurotypical participants (Datta et al., 2011; Galletta et al., 2015; Minjoli et al., 2017; Piastra et al., 2021). However, sample size in these studies ranged from 1 to 16 participants, and it is unknown if the impact of brain lesions could be systematically controlled for in tDCS protocol design across the stroke survivor population. In the presented study, CFM was used to estimate the impact of 'real' stroke lesions in 123 stroke survivors, and findings were compared to simulations conducted in 147 neurotypical participants' MR scans.

4.1.2 CFMs do not account for lesioned tissue.

In addition to small sample size, previous work may be limited by the parameters used in CFM, which relies on accurate segmentation and assignment of tissue-specific conductivity values to different tissue types. Typically, lesions have been assigned the same conductivity as CSF (Datta et al., 2011; Dmochowski et al., 2013; Galletta et al., 2015; Minjoli et al., 2017), justified by evidence that CSF eventually occupies lesioned space in the brain (Mestre et al., 2020). However, a magnetic resonance electrical impedance tomography (MREIT) study reported lesion conductivity of approximately 1.2 S/m in a single patient, significantly lower than the conductivity value assigned to CSF by default in ROAST (1.65 S/m; van Lier et al., 2012). In addition, a meta-analysis of human head tissue electrical conductivity values (McCann et al., 2019) reported significant variation in lesion conductivity, with a weighted average of 0.8757 S/m (range = 0.1 – 1.77 S/m) based on data from 14 participants across 3 studies. This value is higher than the weighted average of grey matter (0.466 S/m) and blood conductivity (0.5737 S/m) though significantly lower than the weighted average of CSF (1.71 S/m). In the absence of consensus over the conductivity value of lesioned tissue, the weighted average value reported by McCann and colleagues (0.8757S/m) was applied to lesions in the following study. The impact of lesion conductivity on tDCS-induced E-field estimates has been directly interrogated elsewhere (Johnstone et al., in review; Piastra et al., 2021), with findings suggesting that more conductive lesions have a more exaggerated

impact on current flow than those with lower conductivity, though the pattern of findings remained unchanged.

4.1.3 Controlling for stroke-induced anatomical changes may reduce tDCS outcome variability.

TDCS has already been widely applied in stroke survivors, with reportedly high outcome variability (for reviews, see Elsner et al., 2018; Lefaucheur et al., 2017; Marquez et al., 2015). In these cases, a conventional motor-targeted tDCS protocol is typically applied to patients with upper limb impairment, often by research teams with limited or no access to CFM; a fixed dose and electrode montage is commonly applied across participants. To interrogate E-field characteristics which might contribute to variable tDCS outcomes in these cases, 1mA conventional tDCS is here simulated in structural MRIs of >100 stroke survivors with FM-UL scores reflecting upper limb impairment without paresis (likely candidates for tDCS intervention in clinical settings) and an identical protocol is also simulated in a large sample of age-matched neurotypical participants. Structural MRIs and FM-UL data were generously provided by the ENIGMA (Enhancing NeuoImaging Genetics through Meta-Analysis) Stroke Recovery Working Group (Liew et al., 2020; Liew et al., 2018, 2022), and simulations were completed with an adapted version of ROAST (Huang, Datta, et al., 2018; Johnstone et al., in review), which assigns lesion-specific conductivity values (McCann et al., 2019) to segmented lesion masks. E-field intensity in $M1_{hand}$ was compared in stroke survivor and neurotypical scans, and lesion characteristics were correlated with the findings to determine whether lesions had a systematic impact on tDCS-induced fields when conventional tDCS was applied across participants.

It is hypothesised first that greater variability in tDCS-induced E-field intensity will be detected in $M1_{hand}$ in stroke survivors compared to neurotypical participants. Second, in light of the findings of Johnstone and colleagues, (Johnstone et al., in review) it is hypothesised that current is drawn towards conductive lesion tissue during tDCS, resulting in altered E-field intensity in $M1_{hand}$. It is unknown if lesion size, distance to $M1_{hand}$, or position will systematically impact tDCS-induced fields in the same way as detected in this synthetic lesion work, as 'real' lesion morphology differs substantially to computer-generated spherical structures. If a systematic effect of specific lesion characteristics is

detected, heuristics may be formed to inform clinicians of the potential impact of lesions which fit a given profile on tDCS fields. Accounting for stroke lesions in tDCS protocol via CFM or through heuristics has promise to reduce variability in tDCS-induced fields in the context of stroke, which in turn may increase the reliability of outcomes.

4.2 Methods.

4.2.1 Inclusion criteria.

Structural MR scans were provided by The ENIGMA Stroke Recovery Working Group (Liew et al., 2020; Liew et al., 2018, 2022) for 1,011 stroke survivors and 167 ageing neurotypical participants. Inclusion criteria for stroke survivor scans were: FM-UL score available, >=3 months post-stroke, presence of upper limb motor weakness with some voluntary movement remaining (<66 FM-UL >=28), unilateral cortical or subcortical stroke, manually segmented lesion mask available, 1mm isotropic structural MR scan available. The inclusion criterion for neurotypical scans was: 1mm isotropic structural MR scan available.

4.2.2 Participants.

One hundred and fifty-five stroke survivors satisfied the inclusion criteria. Simulations failed to complete for 17 scans (12 due to poor tissue segmentation, 3 due to poor electric field estimation, 2 due to mis-placed electrodes). Completed simulations were visually inspected for poor tissue segmentation or electrode placement, or unequal resolution across image panes, after which simulations for 16 stroke survivors and 13 neurotypical participants were discarded. Full analyses were conducted in 123 stroke survivor scans from 16 data collection sites and 147 neurotypical scans from 6 sites.

4.2.3 MR scans.

T1-weighted MR Scans from 19 contributing sites were included in this study. Of these, 3 sites provided both stroke and neurotypical data. Three sites used a 3 tesla (3T) Siemens Trio scanner, 3 used 3T GE scanners (1 specified GE Signa Excite scanner type), 1 used a 3T Siemens MAGNETOMÂ Skyra and 1 site used a 3T Philips Achieva. Scanner brand and type were unknown for 4 sites which provided stroke survivor data only, 5 sites which provided neurotypical data only, and 3 sites which provided data for both groups. Image resolution for included scans was 1mm isotropic, slice dimensions varied per site (range: 139-230 axial

slices, 190-256 coronal slices, 194-256 sagittal slices). The ENIGMA dataset included manually segmented lesion masks alongside T1-weighted brain MRIs.

4.2.4 Current flow modelling.

A custom version of ROAST v2.7 (Huang et al., 2019) previously adapted for modelling tDCS with synthetic lesions (Johnstone et al., in review) was adapted here to accept real lesion masks provided by ENIGMA. The modified version of ROAST (herein referred to as 'ROAST-lesion'; Johnstone et al., in review) differs from the original (Huang et al., 2019) because it incorporates lesion masks as a 7th segmented tissue type with a conductivity value of 0.8757 S/m (McCann et al., 2019). In ROAST-lesion, scans undergo default ROAST processing up to the end of the segmentation stage, where the head image is segmented into 8 features (white matter, grey matter, CSF, bone, skin, air, electrodes, and electrode gel) via SPM12 (http://www.fil.ion.ucl.ac.uk/spm/; Figure 4.1A-B). Here, a custom MATLAB function is inserted into the ROAST workflow where lesion masks are added as a 9th segment and subtracted from previously created masks (Figure 4.1C). Subsequent image processing returns to the default ROAST pipeline: virtual electrode placement, volumetric meshing from 3D multi-domain images using *Iso2Mesh* (Fang & Boas, 2009; http://Iso2Mesh.sourceforge.net/cgi-bin/index.cg) to generate the finite element model (FEM), and numerically solving the FEM using *getDP* (https://getDP.info/; Figure 4.1D-E). Default conductivity values provided by ROAST were used for all segment types except lesions (in S/m, white matter: 0.126, grey matter: 0.276, CSF: 1.65, bone: 0.465, skin: 0.126, air: 2.5e-14, electrode gel: 0.3, electrodes: 5.9e7; lesions: 0.8757. Other ROAST settings were as follows: maximum surface element size for generated meshes was 5, minimum angle of surface triangle was set as 20, maximal distance between the centres of the element bounding sphere and surface bounding circle was 0.3, target maximal tetrahedral element volume was 10, and maximal radius-edge ratio was 3.

Conventional tDCS was simulated in ROAST-lesion with 1mA current injected to an anode placed over the 10-10 EEG coordinate for $M1_{hand}$ (C3/C4) on the ipsilesional hemisphere of stroke survivor scans and left hemisphere of neurotypical scans. A cathode (-1mA) was placed contralaterally to the anode on the supraorbital ridge (FP2/FP1). Both electrodes

were disk-shaped (radius 17mm, height 2mm) and 20 voxels of zero-padding were added to each MR image to ensure simulated electrodes did not extend beyond image boundaries.

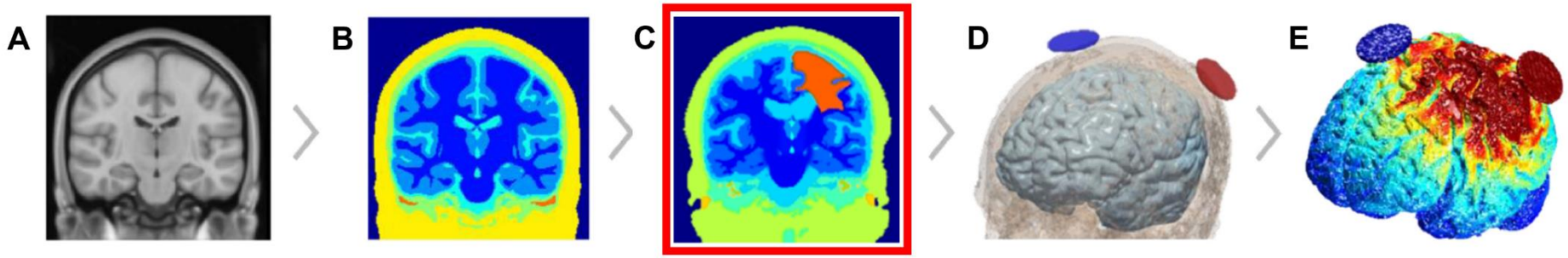

Figure 4.1. Current flow modelling pipeline using ROAST-lesion (Huang et al., 2019; Johnstone et al., in review) A) ROAST requires a structural MR image of an individual participant's head, B) in ROAST, head tissue is segmented into 8 tissue types, calling SPM12, C) ROAST-lesion automatically calls segmented lesion masks which are added as a 7th tissue type using a custom MATLAB script calling SPM12, D) the default ROAST simulation resumes, simulated tDCS electrodes are applied and surfaces are meshed using Iso2Mesh *(Fang & Boas, 2009), E) the FEM is solved using getDP (Dular et al., 1998). Image is adapted from Lee et al., 2021.*

4.2.5 E-field data extraction.

After completion of simulations in ROAST-lesion, output E-field images, structural MR scans and segmented tissue masks were normalised (resampled to 2x2x2mm voxels) into standard space (Montreal Neurological Institute; MNI template) using SPM12 (http://www.fil.ion.ucl.ac.uk/spm/). Scans with right hemisphere lesions were flipped in MATLAB using the *flip_lr* function (Shen, 2022). Normalised grey and white matter tissue masks produced by ROAST-lesion were then used to create explicit binary masks using SPM12 (0.2 intensity threshold), which were then applied to a 1cm diameter ROI sphere centred on MNI coordinates for left $M1_{hand}$ (MNI: −38, −20, 50) based on previous activation likelihood estimations (Eickhoff et al., 2009). Individualised grey and white ROIs are herein referred to simply as $M1_{hand}$. Finally, E-field intensity values in grey and white matter voxels in the ROI were extracted using a custom MATLAB script including SPM's *spm_get_data* command (http://www.fil.ion.ucl.ac.uk/spm/) and averaged to produce an estimate of E-field intensity (in V/m) delivered to $M1_{hand}$ when conventional tDCS protocol is applied.

4.2.6 Lesion characterisation.

Lesion size, distance to an ROI, and location have been reported to significantly alter E-field delivery to an ROI (Handiru et al., 2021; Johnstone et al., in review; Minjoli et al., 2017; Piastra et al., 2021), though a systematic pattern for the impact of 'real' lesions on current flow has not yet been described. Here, I consider intuitive methods to quantify lesion characteristics, with the benefit that recognisable descriptions (for example, "large" or "small" lesions) might improve accessibility of tDCS protocols which account for lesions in clinical settings. Naturally, this approach comes at the cost of precision; advanced machine learning is required to capture the complex characteristics of 3-dimensional (3D) irregularly shaped lesions relative to an ROI and electrodes. In the following I describe methods employed for relatively coarse lesion characterisation, to determine whether the findings reported in controlled synthetic lesion study previously conducted by our group (Johnstone et al., in review), might generalise to the stroke survivor population. Since optimal numerical or categorical descriptions for lesion characteristics are unknown, a number of candidate models were constructed using various parameters to describe key lesion characteristics. For example, models including a continuous numerical value representing lesion volume were statistically compared with models including a categorical descriptor of lesion size (the

model selection process is detailed in section 4.3.2.5) to determine which available variables might best describe the impact of stroke lesions on current flow. In the following I describe the data extraction process for descriptors of 3 lesion characteristics of interest: size, distance to $M1_{hand}$ and location.

4.2.6.1 Lesion size.

Lesion volume was extracted for each subject using individual lesion masks provided by ENIGMA (Liew et al., 2020; Liew et al., 2018, 2022), which were normalised to MNI space and binarised with an inclusion threshold of >0.2 intensity using SPM12 (http://www.fil.ion.ucl.ac.uk/spm/). Two methods for expressing lesion size in statistical models were considered. First, lesion size could be represented as a continuous variable (in cm^3) denoted as *Lesion size*$_{continuous}$, where the number of voxels in binary lesion masks with a value greater than zero represented the volume of lesioned tissue in mm^3. This value was divided by 1000 for conversion to cm^3 in keeping with convention in the literature (Sperber & Karnath, 2016). Second, lesions were described by a categorical variable stratified by lesion per centage of the affected hemisphere, denoted as *Lesion size*$_{categorical}$. To identify lesions in each category, individual brain volume was calculated, in cm^3, as the number of voxels greater than zero in a combined binary segmentation of normalised grey matter, white matter, CSF, and lesioned tissue. Hemisphere volume was approximated by halving total normalised brain volume. Lesions occluding ≤1% of hemisphere volume were categorised as 'small', 'mid-sized' lesions were defined as occluding >1% and ≤10% of hemisphere volume, and lesions which occluded >10% of the target hemisphere were categorised as 'large'. Categorisation of lesions relative to hemisphere volume was conducted because it is unknown if these data are representative of the wider stroke survivor population; categories relative to individual heads were therefore preferred over comparison with other scans in the cohort.

4.2.6.2 Lesion distance to $M1_{hand}$.

Two parameters were considered to describe lesion proximity to $M1_{hand}$: the Euclidean distance between the centre of $M1_{hand}$ and the centre of the irregularly shaped 3D lesion, or the Euclidean distance between $M1_{hand}$ and the nearest voxel of lesioned tissue, denoted as *Lesion distance*$_{centre}$ and *Lesion distance*$_{min}$ respectively (Figure 4.2). A custom MATLAB script

was used to calculate vectors extending from the centre of $M1_{hand}$ to each voxel of lesioned tissue using the formula:

$$3D\ coordinate\ for\ each\ voxel\ in\ lesion - 3D\ coordinate\ for\ centre\ of\ M1hand$$

The average of these vectors was then taken to produce a single vector between the centre of $M1_{hand}$ and the centre of the lesion, using the formula:

$$[mean(Vx), mean(Vy), mean(Vz)]$$

Where *V* are vectors with components *x, y,* and *z*. The MATLAB *norm* function was used to calculate the magnitude of the average vector (*Lesion distance*$_{centre}$). The same function was used to calculate the distance between $M1_{hand}$ and each voxel of lesioned tissue. The vector with minimum magnitude was taken to express the minimum euclidean distance between the centre of $M1_{hand}$ and the lesion in 3D space (*Lesion distance*$_{min}$). Instances where the lesion occluded $M1_{hand}$ were represented by a *Lesion distance*$_{min}$ value of zero.

4.2.6.3 Lesion location.

Eleven anatomical descriptors of lesion location were provided in the ENIGMA dataset, for example, lesions were identified as occluding the Basal Ganglia, Occipital lobe, or Parietal Lobe. In the event that a lesion occupied multiple brain regions, multiple anatomical labels were used to describe the lesion's location, resulting in 50 unique location categories for 123 subjects. These data were not sufficiently powered to include anatomical lesion location in statistical models. Lesion location was therefore expressed in two ways: first, as the per centage of the lesion which occupied space anterior to the centre of $M1_{hand}$, denoted as *Lesion location*$_{continuous}$. Second, as a categorical variable, describing lesions as anterior, medial, or posterior to $M1_{hand}$. Anterior lesions were identified with ≥60% tissue anterior to $M1_{hand}$, medial lesions were positioned with >40%<60% tissue anterior to $M1_{hand}$, and posterior lesions had ≤40% tissue anterior to $M1_{hand}$ (Figure 4.2).

Since previous work indicates that lesion location relative to the path of current flow predicts E-field intensity in an ROI (Johnstone et al., in review), I note that scalp electrode position is a good proxy for the predominant direction of current flow through the brain (Evans et al., 2022; Rawji et al., 2018). Here, electrical current entered the body via an

anode at 10-10 position C3, and exited the body via a cathode at Fp2 (Figure 4.2C). Note that data from scans with right-hemisphere lesions and a C4-FP1 montage were flipped during data extraction. The predominant direction of current flow can therefore be summarised by the relative position of the cathode to the anode: current is approximated to flow right-anterior-inferior (R-A-I) through the brain between scalp electrodes. $M1_{hand}$ is positioned directly below the anode, left-medial-superior relative to the rest of the brain. Since the majority of brain tissue is positioned right-inferior (R-I) to $M1_{hand}$, lesions positioned anteriorly to $M1_{hand}$ are considered more in-line with the path of R-A-I current flow than lesions positioned posteriorly. This coarse descriptor for lesion location relative to the approximated path of current flow was included in analyses because it may be intuitively applied in clinical settings: in the absence of CFM, one might consider the position of a lesion relative to the approximated path of current flow between scalp electrodes.

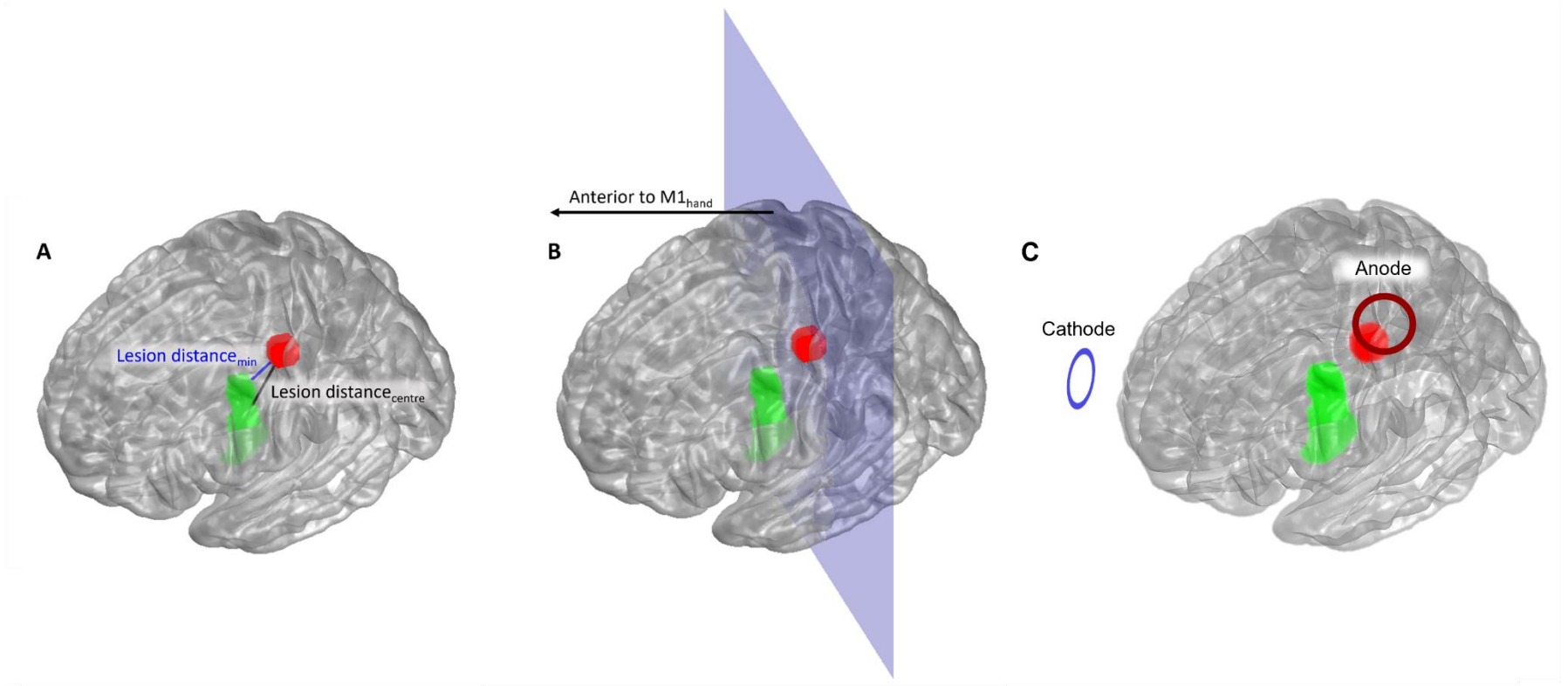

Figure 4.2. Characterisation of lesion location and distance to $M1_{hand}$. Grey matter is shown as a translucent grey surface, lesioned tissue is in green, and the 1cm diameter ROI sphere for $M1_{hand}$ is in red. A) Two parameters were considered to describe the Euclidean distance between lesions and $M1_{hand}$: in blue, the magnitude of a vector extending from the centre of $M1_{hand}$ to the nearest voxel of lesioned tissue (Lesion distance$_{min}$), and in black, the magnitude of a vector extending from the centre of $M1_{hand}$ to the centre of lesioned tissue (Lesion distance$_{centre}$). B) Lesion location is quantified as the per centage of lesioned tissue positioned anteriorly to $M1_{hand}$, the threshold for anterior position is represented by a blue pane which intersects $M1_{hand}$ along the Y-axis. C) Schematic of the conventional electrode montage simulated. An anode (dark red ring) is positioned over $M1_{hand}$ in 10-10 position C3, and a cathode (blue ring) is positioned R-A-I to the anode, in 10-10 position Fp2.

4.3 Analysis.

4.3.1 Comparison of stroke survivor and neurotypical data.

To compare estimated E-field intensity in $M1_{hand}$ in stroke survivor and neurotypical samples when conventional tDCS protocol was simulated, an LMM was constructed with the outcome variable *E-field intensity in* $M1_{hand,}$ a fixed effect of *Group* (stroke or neurotypical), and a random intercept to account for homogeneity of variance per data collection *site*, giving the formula:

$$E\text{-}field\ intensity\ in\ M1_{hand} \sim Group + (1|site)$$

To investigate whether lesion size influenced group comparison, stroke survivor data were stratified into groups by lesion size relative to hemisphere volume (small: <1% hemisphere, mid-sized: >1%≤10% hemisphere, or large: >10% hemisphere). The above model was repeated separately to compare *Groups* (neurotypical participants, or stroke survivors with small, mid-sized, or large lesions).

4.3.2 Do lesion characteristics predict E-field in ROIs?

4.3.2.1 Outcome variables.

LMMs were then constructed for stroke survivor data separately, to determine the impact of lesion size, location, and distance to $M1_{hand}$ on E-field intensity in 2 ROIs: $M1_{hand}$ or lesion tissue. Models interrogating each ROI were constructed separately.

4.3.2.2 Random effects.

All models included a random intercept for data collection *site* to account for lack of independence of data collected at each location, for example differences in image quality and scanner type between sites may have impacted segmentation quality during current flow simulations.

4.3.2.3 Predictors were standardised for comparison across scales.

Multiple parameters on differing scales were available to describe 3 predictors of interest: lesion location, size, and proximity to $M1_{hand}$. Continuous predictors and outcome variables were standardised by subtracting the mean and dividing by the standard deviation, to allow for easier interpretation of regression models, and meaningful comparison of predictors on

differing scales. Results are therefore interpretable as standard deviations instead of raw values.

4.3.2.4 Model exclusion.

To investigate whether *lesion size, distance*, or *location* predicted E-field intensity in each ROI, a series of LMMs were constructed using all viable predictor combinations and a random intercept per data collection *site*. The variance inflation factor (VIF) was calculated using the *vif* function in the R *stats* package (R Core Team, 2021) to estimate how much variance in regression coefficients was inflated due to multicollinearity between predictors.

Models with continuous predictors were excluded from further analyses if VIF values for 1 or more predictors exceeded 5 (James et al., 2013). Models with categorical predictors were assessed for collinearity using generalised VIF (GVIF) values produced by the *vif* function (R Core Team, 2021). GVIF values were taken to the power of 1/(2*degrees of freedom) (DF), to produce a value analogous to the square root of the VIF. The $DVIF^{1/(2*DF)}$ value was therefore squared and the usual VIF threshold of 5 was applied to assess collinearity between categorical predictors (Fox & Monette, 1992). Combinations of predictors which did not violate the multicollinearity assumption are listed in Table 4.1.

4.3.2.5 Model comparison.

To interrogate whether lesions were associated with altered E-field intensity in $M1_{hand}$ when conventional tDCS was simulated, models were constructed to interrogate 3 secondary hypotheses: first, that lesion characteristics such as *size*, *distance* to $M1_{hand}$ and *location* predict E-field intensity in $M1_{hand}$ (hypothesis A). Second, that lesion characteristics predict average E-field intensity in lesion tissue (hypothesis B), and third, that E-field intensity in $M1_{hand}$ is correlated with E-field intensity in lesioned tissue, modulated by lesion characteristics such as *size*, *distance* to $M1_{hand}$ and *location* (hypothesis C). Only models addressing the same hypothesis were compared with each other (Figure 4.3).

Akaike's Information Criterion (AIC) and Bayesian information criterion (BIC) were calculated for model comparison using the *AICcmodavg* R package (Mazerolle, 2020). Lower AIC and BIC values reflected better model fit. Delta-AIC and delta-BIC were calculated to quantify the difference in fit of candidate models, where a delta value of more than -2 was considered to

reflect a significantly better fit of one model compared to another. A model with a delta statistic of zero, for example, is considered the best-fit for available data relative to other candidate models (Figure 4.3). In cases where AIC and BIC values did not converge to suggest the same winning model, conditional R^2 ($R^2_{LMM(c)}$) and marginal R^2 ($R^2_{LLM(m)}$) values were inspected to compare the winning models. Marginal R^2 describes the proportion of variance explained by fixed factor(s) in the LMM alone, while conditional R^2 reflects the proportion of variance explained by both fixed and random factors (Nakagawa & Schielzeth, 2013). AIC and BIC values for each candidate model in Table 4.1 are displayed in Figure 4.3. The winning model used to interrogate each secondary hypothesis (A, B, and C) is highlighted and starred in Table 4.1.

4.3.2.6 Hypothesis A: lesion characteristics predict E-field intensity in $M1_{hand}$.

Secondary hypothesis A states that lesion characteristics such as *size, distance to* $M1_{hand}$, and *location* predict E-field intensity in $M1_{hand}$. AIC and BIC model comparison did not converge on a winning model, with the lowest delta AIC value associated with Mod15, and the lowest delta BIC value found for Mod5. Inspection of conditional R^2 values for each model showed a better fit for Mod15 ($R^2_{LMM(c)}$: Mod15 = .22; Mod5 = .12), herein referred to as model A. Model A was used to investigate hypothesis A, with the formula:

$$E\text{-}field\ intensity\ in\ M1_{hand} \sim Lesion\ distance_{minimum} \times Lesion\ location_{categorical} + (1|site)$$

4.3.2.7 Hypothesis B: lesion characteristics predict E-field intensity in lesions.

Secondary hypothesis B states that lesion characteristics such as *size, distance to* $M1_{hand}$, and *location* predict E-field intensity in lesions. Delta AIC indicated the best fit for Mod6, while delta BIC suggested Mod9. Conditional R^2 revealed a better fit for Mod9 (($R^2_{LMM(c)}$: Mod6 = .32; Mod9 = .36), herein referred to as Model B, which was used to interrogate hypothesis B with the formula:

$$E\text{-}field\ intensity\ in\ lesion \sim Lesion\ size_{continuous} \times Lesion\ distance_{centre} + (1|site)$$

4.3.2.8 *Hypothesis C: E-field intensity in lesions predicts E-field intensity in $M1_{hand}$, modulated by lesion characteristics.*

Finally, to investigate whether the findings of synthetic lesion work translate to data with 'real' stroke lesions, a series of models were constructed to interrogate whether E-field may be re-directed to lesions instead of to $M1_{hand}$, depending on lesion *size, distance to* $M1_{hand}$, and *location*. Delta AIC indicated ModD as the winning model, and delta BIC suggested ModF. Conditional R^2 values were comparable between models ($R^2_{LMM(c)}$: ModD = .29; ModF = .30), while marginal R^2 indicated better predictive power of fixed effects in ModD ($R^2_{LMM(m)}$: ModD = .26; ModF = .21). ModD was selected as the winning model, herein referred to as Model C as it was used to interrogate hypothesis C. The formula for Model C is:

$$E\text{-}field\ intensity\ in\ M1_{hand} \sim Efield\ intensity\ in\ lesion \times Lesion\ location_{categorical} + (1|site)$$

Table 4.1. Summary of predictor variables in candidate LMMs used to interrogate secondary hypotheses A, B, and C. The outcome variable for hypotheses A and C was E-field intensity in $M1_{hand}$. The outcome variable for models addressing hypothesis B was E-field intensity in lesion tissue. Candidate model names (column 1) correspond to AIC and BIC values shown in figure 4.3. Fixed and random effects for each model are listed in column 2. The winning model used to interrogate each hypothesis is shaded and labelled (Models A-C) to correspond to the hypothesis it is used to assess (columns 3-5). All models included a random effect for data collection site (notation: (1|site)). Models addressing different hypotheses were not compared with each other. Candidate models which violated the multicollinearity assumption (VIF > 5) are not included in the table.

Candidate model	**Predictor variables for models predicting E-field intensity in $M1_{hand}$.**	**Hypothesis**		
		A	**B**	**C**
Mod1	Lesion $size_{continuous}$ + (1|site)			
Mod2	Lesion $size_{categorical}$ + (1|site)			
Mod3	Lesion $location_{continuous}$ + (1|site)			
Mod4	Lesion $location_{categorical}$ + (1|site)			
Mod5	Lesion $distance_{min}$ + (1|site)			
Mod6	Lesion $distance_{centre}$ + (1|site)			
Mod7	Lesion $size_{continuous}$ × Lesion $location_{continuous}$ + (1|site)			
Mod8	Lesion $size_{continuous}$ × Lesion $location_{categorical}$ + (1|site)			
Mod9	**Lesion $size_{continuous}$ × Lesion $distance_{centre}$ + (1|site)**		**Model B**	
Mod10	Lesion $size_{categorical}$ × Lesion $location_{continuous}$ + (1|site)			
Mod11	Lesion $size_{categorical}$ × Lesion $distance_{min}$ + (1|site)			
Mod12	Lesion $size_{categorical}$ × Lesion $distance_{centre}$ + (1|site)			
Mod13	Lesion $location_{continuous}$ × Lesion $distance_{min}$ + (1|site)			
Mod14	Lesion $location_{continuous}$ × Lesion $distance_{centre}$ + (1|site)			
Mod15	**Lesion $location_{categorical}$ × Lesion $distance_{min}$ + (1|site)**	**Model A**		
Mod16	Lesion $location_{categorical}$ × Lesion $distance_{centre}$ + (1|site)			
Mod17	Lesion $size_{continuous}$ × Lesion $location_{continuous}$ × Lesion $distance_{centre}$ + (1|site)			
	Predictor variable for models predicting E-field intensity in lesion.			
ModA	Lesion $size_{continuous}$ × E-field intensity in Lesion + (1 | site)			

ModB	Lesion $size_{categorical}$ × E-field intensity in Lesion + (1 | site)	
ModC	Lesion $location_{continuous}$ × E-field intensity in Lesion + (1 | site)	
ModD	**Lesion $location_{categorical}$ × E-field intensity in Lesion + (1 | site)**	**Model C**
ModE	Lesion $distance_{min}$ × E-field intensity in Lesion + (1 | site)	
ModF	Lesion $distance_{centre}$ × E-field intensity in Lesion + (1 | site)	
ModG	Lesion $size_{continuous}$ × Lesion $location_{continuous}$ × E-field intensity in Lesion + (1 | site)	
ModH	Lesion $size_{continuous}$ × Lesion $location_{categorical}$ × E-field intensity in Lesion + (1 | site)	
ModI	Lesion $size_{continuous}$ × Lesion $distance_{min}$ × E-field intensity in Lesion + (1 | site)	
ModJ	Lesion $size_{continuous}$ × Lesion $distance_{centre}$ × E-field intensity in Lesion + (1 | site)	
ModK	Lesion $size_{categorical}$ × Lesion $location_{continuous}$ × E-field intensity in Lesion + (1 | site)	
ModL	Lesion $size_{categorical}$ × Lesion $location_{categorical}$ × E-field intensity in Lesion + (1 | site)	
ModM	Lesion $size_{categorical}$ × Lesion $distance_{min}$ × E-field intensity in Lesion + (1 | site)	
ModN	Lesion $size_{categorical}$ × Lesion $distance_{centre}$ × E-field intensity in Lesion + (1 | site)	
ModO	Lesion $location_{continuous}$ × Lesion $location_{categorical}$ × E-field intensity in Lesion + (1 | site)	
ModP	Lesion $location_{continuous}$ × Lesion $distance_{centre}$ × E-field intensity in Lesion + (1 | site)	
ModQ	Lesion $location_{categorical}$ × Lesion $distance_{min}$ × E-field intensity in Lesion + (1 | site)	
ModR	Lesion $location_{categorical}$ × Lesion $distance_{centre}$ × E-field intensity in Lesion + (1 | site)	
ModS	Lesion $distance_{min}$ × Lesion $distance_{centre}$ × E-field intensity in Lesion + (1 | site)	

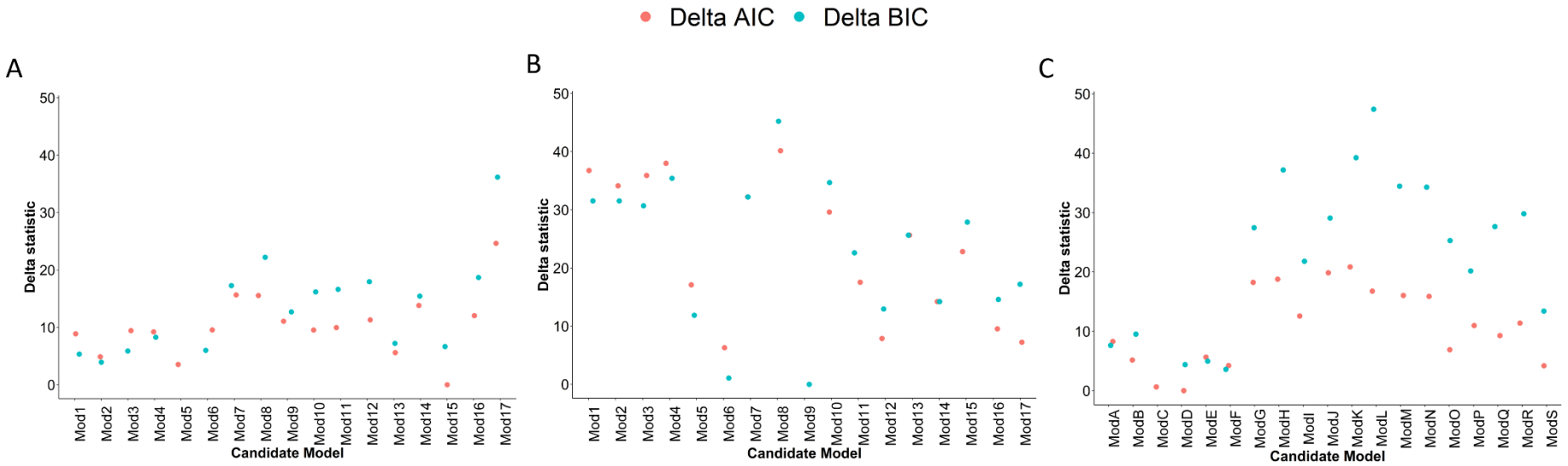

Figure 4.3. Summary of model comparisons. X-axis: model names correspond to candidate models detailed in table 4.1. The y-axis simultaneously shows delta AIC (red) and delta BIC (blue) values for each model, referred to collectively as "delta statistic". Lower delta statistics reflect better model fit. Where AIC and BIC values did converge on the same model, conditional R^2 values were compared to determine the winning model. A) Delta AIC and delta BIC values for models used to interrogate hypothesis A. Mod15 was selected after inspection of conditional R^2 values for Mod5 and Mod15. B) Delta AIC and delta BIC values for models used to interrogate hypothesis B. Mod9 was selected after consulting Conditional R^2 values for Mod6 and Mod9. C) Delta AIC and delta BIC values for models used to interrogate hypothesis C. ModD was selected after comparison of conditional and marginal R^2 values for ModD and ModF.

4.4 Results.

4.4.1 Participant demographics.

Data from 123 stroke survivors (age = 59.88 ± 11.72, age unknown = 1, female = 50, sex unknown = 8) and 147 neurotypical participants (age = 50.18 ± 16.38, age unknown = 43, female = 55, sex unknown = 51) were included in analyses. Stroke survivors were included if they were at least 3 months post-stroke (days post-stroke = 1337.07 ± 1148.66) and had a FM-UL score indicating upper limb impairment without hemiparesis (FM-UL = 46.1 ± 11.47). Participant demographics are summarised in Table 4.2.

Table 4.2. Demographic information for stroke survivors and neurotypical participants whose data were included in final analyses.

Group	N	Age (years)		Sex		Days post-stroke		FM-UL (max = 66)	
		Mean (SD)	NA	F	NA	Mean (SD)	Range	Mean (SD)	Range
Stroke	123	59.88 (11.72)	1	50	8	1337.07 (1148.66)	106-5345	46.1 (11.47)	28-64
Neurotypical	147	50.18 (16.38)	43	55	51	NA	NA	NA	NA

NA = information not available; FM-UL = Fugl-Meyer assessment of upper limb impairment, where a score of 66 reflects no impairment; SD = standard deviation.

4.4.2 Lesion characteristics.

4.4.2.1 Lesion size.

Median lesion volume in this sample was 14.24 cm^3 (25%-quantile = 1.78 cm^3; 75%-quantile = 48.73 cm^3). Forty-eight small lesions covered less than 1% of the affected hemisphere, 45 mid-sized lesions occluded between 1 and 10% of the affected hemisphere, and 30 large lesions occluded more than 10%. Lesion size was smaller in this sample compared to values previously reported in the literature, for example, in a larger sample of 439 human scans, average normalized lesion size was 31.9 cm^3 (25%-quantile = 9.4 cm^3, 75%-quantile = 72.9 cm^3; Sperber & Karnath, 2016). Lesion information is summarised in Table 4.3.

4.4.2.2 Lesion location.

Anatomical lesion location categories included in the ENIGMA database (Liew et al., 2020; Liew et al., 2018, 2022) are summarised in Figure 4.4; 50 unique anatomical tags described lesion location in 123 stroke survivors. After stratification by *lesion location*$_{categorical}$, 85

lesions (70% of the sample) were identified as anterior, 12 as medial (9.5%), and 25 as posterior (20.5%) to $M1_{hand}$. Thirty-one lesions partially occluded $M1_{hand}$ (small = 1, mid-sized = 13, large = 19). Of these, the per centage of $M1_{hand}$ occluded ranged from 0.32% to 99.25% (M = 40.32%, SD = 37.24%). One large medial lesion (volume = 96.51cm^3, 17% of hemisphere) and 1 large posterior lesion (volume = 254.52cm^3, 56% of hemisphere) entirely occluded $M1_{hand}$ and were excluded from analyses of E-field intensity in $M1_{hand}$ (hypotheses A and C). Lesion information is summarised in Table 4.3.

4.4.2.3 Lesion distance to $M1_{hand}$.

Average *lesion distance*$_{min}$ was 17.7mm (SD = 14.2), and average *Lesion distance*$_{centre}$ was 36.5mm (SD = 13.9). On average, small lesions were positioned further from $M1_{hand}$ (*distance*$_{min}$ = 31.2 mm, *distance*$_{centre}$ = 42.6 mm), while mid-sized lesions (*distance*$_{min}$ = 11.3 mm, *distance*$_{centre}$ = 31.6 mm) and large lesions (*distance*$_{min}$ = 5.46 mm, *distance*$_{centre}$ = 33.6 mm) were more proximal. Lesion information is summarised in Table 4.3.

Table 4.3. Summary of lesion characteristics, quantified as lesion size, location, and distance from $M1_{hand}$.

Lesion size$_{categorical}$ (% of hemisphere)	**N**	**Lesion size$_{continuous}$ (cm^3)**		**Lesion location$_{categorical}$ N (% of size group)**			**Lesion distance$_{min}$ (mm)**		**Lesion distance$_{centre}$ (mm)**	
		Mean	**SD**	**A**	**M**	**P**	**Mean**	**SD**	**Mean**	**SD**
Small (<1%)	48	1.86	1.42	43 (89%)	3 (7%)	2 (4%)	31.16	11.17	42.64	10.21
Mid-sized (>1<10%)	44	26.45	15.67	27 (62%)	5 (11%)	12 (27%)	11.34	7.68	31.65	13.22
Large (>10%)	30	101.7	51.58	15 (50%)	4 (13%)	11 (37%)	5.46	5.67	33.61	16.32

A = anterior to $M1_{hand}$, M = medial to $M1_{hand}$, P = posterior to $M1_{hand}$; SD = standard deviation.

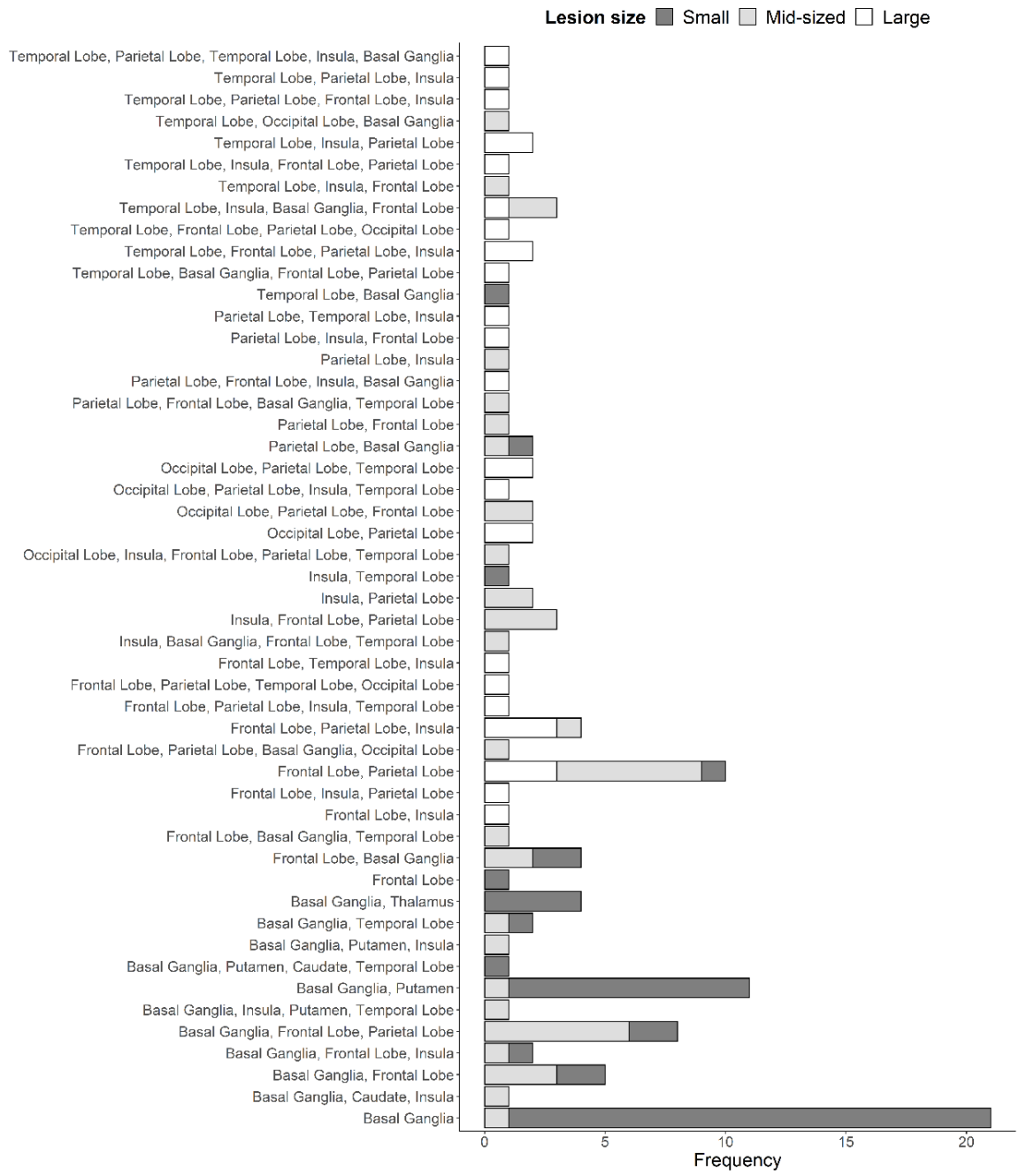

Figure 4.4. Summary of anatomical lesion location descriptors included in the ENIGMA database (Liew et al., 2020; Liew et al., 2018, 2022). Y-axis: list of 50 unique lesion location tags. X-axis, frequency of stroke survivors (total = 123) with small (≤1% hemisphere, white), mid-sized (>1% ≤10% hemisphere, grey) or large (>10% hemisphere) lesions in each anatomical location.

4.4.3 Lower E-field intensity in $M1_{hand}$ for stroke survivors with small lesions compared to neurotypical participants, when conventional tDCS was simulated.

The model selection process is detailed in section 4.3.1. An LMM was selected to compare estimated E-field intensity in $M1_{hand}$ between *groups* (stroke and neurotypical) when conventional tDCS protocol was simulated (formula: E-field intensity in $M1_{hand}$ ~ Group + (1|site)). Neurotypical data were normally distributed while stroke survivor data were not (Shapiro's test: Neurotypical, $p > .05$, Stroke, $p < .01$). Levene's test detected no significant difference in variance between groups ($F(1,226) = .01, p = .93$) though variance was high in both groups; E-field intensity in $M1_{hand}$ varied by 390% across participants in the stroke survivor group (CV = 30.89) and by 310% in the neurotypical group (CV = 25.37).

No significant difference in average E-field intensity in $M1_{hand}$ was detected when all stroke survivors were compared to all neurotypical participants $F(1,55) = 2.82$, $p = .10$ (Neurotypical: Mean = .14 ± .04 V/m, range = .06-.24; Stroke: Mean = .13 ± .04 V/m, range = .06-.31 V/m). After stratification by lesion size, significantly lower E-field intensity in $M1_{hand}$ was found in the 'small lesion' subset of the stroke group compared to the neurotypical group, $t(98) = 3.78$, $p < .01$. No significant difference was found in E-field intensity in $M1_{hand}$ in survivors with mid-sized- and large-lesions compared to the neurotypical group ($p>.05$; Figure 4.5).

Data were further stratified by lesion occlusion of $M1_{hand}$. No significant difference in E-field intensity in $M1_{hand}$ was found between the neurotypical group and stroke survivors with and without $M1_{hand}$ occlusion, $F(2,172) = .61$, $p=.54$. Within the stroke survivor group only, no significant difference in E-field intensity in $M1_{hand}$ was found in subjects with and without partial $M1_{hand}$ occlusion, in each lesion size group ($p>.05$). Ninety per cent of lesions categorised as 'small' were positioned anteriorly to $M1_{hand}$ (89.6%), and 70.8% of small lesions were located in the basil ganglia or thalamus. Group comparison of E-field intensity in $M1_{hand}$ is summarised in Figure 4.5.

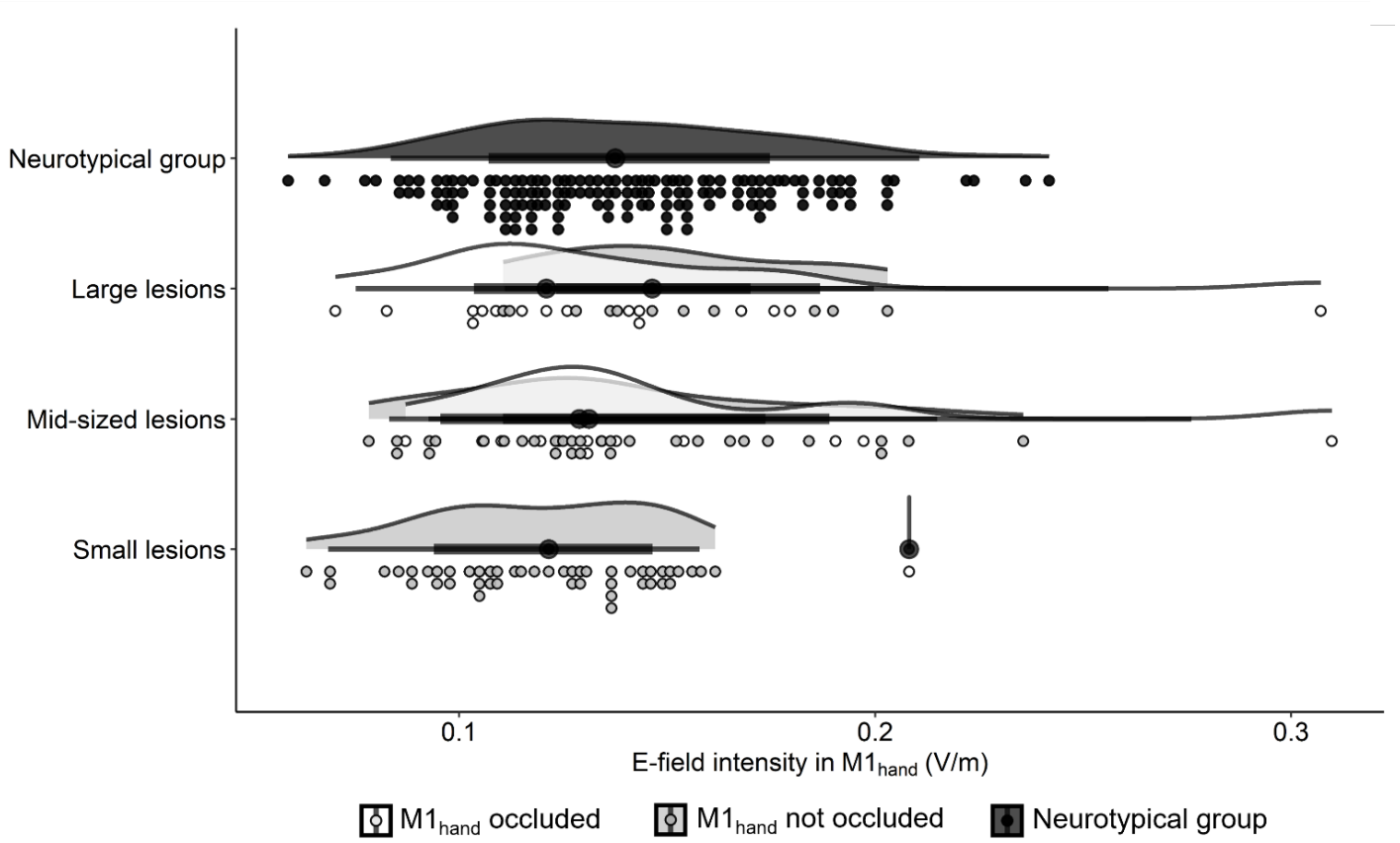

Figure 4.5. Comparison of E-field intensity in $M1_{hand}$ in neurotypical participants and stroke survivors when 1mA conventional tDCS is simulated. X-axis: mean estimated E-field intensity in $M1_{hand}$. Y-axis: data are stratified into 4 groups: neurotypical participants, and stroke survivors with small (≤1% hemisphere), mid-sized (>1% ≤10% hemisphere) or large (>10% hemisphere) lesions. Stroke survivor data are also stratified by those with lesions which partially occluded (white) or did not occlude (grey) $M1_{hand}$. Neurotypical data are shown in black. Shaded areas depict the distribution of data in each group, box plots show 25th, 50th and 75th quartiles, and data points show estimated E-field intensity in $M1_{hand}$ per participant. Estimated E-field intensity in $M1_{hand}$ was significantly lower in stroke survivors with small lesions compared to the neurotypical group ($t(98) = 3.78$, $p < .01$). No significant difference was found between stroke survivors with mid-sized or large lesions and the neurotypical group ($p > .05$).

4.4.4 Model A: lesion distance and location predict E-field intensity in $M1_{hand}$.

The model selection process is described in section 4.3.2.6. Secondary hypothesis A states that lesion characteristics predict E-field intensity in $M1_{hand}$. The winning LMM formula was: E-field intensity in $M1_{hand}$ ~ lesion $distance_{min}$ × lesion $location_{categorical}$ + (1|site). A significant interaction was found between *lesion* $distance_{min}$ and *lesion* $location_{categorical}$, $F(2,114) = 4.69$, $p = 0.01$, $R^2_{LLM(m)} = .15$, $R^2_{LMM(c)} = .22$. (Figure 4.6A, D), whereby the effect of a 1 SD increase in *lesion* $distance_{min}$ resulted in a .89 SD difference in E-field intensity in $M1_{hand}$ for anterior compared to posterior lesions, $\beta = -0.89$, CI = -1.46 – -0.31, $p<0.01$. No significant difference was found in the effect of *lesion* $distance_{min}$ for anterior compared to medial lesions, $\beta = 0.06$, CI = -0.78 – 0.67, $p = 0.88$, and a trend was detected towards increased distance associated with increased E-field intensity in $M1_{hand}$ for posterior compared to medial lesions, $\beta = 0.83$, CI = -0.04 – -1.70, $p = 0.06$. *Lesion* $distance_{min}$ alone was significantly negatively correlated with E-field intensity in $M1_{hand}$ for participants with anterior lesions only ($\beta = -0.43$, CI = -0.64 – -0.22, $p < 0.001$). The effect of *lesion* $distance_{min}$ alone was non-significant for medial and posterior lesion locations (Medial, $\beta = -0.38$, CI = -1.06 – 0.31, $p = 0.28$; Posterior, $\beta = 0.46$, CI = -0.08 – 0.99, $p = 0.09$).

4.4.5 Model B: lesion distance and lesion size predict E-field intensity in lesions, and the effect is more pronounced in small lesions.

Secondary hypothesis B states that lesion characteristics predict E-field intensity in lesions when a conventional 1mA tDCS is simulated. Model selection has been detailed in section 4.3.2.7, giving the winning LMM formula: E-field intensity in lesions ~ lesion $size_{continuous}$ × lesion $distance_{centre}$ + (1|site). A significant interaction was found between *lesion* $distance_{centre}$ and *lesion* $size_{continous}$ predicting E-field intensity in lesioned tissue ($F(1,117) = 15.16$, $p <.001$, $R^2_{LLM(m)} = .32$, $R^2_{LMM(c)} = .36$) and a significant main effect of *Lesion* $distance_{centre}$ was detected, $F(1,116) = 49.51$, $p <.001$ (Figure 4.6B, E). Inspection of beta estimates showed that a 1 SD increase in *lesion* $distance_{centre}$ was associated with a 0.54 SD decrease in E-field in lesioned tissue ($\beta = 0.28$, CI = 0.09 – 0.48, $p = 0.01$). The extent of E-field intensity change significantly interacted with *lesion* $size_{continuous}$, whereby increased *distance* was associated with a greater decrease in E-field intensity in smaller lesions compared to larger ones, $\beta = 0.31$, CI = 0.15 – 0.47, $p<0.001$ Figure 4.6B, E).

4.4.6 Model C: E-Field intensity in $M1_{hand}$ is correlated with E-field in lesioned tissue only when lesions are in the path of current flow.

Hypothesis C states that the relationship between E-field intensity in $M1_{hand}$ and lesions will depend on lesion characteristics such as size, location, and distance to $M1_{hand}$. The model selection process is described in section 4.3.2.8. The winning LMM to describe the relationship between E-field intensity in $M1_{hand}$ and lesioned tissue was: E-field intensity in $M1_{hand}$ ~ E-field intensity in lesion × Lesion $location_{categorical}$ + (1|site). A significant positive correlation was found between mean estimated *E-field intensity in lesioned tissue* and mean E-field intensity in $M1_{hand}$ ($F(1,114) = 21.11$, $p < .001$, $R^2_{LLM(m)} = .18$, $R^2_{LMM(c)} = .22$) and a significant interaction was detected whereby the impact of *E-field intensity in lesioned tissue* on E-field intensity in $M1_{hand}$ depended on *Lesion location*$_{categorical}$ ($F(2,113) = 5.96$, $p < .001$). Beta estimates showed that a 1 SD increase in mean *E-field intensity in lesioned tissue* was associated with 0.54 SD less change in E-field intensity in $M1_{hand}$ for posterior lesions compared to anterior lesions ($\beta = -0.56$, CI = -.90 - -.24, $p < 0.01$), while no difference was detected for medial compared to anterior lesions ($\beta = -.01$, CI = -.55 - .54, $p = 0.96$; Figure 4.6C, F).

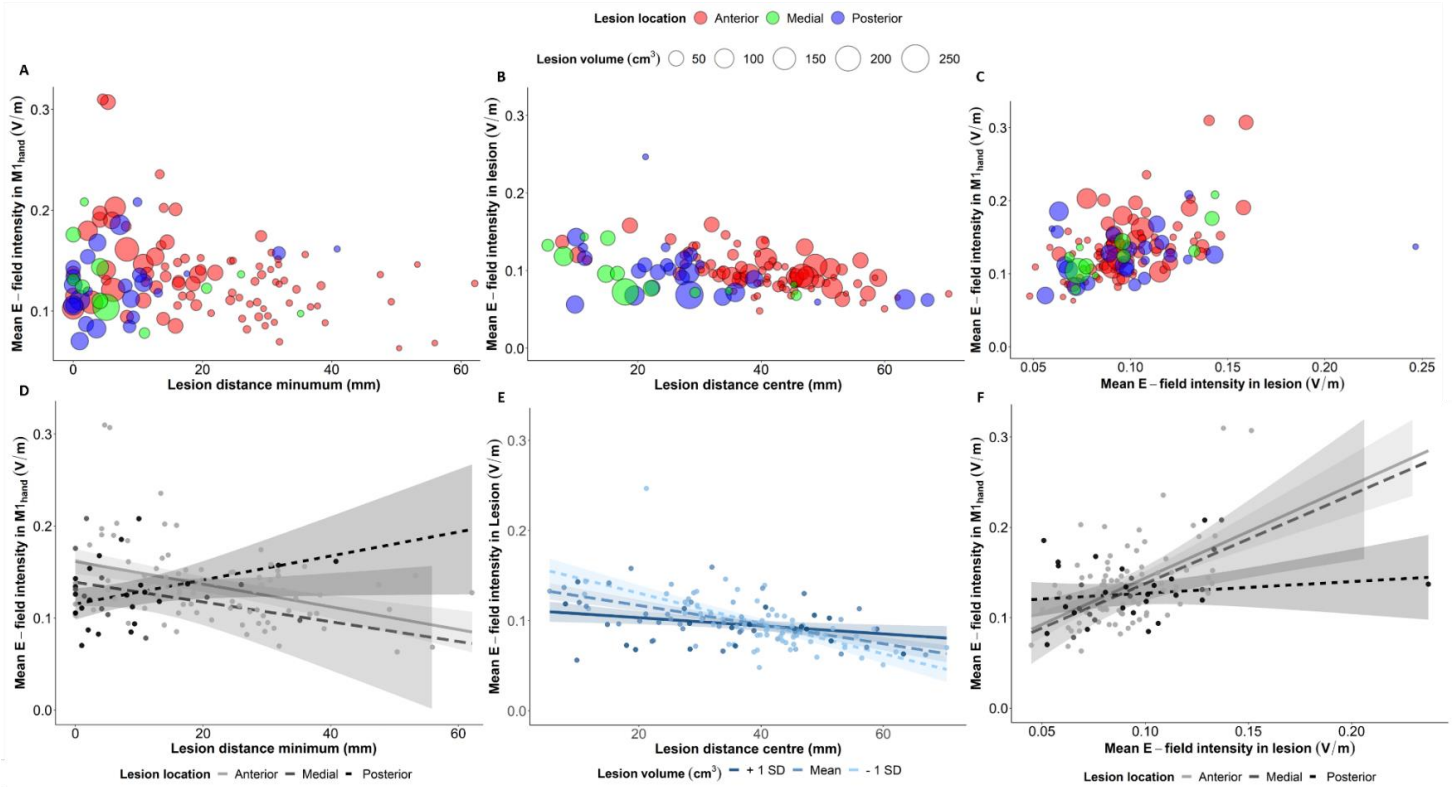

Figure 4.6. The impact of lesions on E-field intensity in $M1_{hand}$ (A, C, D, F) and E-field intensity in lesioned tissue (B, E) when a 1mA conventional tDCS protocol is simulated in ROAST-lesion (Huang et al., 2019; Johnstone et al., in review). Descriptive figures A-C show lesion characteristics (size, distance to $M1_{hand}$, location), while figures D-F show the results of statistical analyses. ***Figures A-C.*** *Each point represents a lesion. Lesion location$_{categorical}$ is depicted by colour (red = anterior, green = medial, blue = posterior to $M1_{hand}$), and point size reflects the lesion size$_{continuous}$ (cm^3). Axes in figures A-C match the figures representing statistical results directly below them, in figures D-F.* ***Figures D-F****. Datapoints represent data for individual participants, shaded areas represent 90% confidence intervals, and lines represent linear relationships between predictors. Data describing the impact of lesion distance$_{min}$ is shown in black, and data describing the impact of lesion distance$_{centre}$ is in blue. D) Lesion distance$_{min}$ is significantly negatively correlated with E-field intensity in $M1_{hand}$ for anterior lesions, significantly different to the relationship with posterior lesions where E-field intensity in $M1_{hand}$ tended to increase with further lesion distance$_{min}$ ($F(2,114) = 4.69$, $p = 0.01$, $R^2_{LMM(c)} = .22$). E) E-field intensity in lesions decreases with greater distance from $M1_{hand}$, and the effect is significantly more dramatic for smaller lesions ($F(1,117) = 15.16$, $p < .001$, $R^2_{LMM(c)} = .36$). F) E-field intensity in anterior lesions is significantly positively correlated with E-field intensity in $M1_{hand}$, significantly different to the relationship with posterior lesions where increasing E-field intensity in the lesion was not associated with a change in E-field intensity in $M1_{hand}$ ($F(2,113) = 5.96$, $p < .001$, $R^2_{LMM(c)} = .22$).*

4.4.7 Case studies.

Lastly, I consider 6 case studies selected from this heterogeneous sample of stroke survivors. The results of Models A and C reported above revealed a significant relationship between lesion characteristics and tDCS-induced E-field intensity in $M1_{hand}$. Model A indicated that lesion $distance_{min}$ is negatively correlated with E-field intensity in $M1_{hand}$ for anterior lesions, significantly different to the relationship with posterior lesions where E-field intensity in $M1_{hand}$ tended to increase with increasing lesion $distance_{min}$ (Model A, Figure 4.6D). Meanwhile, Model C indicated that E-field intensity in anterior lesions is significantly positively correlated with E-field intensity in $M1_{hand}$, significantly different to the relationship with posterior lesions where increasing E-field intensity in the lesion was not associated with a change in E-field intensity in $M1_{hand}$ (Model C, Figure 4.6F). Here I consider whether these relationships could translate to useful heuristics which might apply in clinical settings, to predict the impact of lesions on E-field intensity in $M1_{hand}$ in individual cases. A summary of the information described below can also be found in

Table 4.4 and Figure 4.7.

Participant A is a stroke survivor with a small subcortical lesion occluding part of the basal ganglia and thalamus. The lesion covers less than 1% of the affected hemisphere (volume = 0.91cm^3, 0.2% hemisphere) and is relatively distant from $M1_{hand}$ (*Lesion distance*$_{min}$ = 47.52 mm; *Lesion distance*$_{centre}$ = 56.49 mm). Seventy-three per cent of the lesion is anterior to $M1_{hand}$, and E-field intensity in lesioned tissue is 1.44 SD below the group average. The results of Model A suggested that distant lesions positioned anteriorly to $M1_{hand}$ are associated with lower E-field intensity in $M1_{hand}$ (Figure 4.6D), while Model C indicated that anterior lesions with relatively low E-field intensity in lesioned tissue are associated with relatively low E-field intensity in $M1_{hand}$ (Figure 4.6F). In this case study, E-field intensity in $M1_{hand}$ is indeed .05 SD below the group average.

Participant B has a small cortical lesion occluding part of the frontal and parietal lobes. The lesion covers less than 1% of the affected hemisphere (volume = 4.44cm^3, 0.66% hemisphere) and is proximal to $M1_{hand}$ (*Lesion distance*$_{min}$ = 1.73 mm; *Lesion distance*$_{centre}$ =

11.33 mm). Forty-three per cent of the lesion is anterior to $M1_{hand}$, and mean E-field intensity in lesioned tissue is 1.66 SD above the group average. The findings of Model A suggested that decreasing *lesion distance*$_{min}$ was not significantly associated with a change in E-field intensity in $M1_{hand}$ for medially-positioned lesions (Model A, Figure 4.6D), while Model C also reported no significant relationship between E-field intensity in lesioned tissue and E-field intensity in $M1_{hand}$ for medial lesions (Model C, Figure 4.6F). Estimated E-field intensity in $M1_{hand}$ is 1.80 SD above the group average in participant B, an outcome which aligns more with the findings associated with anterior lesions than posterior ones, but is not directly predicted by the models detailed in the results section.

Participant C has a mid-sized sub-cortical lesion occluding part of the basal ganglia, caudate and Insula. The lesion covers between 1 and 10% of the affected hemisphere (volume = 30.65cm^3, 4.69% hemisphere) and is of middling distance relative to $M1_{hand}$ (*Lesion distance*$_{min}$ = 12.81mm, *Lesion distance*$_{centre}$ = 36.77 mm). The majority of the lesion is anterior to $M1_{hand}$ (76% anterior) though it extends both anteriorly and posteriorly in the brain. Mean E-field intensity in lesioned tissue is .3 SD below the average for the group. The findings of Model A suggested that lesions positioned anteriorly to $M1_{hand}$ at a middling distance are associated with lower E-field intensity in $M1_{hand}$ (Figure 4.6D), while the findings of Model C indicated that anterior lesions with relatively low E-field intensity in lesioned tissue are associated with relatively low E-field intensity in $M1_{hand}$ (Figure 4.6F). E-field intensity in $M1_{hand}$ for participant C is indeed .24 SD below the group average.

Participant D has a large cortical lesion occluding part of the Occipital, Parietal and Temporal lobes. The lesion covers more than 10% of the affected hemisphere (volume = 95.78cm^3, 19% hemisphere) and is proximal to $M1_{hand}$ (*Lesion distance*$_{min}$ = 3.61 mm; Lesion *distance*$_{centre}$ = 35.81mm). The lesion is located posteriorly to $M1_{hand}$ (6% anterior), and average E-field intensity in lesioned tissue is .9 SD below the average for the group. The findings of Model A suggest that proximal lesions positioned posteriorly to $M1_{hand}$ are associated with lower E-field intensity in $M1_{hand,}$ compared to anterior lesions where higher E-field intensity in $M1_{hand}$ is predicted (Figure 4.6D). Model C indicates that posterior lesions with relatively low E-field intensity in lesioned tissue are associated with a shallower

increase in E-field intensity in $M1_{hand}$ compared to anterior and medial lesions (Figure 4.6F). E-field intensity in $M1_{hand}$ is indeed 1.24 SD below the group mean for participant D.

Participant E has a large cortical lesion occluding part of the Frontal and Parietal lobes, and the Insula. The lesion covers more than 10% of the affected hemisphere (volume = 46.91cm^3, 11% hemisphere) and is proximal to $M1_{hand}$ (*Lesion distance*$_{min}$ = 5.39mm; Lesion *distance*$_{centre}$ = 31.97 mm). Eighty-seven per cent of this lesion is anterior to $M1_{hand}$, and mean E-field intensity in lesioned tissue is 2.24 SD above the average for the group. The findings of Model A suggest that proximal lesions positioned anteriorly to $M1_{hand}$ are associated with relatively high E-field intensity in $M1_{hand}$ (Model A, Figure 4.6D), while Model C indicates that anterior lesions with relatively high E-field intensity in lesioned tissue are associated with relatively high E-field intensity in $M1_{hand}$ (Model C, Figure 4.6F). Indeed, E-field intensity in $M1_{hand}$ is 4.19 SD above the group average for participant E.

Finally, **participant F** has a large cortical lesion extending into the Temporal, Frontal, Parietal and Occipital lobes. The lesion covers more than 10% of the affected hemisphere (volume = 228.99cm^3, 39.88% hemisphere) and is proximal to $M1_{hand}$ (*Lesion distance*$_{min}$ = 5.10mm; *Lesion distance*$_{centre}$ = 17.99 mm). This lesion is located medially to $M1_{hand}$ (57% anterior), and average E-field intensity in lesioned tissue is .92 SD below the average for the group. The results of Model A suggest that decreasing *lesion distance*$_{min}$ was not significantly associated with a change in E-field intensity in $M1_{hand}$ for medially-positioned lesions (Figure 4.6D), while Model C also reported no significant relationship between E-field intensity in lesioned tissue and E-field intensity in $M1_{hand}$ for medial lesions (Figure 4.6F). Estimated E-field intensity in $M1_{hand}$ is .73 SD below the group mean for participant F, an effect which is not easily predicted by heuristics which might be deduced from quantitative analyses reported above.

Table 4.4. Lesion characteristics and CFM data for case study participants A-F. Lesion characteristics (size, location, distance to $M1_{hand}$) are quantified for each participant, along with mean E-field in $M1_{hand}$ and lesioned tissue estimated by ROAST-lesion (Huang et al., 2019; Johnstone et al., in review). Participant ID matches labels included in figure 4.7.

Participant	Lesion size category	Primary lesion location	Lesion (sub-) cortical	Lesion Volume (cm^3)	Lesion % of hemisphere	Lesion minimum distance (mm)	Lesion centre distance (mm)	Per cent lesion anterior to $M1_{hand}$	Per cent $M1_{hand}$ occluded by lesion	Mean E-field intensity in $M1_{hand}$ (V/m)	Mean E-field intensity in lesion (V/m)
A	Small	Basal Ganglia, Thalamus	sub-cortical	0.91	0.20	47.52	56.49	73.40	0.00	0.14	0.06
B	Small	Frontal Lobe, Parietal Lobe	cortical	4.44	0.66	1.73	11.33	42.98	18.15	0.21	0.14
C	Mid-sized	Basal Ganglia, Caudate, Insula	sub-cortical	30.65	4.69	12.81	36.77	76.67	0.00	0.12	0.09
D	Large	Occipital Lobe, Parietal Lobe, Temporal Lobe	cortical	95.78	18.59	3.61	35.81	5.98	14.29	0.08	0.07
E	Large	Frontal Lobe, Insula, Parietal Lobe	cortical	46.91	11.12	5.39	31.97	86.68	1.29	0.31	0.16
F	Large	Temporal Lobe, Frontal Lobe, Parietal Lobe, Occipital Lobe	cortical	228.99	39.88	5.10	17.99	57.33	0.97	0.10	0.07

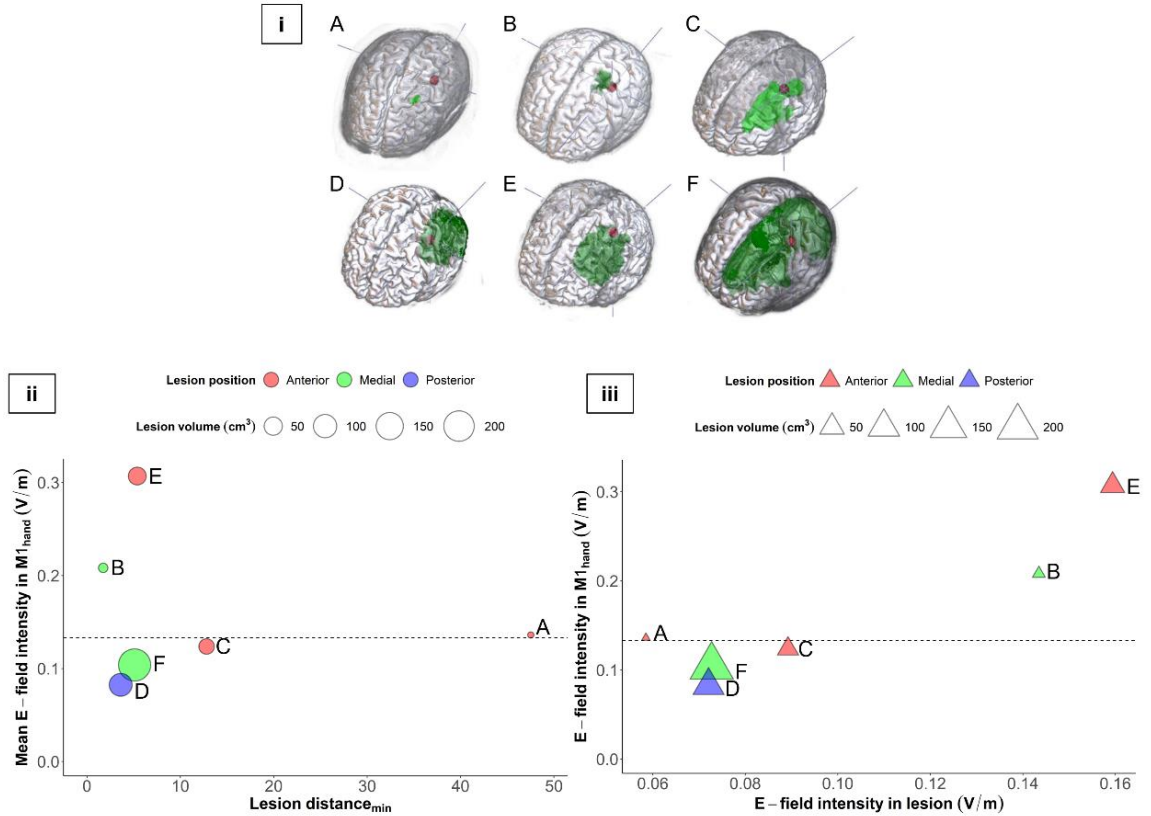

Figure 4.7. Case studies: relationship between lesion characteristics and E-field intensity in $M1_{hand}$ in 6 stroke survivors. Participant IDs correspond to information summarised in table 4.4. Each data point represents a stroke lesion in 1 case study. Lesion $location_{categorical}$ is depicted by colour (red = anterior, green = medial, blue = posterior to $M1_{hand}$) and point size reflects the lesion $size_{continuous}$ (cm^3). Dashed lines show mean E-field intensity in $M1_{hand}$ across participants. Circles show the relationship between variables included in Model A, and triangles show the relationship between variables included in Model C. i) Structural MRIs of 6 stroke survivors (case studies A-F). Grey matter is shown in grey, $M1_{hand}$ in red and lesions in green. ii) Relationship between lesion characteristics and E-field intensity in $M1_{hand}$ (Model A) when a 1mA conventional tDCS protocol is simulated. Quantitative analyses suggest increasing lesion $distance_{min}$ is associated with lower E-field intensity in $M1_{hand}$ for anterior lesions, significantly different to the relationship with posterior lesions where E-field intensity in $M1_{hand}$ tended to increase with further lesion $distance_{min}$. iii) Relationship between E-field intensity in lesions and E-field intensity in $M1_{hand}$ (Model C) when 1mA conventional tDCS is simulated. Quantitative analyses suggest higher E-field intensity in anterior lesions is significantly positively correlated with higher E-field intensity in $M1_{hand}$, significantly different to the relationship with posterior lesions where increasing E-field intensity in the lesion is not associated with a change in E-field intensity in $M1_{hand}$.

4.5 Discussion.

This study aimed to compare tDCS-induced E-field intensity in $M1_{hand}$ in stroke survivors and neurotypical participants, and to investigate the impact of real (instead of synthetic) stroke lesions on simulated current flow in a large sample of MR scans (Liew et al., 2020; Liew et al., 2018, 2022). Customised current flow models (Huang, Datta, et al., 2018; Johnstone et al., in review) were used to estimate the intensity of E-field delivered to $M1_{hand}$, a cortical region of interest (ROI) located under an anode electrode. To further probe the mechanisms by which lesions might impact tDCS current delivery, E-field intensity in lesioned tissue was examined to determine how exogenous DC fields might interact with conductive lesioned tissue positioned in different locations relative to $M1_{hand}$.

4.5.1 E-field intensity in $M1_{hand}$ varied by over 300% in both groups.

First, the intensity of E-field in $M1_{hand}$ did not differ on average between neurotypical and stroke survivor groups. Inter-individual variability in $M1_{hand}$ E-field intensity was very high in both groups, varying by over 300%. By comparison, Evans and colleagues reported ~100% inter-individual E-field variability in a group of younger adults (N = 50, age 22-35 years; Evans et al., 2020) when a similar tDCS montage was simulated. Antonenko and colleagues (Antonenko et al., 2018) however reported higher variability and lower tDCS E-field intensity in cortical ROIs in ageing participants compared to younger adults, possibly due to reduced grey matter volume and increased CSF thickness associated with healthy ageing (Laakso et al., 2015; Mahdavi & Towhidkhah, 2018; McCann & Beltrachini, 2021; Opitz et al., 2015). The impact of age on DC fields is not trivial for the stroke survivor population, where approximately 84% of strokes occur in adults over 49 years of age (Feigin et al., 2022). The optimisation problem for tDCS in stroke therefore requires consideration for anatomical differences due to ageing, as well as the significant impact of lesions on current flow. Without CFM-informed individualisation, high variability in tDCS E-field delivery to an ROI has likely contributed to variability in reported findings of clinical trials investigating the efficacy of tDCS in the stroke population (reviewed recently in Lefaucheur, 2016; Shen et al., 2022; Vergallito et al., 2022).

4.5.2 Low E-field estimated in $M1_{hand}$ for stroke survivors with small lesions.

Further analysis with stroke survivor data stratified by lesion size showed lower E-field intensity in $M1_{hand}$ for stroke survivors with small lesions (<1% of the affected hemisphere) than the neurotypical group. A possible explanation for this can be found in recent work by Kashyap and colleagues (Kashyap et al., 2022), who reported that pockets of tissue with high CSF concentration (i.e. similar to conductive lesions) tend to drag current towards them, altering the pattern of current between anode and cathode electrodes (Datta et al., 2009; Holdefer et al., 2006). Higher current density was reported in the ROI when high CSF pockets were located close to the ROI in the path of current flow, while lower current density was recorded in the ROI when high CSF pockets in the path of current flow were located further from it (Kashyap et al., 2022). Here, the relative locations of scalp electrodes were taken as a proxy for the path of current flow (Evans et al., 2022): due R-A-I between anode and cathode electrodes. Meanwhile, anatomical descriptors provided in the ENIGMA database (Liew et al., 2020; Liew et al., 2018, 2022) showed that the majority of small lesions were located in the basal ganglia, a sub-cortical region which is distant and positioned due R-A-I relative to $M1_{hand}$. Small subcortical lesions may be acting similarly to the pockets of conductive tissue described by Kashyap and colleagues (Kashyap et al., 2022): carrying current away from $M1_{hand}$ towards the cathode, resulting in low E-field intensity in $M1_{hand}$ compared to the neurotypical population. These novel finding suggests that small, sub-cortical lesions may have a larger impact on tDCS E-field delivery than previously thought, if they are positioned in-line with the path of current flow between electrodes.

4.5.3 The impact of lesions on tDCS-induced E-field in $M1_{hand}$ depends on lesion position and proximity to $M1_{hand}$.

Stroke survivor data were also analysed separately, to interrogate the relationship between lesion characteristics and tDCS-induced fields. The findings of Model A suggested that anterior lesions were associated with higher E-field intensity in $M1_{hand}$ if the lesion was proximal to the ROI. Meanwhile, the relationship between lesion proximity and E-field intensity in $M1_{hand}$ differed significantly for posteriorly positioned lesions, where proximal lesions are associated with lower E-field intensity in $M1_{hand}$. The results of Model C and the work of Kashyap and colleagues, described above (Kashyap et al., 2022), hint at the mechanism behind this effect, as results showed E-field intensity in lesions was significantly

positively correlated with E-field intensity in $M1_{hand}$ when lesions were positioned anteriorly (i.e. in-line with the path of current flow) compared to those positioned posteriorly (relatively out-of-line with the path of current flow). This finding supports the theory that lesions draw current towards $M1_{hand}$ if they are in the path of current flow and close to the target (Kashyap et al., 2022), while posterior lesions, out-of-line with the path of current flow, may draw current away from the target. In this way, findings from synthetic lesion work (Johnstone et al., in review) partially generalise to the stroke survivor population, as the impact of lesions on E-field intensity in an ROI depended on the lesion's proximity to target, and its position relative to the path of current flow. In later paragraphs however, I discuss where the findings of this Chapter and synthetic lesion studies diverge.

4.5.4 Lesions act as carriers for tDCS-induced E-field.

Previous work supports the theory that lesions might act as carriers of E-field in the brain. For example, current flow modelling studies have shown that wide pockets of CSF (similar to lesions) are associated with clustering of E-field intensities in sites across the brain (Datta et al., 2009). Furthermore, consistent sub-cortical areas of high current density distant from the intended target have been found even in absence of brain lesions, as current is drawn to conductive structures such as the ventricles (reviewed in Bikson & Dmochowski, 2020). Elsewhere, it has been shown that electric currents are canalised through brain structures with high CSF density, such as the longitudinal fissure, facilitating E-field delivery to deep brain regions (Gomez-Tames et al., 2020). The implications of tDCS current directed away from an ROI via conductive tissue are of particular relevance to the stroke survivor population, where conductive lesions may re-direct current to non-target regions. In contrast to a neurotypical group, prediction of the destination and pattern of re-directed current is confounded by heterogeneity in the size, shape, and location of conductive tissue between stroke survivors. The necessity of individualisation of tDCS protocol particularly in clinical populations is again highlighted to account for the impact of pathological anatomy on tDCS current flow.

4.5.5 Changes in E-field intensity in $M1_{hand}$ do not fully capture the impact of lesions on tDCS-induced fields.

The impact of lesions on E-field in an ROI may not only be limited to altered E-field intensity, as the direction of current flow in a cortical target may also be altered by lesions. Briefly, the direction of current flow through an ROI is of interest because membrane polarisation by endogenous current depends on the direction of current flow relative to the somato-dendritic axes of affected cells (Berzhanskaya et al., 2013; Bikson et al., 2004; Chan et al., 1988; Farahani et al., 2021; Radman et al., 2009; Rahman et al., 2013; detailed in section 1.5.1.2). If current is drawn through conductive lesioned tissue during tDCS, the direction of current flow in surrounding grey matter may shift. This finding demonstrates the potential for increased variability in current direction in lesioned compared to neurotypical brains, which could in turn impact the behavioural effects of tDCS. Furthermore, evidence that lesions might carry current to distributed brain regions (Datta et al., 2009; Gomez-Tames et al., 2020; Kashyap et al., 2022) suggests that the focality of tDCS-induced fields may be impacted by lesions. Individualising electrode montages to counter changes in current direction and to increase focality is a candidate solution for these effects. However, as with a neurotypical population, informed decision-making will be required to prioritise E-field intensity, direction or focality (Lee et al., 2021). While the relative import of each of these parameters remains unknown in the neurotypical literature, the findings of this Chapter suggest brain lesions add complexity to the already vexed issue of tDCS optimisation.

4.5.6 Limitations

4.5.6.1 Lesions are not accurately characterised.

The results of Models A-C describe the impact of lesions on simulated current flow, given the data available. The minimum distance between the centre of $M1_{hand}$ and lesioned tissue ($lesion\ distance_{min}$) may not, for example, accurately describe the proximity of a unique, irregularly shaped 3D lesion to a cortical ROI. In addition, larger lesions in this sample of stroke survivors differ to those of comparable size in synthetic studies, where lesions are often represented by spheres (Johnstone et al., in review). By contrast, 'real' lesions are irregularly shaped three-dimensional structures which can extend across the length of the brain, simultaneously in- and out- of line with the path of current flow, proximal and distant from $M1_{hand}$. Indeed, the profile of lesions described by the same vascular territory location

can vary widely (Kim et al., 2019). However, detailed characterisation of lesions was also not possible with this dataset via machine learning, as the sample size was too small to test and train a lesion characterisation algorithm. While I note that the lesion characterisation methods used here have the benefit of intuitive interpretation, it is also recognised that the descriptors used are subject to more limitations than when used to describe regularly shaped synthetic lesions.

Current flow models used in this study were customised to recognise lesions as a 7th tissue type (Johnstone et al., in review), with a conductivity value lower than CSF but higher than grey matter (McCann et al., 2019). This approach is limited as a way to accurately represent stroke lesions in current flow models for two primary reasons. First, that lesions are not comprised of homogenous tissue, but rather include a gradient of tissue spanning maximally conductive CSF to partially damaged perilesional tissue, scar tissue and healthy tissue (Rekik et al., 2012) all with varying conductivity properties (McCann et al., 2019). Second, lesion composition is likely to vary with time post-stroke, evidenced in diffusion MRI metrics which have shown changes in perilesional tissue conductivity between acute and chronic stages (Beaulieu et al., 1999; Thiel et al., 2004; van der Zijden et al., 2008). Inclusion criteria included a minimum cut-off of 3 months to counter this issue, while maintaining a realistic cohort of survivors likely to be selected for tDCS intervention. To ascertain the true impact of lesions on tDCS-E-field, further work is required to minimise variability in estimates of the head tissue conductivity (McCann et al., 2019) including lesions at varying time points after stroke.

4.5.6.2 The interaction of E-field with smaller lesions was better characterised than for large lesions.

Secondary hypothesis B stated that lesion characteristics such as *size, distance to* $M1_{hand}$*,* and *location* would predict E-field intensity in lesions. In this study, E-field intensity in lesioned tissue was subject to greater change with increasing distance of smaller lesions compared to larger ones. This may not, however, be interpreted as a greater impact of smaller lesions on current flow, but as better characterisation of smaller lesions by the information available. For example, the measure of mean E-field in lesioned tissue may have accurately characterised E-field intensity across tissue in small lesions, while in large lesions

E-field intensity may vary across the structure possibly with higher values found in lesioned tissue positioned more closely to the anode than more distant tissue, within the same lesion.

This issue extends to the findings of Models A and C. Consider, for example the case study of participant F, a stroke survivor with a very large lesion extending across cortical and sub-cortical regions, characterised only as proximal and medially-positioned relative to $M1_{hand}$ in the winning model used to describe the impact of lesions on E-field in $M1_{hand}$ (Model A). Similarly, participant B had a medial lesion positioned proximally to $M1_{hand}$, though model A did not capture the difference in lesion size between participants: E-field intensity in $M1_{hand}$ was above the group average in participant B and below it in participant F. Here, predictions of the impact of lesions on current flow during tDCS deduced from Model A do not translate to individual cases. This may also be the case for the generalisability of work suggesting that conductive structures in the path of current flow may have a systematic impact on current delivery to an ROI (Johnstone et al., in review; Kashyap et al., 2022): it is unknown if these findings extend beyond structures similar to small- or mid-sized lesions, to large lesions which may have an unpredictable impact on the distribution of current through the brain. Rather than pursuing heuristics which might be used to optimise tDCS delivery, these findings further underscore the need for individualised tDCS protocol design particularly in the context of stroke, and a move away from group-level application which might be confounded by high heterogeneity in the *anatomical brain state* of stroke survivors.

4.5.7 Accounting for lesions in current flow models does not solve the optimisation problem of tDCS in stroke.

If current flow models evolve to accurately account for individual stroke lesion size, shape, conductivity, location and proximity to target, the optimisation problem for tDCS use in stroke will remain unsolved. This is first because anatomical changes following stroke are not limited to lesions; recent animal work has reported pervasive stroke-related degeneration of cortical tissue and white matter tracts extending up to 48 weeks post-stroke (Syeda et al., 2022), with implications for the impact of altered CSF thickness and tissue density on the distribution of tDCS current flow (Antonenko et al., 2018; Laakso et al., 2015; Mahdavi & Towhidkhah, 2018; McCann & Beltrachini, 2021; Opitz et al., 2015).

Second, because differences between neurotypical and pathological brains are not limited to anatomy. The neurochemical state of the brain before tDCS is applied is known to impact capacity for tES-induced cortical plasticity (Bradley et al., 2022; Paulus & Rothwell, 2016; Pellegrini et al., 2021; Polanía et al., 2010; Reato et al., 2010; Stagg et al., 2018), and cortical excitability may be subject to significant change after stroke (Bernhardt et al., 2017; Buma et al., 2013; Cramer, 2008; Di Pino, Pellegrino, Assenza, et al., 2014; Krakauer & Carmichael, 2017b; Kwakkel et al., 2004). The expectation that the effects of tDCS in stroke survivors can be predicted from the effects observed in healthy individuals receiving the same intervention is fraught with logical problems (Lee et al., 2021) which cannot be solved by accounting for pathological anatomy alone.

4.5.8 Conclusion.

In this study, a customised current flow modelling pipeline was used to investigate the impact of lesion location, size and distance to target on tDCS-induced E-field intensity in $M1_{hand}$ in over 200 stroke survivors and neurotypical participants, when a commonly used 1mA conventional tDCS protocol was simulated. Some findings from synthetic lesion studies were found to generalise to the stroke survivor population, namely that the impact of lesions on tDCS E-field intensity in an ROI depends on the position of a lesion (in- or out- of line with the path of current flow), and on the distance between a lesion and an ROI. However, a novel finding is described where larger, proximal lesions are not systematically associated with increased E-field intensity in an ROI as previously reported (Johnstone et al., in review; Minjoli et al., 2017; Piastra et al., 2021). Rather, large, irregularly shaped 'real' lesions are poorly quantified by the measures available, and the findings of synthetic lesion work or studies with low sample size may not generalise to survivors with large lesions. Meanwhile, small lesions in the path of current flow can have a larger influence on E-field than previously thought.

Though a systematic pattern of the impact of lesions on tDCS-induced fields could not be described across the heterogeneous stroke population, a significant impact of lesions on current flow is reported. Protocol individualisation is necessary to optimise tDCS application in individual cases, as the impact of lesions may not only result in altered E-field intensity in an ROI, but in altered spatial focality and direction of current flow (Gomez-Tames et al.,

2020; Kashyap et al., 2022). Lesions acting as carriers of electric current could produce hotspots of relatively high E-field intensity in regions distant from the intended target, resulting in collateral neuromodulation of non-target regions. Taken together, lesions may contribute significantly to variability in tDCS-induced fields in stroke survivors, possibly contributing to high variability observed in behavioural outcomes. Implementation of CFM-informed multi-electrode montages may counter some of the issues raised, though this will require detailed current flow modelling and multi-electrode hardware, a potential barrier to optimised protocol application in clinical settings. Nevertheless, the findings reported here may explain the high variability observed in tDCS outcomes in stroke; the promise of tDCS in motor rehabilitation may yet be realised with protocol individualisation.

CHAPTER 5. GENERAL DISCUSSION

Physical therapy improves upper limb rehabilitation after stroke (Biernaskie, 2004; Krakauer & Carmichael, 2017c; Ward et al., 2019; Zeiler & Krakauer, 2013) and it is well-established that increased training dose (quantified as the number of repetitions of an intervention; Dorsch & Elkins, 2020) is positively correlated with improved outcomes (Blennerhassett & Dite, 2004; French et al., 2009; Kwakkel et al., 1997; Lohse et al., 2014; Scrivener et al., 2012). Schneider and colleagues (Schneider et al., 2016) however reported that a 240% increase in training dose was required to improve stroke outcomes, and a recent meta-analysis highlighted that the majority of research into the dose-response relationship for stroke rehabilitation focusses on one-to-one training with a practitioner (Stewart et al., 2017). Under these conditions, an unsustainable increase in time and staff would be required to achieve a meaningful increase in treatment dose for every stroke survivor (Dorsch & Elkins, 2020); innovation is greatly needed to increase efficiency and accessibility of post-stroke rehabilitation.

The focus of this thesis has been on optimising methods for non-invasive maximisation of neuroplastic potential, for increased efficiency of stroke rehabilitation. Two candidate methods were explored: exploitation of an endogenous sensitive period following human stroke, which was hypothesised to occur in the sub-acute phase of recovery (Chapter 2), and application of optimised tDCS to encourage an excitable brain state hypothesised to support potentiation (Chapters 3 and 4).

5.1 Heterogeneity in trajectories of motor recovery and cortical excitability after stroke.

5.1.1 Decoupled timelines of post-stroke motor recovery and cortical excitability.

In Chapter 2, I found that intra-cortical inhibition in $M1_{hand}$ was weaker at 3 weeks post-stroke compared to neurotypical participants, and that it had returned to neurotypical levels by 6 months. This finding is in concurrence with previous research into human post-stroke CSE (Liepert et al., 2000; Manganotti et al., 2002; McDonnell & Stinear, 2017; Swayne et al., 2008). In the context of preclinical work showing that persistently increased GABAergic tone

impedes post-stroke recovery and disinhibitory intervention improves function (Clarkson et al., 2010; Lake et al., 2015; Orfila et al., 2019), the sub-acute endogenous disinhibition observed in mildly impaired participants in Chapter 2 suggests a similar mechanism could underlie stroke recovery in humans, though the findings are limited by relatively small sample size and lack of representation of survivors with more severe symptom severity.

A prevailing hypothesis in stroke rehabilitation literature is summarised in the report of The Stroke Roundtable Consortium (Bernhardt et al., 2017). It posits that accelerated gains often observed in the 'sub-acute' phase of human stroke, followed by relative stability of chronic deficit from approximately 6 months, are underpinned by time-dependent changes in excitatory and inhibitory brain activity which mediate the brain's capacity for neuroplasticity. In Chapter 2Chapter 1, I found that the trajectories of motor recovery (measured by the ARAT and FIM) and change in GABA-mediated intra-cortical inhibition (measured by SICI ratio) were not tightly temporally coupled; motor scores reached ceiling very early in mildly impaired stroke survivors while intra-cortical inhibition continued to change over 6 months.

This finding supports the concept that a 6-month pro-plastic brain environment occurs during the sub-acute phase of stroke, but contends with the hypothesis that it is temporally coupled with motor recovery (Figure 5.1). Further work is needed to assess whether this 6-month window of disinhibited brain activity also occurs in stroke survivors with moderate and severe impairment who tend to experience different trajectories of motor recovery. For example, the trajectories of motor recovery and cortical disinhibition may be temporally coupled in moderate and severe stroke, but not mild stroke. Alternatively, a homogenous 6-month window of endogenous disinhibition may occur in all stroke survivors regardless of recovery trajectory, or this 6-month window could occur with varying magnitude moderating strength of recovery. A fourth possibility could be that impactful changes in excitatory-inhibitory balance occur in brain regions distant from $M1_{hand}$ in moderate-severe stroke, in functionally connected areas which escaped infarction and were not captured by stimulation targeting $M1_{hand}$. These hypotheses are speculative and are not exhaustive. They demonstrate the great need for further research; without direct investigation with more severely impaired survivors, the mechanisms underlying human post-stroke recovery and

the generalisability of pre-clinical findings to survivors with heterogeneous recovery profiles remain unknown.

Given evidence that TMS-assessed changes in excitatory-inhibitory balance were not tightly temporally coupled in mildly impaired human stroke survivors (Chapter 2Chapter 1), one must consider why. Two viable explanations arise: first, since physiology causes behaviour, one might propose that motor recovery observed after stroke is not in fact underpinned by increased excitability and reduced inhibition as preclinical work suggests. Second, one must consider that there are methodological limitations to the use of TMS to measure longitudinal changes in brain activity after stroke. Both explanations are discussed below.

Extensive reorganisation of disrupted networks occurs after stroke (Carmichael et al., 2017; Cramer, 2008), a process thought to require increased cortical excitability to promote functional and structural plasticity (Cheng et al., 2014; Li et al., 2010; Omura et al., 2016; Overman et al., 2012; Tennant et al., 2017; Wahl et al., 2017). However Krakauer and Carmichael (Krakauer & Carmichael, 2017c) point out that the majority of cortical reorganisation processes have not been directly linked to functional gains: they are reactive, not reparative. Branscheidt and colleagues (Branscheidt et al., 2019) highlight the distinction between reactive and reparative processes as a possible explanation for reported decoupling of the trajectories of motor gains and network reorganisation after stroke. Here, I suggest the logic might also apply: in the group of mildly impaired stroke survivors studied in Chapter 2, TMS-assessment of brain activity may have captured a reactive alteration to intra-cortical inhibition which by definition is not coupled with motor gains. Reparative processes underpinned by excitability changes may yet have occurred without being captured, as hypothetically coupled brain activity would have ceased as motor gains reached ceiling by the earliest timepoint examined (3 weeks). This theory is in keeping with the hypothesis that the findings of Chapter 2 may not extend to survivors with more severe impairment, where reparative processes may persist at a greater magnitude for a longer duration (I note however that this contends with the homogenous timeline described by the Stroke Round Table Consortium (Bernhardt et al., 2017)). It also highlights one of the methodological limitations of using TMS to measure functional brain state after stroke: where an effect is detected, it can be difficult to describe the complex neural processes which gave rise to it.

Each TMS-MEP recorded reflects transcortical, intracortical, and spinal projections; a biomarker of CSE rather than a direct measure of brain activity (Bestmann & Krakauer, 2015; Di Lazzaro & Ziemann, 2013; Rusu et al., 2014). MEPs are vulnerable to stroke-induced confounds such as differences in cortico-spinal tract integrity (Kemlin, Moulton, Lamy, et al., 2019; Potter-Baker et al., 2018), variable resting tone in hand muscles (Darling et al., 2006; Kiers et al., 1993), and changes to brain anatomy associated with decreased and more variable TMS-induced E-field in grey matter volumes of interest (Mantell et al., 2021; Minjoli et al., 2017). Increased variability in RMT detected in stroke survivors compared to neurotypical participants in Chapters 2 and 3, for example, could reflect differences in integrity of descending projections in stroke survivors, instead of greater variability in brain activity. Since significantly heightened variance was not also detected in recruitment curve data in Chapter 3, it appears that some TMS measures of CSE are more vulnerable to confounds than others.

Furthermore, the finding of a sub-acute reduction in inhibitory signalling does not capture the full profile of changes in excitatory-inhibitory balance in the post-stroke brain. SICI indexes the operation of transiently activated, cortical GABA interneurons (Ziemann et al., 1996, Ziemann et al., 1996); reduced SICI is thought to be underpinned by reduced 'phasic' synaptic GABAergic inhibition. Classic preclinical work suggested that reduced 'tonic' GABA was linked to functional recovery after stroke (Blicher et al., 2015; Kim et al., 2014; Krakauer & Carmichael, 2017b; Clarkson et al., 2010; Di Lazzaro et al., 1998; Orfila et al., 2019), while more recently enhancement of 'phasic' GABA inhibition has been identified as a therapeutic target (Hiu et al., 2016). While the latter suggests some reparative impact of altered SICI could be captured by TMS, specific probing of different inhibitory systems will be required to describe the *functional state* of the post-stroke brain in humans and inform optimal timing of interventions, a task which may be beyond the scope of TMS alone. As Grigoras and Stagg (Grigoras & Stagg, 2021) point out, regulation of excitatory-inhibitory balance after stroke may not relate to TMS-assessed inhibitory changes in a straightforward way. The complexity of the balance shift after stroke, including mechanisms underlying reparative and reactive processes, is exemplified in the finding that measures of inhibitory activity differ depending on the modality used; MRS-assessed GABA concentration, for example, does not appear to be correlated with TMS-assessed (~3ms SICI) synaptic

inhibition (Dyke et al., 2017; Mooney et al., 2017; Tremblay et al., 2013). While TMS offers valuable insight into the post-stroke brain environment by non-invasive means, multi-modal work is required to interrogate the interplay between various excitatory and inhibitory systems which may be important for optimising the timing of neuromodulatory intervention.

5.1.2 Trajectories of motor recovery after stroke vary with symptom severity.

As discussed in section 2.6, the ARAT and FIM scores described in Chapter 2 may not have captured the full profile of upper limb recovery after stroke. However, a recent longitudinal study of 412 stroke survivors (van der Vliet et al., 2020) reported that individuals with mild impairment (measured with the FM-UL) reached 90% of total recovery within weeks of stroke, in concurrence with the trajectory of ARAT and FIM scores reported in Chapter 2. Furthermore, van der Vliet and colleagues (van der Vliet et al., 2020) identified 5 sub-groups of stroke survivors, stratified by symptom severity, with distinct trajectories of motor recovery. While all sub-groups reached a peak in impairment reduction within the time window defined as 'sub-acute' (1 week – 6 months; Bernhardt et al., 2017) significant differences were found in the temporal profile of recovery within the sub-acute phase: moderately impaired individuals experienced a shallower trajectory of reducing impairment over 6 months, while both mildly and severely impaired survivors tended to reach a 'peak' in recovery (relative to final outcome) within weeks of stroke (Figure 5.1). Emerging work concurs with the notion that motor recovery trajectories after stroke are heterogeneous. For example, Bonkhoff and colleagues (Bonkhoff et al., 2022) described a distinct recovery profile in severely impaired survivors compared to those with moderate or mild symptoms, while elsewhere, some survivors with initially severe impairment have been reported to recover within 10 days of stroke (Grefkes & Fink, 2014).

Heterogeneity within the sub-acute stroke timeline was also acknowledged in The Stroke Roundtable Consortium report (Bernhardt et al., 2017). The authors pointed out that functional gains occur for many survivors within 1-week to 1-month post-stroke, and describe some uncertainty over how early training could be applied (Bernhardt et al., 2006; Dromerick et al., 2009; The AVERT Trial Collaboration group, 2015). The work described above (Bonkhoff et al., 2022; van der Vliet et al., 2020) has since made progress in

characterising heterogeneity in functional recovery trajectories after human stroke, and development of methods to predict stroke outcomes is also progressing quickly (Fleury et al., 2022; Hope et al., 2013, 2019; Quinlan et al., 2015; Selles et al., 2021; Stinear & Byblow, 2017; Walford et al., 2021).

Taken together, improved understanding of human stroke recovery may necessitate a shift away from broad, temporally-defined phases such as “sub-acute” and “chronic”, in light of emerging evidence that the timeline of recovery (and the neural processes which underpin it) is likely subject to high inter-individual variability. Furthermore, there is presently a cavernous gap between the specificity of non-invasive measures of brain activity changes after stroke (e.g. TMS-assessed excitability) and the specificity required for state-dependent neuromodulation by tDCS. A shift is needed towards individualisation of interventions which may benefit some survivors more than others, at different time points after stroke.

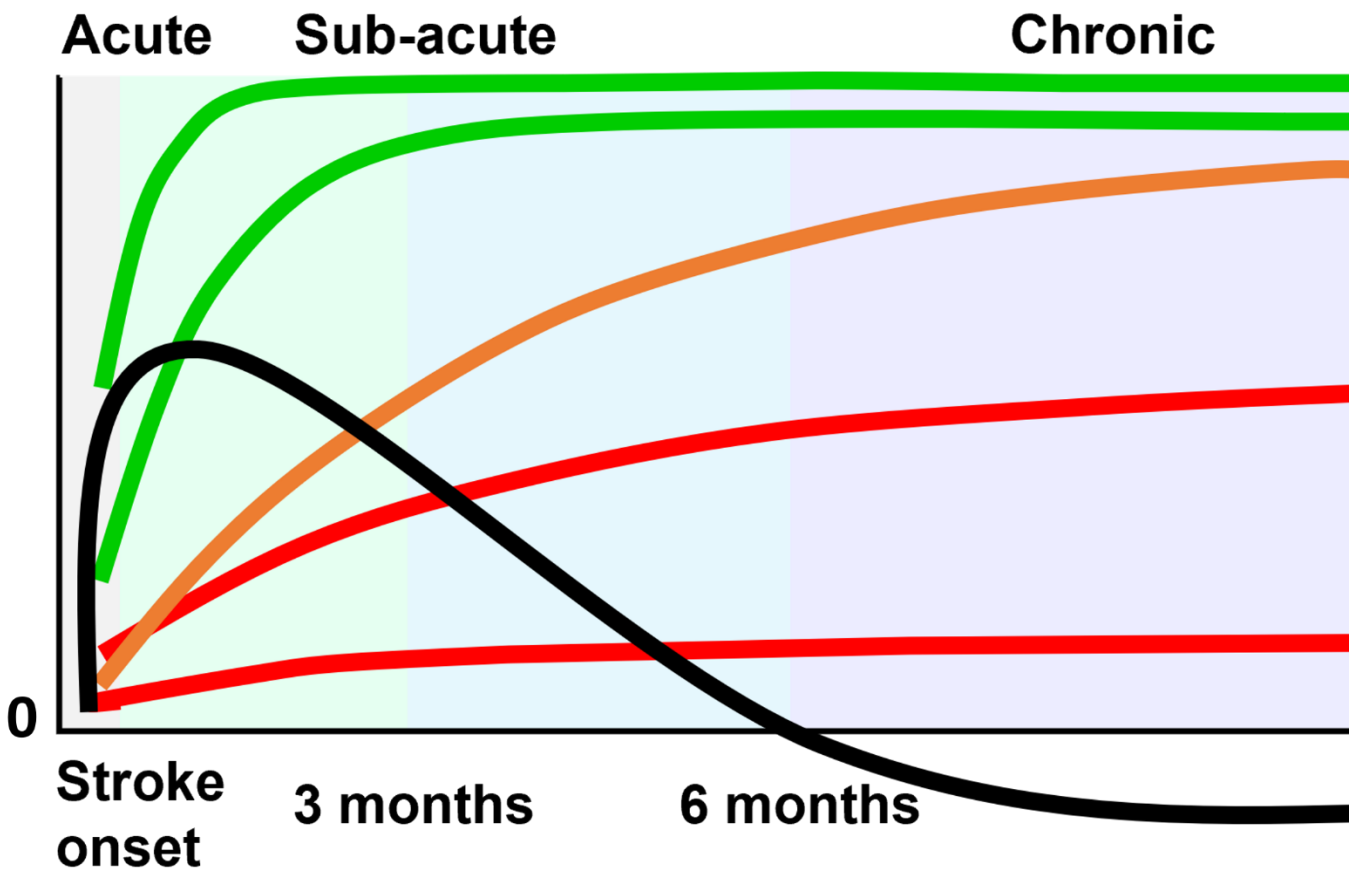

Figure 5.1. A revised schematic of the trajectories of cortical excitability change and functional gains after human stroke, based on the work of van der Vliet and colleagues (van der Vliet et al., 2020) and the findings of Chapters 2 and 3 of this thesis. The timing and magnitude of sub-acute peaks in capacity for endogenous neuroplasticity are moderated by stroke symptom severity, and functional recovery may not be temporally coupled with changes in TMS-assessed cortical excitability. On the y-axis, zero simultaneously represents neurotypical cortical excitability and minimum motor function. Time post-stroke is shown on the x-axis. Coloured lines depict the motor recovery trajectories of sub-groups of survivors with mild (green), moderate (orange) and severe (red) motor impairment. The black line depicts TMS-assessed changes in excitatory-inhibitory balance recorded in mildly impaired stroke survivors in Chapters 2 and 3 of this thesis: a peak in plastic potential is shown at ~3 weeks post-stroke, returning to neurotypical levels by ~6 months (Chapter 2), and a decrease in plastic potential is shown after 6 months (Chapter 3). It is not known if this profile of cortical excitability generalises to stroke survivors with moderate and severe symptom severity.

5.1.3 Optimisation requires identification of individuals best suited to neuromodulation.

The findings of Chapter 2 suggest that excitability-boosting interventions such as tDCS may be redundant in mildly impaired survivors whose motor scores reached ceiling relatively soon after infarction without neuromodulatory intervention. It is not yet known if moderately and severely impaired survivors experience the same 6-month period of reduced synaptic inhibition, or whether this shift in functional brain state might contribute to reparative processes, or simply be reactionary. As mentioned above, heterogeneous trajectories of motor recovery could instead be underpinned by heterogeneous trajectories of cortical excitability, or varying magnitude of neurophysiological change, possibly mediated by symptom severity (Figure 5.1). Further work is needed to understand which mechanisms could be viable and interrogate how they may be best supported.

If varying trajectories of cortical excitability are detected in a large cohort of stroke survivors, and neurophysiological shifts in excitatory balance are found to correlate with symptom trajectory, interventions such as tDCS maintain their promise. Those with atypical functional recovery profiles ('non-fitters') may for example benefit from intervention to shift brain activity towards a typical profile via neuromodulation; reinstatement of brain function comparable to the neurotypical population in chronic stroke has for example been linked to better motor outcomes (Calautti & Baron, 2003).

As discussed throughout this thesis, and in previous work which also considers tDCS use to target non-motor functions (Crinion, 2016; Holland & Crinion, 2012), optimisation will require identification of survivors who might maximally benefit. For example, the timing of tDCS-supported training may be optimal during an individually-assessed period of decreased cortical excitability coupled with sub-optimal reduction of symptom severity, in a survivor who is MEP positive (Stinear et al., 2012), has sufficient cortical structures remaining (not limited to M1) to support network re-organisation (Aswendt et al., 2021; Nouri & Cramer, 2011; van der Cruijsen et al., 2022), and has <63% injury to the CST (Quinlan et al., 2015). I note that the potential for tDCS-assisted intervention is not limitless, as outcomes will depend on the severity of comorbid symptoms such as cognitive deficit (Sanchez-Bezanilla et al., 2021; Verstraeten et al., 2020), reduced upper limb strength (de Sousa et al., 2018), or chronic network dysfunction (Guggisberg et al., 2019). The question here is whether an additional target for intervention is viable or not: is shifting excitatory-inhibitory balance

correlated with neural repair and improvement of symptoms? Could excitatory intervention promote greater recovery in some stroke survivors? The efficacy of tDCS in stroke will depend not only on optimisation of the technique, but careful identification of individuals who may benefit from it.

5.1.4 Optimal timing of neuromodulatory intervention depends on individual functional brain state, not recovery phase.

In addition to 'boosting' cortical excitability which is hypothesised to be heightened in sub-acute stroke, tDCS has been suggested as a means to "re-open" a pro-plastic period of increased excitability in survivors in the chronic phase of recovery. In Chapter 3, I found that TMS-assessed CSE was lower in chronic stroke survivors with mild-moderate impairment, compared to neurotypical participants (Figure 5.1). Meanwhile in Chapter 2, I showed that intra-cortical inhibition was comparable to neurotypical levels after ~6 months. These findings are not conclusive due to relatively small sample size, though they do illustrate heterogeneity in the post-stroke timeline during a temporal "phase" when brain activity is hypothesised to have stabilised to neurotypical levels (Bernhardt et al., 2017). They also contribute to existing evidence (described in section 1.3.2) that excitatory and inhibitory systems do not respond uniformly to stroke. As evidence such as this continues to emerge in the human stroke literature, the applicability of homogenous frameworks for post-stroke neurophysiological changes and their relationship with functional recovery decreases (Figure 5.1).

Pre-clinical work has evidenced the benefit of 're-opening' a post-stroke period, most notably in the work of Zeiler and colleagues (Zeiler et al., 2016) who reported significantly improved motor outcomes after induction of a second stroke, compared to mice who experienced one stroke. TDCS is a candidate tool to non-invasively induce an excitable brain environment after stroke in humans, to re-instate a brain environment thought to modulate functional recovery. However, in addition to the high variability observed in stroke outcomes, a number of barriers prevent translation of preclinical findings to non-invasive intervention in humans. First, the rodent post-stroke timeline occurs on a very different temporal scale to that observed in humans. For example the so-called sensitive period occurs much earlier, and lasts for less time: training initiated 1 day after rodent stroke has been shown to mediate recovery, while no effect is observed if training is delayed by 1 week

(Ng et al., 2015; Zeiler et al., 2013). Findings such as these suggest the rodent sensitive period gives way to a period similar to a "chronic" phase 1 week to 1 month post-stroke (the beginning of the temporally defined "sub-acute" phase in humans). Since the stroke recovery timeline does not translate to the observed duration of functional gains in human stroke survivors, and recent work suggests that (sub-groups of) survivors may enter a period of stabilised chronic deficit at different times (Bonkhoff et al., 2022; Fleury et al., 2022; Selles et al., 2021; van der Vliet et al., 2020; Figure 5.1), a robust method may be required to identify *when* an endogenous sensitive window occurs and excitability-boosting interventions such as tDCS may be best applied. Since the timeline for a critical period for stroke recovery may be subject to heterogeneity, interventions intended to target survivors in a homogeneously defined "chronic" time window may contribute to variable outcomes.

In addition, to my knowledge pre-clinical work does not provide a robust model for human stroke survivors in a late chronic phase, for example 10 years post-stroke. While in theory, concepts such as "re-opening" the post-stroke sensitive period may apply to an individual any time after stroke, chronic changes such as network re-organisation may mediate the impact of a tDCS-induced sensitive period: increasing motor cortical excitability may not benefit a survivor whose primary motor control processes occur in brain regions distant to neurotypical $M1_{hand}$. Mechanistic understanding of optimal tDCS application, and of the trajectory of post-stroke neurophysiology, will be required to translate ideas such as *re-opening the critical period* to a human stroke population.

In the context of evidence that heightened excitability and decreased inhibition support recovery after stroke, one might argue that tDCS would be beneficial regardless of its excitatory profile before stimulation is applied. This approach is likely sub-optimal because tDCS is state-dependent (Lisman, 2001; Monte-Silva et al., 2013; Pellegrini et al., 2021; Stagg et al., 2018), and has a non-linear or even non-monotonic impact on CSE (Esmaeilpour et al., 2018). Applying the same tDCS protocol across a group of neurotypical participants may produce both excitation and inhibition due to differences in *functional* and *anatomical brain state*, and the effect may be exacerbated in stroke where pathological, time-dependent alterations in excitatory-inhibitory balance and anatomy are expected. Heterogeneity in human post-stroke excitability is evident in the work presented in this thesis, for example, as chronic stroke survivors' CSE was comparable to neurotypical participants in Chapter

2,Chapter 1 and significantly lower than the neurotypical group in Chapter 3. Since small variations in brain state may alter tDCS effects, the use of post-stroke "phase" to predict the cortical excitability profile of an individual survivor does not allow for effective individualisation of tDCS. Use of temporally-defined eligibility criteria is a sub-optimal method to select patients who may benefit most from tDCS intervention. Development of robust biomarkers to track individual progression of brain activity after stroke is a therapeutic target of high importance (Boyd et al., 2017), and is required to facilitate a shift towards individualised intervention.

5.2 TDCS optimisation.

5.2.1 CFMs are agnostic to the physiological impact of stimulation.

A reliable method to account for neurophysiological 'state' in tDCS application has not yet been developed for neurotypical individuals or stroke survivors. However, recent advances in current flow models (employed in Chapters 3 and 4) have progressed to provide gyri-precise, validated (Datta et al., 2009; Huang et al., 2017b, 2019a; Opitz et al., 2016) estimates of E-field delivered to the brain during non-invasive stimulation. These models allow researchers to control the intensity, direction, and focality of applied fields (functionality is detailed in section 1.6.2), but do not extend to predicting the impact of tDCS on human behaviour. While it is now possible to use CFM to prescribe a chosen E-field intensity in a cortical ROI for example (Dmochowski et al., 2011, 2013; Huang, Thomas, et al., 2018; Saturnino, Siebner, et al., 2019), the optimal 'dose' of E-field required to meaningfully alter potentiation of a skill remains unknown and is likely subject to individual differences in cellular morphology, brain state at the time of stimulation, and cumulative effects summed across a functional network (Bikson et al., 2004; Chan et al., 1988; Esmaeilpour et al., 2018; Jefferys, 1981; Joucla & Yvert, 2009; Polanía et al., 2010; Reato et al., 2010, 2013).

In the context of stroke, where atypical neuronal activity is hypothesised to promote functional recovery, the dilemma of defining an optimal 'dose' for an individual is exacerbated. In Chapter 2, I found a ~20% decrease in intra-cortical inhibition at 3 weeks post-stroke in survivors who experienced good clinical outcomes after relatively mild initial symptoms. While a hypothesis persists for the benefits of enhanced excitation and reduced

inhibition in stroke rehabilitation (Bernhardt et al., 2017; Carmichael, 2012; Clarkson et al., 2010, 2011, 2015; Di Pino, Pellegrino, Capone, et al., 2014; Fujiwara, 2020; Glykys & Mody, 2007; Hiu et al., 2016; Johnstone et al., 2018; Joy & Carmichael, 2020; Kim et al., 2014; Krakauer & Carmichael, 2017b; Wang et al., 2018), no precedence exists to suggest *how much* disinhibition is optimal. When considering the dose-response relationship of tDCS in human stroke, two primary targets for investigation emerge: what is the relationship between exogenous E-field and cell- and network-specific brain activity? Second, what is the optimal magnitude of change in brain activity required to modulate potentiation of a given skill?

Without answers to these questions, tDCS will continue to be applied in a trial-and-error fashion. Effective methods may still be found, allowing for reverse-calculation to satisfy curiosity. A pattern has for example begun to emerge where PA-tDCS is associated with decreases in neurophysiological markers of cortical excitability (Laakso et al., 2019; Rawji et al., 2018) and behaviour (Hannah et al., 2019). The direction of this effect at first appears counter-intuitive, as PA-tDCS is associated with radial-inward (supposedly excitatory) current flow in $M1_{hand}$ (Evans et al., 2022; Farahani et al., 2021; Laakso et al., 2017; Lafon et al., 2017; Radman et al., 2009; Rahman et al., 2013). Evans and colleagues (Evans et al., 2022) postulate however that the direction of PA-tDCS effects may not only reflect the impact of DC fields in $M1_{hand}$, but interplay with functionally connected regions also affected by DC field. Activity in the primary sensory cortex, positioned in the posterior bank of the central sulcus, or the dorsal pre-motor cortex positioned in the anterior crown may explain the relatively consistent yet counter-intuitive effects of PA-tDCS (Evans et al., 2022; Siebner, 2020). Further research is required to elucidate the mechanisms of DC field acting on varied nodes in a target network, to improve understanding of the tDCS dose-response relationship and in turn to support innovation in the field.

5.2.2 MEPs contribute to tDCS outcome variability.

TMS-tDCS studies are as much an interrogation of TMS variability as tDCS effects. There is a great need to assess the impact of tDCS not only on MEPs and individual neurons, but on more complex network activity which might modulate LTP, the primary therapeutic target in tDCS-augmented stroke rehabilitation. Greater understanding of the impact of tDCS on

relatively small populations of cells (Bikson et al., 2004; Lafon et al., 2017; Radman et al., 2007, 2009b; Rahman et al., 2013; Reato et al., 2010, 2013) has not yet reliably translated to improved predictability of transcranial stimulation outcomes (see Chapter 3). While mechanistically-informed protocol development remains a primary goal of tDCS research, recent findings suggest that tDCS-induced changes in MEP amplitude do not transfer to other neurophysiological measures (Hannah et al., 2019; Horvath et al., 2015). In fact, a comparable increase in MEP amplitude has been recorded with opposite motor behaviours (Bagce et al., 2013), and a recent systematic review concluded that MEP amplitude may not align with changes in motor performance (Ryan et al., 2023). The relationship between MEPs, which probe the state of pre-synaptic intracortical processes and post-synaptic cortical excitability, and motor learning is not straightforward (Bagce et al., 2013; Gelli et al., 2007; McDonnell & Ridding, 2006; Muellbacher et al., 2000; Todd et al., 2009).

That is, if a measurable change in MEP amplitude was reliably reported after application of a given tDCS protocol (Horvath et al., 2015; Laakso et al., 2015), it may have no causal relevance to motor behaviour (Bestmann & Krakauer, 2015). Rather than providing clear evidence of target engagement by DC fields, MEPs may offer no more insight than a colour map of tDCS-induced E-field distribution throughout the brain, providing confirmation that current has reached $M1_{hand}$ without describing what this means for behavioural outcomes. The circular argument completes here when one considers measuring the impact of tDCS on potentiation of a complex task regardless of confirmation of target engagement, to satisfy the question: “does this work” before: “how does this work?”.

5.2.3 Bridging the gap between physics and physiology.

The advent of CFMs propelled tDCS use toward informed design and away from justification by precedence in the literature. Once again, CFM may here offer some resolution to the target engagement problem described above, as development of biophysically accurate models has potential to bridge the gap between the physics of current flow and the physiological effects of stimulation.

A neural twin is a compressed computational rendition of a specific patient’s brain. It is comprised of multi-scale models which aim to link the impact of exogenous field on cellular activity, including polarisation of specific cellular compartments (Aberra et al., 2020;

Bonaiuto et al., 2016; Galan-Gadea et al., 2022; Wang et al., 2018) with neural mass models which describe the dynamics of populations of neurons, for example by modelling network amplification associated with the direct and indirect effects of tDCS across the brain (Clusella et al., 2022; Jansen & Rit, 1995). Recent work has extended to computationally reproduce electrical activity recorded during epileptic seizures, in a first step towards linking electrical field modelling to physiological outcomes (Sanchez-Todo et al., 2022). Biophysically-accurate models may shape the future of tDCS, as dual computational- and empirical-validation methods could allow for tighter control and detailed interrogation of the distribution and impact of transcranially-applied electrical fields. In the next section however, I discuss the unresolved problem of translating neurotypically-informed models to pathological populations.

5.2.4 TDCS optimisation methods must be stroke-specific.

Progress in CFM-informed tDCS is likely to first occur with models of the neurotypical human brain. In Chapter 4 I considered how one aspect of pathological anatomy, stroke lesions, may alter the distribution of exogenous electrical fields. Candidate methods to account for this effect include adjustment of electrode montage or stimulator output in stroke-specific tDCS protocol (Johnstone et al., in review; Minjoli et al., 2017; Piastra et al., 2021), though accounting for the physical properties of DC fields does not address other stroke-induced features which might impact tDCS efficacy. For example, stroke is characterised by abnormalities in several neurotransmitter systems, and the notion that the effects of stimulation in patients can be predicted from the effects observed in healthy individuals receiving the same intervention is fraught with logical problems (Lee et al., 2021).

In addition to a relatively limited understanding of the neurophysiological response to DC fields in the pathological brain, stroke-induced network re-organisation will likely require revision of commonly accepted targets for stimulation in the context of stroke. Van der Cruijsen and colleagues (van der Cruijsen et al., 2022) recently distinguished between ‘anatomical’ and ‘functional’ targets for motor tDCS application, using EEG recordings collected during a robotic wrist-manipulator task to identify the primary brain region involved in active motor engagement. In neurotypical participants, the authors reported

functional targets located ipsilaterally to anatomically-defined dominant $M1_{hand}$. In contrast, functional motor targets were located ipsilesionally in 11 of 20 stroke survivors, and contralesionally in 9 survivors. Functional targets in the stroke survivor population included the premotor cortex, Wernicke's area, intermediate frontal cortex, pars opercularis, primary somatosensory cortex, and the supramarginal gyrus, in addition to the primary motor cortex. Similarly to the data reported in Chapter 4, $M1_{hand}$ was entirely occluded in 2 stroke survivors. Findings such as these underscore the dilemma of translating tDCS protocols designed for a neurotypical population to stroke survivors. In addition to the previously-discussed need to individualise tDCS depending on brain 'state', future work will require individualised identification of cortical targets in participants with network disruption. This may be of particular relevance for chronic stroke survivors, where functional gains could depend more on supporting alternative network activity than on recovery of function of the classic motor control network (Swayne et al., 2008).

Functional tDCS targeting recommendations are not novel; Nouri and colleagues suggested that confirmation of the integrity of the biological target might be included in tDCS eligibility criteria a decade ago (Nouri & Cramer, 2011), and by extension recognised the difficulties of translating neurotypically-defined stimulation targets to a stroke survivor population. The impact of lesions on tDCS-induced E-field may therefore extend across the parameter space for stroke-specific protocol design: E-field **intensity** in an ROI can be altered by lesions (Datta et al., 2011; Galletta et al., 2015; Handiru et al., 2021; Johnstone et al., in review; Minjoli et al., 2017; Piastra et al., 2021; Chapter 4), E-field **direction** in an ROI may be modulated by lesion location and proximity (Johnstone et al., in review; Kashyap et al., 2022), canalising of electric currents through conductive structures such as lesions may result in reduced, and less predictable **focality** of applied fields (Bikson & Dmochowski, 2020; Gomez-Tames et al., 2020), and ROIs themselves may change if neurotypical targets such as $M1_{hand}$ are no longer involved in primary motor behaviour (van der Cruijsen et al., 2022).

The feasibility of accounting for the impact of stroke-induced changes in *functional* and *anatomical state* in tDCS study protocol is at present limited by the additional time, funding, and expertise required particularly in clinical settings. This is an example of the cognitive dissonance which may have curbed innovation in the tDCS field: the original appeal of tDCS

as a cheap, accessible tool for non-invasive neuromodulation contrasts some evidence suggesting that a more complex approach to implementation may be required for effective neuromodulation of the pathological brain.

5.2.4.1 Bayesian statistics may allow for nuanced interpretation of tDCS study outcomes.

The complexity of the multi-variate tDCS optimisation problem may be better approached by Bayesian statistics. For example, the frequentist statistical approach employed in Chapter 3 suggested that the null hypothesis (that PA-tDCS does not significantly alter TMS-assessed CSE) could be accepted based on a p-value threshold ($\alpha = .05$). In Bayesian statistics however, a more flexible and nuanced interpretation of null results is possible; probabilities are assigned to both the null and alternative hypotheses based on prior knowledge, and the collected data is used to update them (Dienes, 2014; Kruschke, 2018). For example, future work is recommended to directly address the following hypothesis: conventional tDCS has a stronger impact on MEP amplitude than an individualised protocol or sham-tDCS. A Bayesian approach could here be used to quantify the degree of evidence for and against the hypothesis, instead of using a p-value threshold to reject or accept the null hypothesis in a binary fashion. Importantly, the Bayesian approach provides information for the relative strength of evidence for competing hypotheses, allowing for more nuanced interpretation of the findings and perhaps clearer direction when designing follow-up studies, particularly when multiple plausible hypotheses exist in the multi-faceted tDCS parameter space. In practice, Bayesian Linear Mixed-Effects Models can be implemented in RStudio using the *blme* package (Chung et al., 2013), an extension of the *lme4* package (Bates et al., 2020) used in this thesis.

5.2.5 Individualised- and optimised-tDCS maintains promise as an adjunct tool for motor rehabilitation after stroke.

While conventional tDCS has been used to great effect (Hashemirad et al., 2016; Horvath et al., 2015; Orrù et al., 2020; O'Shea et al., 2014; Wang et al., 2021), outcome variability remains an issue (Chew et al., 2015; Laakso et al., 2015; Polanía et al., 2018; Vergallito et al., 2022; Wiethoff et al., 2014; Wörsching et al., 2016). Increasingly sophisticated functionality of CFMs (Dannhauer et al., 2012; Dmochowski et al., 2011, 2013; Huang, Thomas, et al., 2018; Huang, Datta, et al., 2018; Huang et al., 2019; Lee et al., 2017; Saturnino, Puonti, et

al., 2019) and increased understanding of the mechanisms of DC fields impacting neuronal excitability (Berzhanskaya et al., 2013; Bikson et al., 2004; Farahani et al., 2021; Radman et al., 2007, 2009b; Rahman et al., 2013b) offer an opportunity to identify and minimise sources of tDCS outcome variability.

In the context of this thesis, further investigation into the E-field properties associated with positive tDCS outcomes is recommended: how might positive changes in motor performance be reproduced reliably by non-invasively applied current? For example, a positive correlation has recently been reported between tDCS-induced E-field intensity and MRS-assessed GABA concentration (Nandi et al., 2022), and MEP amplitude change (Laakso et al., 2018), indicating that individual response to tDCS may depend on individual differences in applied fields. That such a relationship would exist seems highly plausible, but it remains to be seen whether CFMs can be employed to reduce variability sufficiently to warrant the additional effort and resources.

In chapter 3, the PA-tDCS montage was selected because previous work demonstrated the impact of the direction of current flow across $M1_{hand}$ on MEP amplitude (Evans et al., 2022; Rawji et al., 2018) and on neuronal membrane polarisation (Berzhanskaya et al., 2013; Bikson et al., 2004; Chan et al., 1988; Farahani et al., 2021; Radman et al., 2009; Rahman et al., 2013). PA-tDCS was found not to significantly alter MEP amplitude in this thesis, contributing to the on-going exploration of the tDCS parameter space in a field where high outcome variability persists (Chew et al., 2015; Laakso et al., 2015; Polanía et al., 2018; Vergallito et al., 2022; Wiethoff et al., 2014; Wörsching et al., 2016). Further work is recommended to deduce which aspects of tDCS study protocols are associated with positive outcomes, to inform standardised, effective use of tDCS especially in clinical populations. For example, neuronal structures beyond the somatic compartment of pyramidal cells in grey matter $M1_{hand}$ may have a greater impact on neuromodulatory outcomes than the somatic doctrine suggests (Kabakov et al., 2012; Polanía et al., 2010; Purpura & McMurtry, 1965; Reato et al., 2010), and protocol adjustments may be possible to maximise stimulation of non-somatic targets.

To support innovation in future, I suggest revision of the language used to describe tDCS protocol, to encourage mechanistically informed study design and promote transparency in

protocol selection choices. For example, conventional "anodal tDCS" might instead be described as "$M1_A$-SO_C tDCS", where subscript letters are used to indicate electrode polarity (A = anode; C = cathode). I suggest this is necessary because it acknowledges both inward and outward current flow relative to the folded cortical surface between electrodes (Evans et al., 2022; Galletta et al., 2015; Lafon et al., 2017; Rahman et al., 2013b; Salvador et al., 2015). This is relevant because inward and outward current flow is associated with neuronal de- and hyper-polarisation of pyramidal neurons, respectively (Berzhanskaya et al., 2013; Bikson et al., 2004; Chan et al., 1988; Farahani et al., 2021; Radman et al., 2009; Rahman et al., 2013).

Innovation may also be supported by pre-registration of research design, hypotheses, and methods before conducting a study. This process helps to increase the transparency, reproducibility, and credibility of the scientific research, and may reduce confirmatory bias by ensuring that the results are not influenced by researchers' personal beliefs and preferences. Moreover, pre-registration allows reviewers to evaluate the research design (and its mechanistic justification) before the study is conducted, which can help to identify any potential flaws or limitations. Using data to inform future power calculations may also improve the reliability and reproducibility of tDCS findings, as the sample size needed to ensure adequate power for a planned study can be determined, preventing Type II errors and avoiding unnecessary recruitment of participants. In practice, the *simr* package (Green & MacLeod, 2016) can be used in R to simulate data and estimate power for models constructed using the *lme4* package (Bates et al., 2020).

5.3 Concluding remarks

The presented work does not extend to suggest reliable methods through which variability might be reduced, for example in the context of tDCS-augmented motor rehabilitation outcomes in stroke. Given the high heterogeneity reported in excitatory-inhibitory balance at varying time points after stroke and in survivors with varying symptom severity profiles (Chapter 2) and the heterogeneity in stroke-induced anatomical changes and their impact on tDCS-induced E-field (Chapter 4), it is reasonable to suggest that the future for tDCS may lie in individualisation to improve the reliability of outcomes where high variability persists, even when CFM-informed tDCS is applied in neurotypical and stroke populations (Chapter

3). In fact, careful selection of stroke survivors who might be suitable for tDCS intervention may be required, alongside careful design of individualised stimulation protocol. This may first be achieved via multi-modal study design, combining neuroimaging and CFM to ascertain why tDCS works under some conditions, in some participants, but not others. Research showing a relationship between E-field intensity in a cortical target and physiological outcomes (Antonenko et al., 2019; Laakso et al., 2019; Mosayebi-Samani et al., 2021; Nandi et al., 2022) suggests that accounting for subject-specific E-field characteristics could go some way to control for the physiological effects of stimulation, and development of biophysically and morphologically realistic current flow models holds promise as part of the future of optimised tDCS application in health and disease (Aberra et al., 2020; Bonaiuto et al., 2016; Bonaiuto & Bestmann, 2015; Clusella et al., 2022; Galan-Gadea et al., 2022; Jansen & Rit, 1995; Lopez-Sola et al., 2022; Sanchez-Todo et al., 2022; Wang et al., 2018). As models improve, more complex tDCS application techniques are likely to become available which may compete with the conventional tDCS methods hailed as cheap, accessible, and ready-to-use. If computationally optimised tDCS is achieved, development of accessible modelling software is encouraged to ensure its effective use in clinical settings.

REFERENCES

Abe, H., Jitsuki, S., & Takahashi, T. (2019). Pharmacological Enhancement of Stroke Rehabilitation. *Stroke*, *50*(11), 3323–3329. https://doi.org/10.1161/STROKEAHA.119.023720

Aberra, A. S., Wang, B., Grill, W. M., & Peterchev, A. V. (2020). Simulation of transcranial magnetic stimulation in head model with morphologically-realistic cortical neurons. *Brain Stimulation: Basic, Translational, and Clinical Research in Neuromodulation*, *13*(1), 175–189. https://doi.org/10.1016/j.brs.2019.10.002

Akaike, H. (1974). A new look at the statistical model identification. *IEEE Transactions on Automatic Control*, *19*(6), 716–723. https://doi.org/10.1109/TAC.1974.1100705

Allman, C., Amadi, U., Winkler, A. M., Wilkins, L., Filippini, N., Kischka, U., Stagg, C. J., & Johansen-Berg, H. (2016). Ipsilesional anodal tDCS enhances the functional benefits of rehabilitation in patients after stroke. *Science Translational Medicine*, *8*(330), 330re1. https://doi.org/10.1126/scitranslmed.aad5651

Amadi, U., Allman, C., Johansen-Berg, H., & Stagg, C. J. (2015). The Homeostatic Interaction Between Anodal Transcranial Direct Current Stimulation and Motor Learning in Humans is Related to GABAA Activity. *Brain Stimulation*, *8*(5), 898–905. https://doi.org/10.1016/j.brs.2015.04.010

Antonenko, D., Grittner, U., Puonti, O., Flöel, A., & Thielscher, A. (2021). Estimation of individually induced e-field strength during transcranial electric stimulation using the head circumference. *Brain Stimulation*, *14*(5), 1055–1058. https://doi.org/10.1016/j.brs.2021.07.001

Antonenko, D., Nierhaus, T., Meinzer, M., Prehn, K., Thielscher, A., Ittermann, B., & Flöel, A. (2018). Age-dependent effects of brain stimulation on network centrality. *NeuroImage*, *176*, 71–82. https://doi.org/10.1016/j.neuroimage.2018.04.038

Antonenko, D., Schubert, F., Bohm, F., Ittermann, B., Aydin, S., Hayek, D., Grittner, U., & Flöel, A. (2017). TDCS-Induced Modulation of GABA Levels and Resting-State Functional Connectivity in Older Adults. *Journal of Neuroscience*, *37*(15), 4065–4073. https://doi.org/10.1523/JNEUROSCI.0079-17.2017

Antonenko, D., Thielscher, A., Saturnino, G. B., Aydin, S., Ittermann, B., Grittner, U., & Flöel, A. (2019). Towards precise brain stimulation: Is electric field simulation related to neuromodulation? *Brain Stimulation: Basic, Translational, and Clinical Research in Neuromodulation*, *12*(5), 1159–1168. https://doi.org/10.1016/j.brs.2019.03.072

Aswendt, M., Pallast, N., Wieters, F., Baues, M., Hoehn, M., & Fink, G. R. (2021). Lesion Size- and Location-Dependent Recruitment of Contralesional Thalamus and Motor Cortex Facilitates Recovery after Stroke in Mice. *Translational Stroke Research*, *12*(1), 87–97. https://doi.org/10.1007/s12975-020-00802-3

Austin, P. C., & Brunner, L. J. (2003). Type I Error Inflation in the Presence of a Ceiling Effect. *The American Statistician*, *57*(2), 97–104. https://doi.org/10.1198/0003130031450

Ayache, S. S., Ahdab, R., Chalah, M. A., Farhat, W. H., Mylius, V., Goujon, C., Sorel, M., & Lefaucheur, J.-P. (2016). Analgesic effects of navigated motor cortex rTMS in patients with chronic neuropathic pain. *European Journal of Pain*, *20*(9), 1413–1422. https://doi.org/10.1002/ejp.864

Bachtiar, V., Near, J., Johansen-Berg, H., & Stagg, C. J. (2015). Modulation of GABA and resting state functional connectivity by transcranial direct current stimulation. *ELife*, *4*, e08789. https://doi.org/10.7554/eLife.08789

Bagce, H. F., Saleh, S., Adamovich, S. V., Krakauer, J. W., & Tunik, E. (2013). Corticospinal excitability is enhanced after visuomotor adaptation and depends on learning rather than performance or error. *Journal of Neurophysiology*, *109*(4), 1097–1106. https://doi.org/10.1152/jn.00304.2012

Bai, Z., Zhang, J., & Fong, K. N. K. (2022). Effects of transcranial magnetic stimulation in modulating cortical excitability in patients with stroke: A systematic review and meta-analysis. *Journal of NeuroEngineering and Rehabilitation*, *19*(1), 24. https://doi.org/10.1186/s12984-022-00999-4

Balslev, D., Braet, W., McAllister, C., & Miall, R. C. (2007). Inter-individual variability in optimal current direction for transcranial magnetic stimulation of the motor cortex. *Journal of Neuroscience Methods*, *162*(1), 309–313. https://doi.org/10.1016/j.jneumeth.2007.01.021

Baroncelli, L., Braschi, C., Spolidoro, M., Begenisic, T., Sale, A., & Maffei, L. (2010). Nurturing brain plasticity: Impact of environmental enrichment. *Cell Death & Differentiation*, *17*(7), Article 7. https://doi.org/10.1038/cdd.2009.193

Bashir, S., Edwards, D., & Pascual-Leone, A. (2011). Neuronavigation Increases the Physiologic and Behavioral Effects of Low-Frequency rTMS of Primary Motor Cortex in Healthy Subjects. *Brain Topography*, *24*(1), 54–64. https://doi.org/10.1007/s10548-010-0165-7

Bastani, A., & Jaberzadeh, S. (2012). Does anodal transcranial direct current stimulation enhance excitability of the motor cortex and motor function in healthy individuals and subjects with stroke: A systematic review and meta-analysis. *Clinical Neurophysiology*, *123*(4), 644–657. https://doi.org/10.1016/j.clinph.2011.08.029

Bates, D., Mächler, M., Bolker, B., & Walker, S. (2015). Fitting Linear Mixed-Effects Models Using lme4. *Journal of Statistical Software*, *67*(1), Article 1. https://doi.org/10.18637/jss.v067.i01

Bates, D., Maechler, M., Bolker [aut, B., cre, Walker, S., Christensen, R. H. B., Singmann, H., Dai, B., Scheipl, F., Grothendieck, G., Green, P., Fox, J., Bauer, A., & simulate.formula), P. N. K. (shared copyright on. (2020). *lme4: Linear Mixed-Effects Models using 'Eigen' and S4* (1.1-26). https://CRAN.R-project.org/package=lme4

Bavelier, D., Levi, D. M., Li, R. W., Dan, Y., & Hensch, T. K. (2010). Removing brakes on adult brain plasticity: From molecular to behavioral interventions. *The Journal of Neuroscience: The Official Journal of the Society for Neuroscience*, *30*(45), 14964–14971. https://doi.org/10.1523/JNEUROSCI.4812-10.2010

Beaulieu, C., De Crespigny, A., Tong, D. C., Moseley, M. E., Albers, G. W., & Marks, M. P. (1999). Longitudinal magnetic resonance imaging study of perfusion and diffusion in stroke: Evolution of lesion volume and correlation with clinical outcome. *Annals of Neurology*, *46*(4), 568–578. https://doi.org/10.1002/1531-8249(199910)46:4<568::AID-ANA4>3.0.CO;2-R

Bernhardt, J., Dewey, H., Collier, J., Thrift, A., Lindley, R., Moodie, M., & Donnan, G. (2006). A Very Early Rehabilitation Trial (AVERT). *International Journal of Stroke*, *1*(3), 169–171. https://doi.org/10.1111/j.1747-4949.2006.00044.x

Bernhardt, J., Hayward, K. S., Kwakkel, G., Ward, N. S., Wolf, S. L., Borschmann, K., Krakauer, J. W., Boyd, L. A., Carmichael, S. T., Corbett, D., & Cramer, S. C. (2017). Agreed definitions and a shared vision for new standards in stroke recovery research: The Stroke Recovery and Rehabilitation Roundtable taskforce. *International Journal of Stroke*, *12*(5), 444–450. https://doi.org/10.1177/1747493017711816

Berzhanskaya, J., Chernyy, N., Gluckman, B. J., Schiff, S. J., & Ascoli, G. A. (2013). Modulation of hippocampal rhythms by subthreshold electric fields and network topology. *Journal of Computational Neuroscience*, *34*(3), 10.1007/s10827-012-0426–4. https://doi.org/10.1007/s10827-012-0426-4

Bestmann, S., de Berker, A. O., & Bonaiuto, J. (2015). Understanding the behavioural consequences of noninvasive brain stimulation. *Trends in Cognitive Sciences*, *19*(1), 13–20. https://doi.org/10.1016/j.tics.2014.10.003

Bestmann, S., & Krakauer, J. W. (2015). The uses and interpretations of the motor-evoked potential for understanding behaviour. *Experimental Brain Research*, *233*(3), 679–689. https://doi.org/10.1007/s00221-014-4183-7

Biane, J. S., Scanziani, M., Tuszynski, M. H., & Conner, J. M. (2015). Motor Cortex Maturation Is Associated with Reductions in Recurrent Connectivity among Functional Subpopulations and Increases in Intrinsic Excitability. *The Journal of Neuroscience*, *35*(11), 4719–4728. https://doi.org/10.1523/JNEUROSCI.2792-14.2015

Biernaskie, J. (2004). Efficacy of Rehabilitative Experience Declines with Time after Focal Ischemic Brain Injury. *Journal of Neuroscience*, *24*(5), 1245–1254. https://doi.org/10.1523/JNEUROSCI.3834-03.2004

Bikson, M., & Dmochowski, J. (2020). What it means to go deep with non-invasive brain stimulation. *Clinical Neurophysiology*, *131*(3), 752–754. https://doi.org/10.1016/j.clinph.2019.12.003

Bikson, M., Dmochowski, J., & Rahman, A. (2013). The “Quasi-Uniform” Assumption in Animal and Computational Models of Non-Invasive Electrical Stimulation. *Brain Stimulation*, *6*(4), 704–705. https://doi.org/10.1016/j.brs.2012.11.005

Bikson, M., Inoue, M., Akiyama, H., Deans, J. K., Fox, J. E., Miyakawa, H., & Jefferys, J. G. R. (2004). Effects of uniform extracellular DC electric fields on excitability in rat hippocampal slices *in vitro*: Modulation of neuronal function by electric fields. *The Journal of Physiology*, *557*(1), 175–190. https://doi.org/10.1113/jphysiol.2003.055772

Bikson, M., Paulus, W., Esmaeilpour, Z., Kronberg, G., & Nitsche, M. A. (2019). Mechanisms of Acute and After Effects of Transcranial Direct Current Stimulation. In H. Knotkova, M. A. Nitsche, M. Bikson, & A. J. Woods (Eds.), *Practical Guide to Transcranial Direct Current Stimulation: Principles, Procedures and Applications* (pp. 81–113). Springer International Publishing. https://doi.org/10.1007/978-3-319-95948-1_3

Bikson, M., & Rahman, A. (2013). Origins of specificity during tDCS: Anatomical, activity-selective, and input-bias mechanisms. *Frontiers in Human Neuroscience*, *7*, 688. https://doi.org/10.3389/fnhum.2013.00688

Bikson, M., Rahman, A., & Datta, A. (2012). Computational Models of Transcranial Direct Current Stimulation. *Clinical EEG and Neuroscience*, *43*(3), 176–183. https://doi.org/10.1177/1550059412445138

Bikson, M., Rahman, A., Datta, A., Fregni, F., & Merabet, L. (2012). High-resolution Modeling Assisted Design of Customized and Individualized Transcranial Direct Current Stimulation Protocols. *Neuromodulation : Journal of the International Neuromodulation Society*, *15*(4), 306–315. https://doi.org/10.1111/j.1525-1403.2012.00481.x

Bindman, L. J., Lippold, O. C. J., & Redfearn, J. W. T. (1964a). The action of brief polarizing currents on the cerebral cortex of the rat (1) during current flow and (2) in the production of long-lasting after-effects. *The Journal of Physiology*, *172*(3), 369–382.

Bindman, L. J., Lippold, O. C. J., & Redfearn, J. W. T. (1964b). The action of brief polarizing currents on the cerebral cortex of the rat (1) during current flow and (2) in the production of long-lasting after-effects. *The Journal of Physiology*, *172*(3), 369–382.

Birkenmeier, R. L., Prager, E. M., & Lang, C. E. (2010). Translating animal doses of task-specific training to people with chronic stroke in one hour therapy sessions: A proof-of-concept study. *Neurorehabilitation and Neural Repair*, *24*(7), 620–635. https://doi.org/10.1177/1545968310361957

Blennerhassett, J., & Dite, W. (2004). Additional task-related practice improves mobility and upper limb function early after stroke: A randomised controlled trial. *Australian Journal of Physiotherapy*, *50*(4), 219–224. https://doi.org/10.1016/S0004-9514(14)60111-2

Blicher, J. U., Near, J., Næss-Schmidt, E., Stagg, C. J., Johansen-Berg, H., Nielsen, J. F., Østergaard, L., & Ho, Y.-C. L. (2015). GABA Levels Are Decreased After Stroke and GABA Changes During Rehabilitation Correlate With Motor Improvement. *Neurorehabilitation and Neural Repair*, *29*(3), 278–286. https://doi.org/10.1177/1545968314543652

Blomstedt, P., & Hariz, M. I. (2006). Are complications less common in deep brain stimulation than in ablative procedures for movement disorders? *Stereotactic and Functional Neurosurgery*, *84*(2–3), 72–81. https://doi.org/10.1159/000094035

Bonaiuto, J. J., Berker, A. de, & Bestmann, S. (2016). Response repetition biases in human perceptual decisions are explained by activity decay in competitive attractor models. *ELife*, *5*, e20047. https://doi.org/10.7554/eLife.20047

Bonaiuto, J. J., & Bestmann, S. (2015). Chapter 4—Understanding the nonlinear physiological and behavioral effects of tDCS through computational neurostimulation. In S. Bestmann (Ed.), *Progress in Brain Research* (Vol. 222, pp. 75–103). Elsevier. https://doi.org/10.1016/bs.pbr.2015.06.013

Bonkhoff, A. K., Hope, T., Bzdok, D., Guggisberg, A. G., Hawe, R. L., Dukelow, S. P., Chollet, F., Lin, D. J., Grefkes, C., & Bowman, H. (2022). Recovery after stroke: The severely impaired are a distinct group. *Journal of Neurology, Neurosurgery & Psychiatry*, *93*(4), 369–378. https://doi.org/10.1136/jnnp-2021-327211

Borich, M. R., Neva, J. L., & Boyd, L. A. (2015). Evaluation of differences in brain neurophysiology and morphometry associated with hand function in individuals with chronic stroke. *Restorative Neurology and Neuroscience*, *33*(1), 31–42. https://doi.org/10.3233/RNN-140425

Boroojerdi, B., Battaglia, F., Muellbacher, W., & Cohen, L. G. (2001). Mechanisms influencing stimulus-response properties of the human corticospinal system. *Clinical Neurophysiology*, *112*(5), 931–937. https://doi.org/10.1016/S1388-2457(01)00523-5

Boros, K., Poreisz, C., Münchau, A., Paulus, W., & Nitsche, M. A. (2008). Premotor transcranial direct current stimulation (tDCS) affects primary motor excitability in humans. *European Journal of Neuroscience*, *27*(5), 1292–1300. https://doi.org/10.1111/j.1460-9568.2008.06090.x

Boyd, L. A., Hayward, K. S., Ward, N. S., Stinear, C. M., Rosso, C., Fisher, R. J., Carter, A. R., Leff, A. P., Copland, D. A., Carey, L. M., Cohen, L. G., Basso, D. M., Maguire, J. M., & Cramer, S. C. (2017). Biomarkers of stroke recovery: Consensus-based core recommendations from the Stroke Recovery and Rehabilitation Roundtable. *International Journal of Stroke*, *12*(5), 480–493. https://doi.org/10.1177/1747493017714176

Bradley, C., Nydam, A. S., Dux, P. E., & Mattingley, J. B. (2022). State-dependent effects of neural stimulation on brain function and cognition. *Nature Reviews Neuroscience*, 1–17. https://doi.org/10.1038/s41583-022-00598-1

Branscheidt, M., Ejaz, N., Xu, J., Widmer, M., Harran, M. D., Cortés, J. C., Kitago, T., Celnik, P., Hernandez-Castillo, C., Diedrichsen, J., Luft, A., & Krakauer, J. W. (2019). *No evidence for motor recovery-related cortical reorganization after stroke using resting-state fMRI* (p. 681320). bioRxiv. https://doi.org/10.1101/681320

Brasil-Neto, J. P., Cohen, L. G., Panizza, M., Nilsson, J., Roth, B. J., & Hallett, M. (1992). Optimal focal transcranial magnetic activation of the human motor cortex: Effects of coil orientation, shape of the induced current pulse, and stimulus intensity. *Journal of Clinical Neurophysiology: Official Publication of the American Electroencephalographic Society*, *9*(1), 132–136.

Brett, M., Anton, J.-L., Valabregue, R., & Poline, J.-B. (2002). *Region of interest analysis using an SPM toolbox.* https://marsbar-toolbox.github.io/

Brouwer, B. J., & Schryburt-Brown, K. (2006). Hand Function and Motor Cortical Output Poststroke: Are They Related? *Archives of Physical Medicine and Rehabilitation*, *87*(5), 627–634. https://doi.org/10.1016/j.apmr.2006.02.006

Brown, C. E., Aminoltejari, K., Erb, H., Winship, I. R., & Murphy, T. H. (2009). In Vivo Voltage-Sensitive Dye Imaging in Adult Mice Reveals That Somatosensory Maps Lost to Stroke Are Replaced over Weeks by New Structural and Functional Circuits with Prolonged Modes of Activation within Both the Peri-Infarct Zone and Distant Sites. *The Journal of Neuroscience*, *29*(6), 1719–1734. https://doi.org/10.1523/JNEUROSCI.4249-08.2009

BRUK. (2017). *Brain Research UK | Funding world-class brain research*. https://www.brainresearchuk.org.uk/research-project/stroke-optimising-brain-stimulation-to-help-recovery-sven-bestmann

Buchkremer-Ratzmann, I., & Witte, O. W. (1997). Extended brain disinhibition following small photothrombotic lesions in rat frontal cortex. *NeuroReport*, *8*(2), 519–522.

Buma, F., Kwakkel, G., & Ramsey, N. (2013). Understanding upper limb recovery after stroke. *Restorative Neurology and Neuroscience*, *31*(6), 707–722. https://doi.org/10.3233/RNN-130332

Burke, D., Hicks, R., Stephen, J., Woodforth, I., & Crawford, M. (1995). Trial-to-trial variability of corticospinal volleys in human subjects. *Electroencephalography and Clinical Neurophysiology*, *97*(5), 231–237. https://doi.org/10.1016/0013-4694(95)00005-j

Burnham, K. P., & Anderson, D. R. (2004). Multimodel Inference: Understanding AIC and BIC in Model Selection. *Sociological Methods & Research*, *33*, 261–304. https://doi.org/10.1177/0049124104268644

Calautti, C., & Baron, J.-C. (2003). Functional neuroimaging studies of motor recovery after stroke in adults: A review. *Stroke*, *34*(6), 1553–1566. https://doi.org/10.1161/01.STR.0000071761.36075.A6

Capocchi, G., Zampolini, M., & Larson, J. (1992). Theta burst stimulation is optimal for induction of LTP at both apical and basal dendritic synapses on hippocampal CA1 neurons. *Brain Research*, *591*(2), 332–336. https://doi.org/10.1016/0006-8993(92)91715-Q

Caracciolo, L., Marosi, M., Mazzitelli, J., Latifi, S., Sano, Y., Galvan, L., Kawaguchi, R., Holley, S., Levine, M. S., Coppola, G., Portera-Cailliau, C., Silva, A. J., & Carmichael, S. T. (2018). CREB controls cortical circuit plasticity and functional recovery after stroke. *Nature Communications*, *9*(1), Article 1. https://doi.org/10.1038/s41467-018-04445-9

Carmichael, S. T. (2006). Cellular and molecular mechanisms of neural repair after stroke: Making waves. *Annals of Neurology*, *59*(5), 735–742. https://doi.org/10.1002/ana.20845

Carmichael, S. T. (2012). Brain Excitability in Stroke. *Archives of Neurology*, *69*(2), 161–167. https://doi.org/10.1001/archneurol.2011.1175

Carmichael, S. T. (2016). The 3 Rs of Stroke Biology: Radial, Relayed, and Regenerative. *Neurotherapeutics*, *13*(2), 348–359. https://doi.org/10.1007/s13311-015-0408-0

Carmichael, S. T., Kathirvelu, B., Schweppe, C. A., & Nie, E. H. (2017). Molecular, cellular and functional events in axonal sprouting after stroke. *Experimental Neurology*, *287*(Pt 3), 384–394. https://doi.org/10.1016/j.expneurol.2016.02.007

Carroll, T. J., Riek, S., & Carson, R. G. (2001). Reliability of the input–output properties of the cortico-spinal pathway obtained from transcranial magnetic and electrical stimulation. *Journal of Neuroscience Methods*, *112*(2), 193–202. https://doi.org/10.1016/S0165-0270(01)00468-X

Carson, R. G., Nelson, B. D., Buick, A. R., Carroll, T. J., Kennedy, N. C., & Cann, R. M. (2013). Characterizing Changes in the Excitability of Corticospinal Projections to Proximal Muscles of the Upper Limb. *Brain Stimulation: Basic, Translational, and Clinical Research in Neuromodulation*, *6*(5), 760–768. https://doi.org/10.1016/j.brs.2013.01.016

Castro-Alamancos, M., Donoghue, J., & Connors, B. (1995). Different forms of synaptic plasticity in somatosensory and motor areas of the neocortex. *The Journal of Neuroscience*, *15*(7), 5324–5333. https://doi.org/10.1523/JNEUROSCI.15-07-05324.1995

Caulfield, K. A., Badran, B. W., DeVries, W. H., Summers, P. M., Kofmehl, E., Li, X., Borckardt, J. J., Bikson, M., & George, M. S. (2020). Transcranial electrical stimulation motor threshold can estimate individualized tDCS dosage from reverse-calculation electric-field modeling. *Brain Stimulation: Basic, Translational, and Clinical Research in Neuromodulation*, *13*(4), 961–969. https://doi.org/10.1016/j.brs.2020.04.007

Caulo, M., Briganti, C., Mattei, P. A., Perfetti, B., Ferretti, A., Romani, G. L., Tartaro, A., & Colosimo, C. (2007). New Morphologic Variants of the Hand Motor Cortex as Seen with MR Imaging in a Large Study Population. *American Journal of Neuroradiology*, *28*(8), 1480–1485. https://doi.org/10.3174/ajnr.A0597

Chan, C. Y., Hounsgaard, J., & Nicholson, C. (1988). Effects of electric fields on transmembrane potential and excitability of turtle cerebellar Purkinje cells in vitro. *The Journal of Physiology*, *402*(1), 751–771. https://doi.org/10.1113/jphysiol.1988.sp017232

Chang, M. C., Kim, D. Y., & Park, D. H. (2015). Enhancement of Cortical Excitability and Lower Limb Motor Function in Patients With Stroke by Transcranial Direct Current Stimulation. *Brain Stimulation*, *8*(3), 561–566. https://doi.org/10.1016/j.brs.2015.01.411

Cheng, M. Y., Wang, E. H., Woodson, W. J., Wang, S., Sun, G., Lee, A. G., Arac, A., Fenno, L. E., Deisseroth, K., & Steinberg, G. K. (2014). Optogenetic neuronal stimulation promotes functional recovery after stroke. *Proceedings of the National Academy of Sciences*, *111*(35), 12913–12918. https://doi.org/10.1073/pnas.1404109111

Chew, T., Ho, K.-A., & Loo, C. K. (2015). Inter- and Intra-individual Variability in Response to Transcranial Direct Current Stimulation (tDCS) at Varying Current Intensities. *Brain Stimulation*, *8*(6), 1130–1137. https://doi.org/10.1016/j.brs.2015.07.031

Chhatbar, P. Y., Chen, R., Deardorff, R., Dellenbach, B., Kautz, S. A., George, M. S., & Feng, W. (2017). Safety and tolerability of transcranial direct current stimulation to stroke patients – A phase I current escalation study. *Brain Stimulation*, *10*(3), 553–559. https://doi.org/10.1016/j.brs.2017.02.007

Chhatbar, P. Y., Ramakrishnan, V., Kautz, S., George, M. S., Adams, R. J., & Feng, W. (2016). Transcranial Direct Current Stimulation Post-Stroke Upper Extremity Motor Recovery Studies Exhibit a Dose–Response Relationship. *Brain Stimulation*, *9*(1), 16–26. https://doi.org/10.1016/j.brs.2015.09.002

Chollet, F., Tardy, J., Albucher, J.-F., Thalamas, C., Berard, E., Lamy, C., Bejot, Y., Deltour, S., Jaillard, A., Niclot, P., Guillon, B., Moulin, T., Marque, P., Pariente, J., Arnaud, C., & Loubinoux, I. (2011). Fluoxetine for motor recovery after acute ischaemic stroke (FLAME): A randomised placebo-controlled trial. *The Lancet. Neurology*, *10*(2), 123–130. https://doi.org/10.1016/S1474-4422(10)70314-8

Chung, Y., Rabe-Hesketh, S., Dorie, V., Gelman, A., & Liu, J. (2013). A Nondegenerate Penalized Likelihood Estimator for Variance Parameters in Multilevel Models. *Psychometrika*, *78*(4), 685–709. https://doi.org/10.1007/s11336-013-9328-2

Cicinelli, P., Pasqualetti, P., Zaccagnini, M., Traversa, R., Oliveri, M., & Rossini, P. M. (2003). Interhemispheric Asymmetries of Motor Cortex Excitability in the Postacute Stroke Stage. *Stroke*, *34*(11), 2653–2658. https://doi.org/10.1161/01.STR.0000092122.96722.72

Ciechanski, P., Carlson, H. L., Yu, S. S., & Kirton, A. (2018). Modeling Transcranial Direct-Current Stimulation-Induced Electric Fields in Children and Adults. *Frontiers in Human Neuroscience*, *12*. https://doi.org/10.3389/fnhum.2018.00268

Cirillo, J., Mooney, R. A., Ackerley, S. J., Barber, P. A., Borges, V. M., Clarkson, A. N., Mangold, C., Ren, A., Smith, M.-C., Stinear, C. M., & Byblow, W. D. (2020). Neurochemical balance and inhibition at the subacute stage after stroke. *Journal of Neurophysiology*, *123*(5), 1775–1790. https://doi.org/10.1152/jn.00561.2019

Clark, T. A., Sullender, C., Jacob, D., Zuo, Y., Dunn, A. K., & Jones, T. A. (2019). Rehabilitative Training Interacts with Ischemia-Instigated Spine Dynamics to Promote a Lasting Population of New Synapses in Peri-Infarct Motor Cortex. *The Journal of Neuroscience*, *39*(43), 8471–8483. https://doi.org/10.1523/JNEUROSCI.1141-19.2019

Clarkson, A. N., Huang, B. S., Macisaac, S. E., Mody, I., & Carmichael, S. T. (2010). Reducing excessive GABA-mediated tonic inhibition promotes functional recovery after stroke. *Nature*, *468*(7321), 305–309. https://doi.org/10.1038/nature09511

Clarkson, A. N., Overman, J. J., Zhong, S., Mueller, R., Lynch, G., & Carmichael, S. T. (2011). AMPA Receptor-Induced Local Brain-Derived Neurotrophic Factor Signaling Mediates Motor Recovery after Stroke. *The Journal of Neuroscience*, *31*(10), 3766–3775. https://doi.org/10.1523/JNEUROSCI.5780-10.2011

Clarkson, A. N., Parker, K., Nilsson, M., Walker, F. R., & Gowing, E. K. (2015). Combined ampakine and BDNF treatments enhance poststroke functional recovery in aged mice via AKT-CREB signaling. *Journal of Cerebral Blood Flow & Metabolism*, *35*(8), 1272–1279. https://doi.org/10.1038/jcbfm.2015.33

Clusella, P., Köksal-Ersöz, E., Garcia-Ojalvo, J., & Ruffini, G. (2022). Comparison between an exact and a heuristic neural mass model with second-order synapses. *Biological Cybernetics*. https://doi.org/10.1007/s00422-022-00952-7

Cnaan, A., Laird, N. M., & Slasor, P. (1997). Using the general linear mixed model to analyse unbalanced repeated measures and longitudinal data. *Statistics in Medicine*, *16*(20), 2349–2380. https://doi.org/10.1002/(sici)1097-0258(19971030)16:20<2349::aid-sim667>3.0.co;2-e

Corp, D. T., Bereznicki, H. G. K., Clark, G. M., Youssef, G. J., Fried, P. J., Jannati, A., Davies, C. B., Gomes-Osman, J., Kirkovski, M., Albein-Urios, N., Fitzgerald, P. B., Koch, G., Lazzaro, V. D., Pascual-Leone, A., Enticott, P. G., & the Big TMS Data Collaboration. (2021). *Large-scale analysis of interindividual variability in single and paired-pulse TMS data: Results from the 'Big TMS Data Collaboration'* [Preprint]. Neuroscience. https://doi.org/10.1101/2021.01.24.428014

Corp, D. T., Bereznicki, H. G. K., Clark, G. M., Youssef, G. J., Fried, P. J., Jannati, A., Davies, C. B., Gomes-Osman, J., Stamm, J., Chung, S. W., Bowe, S. J., Rogasch, N. C., Fitzgerald, P. B., Koch, G., Di Lazzaro, V., Pascual-Leone, A., & Enticott, P. G. (2020). Large-scale analysis of interindividual variability in theta-burst stimulation data: Results from the 'Big TMS Data Collaboration'. *Brain Stimulation*, *13*(5), 1476–1488. https://doi.org/10.1016/j.brs.2020.07.018

Costa, R. M., Cohen, D., & Nicolelis, M. A. L. (2004). Differential Corticostriatal Plasticity during Fast and Slow Motor Skill Learning in Mice. *Current Biology*, *14*(13), 1124–1134. https://doi.org/10.1016/j.cub.2004.06.053

Cramer, S. C. (2008). Repairing the human brain after stroke: I. Mechanisms of spontaneous recovery. *Annals of Neurology*, *63*(3), 272–287. https://doi.org/10.1002/ana.21393

Cramer, S. C. (2020). Recovery After Stroke. *CONTINUUM: Lifelong Learning in Neurology*, *26*(2), 415. https://doi.org/10.1212/CON.0000000000000838

Crinion, J. T. (2016). Transcranial direct current stimulation as a novel method for enhancing aphasia treatment effects. *European Psychologist*, *21*(1), 65. https://doi.org/10.1027/1016-9040/a000254

Danner, N., Julkunen, P., Könönen, M., Säisänen, L., Nurkkala, J., & Karhu, J. (2008). Navigated transcranial magnetic stimulation and computed electric field strength reduce stimulator-dependent differences in the motor threshold. *Journal of Neuroscience Methods*, *174*(1), 116–122. https://doi.org/10.1016/j.jneumeth.2008.06.032

Dannhauer, M., Brooks, D., Tucker, D., & MacLeod, R. (2012). A pipeline for the Simulation of Transcranial Direct Current Stimulation for Realistic Human Head Models using SCIRun/BioMesh3D. *Conference Proceedings : ... Annual International Conference of*

the IEEE Engineering in Medicine and Biology Society. IEEE Engineering in Medicine and Biology Society. Conference, *2012*. https://doi.org/10.1109/EMBC.2012.6347236

Darling, W. G., Wolf, S. L., & Butler, A. J. (2006). Variability of motor potentials evoked by transcranial magnetic stimulation depends on muscle activation. *Experimental Brain Research. Experimentelle Hirnforschung. Experimentation Cerebrale*, *174*(2), 376. https://doi.org/10.1007/s00221-006-0468-9

DaSilva, A. F., Mendonca, M. E., Zaghi, S., Lopes, M., DosSantos, M. F., Spierings, E. L., Bajwa, Z., Datta, A., Bikson, M., & Fregni, F. (2012). TDCS-Induced Analgesia and Electrical Fields in Pain-Related Neural Networks in Chronic Migraine. *Headache*, *52*(8), 1283–1295. https://doi.org/10.1111/j.1526-4610.2012.02141.x

DaSilva, A. F., Volz, M. S., Bikson, M., & Fregni, F. (2011). Electrode Positioning and Montage in Transcranial Direct Current Stimulation. *Journal of Visualized Experiments : JoVE*, *51*, 2744. https://doi.org/10.3791/2744

Datta, A., Baker, J. M., Bikson, M., & Fridriksson, J. (2011). Individualized model predicts brain current flow during transcranial direct-current stimulation treatment in responsive stroke patient. *Brain Stimulation*, *4*(3), 169–174. https://doi.org/10.1016/j.brs.2010.11.001

Datta, A., Bansal, V., Diaz, J., Patel, J., Reato, D., & Bikson, M. (2009). Gyri-precise head model of transcranial direct current stimulation: Improved spatial focality using a ring electrode versus conventional rectangular pad. *Brain Stimulation: Basic, Translational, and Clinical Research in Neuromodulation*, *2*(4), 201-207.e1. https://doi.org/10.1016/j.brs.2009.03.005

Datta, A., Elwassif, M., Battaglia, F., & Bikson, M. (2008). Transcranial current stimulation focality using disc and ring electrode configurations: FEM analysis. *Journal of Neural Engineering*, *5*(2), 163–174. https://doi.org/10.1088/1741-2560/5/2/007

Datta, A., Truong, D., Minhas, P., Parra, L. C., & Bikson, M. (2012). Inter-Individual Variation during Transcranial Direct Current Stimulation and Normalization of Dose Using MRI-Derived Computational Models. *Frontiers in Psychiatry*, *3*. https://doi.org/10.3389/fpsyt.2012.00091

Davis, S., & Donnan, G. A. (2014). Time Is Penumbra: Imaging, Selection and Outcome. *Cerebrovascular Diseases*, *38*(1), 59–72. https://doi.org/10.1159/000365503

de Sousa, D. G., Harvey, L. A., Dorsch, S., & Glinsky, J. V. (2018). Interventions involving repetitive practice improve strength after stroke: A systematic review. *Journal of Physiotherapy*, *64*(4), 210–221. https://doi.org/10.1016/j.jphys.2018.08.004

Deans, J. K., Powell, A. D., & Jefferys, J. G. R. (2007). Sensitivity of coherent oscillations in rat hippocampus to AC electric fields. *The Journal of Physiology*, *583*(Pt 2), 555–565. https://doi.org/10.1113/jphysiol.2007.137711

Dechent, P., & Frahm, J. (2003). Functional somatotopy of finger representations in human primary motor cortex. *Human Brain Mapping*, *18*(4), 272–283. https://doi.org/10.1002/hbm.10084

Devanne, H., Lavoie, B. A., & Capaday, C. (1997). Input-output properties and gain changes in the human corticospinal pathway: *Experimental Brain Research*, *114*(2), 329–338. https://doi.org/10.1007/PL00005641

Di Lazzaro, V., Pilato, F., Dileone, M., Profice, P., Ranieri, F., Ricci, V., Bria, P., Tonali, P. A., & Ziemann, U. (2007). Segregating two inhibitory circuits in human motor cortex at the level of GABAA receptor subtypes: A TMS study. *Clinical Neurophysiology*, *118*(10), 2207–2214. https://doi.org/10.1016/j.clinph.2007.07.005

Di Lazzaro, V., Pilato, F., Dileone, M., Ranieri, F., Ricci, V., Profice, P., Bria, P., Tonali, P. A., & Ziemann, U. (2006). GABAA receptor subtype specific enhancement of inhibition in human motor cortex. *The Journal of Physiology*, *575*(3), 721–726. https://doi.org/10.1113/jphysiol.2006.114694

Di Lazzaro, V., Profice, P., Pilato, F., Capone, F., Ranieri, F., Pasqualetti, P., Colosimo, C., Pravatà, E., Cianfoni, A., & Dileone, M. (2010). Motor Cortex Plasticity Predicts Recovery in Acute Stroke. *Cerebral Cortex*, *20*(7), 1523–1528. https://doi.org/10.1093/cercor/bhp216

Di Lazzaro, V., Restuccia, D., Oliviero, A., Profice, P., Ferrara, L., Insola, A., Mazzone, P., Tonali, P., & Rothwell, J. C. (1998). Magnetic transcranial stimulation at intensities below active motor threshold activates intracortical inhibitory circuits. *Experimental Brain Research*, *119*(2), 265–268. https://doi.org/10.1007/s002210050341

Di Lazzaro, V., & Ziemann, U. (2013). The contribution of transcranial magnetic stimulation in the functional evaluation of microcircuits in human motor cortex. *Frontiers in Neural Circuits*, *7*. https://doi.org/10.3389/fncir.2013.00018

Di Pino, G., Pellegrino, G., Assenza, G., Capone, F., Ferreri, F., Formica, D., Ranieri, F., Tombini, M., Ziemann, U., Rothwell, J. C., & Di Lazzaro, V. (2014). Modulation of brain plasticity in stroke: A novel model for neurorehabilitation. *Nature Reviews Neurology*, *10*(10), Article 10. https://doi.org/10.1038/nrneurol.2014.162

Di Pino, G., Pellegrino, G., Capone, F., & Di Lazzaro, V. (2014). Human Cerebral Cortex Metaplasticity and Stroke Recovery. *Austin Journal of Cerebrovascular Disease and Stroke*. https://doi.org/10.13140/2.1.2221.8886

Diamond, D. M., Dunwiddie, T. V., & Rose, G. M. (1988). Characteristics of hippocampal primed burst potentiation in vitro and in the awake rat. *Journal of Neuroscience*, *8*(11), 4079–4088. https://doi.org/10.1523/JNEUROSCI.08-11-04079.1988

Dienes, Z. (2014). Using Bayes to get the most out of non-significant results. *Frontiers in Psychology*, *5*, 781. https://doi.org/10.3389/fpsyg.2014.00781

Dmochowski, J. P., Bikson, M., & Parra, L. C. (2012). The point spread function of the human head and its implications for transcranial current stimulation. *Physics in Medicine and Biology*, *57*(20), 6459–6477. https://doi.org/10.1088/0031-9155/57/20/6459

Dmochowski, J. P., Datta, A., Bikson, M., Su, Y., & Parra, L. C. (2011). Optimized multi-electrode stimulation increases focality and intensity at target. *Journal of Neural Engineering*, *8*(4), 046011. https://doi.org/10.1088/1741-2560/8/4/046011

Dmochowski, J. P., Datta, A., Huang, Y., Richardson, J. D., Bikson, M., Fridriksson, J., & Parra, L. C. (2013). Targeted transcranial direct current stimulation for rehabilitation after stroke. *NeuroImage*, *75*, 12–19. https://doi.org/10.1016/j.neuroimage.2013.02.049

Dobkin, B. H., & Carmichael, S. T. (2016). The Specific Requirements of Neural Repair Trials for Stroke. *Neurorehabilitation and Neural Repair*, *30*(5), 470–478. https://doi.org/10.1177/1545968315604400

Dong, Y., Green, T., Saal, D., Marie, H., Neve, R., Nestler, E. J., & Malenka, R. C. (2006). CREB modulates excitability of nucleus accumbens neurons. *Nature Neuroscience*, *9*(4), 475–477. https://doi.org/10.1038/nn1661

Dorsch, S., & Elkins, M. R. (2020). Repetitions and dose in stroke rehabilitation. *Journal of Physiotherapy*, *66*(4), 211–212. https://doi.org/10.1016/j.jphys.2020.04.001

Dromerick, A. W., Edwardson, M. A., Edwards, D. F., Giannetti, M. L., Barth, J., Brady, K. P., Chan, E., Tan, M. T., Tamboli, I., Chia, R., Orquiza, M., Padilla, R. M., Cheema, A. K., Mapstone, M. E., Fiandaca, M. S., Federoff, H. J., & Newport, E. L. (2015). Critical periods after stroke study: Translating animal stroke recovery experiments into a clinical trial. *Frontiers in Human Neuroscience*, *9*, 231. https://doi.org/10.3389/fnhum.2015.00231

Dromerick, A. W., Geed, S., Barth, J., Brady, K., Giannetti, M. L., Mitchell, A., Edwardson, M. A., Tan, M. T., Zhou, Y., Newport, E. L., & Edwards, D. F. (2021). Critical Period After Stroke Study (CPASS): A phase II clinical trial testing an optimal time for motor recovery after stroke in humans. *Proceedings of the National Academy of Sciences of the United States of America*, *118*(39), e2026676118. https://doi.org/10.1073/pnas.2026676118

Dromerick, A. W., Lang, C. E., Birkenmeier, R. L., Wagner, J. M., Miller, J. P., Videen, T. O., Powers, W. J., Wolf, S. L., & Edwards, D. F. (2009). Very Early Constraint-Induced Movement during Stroke Rehabilitation (VECTORS). *Neurology*, *73*(3), 195–201. https://doi.org/10.1212/WNL.0b013e3181ab2b27

Dular, P., Geuzaine, C., Henrotte, F., & Legros, W. (1998). A general environment for the treatment of discrete problems and its application to the finite element method. *IEEE Transactions on Magnetics*, *34*(5), 3395–3398. https://doi.org/10.1109/20.717799

Duncan, P. W., Goldstein, L. B., Matchar, D., Divine, G. W., & Feussner, J. (1992). Measurement of motor recovery after stroke. Outcome assessment and sample size requirements. *Stroke*, *23*(8), 1084–1089. https://doi.org/10.1161/01.STR.23.8.1084

Duncan, P. W., Zorowitz, R., Bates, B., Choi, J. Y., Glasberg, J. J., Graham, G. D., Katz, R. C., Lamberty, K., & Reker, D. (2005). Management of Adult Stroke Rehabilitation Care. *Stroke*, *36*(9), e100–e143. https://doi.org/10.1161/01.STR.0000180861.54180.FF

Dyke, K., Pépés, S. E., Chen, C., Kim, S., Sigurdsson, H. P., Draper, A., Husain, M., Nachev, P., Gowland, P. A., Morris, P. G., & Jackson, S. R. (2017). Comparing GABA-dependent physiological measures of inhibition with proton magnetic resonance spectroscopy

measurement of GABA using ultra-high-field MRI. *Neuroimage*, *152*, 360–370. https://doi.org/10.1016/j.neuroimage.2017.03.011

Edwards, D., Cortes, M., Datta, A., Minhas, P., Wassermann, E. M., & Bikson, M. (2013). Physiological and modeling evidence for focal transcranial electrical brain stimulation in humans: A basis for high-definition tDCS. *NeuroImage*, *74*, 266–275. https://doi.org/10.1016/j.neuroimage.2013.01.042

Eickhoff, S. B., Laird, A. R., Grefkes, C., Wang, L. E., Zilles, K., & Fox, P. T. (2009). Coordinate-based activation likelihood estimation meta-analysis of neuroimaging data: A random-effects approach based on empirical estimates of spatial uncertainty. *Human Brain Mapping*, *30*(9), 2907–2926. https://doi.org/10.1002/hbm.20718

Elsner, B., Kugler, J., & Mehrholz, J. (2018). Transcranial direct current stimulation (tDCS) for upper limb rehabilitation after stroke: Future directions. *Journal of NeuroEngineering and Rehabilitation*, *15*. https://doi.org/10.1186/s12984-018-0459-7

Elsner, B., Kugler, J., Pohl, M., & Mehrholz, J. (2020). Transcranial direct current stimulation (tDCS) for improving activities of daily living, and physical and cognitive functioning, in people after stroke. *The Cochrane Database of Systematic Reviews*, *11*, CD009645. https://doi.org/10.1002/14651858.CD009645.pub4

Engelhardt, M., Schneider, H., Gast, T., & Picht, T. (2019). Estimation of the resting motor threshold (RMT) in transcranial magnetic stimulation using relative-frequency and threshold-hunting methods in brain tumor patients. *Acta Neurochirurgica*, *161*(9), 1845–1851. https://doi.org/10.1007/s00701-019-03997-z

Esmaeilpour, Z., Marangolo, P., Hampstead, B. M., Bestmann, S., Galletta, E., Knotkova, H., & Bikson, M. (2018). Incomplete evidence that increasing current intensity of tDCS boosts outcomes. *Brain Stimulation*, *11*(2), 310–321. https://doi.org/10.1016/j.brs.2017.12.002

Evans, C., Bachmann, C., Lee, J. S. A., Gregoriou, E., Ward, N., & Bestmann, S. (2020). Dose-controlled tDCS reduces electric field intensity variability at a cortical target site. *Brain Stimulation*, *13*(1), 125–136. https://doi.org/10.1016/j.brs.2019.10.004

Evans, C., Zich, C., Lee, J. S. A., Ward, N., & Bestmann, S. (2022). Inter-individual variability in current direction for common tDCS montages. *NeuroImage*, *260*, 119501. https://doi.org/10.1016/j.neuroimage.2022.119501

Fang, Q., & Boas, D. A. (2009). Tetrahedral mesh generation from volumetric binary and grayscale images. *2009 IEEE International Symposium on Biomedical Imaging: From Nano to Macro*, 1142–1145. https://doi.org/10.1109/ISBI.2009.5193259

Faraday, M. (1832). V. Experimental researches in electricity. *Philosophical Transactions of the Royal Society of London*, *122*, 125–162. https://doi.org/10.1098/rstl.1832.0006

Farahani, F., Kronberg, G., FallahRad, M., Oviedo, H. V., & Parra, L. C. (2021). Effects of direct current stimulation on synaptic plasticity in a single neuron. *Brain Stimulation: Basic, Translational, and Clinical Research in Neuromodulation*, *0*(0). https://doi.org/10.1016/j.brs.2021.03.001

Faria, P., Hallett, M., & Miranda, P. C. (2011). A finite element analysis of the effect of electrode area and inter-electrode distance on the spatial distribution of the current density in tDCS. *Journal of Neural Engineering*, *8*(6), 066017. https://doi.org/10.1088/1741-2560/8/6/066017

Faria, P., Leal, A., & Miranda, P. C. (2009). Comparing different electrode configurations using the 10-10 international system in tDCS: A finite element model analysis. *2009 Annual International Conference of the IEEE Engineering in Medicine and Biology Society*, 1596–1599. https://doi.org/10.1109/IEMBS.2009.5334121

Feigin, V. L., Brainin, M., Norrving, B., Martins, S., Sacco, R. L., Hacke, W., Fisher, M., Pandian, J., & Lindsay, P. (2022). World Stroke Organization (WSO): Global Stroke Fact Sheet 2022. *International Journal of Stroke*, *17*(1), 18–29. https://doi.org/10.1177/17474930211065917

Fernández-Klett, F., & Priller, J. (2014). The Fibrotic Scar in Neurological Disorders. *Brain Pathology*, *24*(4), 404–413. https://doi.org/10.1111/bpa.12162

Figlewski, K., Blicher, J. U., Mortensen, J., Severinsen, K. E., Nielsen, J. F., & Andersen, H. (2017). Transcranial Direct Current Stimulation Potentiates Improvements in Functional Ability in Patients With Chronic Stroke Receiving Constraint-Induced Movement Therapy. *Stroke*, *48*(1), 229–232. https://doi.org/10.1161/STROKEAHA.116.014988

Fitzgerald, P. B., Hoy, K., McQueen, S., Maller, J. J., Herring, S., Segrave, R., Bailey, M., Been, G., Kulkarni, J., & Daskalakis, Z. J. (2009). A Randomized Trial of rTMS Targeted with MRI Based Neuro-Navigation in Treatment-Resistant Depression. *Neuropsychopharmacology*, *34*(5), Article 5. https://doi.org/10.1038/npp.2008.233

Fleury, L., Koch, P., Wessel, M., Bonvin, C., San Millan, D., Constantin, C., Vuadens, P., Adolphsen, J., Cadic-Melchior, A., Brügger, J., Beanato, E., Ceroni, M., Menoud, P., de Leon Rodriguez, D., Zufferey, V., Meyer, N., Egger, P., Harquel, S., Popa, T., … Hummel, F. (2022). *Towards individualized Medicine in Stroke – the TiMeS project: Protocol of longitudinal, multi-modal, multi-domain study in stroke* [Preprint]. Neurology. https://doi.org/10.1101/2022.05.18.22274612

Ford, C. (2018, August 17). *Interpreting Log Transformations in a Linear Model | University of Virginia Library Research Data Services + Sciences*. Research Data Services and Sciences, University of Virginia Library. https://data.library.virginia.edu/interpreting-log-transformations-in-a-linear-model/

Fox, J., & Monette, G. (1992). Generalized Collinearity Diagnostics. *Journal of the American Statistical Association*, *87*(417), 178–183. https://doi.org/10.1080/01621459.1992.10475190

Fox, J., & Weisberg, S. (2019). *An R Companion to Applied Regression*. https://socialsciences.mcmaster.ca/jfox/Books/Companion/

Frank, A. C., Huang, S., Zhou, M., Gdalyahu, A., Kastellakis, G., Silva, T. K., Lu, E., Wen, X., Poirazi, P., Trachtenberg, J. T., & Silva, A. J. (2018). Hotspots of dendritic spine

turnover facilitate clustered spine addition and learning and memory. *Nature Communications*, *9*(1), Article 1. https://doi.org/10.1038/s41467-017-02751-2

French, B., Thomas, L. H., Leathley, M. J., Sutton, C. J., McAdam, J., Forster, A., Langhorne, P., Price, C. I. M., Walker, A., & Watkins, C. L. (2009). Repetitive Task Training for Improving Functional Ability After Stroke. *Stroke*, *40*(4), e98–e99. https://doi.org/10.1161/STROKEAHA.108.519553

Freundlieb, N., Philipp, S., Drabik, A., Gerloff, C., Forkert, N. D., & Hummel, F. C. (2015). Ipsilesional motor area size correlates with functional recovery after stroke: A 6-month follow-up longitudinal TMS motor mapping study. *Restorative Neurology and Neuroscience*, *33*(2), 221–231. https://doi.org/10.3233/RNN-140454

Fröhlich, F., & McCormick, D. A. (2010). Endogenous Electric Fields May Guide Neocortical Network Activity. *Neuron*, *67*(1), 129–143. https://doi.org/10.1016/j.neuron.2010.06.005

Fu, M., Yu, X., Lu, J., & Zuo, Y. (2012). Repetitive motor learning induces coordinated formation of clustered dendritic spines in vivo. *Nature*, *483*(7387), 92–95. https://doi.org/10.1038/nature10844

Fugl-Meyer, A. R., Jääskö, L., Leyman, I., Olsson, S., & Steglind, S. (1975). The post-stroke hemiplegic patient. 1. A method for evaluation of physical performance. *Scandinavian Journal of Rehabilitation Medicine*, *7*(1), 13–31.

Fujiwara, T. (2020). Mini-review article: The role of spinal reciprocal inhibition and intracortical inhibition in functional recovery from stroke. *Experimental Brain Research*, *238*(7), 1701–1705. https://doi.org/10.1007/s00221-020-05849-0

Galan-Gadea, A., Salvador, R., Bartolomei, F., Wendling, F., & Ruffini, G. (2022). *Spherical harmonics representation of the steady-state membrane potential shift induced by tDCS in realistic neuron models* (p. 2022.07.19.500653). bioRxiv. https://doi.org/10.1101/2022.07.19.500653

Galletta, E. E., Cancelli, A., Cottone, C., Simonelli, I., Tecchio, F., Bikson, M., & Marangolo, P. (2015). Use of Computational Modeling to Inform tDCS Electrode Montages for the Promotion of Language Recovery in Post-stroke Aphasia. *Brain Stimulation*, *8*(6), 1108–1115. https://doi.org/10.1016/j.brs.2015.06.018

Gelli, F., Del Santo, F., Popa, T., Mazzocchio, R., & Rossi, A. (2007). Factors influencing the relation between corticospinal output and muscle force during voluntary contractions. *European Journal of Neuroscience*, *25*(11), 3469–3475. https://doi.org/10.1111/j.1460-9568.2007.05590.x

Geroin, C., Picelli, A., Munari, D., Waldner, A., Tomelleri, C., & Smania, N. (2011). Combined transcranial direct current stimulation and robot-assisted gait training in patients with chronic stroke: A preliminary comparison. *Clinical Rehabilitation*, *25*(6), 537–548. https://doi.org/10.1177/0269215510389497

Ginhoux, R., Renaud, P., Zorn, L., Goffin, L., Bayle, B., Foucher, J., Lamy, J., Armspach, J. P., & de Mathelin, M. (2013). A custom robot for Transcranial Magnetic Stimulation: First assessment on healthy subjects. *Annual International Conference of the IEEE*

Engineering in Medicine and Biology Society. IEEE Engineering in Medicine and Biology Society. Annual International Conference, *2013*, 5352–5355. https://doi.org/10.1109/EMBC.2013.6610758

Glykys, J., & Mody, I. (2007). Activation of GABAA Receptors: Views from Outside the Synaptic Cleft. *Neuron*, *56*(5), 763–770. https://doi.org/10.1016/j.neuron.2007.11.002

Gomez-Tames, J., Asai, A., & Hirata, A. (2020). Significant group-level hotspots found in deep brain regions during transcranial direct current stimulation (tDCS): A computational analysis of electric fields. *Clinical Neurophysiology*, *131*(3), 755–765. https://doi.org/10.1016/j.clinph.2019.11.018

Gouty-Colomer, L. A., Hosseini, B., Marcelo, I. M., Schreiber, J., Slump, D. E., Yamaguchi, S., Houweling, A. R., Jaarsma, D., Elgersma, Y., & Kushner, S. A. (2016). Arc expression identifies the lateral amygdala fear memory trace. *Molecular Psychiatry*, *21*(3), Article 3. https://doi.org/10.1038/mp.2015.18

Green, P., & MacLeod, C. J. (2016). SIMR: An R package for power analysis of generalized linear mixed models by simulation. *Methods in Ecology and Evolution*, *7*(4), 493–498. https://doi.org/10.1111/2041-210X.12504

Grefkes, C., & Fink, G. R. (2012). Disruption of motor network connectivity post-stroke and its noninvasive neuromodulation. *Current Opinion in Neurology*, *25*(6), 670–675. https://doi.org/10.1097/WCO.0b013e3283598473

Grefkes, C., & Fink, G. R. (2014). Connectivity-based approaches in stroke and recovery of function. *The Lancet Neurology*, *13*(2), 206–216. https://doi.org/10.1016/S1474-4422(13)70264-3

Grefkes, C., & Fink, G. R. (2020). Recovery from stroke: Current concepts and future perspectives. *Neurological Research and Practice*, *2*(1), 17. https://doi.org/10.1186/s42466-020-00060-6

Grigoras, I.-F., & Stagg, C. J. (2021). Recent advances in the role of excitation-inhibition balance in motor recovery post-stroke. *Faculty Reviews*, *10*, 58. https://doi.org/10.12703/r/10-58

Groppa, S., Oliviero, A., Eisen, A., Quartarone, A., Cohen, L. G., Mall, V., Kaelin-Lang, A., Mima, T., Rossi, S., Thickbroom, G. W., Rossini, P. M., Ziemann, U., Valls-Solé, J., & Siebner, H. R. (2012). A practical guide to diagnostic transcranial magnetic stimulation: Report of an IFCN committee. *Clinical Neurophysiology*, *123*(5), 858–882. https://doi.org/10.1016/j.clinph.2012.01.010

Grubbs, F. E. (1969). Procedures for Detecting Outlying Observations in Samples. *Technometrics*, *11*(1), 1–21. https://doi.org/10.1080/00401706.1969.10490657

Guggisberg, A. G., Koch, P. J., Hummel, F. C., & Buetefisch, C. (2019). Brain networks and their relevance for stroke rehabilitation. *Clinical Neurophysiology : Official Journal of the International Federation of Clinical Neurophysiology*, *130*(7), 1098–1124. https://doi.org/10.1016/j.clinph.2019.04.004

Hagemann, G., Redecker, C., Neumann-Haefelin, T., Freund, H.-J., & Witte, O. W. (1998). Increased long-term potentiation in the surround of experimentally induced focal cortical infarction. *Annals of Neurology*, *44*(2), 255–258. https://doi.org/10.1002/ana.410440217

Hallett, M. (2000). Transcranial magnetic stimulation and the human brain. *Nature*, *406*(6792), 147–150. https://doi.org/10.1038/35018000

Hamoudi, M., Schambra, H. M., Fritsch, B., Schoechlin-Marx, A., Weiller, C., Cohen, L. G., & Reis, J. (2018). Transcranial Direct Current Stimulation Enhances Motor Skill Learning but Not Generalization in Chronic Stroke. *Neurorehabilitation and Neural Repair*, *32*(4–5), 295–308. https://doi.org/10.1177/1545968318769164

Han, J.-H., Kushner, S. A., Yiu, A. P., Cole, C. J., Matynia, A., Brown, R. A., Neve, R. L., Guzowski, J. F., Silva, A. J., & Josselyn, S. A. (2007). Neuronal Competition and Selection During Memory Formation. *Science*, *316*(5823), 457–460. https://doi.org/10.1126/science.1139438

Handiru, V. S., Mark, D., Hoxha, A., & Allexandre, D. (2021). An Automated Workflow for the Electric Field Modeling of High-definition Transcranial Direct Current Stimulation (HD-tDCS) in Chronic Stroke with Lesions. *2021 43rd Annual International Conference of the IEEE Engineering in Medicine & Biology Society (EMBC)*, 6663–6666. https://doi.org/10.1109/EMBC46164.2021.9629584

Hankey, G. J., Spiesser, J., Hakimi, Z., Bego, G., Carita, P., & Gabriel, S. (2007). Rate, degree, and predictors of recovery from disability following ischemic stroke. *Neurology*, *68*(19), 1583–1587. https://doi.org/10.1212/01.wnl.0000260967.77422.97

Hannah, R., Iacovou, A., & Rothwell, J. C. (2019). Direction of TDCS current flow in human sensorimotor cortex influences behavioural learning. *Brain Stimulation: Basic, Translational, and Clinical Research in Neuromodulation*, *12*(3), 684–692. https://doi.org/10.1016/j.brs.2019.01.016

Hashemirad, F., Zoghi, M., Fitzgerald, P. B., & Jaberzadeh, S. (2016). The effect of anodal transcranial direct current stimulation on motor sequence learning in healthy individuals: A systematic review and meta-analysis. *Brain and Cognition*, *102*, 1–12. https://doi.org/10.1016/j.bandc.2015.11.005

Hayashi-Takagi, A., Yagishita, S., Nakamura, M., Shirai, F., Wu, Y. I., Loshbaugh, A. L., Kuhlman, B., Hahn, K. M., & Kasai, H. (2015). Labelling and optical erasure of synaptic memory traces in the motor cortex. *Nature*, *525*(7569), Article 7569. https://doi.org/10.1038/nature15257

Hebbali, A. (2017). *olsrr: Tools for Building OLS Regression Models* (0.4.0). https://CRAN.R-project.org/package=olsrr

Hess, C. W., Mills, K. R., & Murray, N. M. (1987). Responses in small hand muscles from magnetic stimulation of the human brain. *The Journal of Physiology*, *388*(1), 397–419. https://doi.org/10.1113/jphysiol.1987.sp016621

Hesse, S., Waldner, A., Mehrholz, J., Tomelleri, C., Pohl, M., & Werner, C. (2011). Combined Transcranial Direct Current Stimulation and Robot-Assisted Arm Training in Subacute

Stroke Patients: An Exploratory, Randomized Multicenter Trial. *Neurorehabilitation and Neural Repair*, *25*(9), 838–846. https://doi.org/10.1177/1545968311413906

Heusler, P., Cebulla, B., Boehmer, G., & Dinse, H. R. (2000). A repetitive intracortical microstimulation pattern induces long-lasting synaptic depression in brain slices of the rat primary somatosensory cortex. *Experimental Brain Research*, *135*(3), 300–310. Scopus. https://doi.org/10.1007/s002210000530

Hiu, T., Farzampour, Z., Paz, J. T., Wang, E. H. J., Badgely, C., Olson, A., Micheva, K. D., Wang, G., Lemmens, R., Tran, K. V., Nishiyama, Y., Liang, X., Hamilton, S. A., O'Rourke, N., Smith, S. J., Huguenard, J. R., Bliss, T. M., & Steinberg, G. K. (2016). Enhanced phasic GABA inhibition during the repair phase of stroke: A novel therapeutic target. *Brain*, *139*(2), 468–480. https://doi.org/10.1093/brain/awv360

Holdefer, R. N., Sadleir, R., & Russell, M. J. (2006). Predicted current densities in the brain during transcranial electrical stimulation. *Clinical Neurophysiology*, *117*(6), 1388–1397. https://doi.org/10.1016/j.clinph.2006.02.020

Holland, R., & Crinion, J. (2012). Can tDCS enhance treatment of aphasia after stroke? *Aphasiology*, *26*(9), 1169–1191. https://doi.org/10.1080/02687038.2011.616925

Honaga, K., Fujiwara, T., Tsuji, T., Hase, K., Ushiba, J., & Liu, M. (2013). State of intracortical inhibitory interneuron activity in patients with chronic stroke. *Clinical Neurophysiology*, *124*(2), 364–370. https://doi.org/10.1016/j.clinph.2012.08.005

Hope, T. M. H., Friston, K., Price, C. J., Leff, A. P., Rotshtein, P., & Bowman, H. (2019). Recovery after stroke: Not so proportional after all? *Brain*, *142*(1), 15–22. https://doi.org/10.1093/brain/awy302

Hope, T. M. H., Seghier, M. L., Leff, A. P., & Price, C. J. (2013). Predicting outcome and recovery after stroke with lesions extracted from MRI images. *NeuroImage: Clinical*, *2*, 424–433. https://doi.org/10.1016/j.nicl.2013.03.005

Hordacre, B., Austin, D., Brown, K. E., Graetz, L., Pareés, I., De Trane, S., Vallence, A.-M., Koblar, S., Kleinig, T., McDonnell, M. N., Greenwood, R., Ridding, M. C., & Rothwell, J. C. (2021). Evidence for a Window of Enhanced Plasticity in the Human Motor Cortex Following Ischemic Stroke. *Neurorehabilitation and Neural Repair*, *35*(4), 307–320. https://doi.org/10.1177/1545968321992330

Hordacre, B., McCambridge, A. B., Ridding, M. C., & Bradnam, L. V. (2021). Can Transcranial Direct Current Stimulation Enhance Poststroke Motor Recovery?: Development of a Theoretical Patient-Tailored Model. *Neurology*, *97*(4), 170–180. https://doi.org/10.1212/WNL.0000000000012187

Horvath, J. C., Forte, J. D., & Carter, O. (2015). Evidence that transcranial direct current stimulation (tDCS) generates little-to-no reliable neurophysiologic effect beyond MEP amplitude modulation in healthy human subjects: A systematic review. *Neuropsychologia*, *66*, 213–236. https://doi.org/10.1016/j.neuropsychologia.2014.11.021

Huang, Q., Li, C., Xia, N., Zhao, L., Wang, D., Yang, Y., & Gao, H. (2018). Neurochemical changes in unilateral cerebral hemisphere during the subacute stage of focal cerebral

ischemia-reperfusion in rats: An ex vivo 1H magnetic resonance spectroscopy study. *Brain Research*, *1684*, 67–74. https://doi.org/10.1016/j.brainres.2018.01.026

Huang, Thomas, C., Datta, A., & Parra, L. C. (2018). Optimized tDCS for Targeting Multiple Brain Regions: An Integrated Implementation. *2018 40th Annual International Conference of the IEEE Engineering in Medicine and Biology Society (EMBC)*, 3545–3548. https://doi.org/10.1109/EMBC.2018.8513034

Huang, Y., Datta, A., Bikson, M., & Parra, L. C. (2018). ROAST: An Open-Source, Fully-Automated, Realistic Volumetric-Approach-Based Simulator For TES. *2018 40th Annual International Conference of the IEEE Engineering in Medicine and Biology Society (EMBC)*, 3072–3075. https://doi.org/10.1109/EMBC.2018.8513086

Huang, Y., Datta, A., Bikson, M., & Parra, L. C. (2019a). Realistic volumetric-approach to simulate transcranial electric stimulation—ROAST—a fully automated open-source pipeline. *Journal of Neural Engineering*, *16*(5), 056006. https://doi.org/10.1088/1741-2552/ab208d

Huang, Y., Datta, A., Bikson, M., & Parra, L. C. (2019b). Realistic volumetric-approach to simulate transcranial electric stimulation—ROAST—a fully automated open-source pipeline. *Journal of Neural Engineering*, *16*(5), 056006. https://doi.org/10.1088/1741-2552/ab208d

Huang, Y., Dmochowski, J. P., Su, Y., Datta, A., Rorden, C., & Parra, L. C. (2013). Automated MRI segmentation for individualized modeling of current flow in the human head. *Journal of Neural Engineering*, *10*(6), 066004. https://doi.org/10.1088/1741-2560/10/6/066004

Huang, Y., Liu, A. A., Lafon, B., Friedman, D., Dayan, M., Wang, X., Bikson, M., Doyle, W. K., Devinsky, O., & Parra, L. C. (2017). Measurements and models of electric fields in the in vivo human brain during transcranial electric stimulation. *ELife*, *6*, e18834. https://doi.org/10.7554/eLife.18834

Huang, Y., Liu, A. A., Lafon, B., Friedman, D., Dayan, M., Wang, X., Bikson, M., Doyle, W. K., Devinsky, O., & Parra, L. C. (2018). Correction: Measurements and models of electric fields in the in vivo human brain during transcranial electric stimulation. *ELife*, *7*, e35178. https://doi.org/10.7554/eLife.35178

Huang, Y.-Z., Chen, R.-S., Rothwell, J. C., & Wen, H.-Y. (2007). The after-effect of human theta burst stimulation is NMDA receptor dependent. *Clinical Neurophysiology*, *118*(5), 1028–1032. https://doi.org/10.1016/j.clinph.2007.01.021

Hummel, F. C., & Cohen, L. G. (2006). Non-invasive brain stimulation: A new strategy to improve neurorehabilitation after stroke? *The Lancet Neurology*, *5*(8), 708–712. https://doi.org/10.1016/S1474-4422(06)70525-7

Hummel, F. C., Steven, B., Hoppe, J., Heise, K., Thomalla, G., Cohen, L. G., & Gerloff, C. (2009). Deficient intracortical inhibition (SICI) during movement preparation after chronic stroke. *Neurology*, *72*(20), 1766–1772. https://doi.org/10.1212/WNL.0b013e3181a609c5

Hummel, F., & Cohen, L. G. (2005). Improvement of Motor Function with Noninvasive Cortical Stimulation in a Patient with Chronic Stroke. *Neurorehabilitation and Neural Repair*, *19*(1), 14–19. https://doi.org/10.1177/1545968304272698

Iyer, P. C., & Madhavan, S. (2019). Characterization of stimulus response curves obtained with transcranial magnetic stimulation from bilateral tibialis anterior muscles post stroke. *Neuroscience Letters*, *713*, 134530. https://doi.org/10.1016/j.neulet.2019.134530

Jackson, M. P., Rahman, A., Lafon, B., Kronberg, G., Ling, D., Parra, L. C., & Bikson, M. (2016). Animal models of transcranial direct current stimulation: Methods and mechanisms. *Clinical Neurophysiology*, *127*(11), 3425–3454. https://doi.org/10.1016/j.clinph.2016.08.016

James, G., Witten, D., Hastie, T., & Tibshirani, R. (2013). Linear Regression. In G. James, D. Witten, T. Hastie, & R. Tibshirani (Eds.), *An Introduction to Statistical Learning: With Applications in R* (pp. 59–126). Springer. https://doi.org/10.1007/978-1-4614-7138-7_3

Jansen, B. H., & Rit, V. G. (1995). Electroencephalogram and visual evoked potential generation in a mathematical model of coupled cortical columns. *Biological Cybernetics*, *73*(4), 357–366. https://doi.org/10.1007/BF00199471

Jayaraj, R. L., Azimullah, S., Beiram, R., Jalal, F. Y., & Rosenberg, G. A. (2019). Neuroinflammation: Friend and foe for ischemic stroke. *Journal of Neuroinflammation*, *16*, 142. https://doi.org/10.1186/s12974-019-1516-2

Jefferys, J. G. (1981). Influence of electric fields on the excitability of granule cells in guinea-pig hippocampal slices. *The Journal of Physiology*, *319*, 143–152.

Johnstone, A., Levenstein, J. M., Hinson, E. L., & Stagg, C. J. (2018). Neurochemical changes underpinning the development of adjunct therapies in recovery after stroke: A role for GABA? *Journal of Cerebral Blood Flow and Metabolism: Official Journal of the International Society of Cerebral Blood Flow and Metabolism*, *38*(9), 1564–1583. https://doi.org/10.1177/0271678X17727670

Johnstone, A., Zich, C., Evans, C., Lee, J., Ward, N., & Bestmann, S. (in review). The impact of brain lesions on tDCS-induced electric field magnitude. *BioRxiv*, 2021.03.19.436124. https://doi.org/10.1101/2021.03.19.436124

Jorgensen, H. S., Nakayama, H., Raaschou, H. O., & Olsen, T. S. (1999). *Stroke. Neurologic and functional recovery the Copenhagen Stroke Study. 10*(4), 887–906.

Josselyn, S. A., Köhler, S., & Frankland, P. W. (2015). Finding the engram. *Nature Reviews Neuroscience*, *16*(9), Article 9. https://doi.org/10.1038/nrn4000

Joucla, S., & Yvert, B. (2009). The “Mirror” Estimate: An Intuitive Predictor of Membrane Polarization during Extracellular Stimulation. *Biophysical Journal*, *96*(9), 3495–3508. https://doi.org/10.1016/j.bpj.2008.12.3961

Joy, M. T., & Carmichael, S. T. (2020). Encouraging an excitable brain state: Mechanisms of brain repair in stroke. *Nature Reviews Neuroscience*, 1–16. https://doi.org/10.1038/s41583-020-00396-7

Jp, B.-N., Lg, C., M, P., J, N., Bj, R., & M, H. (1992). Optimal focal transcranial magnetic activation of the human motor cortex: Effects of coil orientation, shape of the induced current pulse, and stimulus intensity. *Journal of Clinical Neurophysiology : Official Publication of the American Electroencephalographic Society*, *9*(1), 132–136.

Kabakov, A. Y., Muller, P. A., Pascual-Leone, A., Jensen, F. E., & Rotenberg, A. (2012). Contribution of axonal orientation to pathway-dependent modulation of excitatory transmission by direct current stimulation in isolated rat hippocampus. *Journal of Neurophysiology*, *107*(7), 1881–1889. https://doi.org/10.1152/jn.00715.2011

Kaelin-Lang, A., Luft, A. R., Sawaki, L., Burstein, A. H., Sohn, Y. H., & Cohen, L. G. (2002). Modulation of human corticomotor excitability by somatosensory input. *The Journal of Physiology*, *540*(Pt 2), 623–633. https://doi.org/10.1113/jphysiol.2001.012801

Kashyap, R., Bhattacharjee, S., Bharath, R. D., Venkatasubramanian, G., Udupa, K., Bashir, S., Oishi, K., Desmond, J. E., Chen, S. H. A., & Guan, C. (2022). Variation of cerebrospinal fluid in specific regions regulates focality in transcranial direct current stimulation. *Frontiers in Human Neuroscience*, *16*, 952602. https://doi.org/10.3389/fnhum.2022.952602

Kemlin, C., Moulton, E., Lamy, J.-C., Houot, M., Valabregue, R., Leder, S., Obadia, M. A., Meseguer, E., Yger, M., Brochard, V., Corvol, J.-C., Samson, Y., & Rosso, C. (2019). Elucidating the Structural and Functional Correlates of Upper-Limb Poststroke Motor Impairment. *Stroke*, *50*(12), 3647–3649. https://doi.org/10.1161/STROKEAHA.119.027126

Kemlin, C., Moulton, E., Leder, S., Houot, M., Meunier, S., Rosso, C., & Lamy, J.-C. (2019). Redundancy Among Parameters Describing the Input-Output Relation of Motor Evoked Potentials in Healthy Subjects and Stroke Patients. *Frontiers in Neurology*, *10*. https://doi.org/10.3389/fneur.2019.00535

Kessler, S. K., Minhas, P., Woods, A. J., Rosen, A., Gorman, C., & Bikson, M. (2013). Dosage Considerations for Transcranial Direct Current Stimulation in Children: A Computational Modeling Study. *PLOS ONE*, *8*(9), e76112. https://doi.org/10.1371/journal.pone.0076112

Khedr, E. M., Shawky, O. A., El-Hammady, D. H., Rothwell, J. C., Darwish, E. S., Mostafa, O. M., & Tohamy, A. M. (2013). Effect of Anodal Versus Cathodal Transcranial Direct Current Stimulation on Stroke Rehabilitation: A Pilot Randomized Controlled Trial. *Neurorehabilitation and Neural Repair*, *27*(7), 592–601. https://doi.org/10.1177/1545968313484808

Kiers, L., Cros, D., Chiappa, K. H., & Fang, J. (1993). Variability of motor potentials evoked by transcranial magnetic stimulation. *Electroencephalography and Clinical Neurophysiology/Evoked Potentials Section*, *89*(6), 415–423. https://doi.org/10.1016/0168-5597(93)90115-6

Kim, D.-E., Park, J.-H., Schellingerhout, D., Ryu, W.-S., Lee, S.-K., Jang, M. U., Jeong, S.-W., Na, J.-Y., Park, J. E., Lee, E. J., Cho, K.-H., Kim, J.-T., Kim, B. J., Han, M.-K., Lee, J., Cha, J.-K., Kim, D.-H., Lee, S. J., Ko, Y., … Bae, H.-J. (2019). Mapping the Supratentorial Cerebral Arterial Territories Using 1160 Large Artery Infarcts. *JAMA Neurology*, *76*(1), 72–80. https://doi.org/10.1001/jamaneurol.2018.2808

Kim, J., Kwon, J.-T., Kim, H.-S., & Han, J.-H. (2013). CREB and neuronal selection for memory trace. *Frontiers in Neural Circuits*, *7*. https://www.frontiersin.org/articles/10.3389/fncir.2013.00044

Kim, S., Stephenson, M. C., Morris, P. G., & Jackson, S. R. (2014). tDCS-induced alterations in GABA concentration within primary motor cortex predict motor learning and motor memory: A 7 T magnetic resonance spectroscopy study. *NeuroImage*, *99*, 237–243. https://doi.org/10.1016/j.neuroimage.2014.05.070

Kim, Y. K., Yang, E. J., Cho, K., Lim, J. Y., & Paik, N.-J. (2014). Functional Recovery After Ischemic Stroke Is Associated With Reduced GABAergic Inhibition in the Cerebral Cortex: A GABA PET Study. *Neurorehabilitation and Neural Repair*, *28*(6), 576–583. https://doi.org/10.1177/1545968313520411

Kimiskidis, V., Papagiannopoulos, S., Sotirakoglou, K., Kazis, D., Dimopoulos, G., Kazis, A., & Mills, K. (2005). The repeatability of corticomotor threshold measurements. *Neurophysiologie Clinique = Clinical Neurophysiology*, *34*, 259–266. https://doi.org/10.1016/j.neucli.2004.10.002

King, D., Wittenberg, R., Patel, A., Quayyum, Z., Berdunov, V., & Knapp, M. (2020). The future incidence, prevalence and costs of stroke in the UK. *Age and Ageing*, *49*(2), 277–282. https://doi.org/10.1093/ageing/afz163

Kirimoto, H., Ogata, K., Onishi, H., Oyama, M., Goto, Y., & Tobimatsu, S. (2011). Transcranial direct current stimulation over the motor association cortex induces plastic changes in ipsilateral primary motor and somatosensory cortices. *Clinical Neurophysiology*, *122*(4), 777–783. https://doi.org/10.1016/j.clinph.2010.09.025

Koessler, L., Colnat-Coulbois, S., Cecchin, T., Hofmanis, J., Dmochowski, J. P., Norcia, A. M., & Maillard, L. G. (2016). In-vivo measurements of human brain tissue conductivity using focal electrical current injection through intracerebral multicontact electrodes. *Human Brain Mapping*, *38*(2), 974–986. https://doi.org/10.1002/hbm.23431

Kojima, S., Miyaguchi, S., Sasaki, R., Tsuiki, S., Saito, K., Inukai, Y., Otsuru, N., & Onishi, H. (2019). The effects of mechanical tactile stimulation on corticospinal excitability and motor function depend on pin protrusion patterns. *Scientific Reports*, *9*(1), Article 1. https://doi.org/10.1038/s41598-019-53275-2

Kolasinski, J., Hinson, E. L., Divanbeighi Zand, A. P., Rizov, A., Emir, U. E., & Stagg, C. J. (2019). The dynamics of cortical GABA in human motor learning. *The Journal of Physiology*, *597*(1), 271–282. https://doi.org/10.1113/JP276626

Kornhauser, J. M., Cowan, C. W., Shaywitz, A. J., Dolmetsch, R. E., Griffith, E. C., Hu, L. S., Haddad, C., Xia, Z., & Greenberg, M. E. (2002). CREB Transcriptional Activity in

Neurons Is Regulated by Multiple, Calcium-Specific Phosphorylation Events. *Neuron*, *34*(2), 221–233. https://doi.org/10.1016/S0896-6273(02)00655-4

Krakauer, J. W., & Carmichael, S. T. (2017a). A Hierarchical Framework for Tissue Repair after Stroke. In *Broken Movement: The Neurobiology of Motor Recovery after Stroke*. The MIT Press. https://doi-org.libproxy.ucl.ac.uk/10.7551/mitpress/9310.001.0001

Krakauer, J. W., & Carmichael, S. T. (2017b). Acute Hemiparesis: Spontaneous Biological Recovery, the Effect of Training, Sensitive Periods, and Reorganization. In *Broken Movement*. The MIT Press. https://doi.org/10.7551/mitpress/9310.003.0005

Krakauer, J. W., & Carmichael, S. T. (2017c). The Molecular and Cellular Biology of the Peri-Infarct Cortex and Beyond: Repair versus Reorganization. In *Broken Movement*. The MIT Press. https://doi.org/10.7551/mitpress/9310.003.0006

Krakauer, J. W., Carmichael, S. T., Corbett, D., & Wittenberg, G. F. (2012). Getting Neurorehabilitation Right: What Can Be Learned From Animal Models? *Neurorehabilitation and Neural Repair*, *26*(8), 923–931. https://doi.org/10.1177/1545968312440745

Kronberg, G., Bridi, M., Abel, T., Bikson, M., & Parra, L. C. (2017). Direct Current Stimulation Modulates LTP and LTD: Activity Dependence and Dendritic Effects. *Brain Stimulation*, *10*(1), 51–58. https://doi.org/10.1016/j.brs.2016.10.001

Kronberg, G., Rahman, A., Bikson, M., & Parra, L. (2019). A Hebbian framework for predicting modulation of synaptic plasticity with tDCS. *Brain Stimulation: Basic, Translational, and Clinical Research in Neuromodulation*, *12*(2), 554. https://doi.org/10.1016/j.brs.2018.12.831

Kruschke, J. K. (2018). Rejecting or Accepting Parameter Values in Bayesian Estimation. *Advances in Methods and Practices in Psychological Science*, *1*(2), 270–280. https://doi.org/10.1177/2515245918771304

Kubis, N. (2016). Non-Invasive Brain Stimulation to Enhance Post-Stroke Recovery. *Frontiers in Neural Circuits*, *10*, 56. https://doi.org/10.3389/fncir.2016.00056

Kujirai, T., Caramia, M. D., Rothwell, J. C., Day, B. L., Thompson, P. D., Ferbert, A., Wroe, S., Asselman, P., & Marsden, C. D. (1993). Corticocortical inhibition in human motor cortex. *The Journal of Physiology*, *471*, 501–519.

Kukke, S. N., Paine, R. W., Chao, C., de Campos, A. C., & Hallett, M. (2014). Efficient and reliable characterization of the corticospinal system using transcranial magnetic stimulation. *Journal of Clinical Neurophysiology : Official Publication of the American Electroencephalographic Society*, *31*(3), 246–252. https://doi.org/10.1097/WNP.0000000000000057

Kundert, R., Goldsmith, J., Veerbeek, J. M., Krakauer, J. W., & Luft, A. R. (2019). What the Proportional Recovery Rule Is (and Is Not): Methodological and Statistical Considerations. *Neurorehabilitation and Neural Repair*, *33*(11), 876–887. https://doi.org/10.1177/1545968319872996

Kuznetsova, A., Brockhoff, P. B., & Christensen, R. H. B. (2017). *lmerTest Package: Tests in Linear Mixed Effects Models*. 27.

Kwakkel, G., Kollen, B. J., van der Grond, J., & Prevo, A. J. H. (2003). Probability of Regaining Dexterity in the Flaccid Upper Limb. *Stroke*, *34*(9), 2181–2186. https://doi.org/10.1161/01.STR.0000087172.16305.CD

Kwakkel, G., Kollen, B., & Lindeman, E. (2004). Understanding the pattern of functional recovery after stroke: Facts and theories. *Restorative Neurology and Neuroscience*, *22*, 281–299.

Kwakkel, G., Wagenaar, R. C., Koelman, T. W., Lankhorst, G. J., & Koetsier, J. C. (1997). Effects of Intensity of Rehabilitation After Stroke. *Stroke*, *28*(8), 1550–1556. https://doi.org/10.1161/01.STR.28.8.1550

Laakso, I., Mikkonen, M., Koyama, S., Hirata, A., & Tanaka, S. (2019). Can electric fields explain inter-individual variability in transcranial direct current stimulation of the motor cortex? *Scientific Reports*, *9*(1), Article 1. https://doi.org/10.1038/s41598-018-37226-x

Laakso, I., Mikkonen, M., Koyama, S., Ito, D., Yamaguchi, T., Hirata, A., & Tanaka, S. (2018). *Electric field dependent effects of motor cortical TDCS*. https://doi.org/10.1101/327361

Laakso, I., Tanaka, S., Koyama, S., Santis, V. D., & Hirata, A. (2015). Inter-subject Variability in Electric Fields of Motor Cortical tDCS. *Brain Stimulation: Basic, Translational, and Clinical Research in Neuromodulation*, *8*(5), 906–913. https://doi.org/10.1016/j.brs.2015.05.002

Laakso, I., Tanaka, S., Mikkonen, M., Koyama, S., & Hirata, A. (2017). *Variability in TDCS electric fields: Effects of electrode size and configuration*. 1–4. https://doi.org/10.23919/URSIGASS.2017.8105344

Lackland Daniel T., Roccella Edward J., Deutsch Anne F., Fornage Myriam, George Mary G., Howard George, Kissela Brett M., Kittner Steven J., Lichtman Judith H., Lisabeth Lynda D., Schwamm Lee H., Smith Eric E., & Towfighi Amytis. (2014). Factors Influencing the Decline in Stroke Mortality. *Stroke*, *45*(1), 315–353. https://doi.org/10.1161/01.str.0000437068.30550.cf

Lafon, B., Rahman, A., Bikson, M., & Parra, L. C. (2017). Direct Current Stimulation Alters Neuronal Input/Output Function. *Brain Stimulation: Basic, Translational, and Clinical Research in Neuromodulation*, *10*(1), 36–45. https://doi.org/10.1016/j.brs.2016.08.014

Lai, T. W., Zhang, S., & Wang, Y. T. (2014). Excitotoxicity and stroke: Identifying novel targets for neuroprotection. *Progress in Neurobiology*, *115*, 157–188. https://doi.org/10.1016/j.pneurobio.2013.11.006

Lake, E. M., Chaudhuri, J., Thomason, L., Janik, R., Ganguly, M., Brown, M., McLaurin, J., Corbett, D., Stanisz, G. J., & Stefanovic, B. (2015). The Effects of Delayed Reduction of Tonic Inhibition on Ischemic Lesion and Sensorimotor Function. *Journal of Cerebral*

Blood Flow & Metabolism, *35*(10), 1601–1609. https://doi.org/10.1038/jcbfm.2015.86

Lang, N., Siebner, H. R., Ward, N. S., Lee, L., Nitsche, M. A., Paulus, W., Rothwell, J. C., Lemon, R. N., & Frackowiak, R. S. (2005). How does transcranial DC stimulation of the primary motor cortex alter regional neuronal activity in the human brain? *European Journal of Neuroscience*, *22*(2), 495–504. https://doi.org/10.1111/j.1460-9568.2005.04233.x

Langhorne, P., Coupar, F., & Pollock, A. (2009). Motor recovery after stroke: A systematic review. *The Lancet Neurology*, *8*(8), 741–754. https://doi.org/10.1016/S1474-4422(09)70150-4

Larson, J., & Lynch, G. (1986). Induction of Synaptic Potentiation in Hippocampus by Patterned Stimulation Involves Two Events. *Science*, *232*(4753), 985–988. https://doi.org/10.1126/science.3704635

Larson, J., & Lynch, G. (1989). Theta pattern stimulation and the induction of LTP: The sequence in which synapses are stimulated determines the degree to which they potentiate. *Brain Research*, *489*(1), 49–58. https://doi.org/10.1016/0006-8993(89)90007-3

Larson, J., Wong, D., & Lynch, G. (1986). Patterned stimulation at the theta frequency is optimal for the induction of hippocampal long-term potentiation. *Brain Research*, *368*(2), 347–350. https://doi.org/10.1016/0006-8993(86)90579-2

Lee, C., Jung, Y.-J., Lee, S. J., & Im, C.-H. (2017). COMETS2: An advanced MATLAB toolbox for the numerical analysis of electric fields generated by transcranial direct current stimulation. *Journal of Neuroscience Methods*, *277*, 56–62. https://doi.org/10.1016/j.jneumeth.2016.12.008

Lee, J. S. A., Bestmann, S., & Evans, C. (2021a). A Future of Current Flow Modelling for Transcranial Electrical Stimulation? *Current Behavioral Neuroscience Reports*, *8*(4), 150–159. https://doi.org/10.1007/s40473-021-00238-5

Lee, J. S. A., Bestmann, S., & Evans, C. (2021b). A Future of Current Flow Modelling for Transcranial Electrical Stimulation? *Current Behavioral Neuroscience Reports*, *8*(4), 150–159. https://doi.org/10.1007/s40473-021-00238-5

Lefaucheur, J.-P. (2016). A comprehensive database of published tDCS clinical trials (2005–2016). *Neurophysiologie Clinique/Clinical Neurophysiology*, *46*(6), 319–398. https://doi.org/10.1016/j.neucli.2016.10.002

Lefaucheur, J.-P., Antal, A., Ayache, S. S., Benninger, D. H., Brunelin, J., Cogiamanian, F., Cotelli, M., De Ridder, D., Ferrucci, R., Langguth, B., Marangolo, P., Mylius, V., Nitsche, M. A., Padberg, F., Palm, U., Poulet, E., Priori, A., Rossi, S., Schecklmann, M., … Paulus, W. (2017). Evidence-based guidelines on the therapeutic use of transcranial direct current stimulation (tDCS). *Clinical Neurophysiology*, *128*(1), 56–92. https://doi.org/10.1016/j.clinph.2016.10.087

Lenz, M., Platschek, S., Priesemann, V., Becker, D., Willems, L. M., Ziemann, U., Deller, T., Müller-Dahlhaus, F., Jedlicka, P., & Vlachos, A. (2015). Repetitive magnetic

stimulation induces plasticity of excitatory postsynapses on proximal dendrites of cultured mouse CA1 pyramidal neurons. *Brain Structure and Function*, *220*(6), 3323–3337. https://doi.org/10.1007/s00429-014-0859-9

Levy, R., Ruland, S., Weinand, M., Lowry, D., Dafer, R., & Bakay, R. (2008). Cortical stimulation for the rehabilitation of patients with hemiparetic stroke: A multicenter feasibility study of safety and efficacy. *Journal of Neurosurgery*, *108*(4), 707–714. https://doi.org/10.3171/JNS/2008/108/4/0707

Li, S., Nie, E., Yin, Y., Benowitz, L., Tung, S., Vinters, H., Bahjat, F., Stenzel-Poore, M., Kawaguchi, R., Coppola, G., & Carmichael, S. (2015). GDF10 Is a Signal for Axonal Sprouting and Functional Recovery after Stroke. *Nature Neuroscience*, *18*(12), 1737–1745. https://doi.org/10.1038/nn.4146

Li, S., Overman, J. J., Katsman, D., Kozlov, S. V., Donnelly, C. J., Twiss, J. L., Giger, R. J., Coppola, G., Geschwind, D. H., & Carmichael, S. T. (2010). An age-related sprouting transcriptome provides molecular control of axonal sprouting after stroke. *Nature Neuroscience*, *13*(12), 1496–1504. https://doi.org/10.1038/nn.2674

Liepert, J., Storch, P., Fritsch, A., & Weiller, C. (2000). Motor cortex disinhibition in acute stroke. *Clinical Neurophysiology*, *111*(4), 671–676. https://doi.org/10.1016/S1388-2457(99)00312-0

Liew, S., Zavaliangos-Petropulu, A., Jahanshad, N., Lang, C. E., Hayward, K. S., Lohse, K. R., Juliano, J. M., Assogna, F., Baugh, L. A., Bhattacharya, A. K., Bigjahan, B., Borich, M. R., Boyd, L. A., Brodtmann, A., Buetefisch, C. M., Byblow, W. D., Cassidy, J. M., Conforto, A. B., Craddock, R. C., … Thompson, P. M. (2020). The ENIGMA Stroke Recovery Working Group: Big data neuroimaging to study brain–behavior relationships after stroke. *Human Brain Mapping*, *43*(1), 129–148. https://doi.org/10.1002/hbm.25015

Liew, S.-L., Anglin, J. M., Banks, N. W., Sondag, M., Ito, K. L., Kim, H., Chan, J., Ito, J., Jung, C., Khoshab, N., Lefebvre, S., Nakamura, W., Saldana, D., Schmiesing, A., Tran, C., Vo, D., Ard, T., Heydari, P., Kim, B., … Stroud, A. (2018). A large, open source dataset of stroke anatomical brain images and manual lesion segmentations. *Scientific Data*, *5*, 180011. https://doi.org/10.1038/sdata.2018.11

Liew, S.-L., Lo, B. P., Donnelly, M. R., Zavaliangos-Petropulu, A., Jeong, J. N., Barisano, G., Hutton, A., Simon, J. P., Juliano, J. M., Suri, A., Wang, Z., Abdullah, A., Kim, J., Ard, T., Banaj, N., Borich, M. R., Boyd, L. A., Brodtmann, A., Buetefisch, C. M., … Yu, C. (2022). A large, curated, open-source stroke neuroimaging dataset to improve lesion segmentation algorithms. *Scientific Data*, *9*(1), Article 1. https://doi.org/10.1038/s41597-022-01401-7

Lim, D. H., LeDue, J. M., Mohajerani, M. H., & Murphy, T. H. (2014). Optogenetic Mapping after Stroke Reveals Network-Wide Scaling of Functional Connections and Heterogeneous Recovery of the Peri-Infarct. *The Journal of Neuroscience*, *34*(49), 16455–16466. https://doi.org/10.1523/JNEUROSCI.3384-14.2014

Lindau, N. T., Bänninger, B. J., Gullo, M., Good, N. A., Bachmann, L. C., Starkey, M. L., & Schwab, M. E. (2014). Rewiring of the corticospinal tract in the adult rat after

unilateral stroke and anti-Nogo-A therapy. *Brain*, *137*(3), 739–756. https://doi.org/10.1093/brain/awt336

Lindmark, B., & Hamrin, E. (1988). Evaluation of functional capacity after stroke as a basis for active intervention. Presentation of a modified chart for motor capacity assessment and its reliability. *Scandinavian Journal of Rehabilitation Medicine*, *20*(3), 103–109.

Lisman, J. E. (2001). Three Ca2+ levels affect plasticity differently: The LTP zone, the LTD zone and no man's land. *The Journal of Physiology*, *532*(Pt 2), 285. https://doi.org/10.1111/j.1469-7793.2001.0285f.x

Liu, G., Yang, X., Xue, T., Chen, S., Wu, X., Yan, Z., Wang, Z., Wu, D., Chen, Z., & Wang, Z. (2021). Is Fluoxetine Good for Subacute Stroke? A Meta-Analysis Evidenced From Randomized Controlled Trials. *Frontiers in Neurology*, *12*. https://www.frontiersin.org/articles/10.3389/fneur.2021.633781

Liu, J., Zhang, J., & Wang, L.-N. (2018). Gamma aminobutyric acid (GABA) receptor agonists for acute stroke. *The Cochrane Database of Systematic Reviews*, *10*, CD009622. https://doi.org/10.1002/14651858.CD009622.pub5

Liu, Y.-H., Chan, S. J., Pan, H.-C., Bandla, A., King, N. K. K., Wong, P. T. H., Chen, Y.-Y., Ng, W. H., Thakor, N. V., & Liao, L.-D. (2017). Integrated treatment modality of cathodal-transcranial direct current stimulation with peripheral sensory stimulation affords neuroprotection in a rat stroke model. *Neurophotonics*, *4*(04), 1. https://doi.org/10.1117/1.NPh.4.4.045002

Lohse Keith R., Lang Catherine E., & Boyd Lara A. (2014). Is More Better? Using Metadata to Explore Dose–Response Relationships in Stroke Rehabilitation. *Stroke*, *45*(7), 2053–2058. https://doi.org/10.1161/STROKEAHA.114.004695

Long, J. A. (2020). *interactions: Comprehensive, User-Friendly Toolkit for Probing Interactions* (1.1.3). https://CRAN.R-project.org/package=interactions

Long, J. A. (2021). *jtools: Analysis and Presentation of Social Scientific Data* (2.1.2). https://CRAN.R-project.org/package=jtools

López-Alonso, V., Fernández-del-Olmo, M., Costantini, A., Gonzalez-Henriquez, J. J., & Cheeran, B. (2015). Intra-individual variability in the response to anodal transcranial direct current stimulation. *Clinical Neurophysiology*, *126*(12), 2342–2347. https://doi.org/10.1016/j.clinph.2015.03.022

Lopez-Sola, E., Sanchez-Todo, R., Lleal, È., Köksal-Ersöz, E., Yochum, M., Makhalova, J., Mercadal, B., Guasch, M., Salvador, R., Lozano-Soldevilla, D., Modolo, J., Bartolomei, F., Wendling, F., Benquet, P., & Ruffini, G. (2022). *A personalizable autonomous neural mass model of epileptic seizures* (p. 2021.12.24.474090). bioRxiv. https://doi.org/10.1101/2021.12.24.474090

Lundström, E., Isaksson, E., Greilert Norin, N., Näsman, P., Wester, P., Mårtensson, B., Norrving, B., Wallén, H., Borg, J., Hankey, G. J., Hackett, M. L., Mead, G. E., Dennis, M. S., Sunnerhagen, K. S., & null, null. (2021). Effects of Fluoxetine on Outcomes at 12 Months After Acute Stroke. *Stroke*, *52*(10), 3082–3087. https://doi.org/10.1161/STROKEAHA.121.034705

Mahdavi, S., & Towhidkhah, F. (2018). Computational human head models of tDCS: Influence of brain atrophy on current density distribution. *Brain Stimulation*, *11*(1), 104–107. https://doi.org/10.1016/j.brs.2017.09.013

Malcolm, M. P., Enney, L., & Cramer, S. C. (2014). Methods for an International Randomized Clinical Trial to Investigate the Effect of Gsk249320 on Motor Cortex Neurophysiology using Transcranial Magnetic Stimulation in Survivors of Stroke. *Journal of Clinical Trials*, *4*(6), 1–9. https://doi.org/10.4172/2167-0870.1000199

Manganotti, P., Acler, M., Zanette, G. P., Smania, N., & Fiaschi, A. (2008). Motor Cortical Disinhibition During Early and Late Recovery After Stroke. *Neurorehabilitation and Neural Repair*, *22*(4), 396–403. https://doi.org/10.1177/1545968307313505

Manganotti, P., Patuzzo, S., Cortese, F., Palermo, A., Smania, N., & Fiaschi, A. (2002). Motor disinhibition in affected and unaffected hemisphere in the early period of recovery after stroke. *Clinical Neurophysiology*, *113*(6), 936–943. https://doi.org/10.1016/S1388-2457(02)00062-7

Mantell, K. E., Sutter, E. N., Shirinpour, S., Nemanich, S. T., Lench, D. H., Gillick, B. T., & Opitz, A. (2021). Evaluating transcranial magnetic stimulation (TMS) induced electric fields in pediatric stroke. *NeuroImage : Clinical*, *29*, 102563. https://doi.org/10.1016/j.nicl.2021.102563

Marc J. Mazerolle. (2020). *AICcmodavg: Model selection and multimodel inference based on (Q)AIC(c)*. https://cran.r-project.org/package=AICcmodavg

Marquez, J., van Vliet, P., McElduff, P., Lagopoulos, J., & Parsons, M. (2015). Transcranial Direct Current Stimulation (tDCS): Does it Have Merit in Stroke Rehabilitation? A Systematic Review. *International Journal of Stroke*, *10*(3), 306–316. https://doi.org/10.1111/ijs.12169

MATLAB (Version 2018b). (2018). The Mathworks, Inc.

McCann, H., & Beltrachini, L. (2021). Does participant's age impact on tDCS induced fields? Insights from computational simulations. *Biomedical Physics & Engineering Express*, *7*(4), 045018. https://doi.org/10.1088/2057-1976/ac0547

McCann, H., Pisano, G., & Beltrachini, L. (2019). Variation in Reported Human Head Tissue Electrical Conductivity Values. *Brain Topography*, *32*(5), 825–858. https://doi.org/10.1007/s10548-019-00710-2

McDonald, M. W., Hayward, K. S., Rosbergen, I. C. M., Jeffers, M. S., & Corbett, D. (2018). Is Environmental Enrichment Ready for Clinical Application in Human Post-stroke Rehabilitation? *Frontiers in Behavioral Neuroscience*, *12*, 135. https://doi.org/10.3389/fnbeh.2018.00135

McDonnell, M. N., & Ridding, M. C. (2006). Transient motor evoked potential suppression following a complex sensorimotor task. *Clinical Neurophysiology: Official Journal of the International Federation of Clinical Neurophysiology*, *117*(6), 1266–1272. https://doi.org/10.1016/j.clinph.2006.02.008

McDonnell, M. N., & Stinear, C. M. (2017a). TMS measures of motor cortex function after stroke: A meta-analysis. *Brain Stimulation*, *10*(4), 721–734. https://doi.org/10.1016/j.brs.2017.03.008

McDonnell, M. N., & Stinear, C. M. (2017b). TMS measures of motor cortex function after stroke: A meta-analysis. *Brain Stimulation*, *10*(4), 721–734. https://doi.org/10.1016/j.brs.2017.03.008

Mead, G. E., Hsieh, C.-F., Lee, R., Kutlubaev, M., Claxton, A., Hankey, G. J., & Hackett, M. (2013). Selective Serotonin Reuptake Inhibitors for Stroke Recovery. *Stroke*, *44*(3), 844–850. https://doi.org/10.1161/STROKEAHA.112.673947

Mestre, H., Du, T., Sweeney, A. M., Liu, G., Samson, A. J., Peng, W., Mortensen, K. N., Stæger, F. F., Bork, P. A. R., Bashford, L., Toro, E. R., Tithof, J., Kelley, D. H., Thomas, J. H., Hjorth, P. G., Martens, E. A., Mehta, R. I., Solis, O., Blinder, P., … Nedergaard, M. (2020). Cerebrospinal fluid influx drives acute ischemic tissue swelling. *Science (New York, N.Y.)*, *367*(6483), eaax7171. https://doi.org/10.1126/science.aax7171

Mikkonen, M., Laakso, I., Tanaka, S., & Hirata, A. (2020). Cost of focality in TDCS: Interindividual variability in electric fields. *Brain Stimulation*, *13*(1), 117–124. https://doi.org/10.1016/j.brs.2019.09.017

Mills, K. R., Boniface, S. J., & Schubert, M. (1992). Magnetic brain stimulation with a double coil: The importance of coil orientation. *Electroencephalography and Clinical Neurophysiology/Evoked Potentials Section*, *85*(1), 17–21. https://doi.org/10.1016/0168-5597(92)90096-T

Minhas, P., Bansal, V., Patel, J., Ho, J. S., Diaz, J., Datta, A., & Bikson, M. (2010). Electrodes for high-definition transcutaneous DC stimulation for applications in drug delivery and electrotherapy, including tDCS. *Journal of Neuroscience Methods*, *190*(2), 188–197. https://doi.org/10.1016/j.jneumeth.2010.05.007

Minjoli, S., Saturnino, G. B., Blicher, J. U., Stagg, C. J., Siebner, H. R., Antunes, A., & Thielscher, A. (2017). The impact of large structural brain changes in chronic stroke patients on the electric field caused by transcranial brain stimulation. *NeuroImage: Clinical*, *15*, 106–117. https://doi.org/10.1016/j.nicl.2017.04.014

Miranda, P. C. (2013). Physics of effects of transcranial brain stimulation. In *Handbook of Clinical Neurology* (Vol. 116, pp. 353–366). Elsevier. https://doi.org/10.1016/B978-0-444-53497-2.00029-2

Miranda, P. C., Correia, L., Salvador, R., & Basser, P. J. (2007). Tissue heterogeneity as a mechanism for localized neural stimulation by applied electric fields. *Physics in Medicine and Biology*, *52*(18), 5603–5617. https://doi.org/10.1088/0031-9155/52/18/009

Miranda, P. C., Lomarev, M., & Hallett, M. (2006). Modeling the current distribution during transcranial direct current stimulation. *Clinical Neurophysiology*, *117*(7), 1623–1629. https://doi.org/10.1016/j.clinph.2006.04.009

Monte-Silva, K., Kuo, M.-F., Hessenthaler, S., Fresnoza, S., Liebetanz, D., Paulus, W., & Nitsche, M. A. (2013). Induction of Late LTP-Like Plasticity in the Human Motor

Cortex by Repeated Non-Invasive Brain Stimulation. *Brain Stimulation: Basic, Translational, and Clinical Research in Neuromodulation*, *6*(3), 424–432. https://doi.org/10.1016/j.brs.2012.04.011

Mooney, R. A., Cirillo, J., & Byblow, W. D. (2017). GABA and primary motor cortex inhibition in young and older adults: A multimodal reliability study. *Journal of Neurophysiology*, *118*(1), 425–433. https://doi.org/10.1152/jn.00199.2017

Mosayebi-Samani, M., Jamil, A., Salvador, R., Ruffini, G., Haueisen, J., & Nitsche, M. A. (2021). The impact of individual electrical fields and anatomical factors on the neurophysiological outcomes of tDCS: A TMS-MEP and MRI study. *Brain Stimulation*, *14*(2), 316–326. https://doi.org/10.1016/j.brs.2021.01.016

Moustafa, R. R., & Baron, J.-C. (2008). Pathophysiology of ischaemic stroke: Insights from imaging, and implications for therapy and drug discovery. *British Journal of Pharmacology*, *153*(Suppl 1), S44–S54. https://doi.org/10.1038/sj.bjp.0707530

Muellbacher, W., Ziemann, U., Boroojerdi, B., & Hallett, M. (2000). Effects of low-frequency transcranial magnetic stimulation on motor excitability and basic motor behavior. *Clinical Neurophysiology*, *111*(6), 1002–1007. https://doi.org/10.1016/S1388-2457(00)00284-4

Murata, Y., Higo, N., Oishi, T., Yamashita, A., Matsuda, K., Hayashi, M., & Yamane, S. (2008). Effects of Motor Training on the Recovery of Manual Dexterity After Primary Motor Cortex Lesion in Macaque Monkeys. *Journal of Neurophysiology*, *99*(2), 773–786. https://doi.org/10.1152/jn.01001.2007

Murphy, T. H., & Corbett, D. (2009). Plasticity during stroke recovery: From synapse to behaviour. *Nature Reviews Neuroscience*, *10*(12), 861–872. https://doi.org/10.1038/nrn2735

Nakagawa, S., & Schielzeth, H. (2013). A general and simple method for obtaining R^2 from generalized linear mixed-effects models. *Methods in Ecology and Evolution*, *4*(2), 133–142. https://doi.org/10.1111/j.2041-210x.2012.00261.x

Nandi, T., Puonti, O., Clarke, W. T., Nettekoven, C., Barron, H. C., Kolasinski, J., Hanayik, T., Hinson, E. L., Berrington, A., Bachtiar, V., Johnstone, A., Winkler, A. M., Thielscher, A., Johansen-Berg, H., & Stagg, C. J. (2022). TDCS induced GABA change is associated with the simulated electric field in M1, an effect mediated by grey matter volume in the MRS voxel. *Brain Stimulation*, *15*(5), 1153–1162. https://doi.org/10.1016/j.brs.2022.07.049

Ng, K., Gibson, E. M., Hubbard, R., Yang, J., Caffo, B., O'Brien, R., Krakauer, J. W., & Zeiler, S. R. (2015). Fluoxetine maintains a state of heightened responsiveness to motor training early after stroke in a mouse model. *Stroke; a Journal of Cerebral Circulation*, *46*(10), 2951–2960. https://doi.org/10.1161/STROKEAHA.115.010471

Nikolin, S., Loo, C. K., Bai, S., Dokos, S., & Martin, D. M. (2015). Focalised stimulation using high definition transcranial direct current stimulation (HD-tDCS) to investigate declarative verbal learning and memory functioning. *NeuroImage*, *117*, 11–19. https://doi.org/10.1016/j.neuroimage.2015.05.019

Nishimura, Y., Onoe, H., Morichika, Y., Perfiliev, S., Tsukada, H., & Isa, T. (2007). Time-Dependent Central Compensatory Mechanisms of Finger Dexterity After Spinal Cord Injury. *Science*, *318*(5853), 1150–1155. https://doi.org/10.1126/science.1147243

NITRC: MRIcron: Tool/Resource Info. (n.d.). Retrieved 24 February 2021, from https://www.nitrc.org/projects/mricron

Nitsche, M. A., Fricke, K., Henschke, U., Schlitterlau, A., Liebetanz, D., Lang, N., Henning, S., Tergau, F., & Paulus, W. (2003). Pharmacological Modulation of Cortical Excitability Shifts Induced by Transcranial Direct Current Stimulation in Humans. *The Journal of Physiology*, *553*(1), 293–301. https://doi.org/10.1113/jphysiol.2003.049916

Nitsche, M. A., & Paulus, W. (2000). Excitability changes induced in the human motor cortex by weak transcranial direct current stimulation. *The Journal of Physiology*, *527*(3), 633–639. https://doi.org/10.1111/j.1469-7793.2000.t01-1-00633.x

Nitsche, M. A., & Paulus, W. (2011). Transcranial direct current stimulation – update 2011. *Restorative Neurology and Neuroscience*, *29*(6), 463–492. https://doi.org/10.3233/RNN-2011-0618

Nitsche, M. A., Seeber, A., Frommann, K., Klein, C. C., Rochford, C., Nitsche, M. S., Fricke, K., Liebetanz, D., Lang, N., Antal, A., Paulus, W., & Tergau, F. (2005). Modulating parameters of excitability during and after transcranial direct current stimulation of the human motor cortex. *The Journal of Physiology*, *568*(Pt 1), 291–303. https://doi.org/10.1113/jphysiol.2005.092429

Notturno, F., Pace, M., Zappasodi, F., Cam, E., Bassetti, C. L., & Uncini, A. (2014). Neuroprotective effect of cathodal transcranial direct current stimulation in a rat stroke model. *Journal of the Neurological Sciences*, *342*(1–2), 146–151. https://doi.org/10.1016/j.jns.2014.05.017

Nouri, S., & Cramer, S. C. (2011). Anatomy and physiology predict response to motor cortex stimulation after stroke. *Neurology*, *77*(11), 1076–1083. https://doi.org/10.1212/WNL.0b013e31822e1482

Nudo, R. J., & Milliken, G. W. (1996). *Reorganization of movement representations in primary motor cortex following focal ischemic infarcts in adult squirrel monkeys*. https://doi.org/10.1152/jn.1996.75.5.2144

Ogden, R., & Franz, S. I. (1917). On cerebral motor control: The recovery from experimentally produced hemiplegia. *Psychobiology*, *1*(1), 33–49. https://doi.org/10.1037/h0074814

Ohashi, H., Gribble, P. L., & Ostry, D. J. (2019). Somatosensory cortical excitability changes precede those in motor cortex during human motor learning. *Journal of Neurophysiology*, *122*(4), 1397–1405. https://doi.org/10.1152/jn.00383.2019

Omura, T., Omura, K., Tedeschi, A., Riva, P., Painter, M. W., Rojas, L., Martin, J., Lisi, V., Huebner, E. A., Latremoliere, A., Yin, Y., Barrett, L. B., Singh, B., Lee, S., Crisman, T., Gao, F., Li, S., Kapur, K., Geschwind, D. H., … Woolf, C. J. (2016). Robust Axonal Regeneration Occurs in the Injured CAST/Ei Mouse CNS. *Neuron*, *90*(3), 662. https://doi.org/10.1016/j.neuron.2016.04.025

Opitz, A., Falchier, A., Yan, C.-G., Yeagle, E. M., Linn, G. S., Megevand, P., Thielscher, A., Deborah A., R., Milham, M. P., Mehta, A. D., & Schroeder, C. E. (2016). Spatiotemporal structure of intracranial electric fields induced by transcranial electric stimulation in humans and nonhuman primates. *Scientific Reports*, *6*(1). https://doi.org/10.1038/srep31236

Opitz, A., Paulus, W., Will, S., Antunes, A., & Thielscher, A. (2015). Determinants of the electric field during transcranial direct current stimulation. *NeuroImage*, *109*, 140–150. https://doi.org/10.1016/j.neuroimage.2015.01.033

Orfila, J. E., Grewal, H., Dietz, R. M., Strnad, F., Shimizu, T., Moreno, M., Schroeder, C., Yonchek, J., Rodgers, K. M., Dingman, A., Bernard, T. J., Quillinan, N., Macklin, W. B., Traystman, R. J., & Herson, P. S. (2019). Delayed inhibition of tonic inhibition enhances functional recovery following experimental ischemic stroke. *Journal of Cerebral Blood Flow & Metabolism*, *39*(6), 1005–1014. https://doi.org/10.1177/0271678X17750761

Orrù, G., Conversano, C., Hitchcott, P. K., & Gemignani, A. (2020). Motor stroke recovery after tDCS: A systematic review. *Reviews in the Neurosciences*, *31*(2), 201–218. https://doi.org/10.1515/revneuro-2019-0047

O'Shea, J., Boudrias, M.-H., Stagg, C. J., Bachtiar, V., Kischka, U., Blicher, J. U., & Johansen-Berg, H. (2014). Predicting behavioural response to TDCS in chronic motor stroke. *NeuroImage*, *85 Pt 3*, 924–933. https://doi.org/10.1016/j.neuroimage.2013.05.096

Overman, J. J., Clarkson, A. N., Wanner, I. B., Overman, W. T., Eckstein, I., Maguire, J. L., Dinov, I. D., Toga, A. W., & Carmichael, S. T. (2012). A role for ephrin-A5 in axonal sprouting, recovery, and activity-dependent plasticity after stroke. *Proceedings of the National Academy of Sciences of the United States of America*, *109*(33), E2230–E2239. https://doi.org/10.1073/pnas.1204386109

Patil, I. (2021). Visualizations with statistical details: The 'ggstatsplot' approach. *Journal of Open Source Software*, *6*(61), 3167. https://doi.org/10.21105/joss.03167

Paulus, W., & Rothwell, J. C. (2016). Membrane resistance and shunting inhibition: Where biophysics meets state-dependent human neurophysiology. *The Journal of Physiology*, *594*(10), 2719–2728. https://doi.org/10.1113/JP271452

Pavlova, E. L., Semenov, R. V., & Guekht, A. B. (2020). Effect of tDCS on Fine Motor Control of Patients in Subacute and Chronic Post-Stroke Stages. *Journal of Motor Behavior*, *52*(4), 383–395. https://doi.org/10.1080/00222895.2019.1639608

Pellegrini, M., Zoghi, M., & Jaberzadeh, S. (2021). Can genetic polymorphisms predict response variability to anodal transcranial direct current stimulation of the primary motor cortex? *The European Journal of Neuroscience*, *53*(5), 1569–1591. https://doi.org/10.1111/ejn.15002

Peruzzotti-Jametti, L., Cambiaghi, M., Bacigaluppi, M., Gallizioli, M., Gaude, E., Mari, S., Sandrone, S., Cursi, M., Teneud, L., Comi, G., Musco, G., Martino, G., & Leocani, L. (2013). Safety and Efficacy of Transcranial Direct Current Stimulation in Acute

Experimental Ischemic Stroke. *Stroke*, *44*(11), 3166–3174. https://doi.org/10.1161/STROKEAHA.113.001687

Piastra, C., van der Cruijsen, Joris, Piai, V., Jeukens, F. E. M., Manoochehri, M., Schouten, A. C., Selles, R. W., & Oostendorp, T. (2021). ASH: An Automatic pipeline to generate realistic and individualized chronic Stroke volume conduction Head models. *Journal of Neural Engineering*, *18*(4), 044001. https://doi.org/10.1088/1741-2552/abf00b

Pilloni, G., Vogel-Eyny, A., Lustberg, M., Best, P., Malik, M., Walton-Masters, L., George, A., Mirza, I., Zhovtis, L., Datta, A., Bikson, M., Krupp, L., & Charvet, L. (2022). Tolerability and feasibility of at-home remotely supervised transcranial direct current stimulation (RS-tDCS): Single-center evidence from 6,779 sessions. *Brain Stimulation: Basic, Translational, and Clinical Research in Neuromodulation*, *15*(3), 707–716. https://doi.org/10.1016/j.brs.2022.04.014

Pitcher, J. B., Ogston, K. M., & Miles, T. S. (2003). Age and sex differences in human motor cortex input–output characteristics. *The Journal of Physiology*, *546*(2), 605–613. https://doi.org/10.1113/jphysiol.2002.029454

Podda, M. V., Cocco, S., Mastrodonato, A., Fusco, S., Leone, L., Barbati, S. A., Colussi, C., Ripoli, C., & Grassi, C. (2016). Anodal transcranial direct current stimulation boosts synaptic plasticity and memory in mice via epigenetic regulation of Bdnf expression. *Scientific Reports*, *6*(1), Article 1. https://doi.org/10.1038/srep22180

Polanía, R., Nitsche, M. A., & Paulus, W. (2010). Modulating functional connectivity patterns and topological functional organization of the human brain with transcranial direct current stimulation. *Human Brain Mapping*, *32*(8), 1236–1249. https://doi.org/10.1002/hbm.21104

Polanía, R., Nitsche, M. A., & Ruff, C. C. (2018). Studying and modifying brain function with non-invasive brain stimulation. *Nature Neuroscience*, *21*(2), Article 2. https://doi.org/10.1038/s41593-017-0054-4

Potter-Baker, K. A., Lin, Y.-L., Machado, A. G., Conforto, A. B., Cunningham, D. A., Sankarasubramanian, V., Sakaie, K., & Plow, E. B. (2018). Variability of motor evoked potentials in stroke explained by corticospinal pathway integrity. *Brain Stimulation*, *11*(4), 929–931. https://doi.org/10.1016/j.brs.2018.03.004

Potter-Baker, K. A., Varnerin, N. M., Cunningham, D. A., Roelle, S. M., Sankarasubramanian, V., Bonnett, C. E., Machado, A. G., Conforto, A. B., Sakaie, K., & Plow, E. B. (2016). Influence of Corticospinal Tracts from Higher Order Motor Cortices on Recruitment Curve Properties in Stroke. *Frontiers in Neuroscience*, *10*. https://doi.org/10.3389/fnins.2016.00079

Prabhakaran, S., Zarahn, E., Riley, C., Speizer, A., Chong, J. Y., Lazar, R. M., Marshall, R. S., & Krakauer, J. W. (2008). Inter-individual Variability in the Capacity for Motor Recovery After Ischemic Stroke. *Neurorehabilitation and Neural Repair*, *22*(1), 64–71. https://doi.org/10.1177/1545968307305302

Priori, A., Berardelli, A., Rona, S., Accornero, N., & Manfredi, M. (1998). Polarization of the human motor cortex through the scalp. *NeuroReport*, *9*(10), 2257–2260.

Pruvost-Robieux, E., Calvet, D., Ben Hassen, W., Turc, G., Marchi, A., Mélé, N., Seners, P., Oppenheim, C., Baron, J.-C., Mas, J.-L., & Gavaret, M. (2018). Design and Methodology of a Pilot Randomized Controlled Trial of Transcranial Direct Current Stimulation in Acute Middle Cerebral Artery Stroke (STICA). *Frontiers in Neurology*, *9*, 816. https://doi.org/10.3389/fneur.2018.00816

Purpura, D. P., & McMurtry, J. G. (1965). INTRACELLULAR ACTIVITIES AND EVOKED POTENTIAL CHANGES DURING POLARIZATION OF MOTOR CORTEX. *Journal of Neurophysiology*. https://doi.org/10.1152/jn.1965.28.1.166

Qü, M., Buchkremer-Ratzmann, I., Schiene, K., Schroeter, M., Witte, O. W., & Zilles, K. (1998). Bihemispheric reduction of GABAA receptor binding following focal cortical photothrombotic lesions in the rat brain. *Brain Research*, *813*(2), 374–380. https://doi.org/10.1016/S0006-8993(98)01063-4

Quinlan, E. B., Dodakian, L., See, J., McKenzie, A., Le, V., Wojnowicz, M., Shahbaba, B., & Cramer, S. C. (2015). Neural function, injury, and stroke subtype predict treatment gains after stroke. *Annals of Neurology*, *77*(1), 132–145. https://doi.org/10.1002/ana.24309

Quinn, T. J., Paolucci, S., Sunnerhagen, K. S., Sivenius, J., Walker, M. F., Toni, D., Lees, K. R., European Stroke Organisation (ESO) Executive Committee, & ESO Writing Committee. (2009). Evidence-based stroke r-ehabilitation: An expanded guidance document from the european stroke organisation (ESO) guidelines for management of ischaemic stroke and transient ischaemic attack 2008. *Journal of Rehabilitation Medicine*, *41*(2), 99–111. https://doi.org/10.2340/16501977-0301

R Core Team. (2017). *R: A language and environment for statistical computing.* R Foundation for Statistical Computing. https://www.r-project.org/

R Core Team. (2021). *R: A Language and Environment for Statistical Computing*. R Foundation for Statistical Computing. https://www.R-project.org/

Radman, T., Ramos, R. L., Brumberg, J. C., & Bikson, M. (2009a). Role of cortical cell type and morphology in subthreshold and suprathreshold uniform electric field stimulation in vitro. *Brain Stimulation*, *2*(4), 215-228.e3. https://doi.org/10.1016/j.brs.2009.03.007

Radman, T., Ramos, R. L., Brumberg, J. C., & Bikson, M. (2009b). Role of Cortical Cell Type and Morphology in Sub- and Suprathreshold Uniform Electric Field Stimulation. *Brain Stimulation*, *2*(4), 215–228. https://doi.org/10.1016/j.brs.2009.03.007

Radman, T., Su, Y., An, J. H., Parra, L. C., & Bikson, M. (2007). Spike Timing Amplifies the Effect of Electric Fields on Neurons: Implications for Endogenous Field Effects. *Journal of Neuroscience*, *27*(11), 3030–3036. https://doi.org/10.1523/JNEUROSCI.0095-07.2007

Rahman, A., Lafon, B., & Bikson, M. (2015). Chapter 2—Multilevel computational models for predicting the cellular effects of noninvasive brain stimulation. In S. Bestmann (Ed.), *Progress in Brain Research* (Vol. 222, pp. 25–40). Elsevier. https://doi.org/10.1016/bs.pbr.2015.09.003

Rahman, A., Reato, D., Arlotti, M., Gasca, F., Datta, A., Parra, L. C., & Bikson, M. (2013a). Cellular effects of acute direct current stimulation: Somatic and synaptic terminal effects. *The Journal of Physiology*, *591*(10), 2563–2578. https://doi.org/10.1113/jphysiol.2012.247171

Rahman, A., Reato, D., Arlotti, M., Gasca, F., Datta, A., Parra, L. C., & Bikson, M. (2013b). Cellular effects of acute direct current stimulation: Somatic and synaptic terminal effects. *The Journal of Physiology*, *591*(10), 2563–2578. https://doi.org/10.1113/jphysiol.2012.247171

Rampersad, S. M., Janssen, A. M., Lucka, F., Aydin, Ü., Lanfer, B., Lew, S., Wolters, C. H., Stegeman, D. F., & Oostendorp, T. F. (2014). Simulating Transcranial Direct Current Stimulation With a Detailed Anisotropic Human Head Model. *IEEE Transactions on Neural Systems and Rehabilitation Engineering*, *22*(3), 441–452. https://doi.org/10.1109/TNSRE.2014.2308997

Ranieri, F., Podda, M. V., Riccardi, E., Frisullo, G., Dileone, M., Profice, P., Pilato, F., Di Lazzaro, V., & Grassi, C. (2012). Modulation of LTP at rat hippocampal CA3-CA1 synapses by direct current stimulation. *Journal of Neurophysiology*, *107*(7), 1868–1880. https://doi.org/10.1152/jn.00319.2011

Ravazzani, P., Ruohonen, J., Grandori, F., & Tognola, G. (1996). Magnetic stimulation of the nervous system: Induced electric field in unbounded, semi-infinite, spherical, and cylindrical media. *Annals of Biomedical Engineering*, *24*(5), 606–616. https://doi.org/10.1007/BF02684229

Rawji, V., Ciocca, M., Zacharia, A., Soares, D., Truong, D., Bikson, M., Rothwell, J., & Bestmann, S. (2018). TDCS changes in motor excitability are specific to orientation of current flow. *Brain Stimulation*, *11*(2), 289–298. https://doi.org/10.1016/j.brs.2017.11.001

Reato, D., Rahman, A., Bikson, M., & Parra, L. C. (2010). Low-Intensity Electrical Stimulation Affects Network Dynamics by Modulating Population Rate and Spike Timing. *The Journal of Neuroscience*, *30*(45), 15067–15079. https://doi.org/10.1523/JNEUROSCI.2059-10.2010

Reato, D., Rahman, A., Bikson, M., & Parra, L. C. (2013). Effects of weak transcranial alternating current stimulation on brain activity—A review of known mechanisms from animal studies. *Frontiers in Human Neuroscience*, *7*. https://doi.org/10.3389/fnhum.2013.00687

Reato, D., Salvador, R., Bikson, M., Opitz, A., Dmochowski, J., & Miranda, P. C. (2019). Principles of Transcranial Direct Current Stimulation (tDCS): Introduction to the Biophysics of tDCS. In H. Knotkova, M. A. Nitsche, M. Bikson, & A. J. Woods (Eds.), *Practical Guide to Transcranial Direct Current Stimulation: Principles, Procedures and Applications* (pp. 45–80). Springer International Publishing. https://doi.org/10.1007/978-3-319-95948-1_2

Reckow, J., Rahman-Filipiak, A., Garcia, S., Schlaefflin, S., Calhoun, O., DaSilva, A. F., Bikson, M., & Hampstead, B. M. (2018). Tolerability and blinding of 4x1 High-Definition

transcranial direct current stimulation (HD-tDCS) at two and three milliamps. *Brain Stimulation*. https://doi.org/10.1016/j.brs.2018.04.022

Rekik, I., Allassonnière, S., Carpenter, T. K., & Wardlaw, J. M. (2012). Medical image analysis methods in MR/CT-imaged acute-subacute ischemic stroke lesion: Segmentation, prediction and insights into dynamic evolution simulation models. A critical appraisal. *NeuroImage : Clinical*, *1*(1), 164–178. https://doi.org/10.1016/j.nicl.2012.10.003

Ridding, M. C., Brouwer, B., Miles, T. S., Pitcher, J. B., & Thompson, P. D. (2000). Changes in muscle responses to stimulation of the motor cortex induced by peripheral nerve stimulation in human subjects. *Experimental Brain Research*, *131*(1), 135–143. https://doi.org/10.1007/s002219900269

Ridding, M. C., & Rothwell, J. C. (1997). Stimulus/response curves as a method of measuring motor cortical excitability in man. *Electroencephalography and Clinical Neurophysiology/Electromyography and Motor Control*, *105*(5), 340–344. https://doi.org/10.1016/S0924-980X(97)00041-6

Ridding, M. C., & Taylor, J. L. (2001). Mechanisms of motor-evoked potential facilitation following prolonged dual peripheral and central stimulation in humans. *The Journal of Physiology*, *537*(Pt 2), 623–631. https://doi.org/10.1111/j.1469-7793.2001.00623.x

Rorden, C., & Brett, M. (2000). Stereotaxic display of brain lesions. *Behavioural Neurology*, *12*(4), 191–200. https://doi.org/10.1155/2000/421719

Rossi, S., Antal, A., Bestmann, S., Bikson, M., Brewer, C., Brockmöller, J., Carpenter, L. L., Cincotta, M., Chen, R., Daskalakis, J. D., Di Lazzaro, V., Fox, M. D., George, M. S., Gilbert, D., Kimiskidis, V. K., Koch, G., Ilmoniemi, R. J., Pascal Lefaucheur, J., Leocani, L., … Hallett, M. (2021). Safety and recommendations for TMS use in healthy subjects and patient populations, with updates on training, ethical and regulatory issues: Expert Guidelines. *Clinical Neurophysiology*, *132*(1), 269–306. https://doi.org/10.1016/j.clinph.2020.10.003

Rossini, P. M., Barker, A. T., Berardelli, A., Caramia, M. D., Caruso, G., Cracco, R. Q., Dimitrijević, M. R., Hallett, M., Katayama, Y., Lücking, C. H., Maertens de Noordhout, A. L., Marsden, C. D., Murray, N. M. F., Rothwell, J. C., Swash, M., & Tomberg, C. (1994). Non-invasive electrical and magnetic stimulation of the brain, spinal cord and roots: Basic principles and procedures for routine clinical application. Report of an IFCN committee. *Electroencephalography and Clinical Neurophysiology*, *91*(2), 79–92. https://doi.org/10.1016/0013-4694(94)90029-9

Rossini, P. M., Burke, D., Chen, R., Cohen, L. G., Daskalakis, Z., Di Iorio, R., Di Lazzaro, V., Ferreri, F., Fitzgerald, P. B., George, M. S., Hallett, M., Lefaucheur, J. P., Langguth, B., Matsumoto, H., Miniussi, C., Nitsche, M. A., Pascual-Leone, A., Paulus, W., Rossi, S., … Ziemann, U. (2015). Non-invasive electrical and magnetic stimulation of the brain, spinal cord, roots and peripheral nerves: Basic principles and procedures for routine clinical and research application. An updated report from an I.F.C.N. Committee.

Clinical Neurophysiology, *126*(6), 1071–1107. https://doi.org/10.1016/j.clinph.2015.02.001

Rosso, C., & Lamy, J.-C. (2018). Does Resting Motor Threshold Predict Motor Hand Recovery After Stroke? *Frontiers in Neurology*, *9*, 1020. https://doi.org/10.3389/fneur.2018.01020

Rosso, C., & Samson, Y. (2014). The ischemic penumbra: The location rather than the volume of recovery determines outcome. *Current Opinion in Neurology*, *27*(1), 35–41. https://doi.org/10.1097/WCO.0000000000000047

Roy, D. S., Arons, A., Mitchell, T. I., Pignatelli, M., Ryan, T. J., & Tonegawa, S. (2016). Memory retrieval by activating engram cells in mouse models of early Alzheimer's disease. *Nature*, *531*(7595), 508–512. https://doi.org/10.1038/nature17172

Roy, D. S., Muralidhar, S., Smith, L. M., & Tonegawa, S. (2017). Silent memory engrams as the basis for retrograde amnesia. *Proceedings of the National Academy of Sciences of the United States of America*, *114*(46), E9972–E9979. https://doi.org/10.1073/pnas.1714248114

Rubio Ballester, B., Duff, A., Maier, M., Cameirao, M., Bermudez, S., Duarte, E., Cuxart, A., Rodriguez, S., & Verschure, P. F. M. J. (2018). *Revealing an extended critical window of recovery post-stroke*. https://doi.org/10.1101/458745

Ruffini, G., Fox, M. D., Ripolles, O., Miranda, P. C., & Pascual-Leone, A. (2014). Optimization of multifocal transcranial current stimulation for weighted cortical pattern targeting from realistic modeling of electric fields. *NeuroImage*, *89*, 216–225. https://doi.org/10.1016/j.neuroimage.2013.12.002

Ruohonen, J., & Karhu, J. (2010). Navigated transcranial magnetic stimulation. *Neurophysiologie Clinique/Clinical Neurophysiology*, *40*(1), 7–17. https://doi.org/10.1016/j.neucli.2010.01.006

Rush, S., & Driscoll, D. A. (1968). Current Distribution in the Brain From Surface Electrodes: *Anesthesia & Analgesia*, *47*(6), 717???723. https://doi.org/10.1213/00000539-196811000-00016

Rusu, C. V., Murakami, M., Ziemann, U., & Triesch, J. (2014). A Model of TMS-induced I-waves in Motor Cortex. *Brain Stimulation*, *7*(3), 401–414. https://doi.org/10.1016/j.brs.2014.02.009

Ryan, J. L., Eng, E., Fehlings, D. L., Wright, F. V., Levac, D. E., & Beal, D. S. (2023). Motor Evoked Potential Amplitude in Motor Behavior-based Transcranial Direct Current Stimulation Studies: A Systematic Review. *Journal of Motor Behavior*, *55*(3), 313–329. https://doi.org/10.1080/00222895.2023.2184320

Sack, A. T., Cohen Kadosh, R., Schuhmann, T., Moerel, M., Walsh, V., & Goebel, R. (2008). Optimizing Functional Accuracy of TMS in Cognitive Studies: A Comparison of Methods. *Journal of Cognitive Neuroscience*, *21*(2), 207–221. https://doi.org/10.1162/jocn.2009.21126

Salvador, R., Wenger, C., Nitsche, M. A., & Miranda, P. C. (2015). How electrode montage affects transcranial direct current stimulation of the human motor cortex. *2015 37th Annual International Conference of the IEEE Engineering in Medicine and Biology Society (EMBC)*, 6924–6927. https://doi.org/10.1109/EMBC.2015.7319985

Sampaio-Baptista, C., Filippini, N., Stagg, C. J., Near, J., Scholz, J., & Johansen-Berg, H. (2015). Changes in functional connectivity and GABA levels with long-term motor learning. *Neuroimage*, *106*, 15–20. https://doi.org/10.1016/j.neuroimage.2014.11.032

Sanchez-Bezanilla, S., Hood, R. J., Collins-Praino, L. E., Turner, R. J., Walker, F. R., Nilsson, M., & Ong, L. K. (2021). More than motor impairment: A spatiotemporal analysis of cognitive impairment and associated neuropathological changes following cortical photothrombotic stroke. *Journal of Cerebral Blood Flow & Metabolism*, *41*(9), 2439–2455. https://doi.org/10.1177/0271678X211005877

Sanchez-Todo, R., Bastos, A. M., Sola, E. L., Mercadal, B., Santarnecchi, E., Miller, E. K., Deco, G., & Ruffini, G. (2022). *A physical neural mass model framework for the analysis of oscillatory generators from laminar electrophysiological recordings* (p. 2022.07.19.500618). bioRxiv. https://doi.org/10.1101/2022.07.19.500618

Sargin, D., Mercaldo, V., Yiu, A. P., Higgs, G., Han, J.-H., Frankland, P. W., & Josselyn, S. A. (2013). CREB regulates spine density of lateral amygdala neurons: Implications for memory allocation. *Frontiers in Behavioral Neuroscience*, *7*, 209. https://doi.org/10.3389/fnbeh.2013.00209

Saturnino, G. B., Antunes, A., & Thielscher, A. (2015). On the importance of electrode parameters for shaping electric field patterns generated by tDCS. *NeuroImage*, *120*, 25–35. https://doi.org/10.1016/j.neuroimage.2015.06.067

Saturnino, G. B., Puonti, O., Nielsen, J. D., Antonenko, D., Madsen, K. H., & Thielscher, A. (2019). SimNIBS 2.1: A Comprehensive Pipeline for Individualized Electric Field Modelling for Transcranial Brain Stimulation. In S. Makarov, M. Horner, & G. Noetscher (Eds.), *Brain and Human Body Modeling: Computational Human Modeling at EMBC 2018* (pp. 3–25). Springer International Publishing. https://doi.org/10.1007/978-3-030-21293-3_1

Saturnino, G. B., Siebner, H. R., Thielscher, A., & Madsen, K. H. (2019). Accessibility of cortical regions to focal TES: Dependence on spatial position, safety, and practical constraints. *NeuroImage*, *203*, 116183. https://doi.org/10.1016/j.neuroimage.2019.116183

Schepers, V. P. M., Ketelaar, M., van de Port, I. G. L., Visser-Meily, J. M. A., & Lindeman, E. (2007). Comparing contents of functional outcome measures in stroke rehabilitation using the International Classification of Functioning, Disability and Health. *Disability and Rehabilitation*, *29*(3), 221–230. https://doi.org/10.1080/09638280600756257

Schiene, K., Bruehl, C., Zilles, K., Qu, M., Hagemann, G., Kraemer, M., & Witte, O. W. (1996a). Neuronal Hyperexcitability and Reduction of GABAA-Receptor Expression in the Surround of Cerebral Photothrombosis. *Journal of Cerebral Blood Flow & Metabolism*, *16*(5), 906–914. https://doi.org/10.1097/00004647-199609000-00014

Schiene, K., Bruehl, C., Zilles, K., Qu, M., Hagemann, G., Kraemer, M., & Witte, O. W. (1996b). Neuronal Hyperexcitability and Reduction of GABAA-Receptor Expression in the Surround of Cerebral Photothrombosis. *Journal of Cerebral Blood Flow & Metabolism*, *16*(5), 906–914. https://doi.org/10.1097/00004647-199609000-00014

Schmidt, S. L., Iyengar, A. K., Foulser, A. A., Boyle, M. R., & Fröhlich, F. (2014). Endogenous Cortical Oscillations Constrain Neuromodulation by Weak Electric Fields. *Brain Stimulation*, *7*(6), 878–889. https://doi.org/10.1016/j.brs.2014.07.033

Schneider, E. J., Lannin, N. A., Ada, L., & Schmidt, J. (2016). Increasing the amount of usual rehabilitation improves activity after stroke: A systematic review. *Journal of Physiotherapy*, *62*(4), 182–187. https://doi.org/10.1016/j.jphys.2016.08.006

Schwarz, G. (1978). Estimating the Dimension of a Model. *The Annals of Statistics*, *6*(2), 461–464. https://doi.org/10.1214/aos/1176344136

Scrivener, K., Sherrington, C., & Schurr, K. (2012). Exercise dose and mobility outcome in a comprehensive stroke unit: Description and prediction from a prospective cohort study. *Journal of Rehabilitation Medicine*, *44*(10), 824–829. https://doi.org/10.2340/16501977-1028

Selles, R. W., Andrinopoulou, E.-R., Nijland, R. H., van der Vliet, R., Slaman, J., van Wegen, E. E., Rizopoulos, D., Ribbers, G. M., Meskers, C. G., & Kwakkel, G. (2021). Computerised patient-specific prediction of the recovery profile of upper limb capacity within stroke services: The next step. *Journal of Neurology, Neurosurgery & Psychiatry*, *92*(6), 574–581. https://doi.org/10.1136/jnnp-2020-324637

Seo, H., & Jun, S. C. (2019). Relation between the electric field and activation of cortical neurons in transcranial electrical stimulation. *Brain Stimulation: Basic, Translational, and Clinical Research in Neuromodulation*, *12*(2), 275–289. https://doi.org/10.1016/j.brs.2018.11.004

Sharp, F. R., Lu, A., Tang, Y., & Millhorn, D. E. (2000). Multiple Molecular Penumbras after Focal Cerebral Ischemia. *Journal of Cerebral Blood Flow & Metabolism*, *20*(7), 1011–1032. https://doi.org/10.1097/00004647-200007000-00001

Shen, J. (2022). *Tools for NIfTI and ANALYZE image* (MATLAB Central File Exchange). https://www.mathworks.com/matlabcentral/fileexchange/8797-tools-for-nifti-and-analyze-image

Shen, Q., Hu, M., Feng, W., Li, K.-P., & Wang, W. (2022). Narrative Review of Noninvasive Brain Stimulation in Stroke Rehabilitation. *Medical Science Monitor*, *28*. https://doi.org/10.12659/MSM.938298

Shen, Z., Xiang, M., Chen, C., Ding, F., Wang, Y., Shang, C., Xin, L., Zhang, Y., & Cui, X. (2022). Glutamate excitotoxicity: Potential therapeutic target for ischemic stroke. *Biomedicine & Pharmacotherapy*, *151*, 113125. https://doi.org/10.1016/j.biopha.2022.113125

Siebner, H. R. (2020). Does TMS of the precentral motor hand knob primarily stimulate the dorsal premotor cortex or the primary motor hand area? *Brain Stimulation*, *13*(2), 517–518. https://doi.org/10.1016/j.brs.2019.12.015

Siebner, H. R., Funke, K., Aberra, A. S., Antal, A., Bestmann, S., Chen, R., Classen, J., Davare, M., Di Lazzaro, V., Fox, P. T., Hallett, M., Karabanov, A. N., Kesselheim, J., Beck, M. M., Koch, G., Liebetanz, D., Meunier, S., Miniussi, C., Paulus, W., … Ugawa, Y. (2022). Transcranial magnetic stimulation of the brain: What is stimulated? – A consensus and critical position paper. *Clinical Neurophysiology*, *140*, 59–97. https://doi.org/10.1016/j.clinph.2022.04.022

Siegel, J. S., Ramsey, L. E., Snyder, A. Z., Metcalf, N. V., Chacko, R. V., Weinberger, K., Baldassarre, A., Hacker, C. D., Shulman, G. L., & Corbetta, M. (2016). Disruptions of network connectivity predict impairment in multiple behavioral domains after stroke. *Proceedings of the National Academy of Sciences*, *113*(30), E4367–E4376. https://doi.org/10.1073/pnas.1521083113

Skilbeck, C. E., Wade, D. T., Hewer, R. L., & Wood, V. A. (1983). Recovery after stroke. *Journal of Neurology, Neurosurgery, and Psychiatry*, *46*(1), 5–8.

Skriver, E. B., Olsen, T. S., & McNair, P. (1990). Mass effect and atrophy after stroke. *Acta Radiologica (Stockholm, Sweden: 1987)*, *31*(5), 431–438.

Speekenbrink, M. (2022). *Statistics: Data analysis and modelling*. https://mspeekenbrink.github.io/sdam-book/index.html

Sperber, C., & Karnath, H.-O. (2016). Topography of acute stroke in a sample of 439 right brain damaged patients. *NeuroImage: Clinical*, *10*, 124–128. https://doi.org/10.1016/j.nicl.2015.11.012

Stagg, C. J., Antal, A., & Nitsche, M. A. (2018). Physiology of Transcranial Direct Current Stimulation: *The Journal of ECT*, *34*(3), 144–152. https://doi.org/10.1097/YCT.0000000000000510

Stagg, C. J., Bachtiar, V., & Johansen-Berg, H. (2011). The Role of GABA in Human Motor Learning. *Current Biology*, *21*(6), 480–484. https://doi.org/10.1016/j.cub.2011.01.069

Stewart, C., McCluskey, A., Ada, L., & Kuys, S. (2017). Structure and feasibility of extra practice during stroke rehabilitation: A systematic scoping review. *Australian Occupational Therapy Journal*, *64*(3), 204–217. https://doi.org/10.1111/1440-1630.12351

Stinear, C. M., Barber, P. A., Petoe, M., Anwar, S., & Byblow, W. D. (2012). The PREP algorithm predicts potential for upper limb recovery after stroke. *Brain*, *135*(8), 2527–2535. https://doi.org/10.1093/brain/aws146

Stinear, C. M., & Byblow, W. D. (2017). The Role of TMS for Predicting Motor Recovery and Outcomes After Stroke. In P. A. Lapchak & G.-Y. Yang (Eds.), *Translational Research in Stroke* (pp. 537–553). Springer. https://doi.org/10.1007/978-981-10-5804-2_25

Stinear, C. M., Petoe, M. A., & Byblow, W. D. (2015). Primary Motor Cortex Excitability During Recovery After Stroke: Implications for Neuromodulation. *Brain Stimulation*, *8*(6), 1183–1190. https://doi.org/10.1016/j.brs.2015.06.015

Suppa, A., Huang, Y.-Z., Funke, K., Ridding, M. C., Cheeran, B., Di Lazzaro, V., Ziemann, U., & Rothwell, J. C. (2016). Ten Years of Theta Burst Stimulation in Humans: Established Knowledge, Unknowns and Prospects. *Brain Stimulation*, *9*(3), 323–335. https://doi.org/10.1016/j.brs.2016.01.006

Svirskis, G., Gutman, A., & Hounsgaard, J. (1997). Detection of a Membrane Shunt by DC Field Polarization During Intracellular and Whole Cell Recording. *Journal of Neurophysiology*, *77*(2), 579–586. https://doi.org/10.1152/jn.1997.77.2.579

Swayne, O. B. C., Rothwell, J. C., Ward, N. S., & Greenwood, R. J. (2008). Stages of Motor Output Reorganization after Hemispheric Stroke Suggested by Longitudinal Studies of Cortical Physiology. *Cerebral Cortex*, *18*(8), 1909–1922. https://doi.org/10.1093/cercor/bhm218

Syeda, W., Ermine, C. M., Khilf, M. S., Wright, D., Brait, V. H., Nithianantharajah, J., Kolbe, S., Johnston, L. A., Thompson, L. H., & Brodtmann, A. (2022). Long-term structural brain changes in adult rats after mild ischaemic stroke. *Brain Communications*, *4*(4), fcac185. https://doi.org/10.1093/braincomms/fcac185

Takita, M., Izaki, Y., Jay, T. M., Kaneko, H., & Suzuki, S. S. (1999). Induction of stable long-term depression in vivo in the hippocampal-prefrontal cortex pathway. *European Journal of Neuroscience*, *11*(11), 4145–4148. Scopus. https://doi.org/10.1046/j.1460-9568.1999.00870.x

Tang, E., Mattar, M. G., Giusti, C., Lydon-Staley, D. M., Thompson-Schill, S. L., & Bassett, D. S. (2019). Effective learning is accompanied by high-dimensional and efficient representations of neural activity. *Nature Neuroscience*, *22*(6), Article 6. https://doi.org/10.1038/s41593-019-0400-9

Tennant, K. A., Taylor, S. L., White, E. R., & Brown, C. E. (2017). Optogenetic rewiring of thalamocortical circuits to restore function in the stroke injured brain. *Nature Communications*, *8*, 15879. https://doi.org/10.1038/ncomms15879

ter Braack, E. M., de Goede, A. A., & van Putten, M. J. A. M. (2019). Resting Motor Threshold, MEP and TEP Variability During Daytime. *Brain Topography*, *32*(1), 17–27. https://doi.org/10.1007/s10548-018-0662-7

Terzuolo, C. A., & Bullock, T. H. (1956). MEASUREMENT OF IMPOSED VOLTAGE GRADIENT ADEQUATE TO MODULATE NEURONAL FIRING*. *Proceedings of the National Academy of Sciences of the United States of America*, *42*(9), 687–694.

The AVERT Trial Collaboration group. (2015). Efficacy and safety of very early mobilisation within 24 h of stroke onset (AVERT): A randomised controlled trial. *The Lancet*, *386*(9988), 46–55. https://doi.org/10.1016/S0140-6736(15)60690-0

Thiel, C. M., Zilles, K., & Fink, G. R. (2004). Cerebral correlates of alerting, orienting and reorienting of visuospatial attention: An event-related fMRI study. *NeuroImage*, *21*(1), 318–328. https://doi.org/10.1016/j.neuroimage.2003.08.044

Thielscher, A., Antunes, A., & Saturnino, G. B. (2015). Field modeling for transcranial magnetic stimulation: A useful tool to understand the physiological effects of TMS?

2015 37th Annual International Conference of the IEEE Engineering in Medicine and Biology Society (EMBC), 222–225. https://doi.org/10.1109/EMBC.2015.7318340

Thielscher, A., & Kammer, T. (2002). Linking physics with physiology in TMS: A sphere field model to determine the cortical stimulation site in TMS. *NeuroImage*, *17*(3), 1117–1130. https://doi.org/10.1006/nimg.2002.1282

Todd, G., Rogasch, N. C., Flavel, S. C., & Ridding, M. C. (2009). Voluntary movement and repetitive transcranial magnetic stimulation over human motor cortex. *Journal of Applied Physiology*, *106*(5), 1593–1603. https://doi.org/10.1152/japplphysiol.91364.2008

Tonegawa, S., Liu, X., Ramirez, S., & Redondo, R. (2015). Memory Engram Cells Have Come of Age. *Neuron*, *87*(5), 918–931. https://doi.org/10.1016/j.neuron.2015.08.002

Toschi, N., Welt, T., Guerrisi, M., & Keck, M. E. (2008). A reconstruction of the conductive phenomena elicited by transcranial magnetic stimulation in heterogeneous brain tissue. *Physica Medica: European Journal of Medical Physics*, *24*(2), 80–86. https://doi.org/10.1016/j.ejmp.2008.01.005

Tremblay, S., Beaulé, V., Proulx, S., de Beaumont, L., Marjańska, M., Doyon, J., Pascual-Leone, A., Lassonde, M., & Théoret, H. (2013). Relationship between transcranial magnetic stimulation measures of intracortical inhibition and spectroscopy measures of GABA and glutamate+glutamine. *Journal of Neurophysiology*, *109*(5), 1343–1349. https://doi.org/10.1152/jn.00704.2012

Twitchell, T. E. (1951). The restoration of motor function following hemiplegia in man. *Brain*, *74*(4), 443–480. https://doi.org/10.1093/brain/74.4.443

van der Cruijsen, J., Dooren, R. F., Schouten, A. C., Oostendorp, T. F., Frens, M. A., Ribbers, G. M., van der Helm, F. C. T., Kwakkel, G., & Selles, R. W. (2022). Addressing the inconsistent electric fields of tDCS by using patient-tailored configurations in chronic stroke: Implications for treatment. *NeuroImage: Clinical*, *36*, 103178. https://doi.org/10.1016/j.nicl.2022.103178

van der Vliet, R., Selles, R. W., Andrinopoulou, E.-R., Nijland, R., Ribbers, G. M., Frens, M. A., Meskers, C., & Kwakkel, G. (2020). Predicting Upper Limb Motor Impairment Recovery after Stroke: A Mixture Model. *Annals of Neurology*, *87*(3), 383–393. https://doi.org/10.1002/ana.25679

van der Zijden, J. P., van der Toorn, A., van der Marel, K., & Dijkhuizen, R. M. (2008). Longitudinal in vivo MRI of alterations in perilesional tissue after transient ischemic stroke in rats. *Experimental Neurology*, *212*(1), 207–212. https://doi.org/10.1016/j.expneurol.2008.03.027

van Lier, A. L. H. M. W., van der Kolk, A. G., Brundel, M., Hendrikse, J., Luijten, P. R., Lagendijk, J. J. W., & van den Berg. (2012). Electrical Conductivity in Ischemic Stroke at 7.0 Tesla: A Case Study. *Paper Presented at the Proceedings of the 20th Scientific Meeting of the International Society of Magnetic Resonance in Medicine (ISMRM'12)*.

Veldema, J., Nowak, D. A., & Gharabaghi, A. (2021). Resting motor threshold in the course of hand motor recovery after stroke: A systematic review. *Journal of NeuroEngineering and Rehabilitation*, *18*, 158. https://doi.org/10.1186/s12984-021-00947-8

Vergallito, A., Feroldi, S., Pisoni, A., & Romero Lauro, L. J. (2022). Inter-Individual Variability in tDCS Effects: A Narrative Review on the Contribution of Stable, Variable, and Contextual Factors. *Brain Sciences*, *12*(5), 522. https://doi.org/10.3390/brainsci12050522

Verstraeten, S., Mark, R. E., Dieleman, J., Rijsbergen, M. van, Kort, P. de, & Sitskoorn, M. M. (2020). Motor Impairment Three Months Post Stroke Implies A Corresponding Cognitive Deficit. *Journal of Stroke and Cerebrovascular Diseases*, *29*(10). https://doi.org/10.1016/j.jstrokecerebrovasdis.2020.105119

Viana, R. T., Laurentino, G. E. C., Souza, R. J. P., Fonseca, J. B., Silva Filho, E. M., Dias, S. N., Teixeira-Salmela, L. F., & Monte-Silva, K. K. (2014). Effects of the addition of transcranial direct current stimulation to virtual reality therapy after stroke: A pilot randomized controlled trial. *NeuroRehabilitation*, *34*(3), 437–446. https://doi.org/10.3233/NRE-141065

Waddell, K. J., Birkenmeier, R. L., Moore, J. L., Hornby, T. G., & Lang, C. E. (2014). Feasibility of High-Repetition, Task-Specific Training for Individuals With Upper-Extremity Paresis. *The American Journal of Occupational Therapy*, *68*(4), 444–453. https://doi.org/10.5014/ajot.2014.011619

Wagner, T. A., Zahn, M., Grodzinsky, A. J., & Pascual-Leone, A. (2004). Three-dimensional head model Simulation of transcranial magnetic stimulation. *IEEE Transactions on Biomedical Engineering*, *51*(9), 1586–1598. https://doi.org/10.1109/TBME.2004.827925

Wagner, T., Fregni, F., Fecteau, S., Grodzinsky, A., Zahn, M., & Pascual-Leone, A. (2007). Transcranial direct current stimulation: A computer-based human model study. *NeuroImage*, *35*(3), 1113–1124. https://doi.org/10.1016/j.neuroimage.2007.01.027

Wahl, A. S., Büchler, U., Brändli, A., Brattoli, B., Musall, S., Kasper, H., Ineichen, B. V., Helmchen, F., Ommer, B., & Schwab, M. E. (2017). Optogenetically stimulating intact rat corticospinal tract post-stroke restores motor control through regionalized functional circuit formation. *Nature Communications*, *8*(1), Article 1. https://doi.org/10.1038/s41467-017-01090-6

Walford, I., Rondina, J. M., & Ward, N. (2021). Patient-specific prediction of long-term outcomes will change stroke rehabilitation for the better. *Journal of Neurology, Neurosurgery & Psychiatry*, *92*(6), 572–572. https://doi.org/10.1136/jnnp-2020-325981

Wang, B., Aberra, A. S., Grill, W. M., & Peterchev, A. V. (2018). Modified cable equation incorporating transverse polarization of neuronal membranes for accurate coupling of electric fields. *Journal of Neural Engineering*, *15*(2), 026003. https://doi.org/10.1088/1741-2552/aa8b7c

Wang, B., Xiao, S., Yu, C., Zhou, J., & Fu, W. (2021). Effects of Transcranial Direct Current Stimulation Combined With Physical Training on the Excitability of the Motor Cortex, Physical Performance, and Motor Learning: A Systematic Review. *Frontiers in Neuroscience*, *15*, 648354. https://doi.org/10.3389/fnins.2021.648354

Wang, Y., Dzyubenko, E., Sanchez-Mendoza, E. H., Sardari, M., Silva de Carvalho, T., Doeppner, T. R., Kaltwasser, B., Machado, P., Kleinschnitz, C., Bassetti, C. L., & Hermann, D. M. (2018). Postacute Delivery of GABAA α5 Antagonist Promotes Postischemic Neurological Recovery and Peri-infarct Brain Remodeling. *Stroke*, *49*(10), 2495–2503. https://doi.org/10.1161/STROKEAHA.118.021378

Wankerl, K., Weise, D., Gentner, R., Rumpf, J.-J., & Classen, J. (2010). L-type voltage-gated Ca2+ channels: A single molecular switch for long-term potentiation/long-term depression-like plasticity and activity-dependent metaplasticity in humans. *Journal of Neuroscience*, *30*(18), 6197–6204. Scopus. https://doi.org/10.1523/JNEUROSCI.4673-09.2010

Ward, N. S. (2016). Non-invasive brain stimulation for stroke recovery: Ready for the big time? *Journal of Neurology, Neurosurgery & Psychiatry*, *87*(4), 343–344. https://doi.org/10.1136/jnnp-2015-311991

Ward, N. S. (2017). Restoring brain function after stroke—Bridging the gap between animals and humans. *Nature Reviews Neurology*, *13*(4), 244–255. https://doi.org/10.1038/nrneurol.2017.34

Ward, N. S., Brander, F., & Kelly, K. (2019). Intensive upper limb neurorehabilitation in chronic stroke: Outcomes from the Queen Square programme. *Journal of Neurology, Neurosurgery & Psychiatry*, jnnp-2018-319954. https://doi.org/10.1136/jnnp-2018-319954

Wickham, H. (2016). *ggplot2: Elegant Graphics for Data Analysis* [R]. https://ggplot2.tidyverse.org

Wiethoff, S., Hamada, M., & Rothwell, J. C. (2014). Variability in Response to Transcranial Direct Current Stimulation of the Motor Cortex. *Brain Stimulation*, *7*(3), 468–475. https://doi.org/10.1016/j.brs.2014.02.003

Winstein, C., Kim, B., Kim, S., Martinez, C., & Schweighofer, N. (2019). Dosage Matters. *Stroke*, *50*(7), 1831–1837. https://doi.org/10.1161/STROKEAHA.118.023603

Wörsching, J., Padberg, F., Ertl-Wagner, B., Kumpf, U., Kirsch, B., & Keeser, D. (2016). Imaging transcranial direct current stimulation (tDCS) of the prefrontal cortex—Correlation or causality in stimulation-mediated effects? *Neuroscience & Biobehavioral Reviews*, *69*, 333–356. https://doi.org/10.1016/j.neubiorev.2016.08.001

Wu, H., Zhou, Y., & Xiong, Z.-Q. (2007). Transducer of regulated CREB and late phase long-term synaptic potentiation. *The FEBS Journal*, *274*(13), 3218–3223. https://doi.org/10.1111/j.1742-4658.2007.05891.x

Yoon, K. J., Oh, B.-M., & Kim, D.-Y. (2012). Functional improvement and neuroplastic effects of anodal transcranial direct current stimulation (tDCS) delivered 1day vs. 1week

after cerebral ischemia in rats. *Brain Research*, *1452*, 61–72. https://doi.org/10.1016/j.brainres.2012.02.062

Yousry, T. (1997). Localization of the motor hand area to a knob on the precentral gyrus. A new landmark. *Brain*, *120*(1), 141–157. https://doi.org/10.1093/brain/120.1.141

Zeiler, S. R., Gibson, E. M., Hoesch, R. E., Li, M. Y., Worley, P. F., O'Brien, R. J., & Krakauer, J. W. (2013). Medial Premotor Cortex Shows a Reduction in Inhibitory Markers and Mediates Recovery in a Mouse Model of Focal Stroke. *Stroke; a Journal of Cerebral Circulation*, *44*(2), 483–489. https://doi.org/10.1161/STROKEAHA.112.676940

Zeiler, S. R., Hubbard, R., Gibson, E. M., Zheng, T., Ng, K., O'Brien, R., & Krakauer, J. W. (2016). Paradoxical motor recovery from a first stroke after induction of a second stroke: Re-opening a post-ischemic sensitive period. *Neurorehabilitation and Neural Repair*, *30*(8), 794–800. https://doi.org/10.1177/1545968315624783

Zeiler, S. R., & Krakauer, J. W. (2013). The interaction between training and plasticity in the post-stroke brain. *Current Opinion in Neurology*, *26*(6), 609–616. https://doi.org/10.1097/WCO.0000000000000025

Zhou, Y., Won, J., Karlsson, M. G., Zhou, M., Rogerson, T., J., B., Neve, R., Poirazi, P., & Silva, A. J. (2009). CREB regulates excitability and the allocation of memory to subsets of neurons in the amygdala. *Nature Neuroscience*, *12*(11), 1438–1443. https://doi.org/10.1038/nn.2405

Ziemann, U., Lönnecker, S., Steinhoff, B. J., & Paulus, W. (1996). Effects of antiepileptic drugs on motor cortex excitability in humans: A transcranial magnetic stimulation study. *Annals of Neurology*, *40*(3), 367–378. https://doi.org/10.1002/ana.410400306

Ziemann, U., Rothwell, J. C., & Ridding, M. C. (1996). Interaction between intracortical inhibition and facilitation in human motor cortex. *The Journal of Physiology*, *496*(Pt 3), 873–881.

Zorn, L., Renaud, P., Bayle, B., Goffin, L., Lebosse, C., Mathelin, M. de, & Foucher, J. (2012). Design and Evaluation of a Robotic System for Transcranial Magnetic Stimulation. *IEEE Transactions on Biomedical Engineering*, *59*(3), 805–815. https://doi.org/10.1109/TBME.2011.2179938

APPENDICES

A. Does deviation of TMS coil from hotspot predict MEP amplitude?

Rationale.

Motor evoked potentials (MEPs) elicited in a peripheral muscle by transcranial magnetic stimulation (TMS) are routinely used to quantify corticospinal excitability (Bestmann & Krakauer, 2015). In the context of tDCS studies, TMS-MEPs are often used as a read-out of excitability alterations, for example by measurement of MEP size before and after tDCS is applied. However, the peak-to-peak amplitude of an MEP is inherently variable because it is the result of a combination of cortical and spinal projections of varied origin (Bestmann & Krakauer, 2015; Burke et al., 1995; Kukke et al., 2014). Some variability in trial-to-trial MEP amplitude is therefore expected in TMS studies, but variance which may instead be attributed to deviation in TMS coil position within a range expected when TMS is delivered by trained coil operators has not yet been assessed.

'Hotspotting' is the name given to the process of identifying the optimal TMS coil position on a participant's scalp to elicit an MEP, which is itself measured by electromyography (EMG) electrodes applied to the skin above the target muscle. When targeting M1 to elicit an MEP in the FDI muscle, as is the case for the following study, the hotspot is taken as the cortical target from which a TMS pulse elicits an MEP of a given amplitude in 5 of 10 trials (approximately position C3 to target left M1). Once found, the coil's target position should remain constant throughout a session.

Protocol for TMS application varies between studies. In order to maintain the TMS coil's hotspot position throughout a session, researchers rely on techniques including manually tracing the coil's position onto a participant's scalp with a marker ($_{M}$TMS), or using neuro-navigation software, which provides online coil positioning feedback ($_{NN}$TMS). Neuro-navigation software has been shown to improve the accuracy of TMS targeting (Ayache et al., 2016; Bashir et al., 2011; Fitzgerald et al., 2009; Sack et al., 2008), though it does not eliminate error and is not used universally, due to added equipment costs and protocol complexity.

It is not yet known if deviation of the TMS coil from the hotspot position, during a typical study session where experienced coil operators endeavour to minimise coil movement, contributes to the variability seen in MEP measures. In tDCS studies, where the physiological effects of motor-cortical stimulation are quantified by MEP size, it is important to disentangle systematic sources of variability in stimulation outcome measures. The advantages of having a non-invasive marker of excitability may outweigh the cost of known intrinsic variability in the measure. However, there is a need to investigate if systematic variability associated with methodological error is present in TMS recordings, to guide future study design.

In the following study, we used Brainsight® TMS Navigation (Brainbox Ltd.) to monitor TMS coil position throughout a session. Brainsight® tracks the position of the coil relative to the target via infrared sensors attached to both the TMS coil and the participant's head (figure 7). Online feedback of TMS coil position error is provided on-screen, whereby deviation of the TMS coil from the target position is given as four error types: *Distance to target* (in mm) describes the Euclidean distance between the coil's centre and the target coil position; *angular error* (in degrees, °) represents the difference in tilt between the coil's position and the target angle; *twist error* (in degrees, °) is the coil's rotation within in the plane perpendicular to the target coil trajectory. The fourth coil error type: *target error* is a compound measure, which represents the shortest distance between the hotspot and the vector projecting into the head from the centre of the coil.

An example of the on-line feedback used by coil operators is given in Figure A.1. *Distance to target* is visually represented as an empty red circle, *angular error* is shown as a filled red circle, and *twist error* is visually depicted as a small red line extending from the target circle, which can be compared to the large green crosshairs, of which the y-axis extending towards the top of the screen depicts the coil's *twist* when in hotspot position.

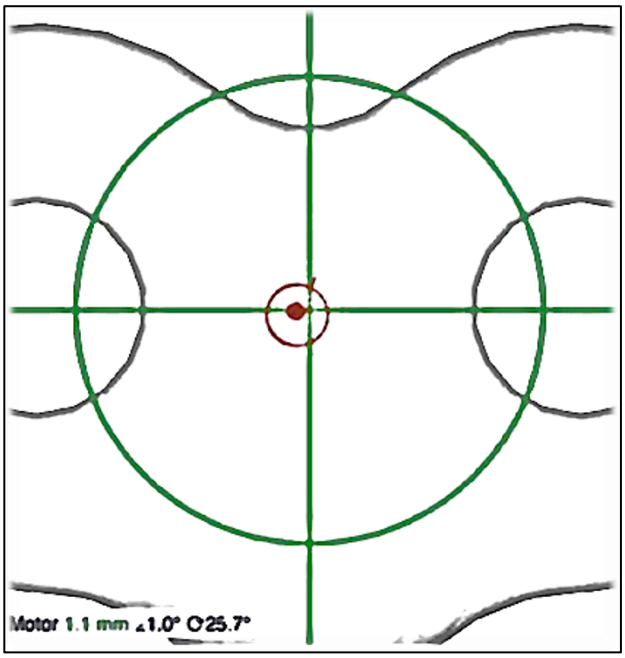

Figure A.1. Example schematic of visual feedback in Brainsight® TMS Navigation (Brainbox Ltd.). *Coil position error is broken down into 3 types: Distance from target position is represented by an empty red circle, angular error is shown as a filled red circle, and twist error is depicted as a small red line extending from the target circle.*

Given the intrinsic variability already present in MEPs, it is important to account for and minimise variance which may instead be attributed to TMS coil error. The following study will investigate how much variance in MEP size can in fact be attributed to deviations in TMS coil position.

Key Questions.

Does deviation of TMS coil from hotspot position predict MEP amplitude?

Methods.

***Participants*.** 5 healthy participants (age M = 29.80, SD = 9.98; 3 females; 4 right-handed, 1 left-handed) attended 2 sessions of identical protocol. The participants were all members of the same research group and had experience conducting TMS research; they were familiar with their surroundings and study protocol. Of the 4 coil operators in this study, 3 were participants. The fourth coil operator did not participate because they did not meet the eligibility criteria for TMS.

Protocol. Motor evoked potentials were recorded using electromyography (EMG) electrodes placed on the belly of the First dorsal interosseous (FDI) musle of the right hand, with a

reference and ground electrodes placed on the proximal interphalangeal joint of index finger of the same hand, and on the head of the ulna bone on the wrist.

The position of the TMS coil was monitored throughout the experiment using Brainsight®. Infrared sensors were attached to the TMS coil and to the participant's head with an elasticated strap, and calibration to an MNI example head was carried out by a researcher sampling the position of the nasion, nose tip, nose base, and the Left and Right Pre-Auricular (LPA and RPA) points of each participant.

Four different researchers operated the TMS coil in this study. In each session, 3 of the possible 4 coil operators applied TMS. This design was chosen to reflect a realistic range of deviation from hotspot position by researchers in the field. The order of coil operators was randomised and the first coil operator in each session carried out hotspotting protocol. During hotspotting, the operator identified the TMS coil position on the scalp and stimulator intensity which elicited 1.0 millivolt (mV) MEPs when 5 out of 10 TMS pulses were applied. This stimulator intensity was recorded as the participant's resting motor threshold (rMT). Once found, the hotspot was sampled and saved using Brainsight®, and the coil position was also manually drawn on the participant's scalp using a chinagraph pencil.

Single-pulse TMS was delivered at rMT intensity using The Magstim® 200² (The Magstim Co. Ltd, Whitland, UK), with a figure-of-eight alpha coil (70 mm) positioned over the dominant primary motor cortex (M1) of each participant. The experiment consisted of 12 blocks of 37 TMS pulses, delivered at a frequency of ~0.25 Hz with a 10% jitter. Three coil operators delivered 4 blocks of TMS pulses each. Two of these blocks were applied using Brainsight® on-line feedback of coil error (TMS_{NN}), and two blocks were applied manually without on-line feedback: the coil operator relied on pencil markings on the scalp to maintain coil position (TMS_{M}). In the TMS_{M} condition, the NeuroNavigation software continued recording coil position, but the monitor display was turned off. Between blocks, operators returned the coil to its holder and then re-applied it to the head, taking care to match the hotspot position as accurately as possible. The protocol is summarised in Figure A.2.

Figure A.2. protocol outline. In black: hotspotting was carried out by the first coil operator for each session. Purple, blue and yellow arrows represent TMS blocks carried out by the 3 different operators. Opaque arrows represent neuro-navigated TMS blocks (TMS_{NS}) and translucent arrows represent manual TMS blocks, where pencil marking on the head were used to guide coil positioning (TMS_{M}).

Results.

Average MEP amplitude was comparable between TMS methods, despite higher coil errors recorded when TMS was applied manually (Table A.1).

Table A.1. Descriptive statistics, session 1.

Method	MEP (mV)	Distance to Target (mm)	Angular Error (°)	Twist Error (°)
Manual	0.76 (0.73)	5.91 (3.82)	6.17 (3.56)	3.47 (2.78)
Neuro-navigated	0.76 (0.88)	1.63 (1.22)	3.51 (2.27)	3.16 (2.56)

Mean and standard deviation (SD, in brackets) of MEP amplitude and coil errors recorded when manual and neuro-navigated TMS were applied.

R version 4.0.2 (https://www.R-project.org) was used to assess the relationship between the coil errors and *MEP size.* The t*wist error* predictor included negative values representing leftward, as opposed to rightward, direction of twist. Since the extent of error and not its direction is of interest for this study, absolute values for *twist error* were used in analyses.

Collinearity checks were carried out using the the *olsrr* R package (Hebbali, 2017) to calculate the variance inflation factor (VIF) for each coil error, which represents the proportion of variance in each predictor that is accounted for by others in the model. *Distance to target* and *target error* were shown to be highly correlated (*Target Error*: VIF = 14.45; *Distance to target*: VIF = 14.84), and so *target error* was discarded from the model. VIF was re-calculated for the revised model which confirmed very low correlation between remaining predictors (VIF ≤ 1.43).

This dataset is characterised by a low participant number and a high volume of samples resulting in high degrees of freedom. Preliminary analysis also showed clustering of datapoints for two of the three coil errors under the $_{NN}$TMS condition (see Figure A.3). Clustering was addressed by discarding $_{NN}$TMS blocks from the analysis. In order to reduce degrees of freedom further, data from sessions 1 and 2 were analysed as separate replication datasets.

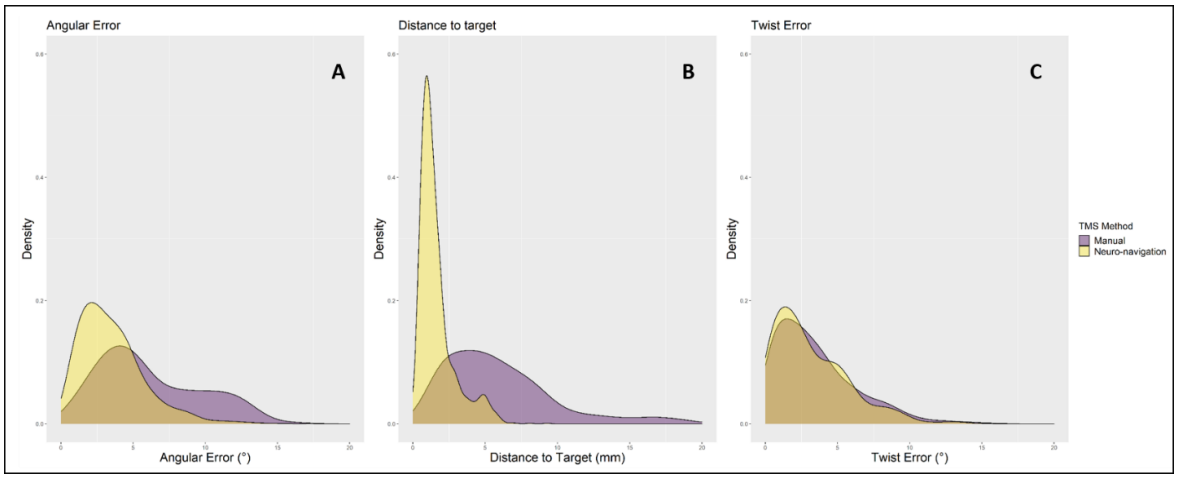

Figure A.3. Density plots representing frequency of MEP datapoints collected during MTMS blocks (purple) and NNTMS blocks (yellow) at varying TMS coil position errors. A: angular error, B: coil distance to target, C: twist error.

A linear regression was first conducted using the *stats* package in R (R Core Team, 2017). Preliminary inspection of the model revealed violation of the multivariate normality assumption, demonstrated by Quantile-Quantile Plots using the *qqnorm* function (R Core Team, 2017). This was remedied by log transformation of the dependent variable, *MEP size*, and qqplots confirmed normal distribution of residuals for the revised model.

To address the main question for this study: does deviation of TMS coil from hotspot predict MEP amplitude? Models of increasing complexity were built around a core linear regression model which included the three coil errors and their interaction predicting log transformed MEP size:

$$\log(MEP\ size) \sim Coil\ distance\ to\ target * coil\ angular\ error * absolute\ coil\ twist\ error$$

Model selection. We then calculated Akaike's Information Criterion (AIC) to distinguish between possible models describing the relationship between the 3 remaining coil errors and log-transformed *MEP size* in sessions 1 and 2.

Potential models included simple linear regressions and linear mixed-effects models (LMMs) which were built using the lme4 package in R (Bates et al., 2015, p. 4). LMMs were considered because they are able to account for non-independence of observations within participants by incorporating this error into the total for the model. The three coil errors and

their interactions were built into the LMMs as fixed effects and *participant* as included as a random effect (therein creating the 'mixed effects' model).

For both session 1 and 2, models which incorporated a random slope for *participant* failed to converge due to the limited model complexity supported by the small datasets and were therefore removed from model comparisons.

Results of the AIC for each session are summarised in Table A.2. The mean (M), standard deviation (SD) and range for MEP amplitude and each level of coil error are summarised in Table A.3; values were comparable between sessions. The best-fitting model for both sessions was an LMM which included a random effect of participant impacting intercept, and fixed effects for the three coil errors: *distance to target, angular error, twist error* and their interactions:

$$\log\ (MEP\ size) \sim Coil\ distance\ to\ target * Coil\ angular\ error * Absolute\ coil\ twist\ error + (1|Participant)$$

Table A.2. Results of AIC model comparison for sessions 1 and 2.

	Model	dAIC	df
Session 1			
	Distance to target*Angular error*Twist error + (1|participant)	0	10
	Distance to target*Angular error*Twist error	10.9	9
Session 2			
	Distance to target*Angular error*Twist error + (1|participant)	0	10
	Distance to target*Angular error*Twist error	20.4	9

dAIC = delta AIC, representing the difference in AIC score between the given and best-fitting models.
df = degrees of freedom.

Table A.3. Descriptive statistics, sessions 1 and 2. Mean and standard deviation (SD, in brackets) of MEP amplitude and coil errors.

	MEP (mV)	Distance to Target (mm)	Angular Error (°)	Twist Error (°)
Session 1				
Mean (SD)	0.73 (0.78)	6.66 (4.80)	6.43 (3.55)	4.07 (3.28)
Range	0.01-5.13	0.28-19.88	0.13-16.97	0.01-16.13
Session 2				
Mean (SD)	0.78 (0.68)	5.18 (2.32)	5.91 (3.56)	2.88 (2.03)
Range	0.01-4.73	0.22-12.18	0.30-15.03	0.01-10.27

Session 1: results

MEPs were inspected on a trial-to-trial basis. Outliers were identified using Grubbs' Test (Grubbs, 1969). 58 trials were discarded in total due to outliers, the presence of a peak-to-peak pre-contraction MEP size exceeding the root mean square for the 37-trial block, or due to missing coil error information.

The *jtools* R package (Long, 2021) was used to obtain p-values for each model and the significance threshold for null-hypothesis testing was set as $p < 0.05$. The proportion of variance explained by fixed factors in the model alone was $R^2_{LMM(m)} = .05$, $p = .12$. The proportion of variance explained by both the fixed and random factors was $R^2_{LMM(c)} = .31$, $p = .12$. Table A.4.a provides results of the fixed effects of the model and random effects are summarised in Table A.4.b. Participant accounted for 27% of total variance.

Table A.4.a, Results summary: impact of coil error on MEPs. Fixed effects, session 1.

	β	CI (2.5%-97.5%)		*p*	
(Intercept)	0.05	-0.79	0.91	0.91	
Distance to target	-0.12	-0.21	-0.03	0.01	**
Angular error	-0.04	-0.11	0.03	0.24	
Absolute twist error	-0.12	-0.22	-0.01	0.03	*
Distance to target*Angular error	0.01	0.00	0.01	0.12	
Distance to target*Absolute twist error	0.01	0.00	0.02	0.07	
Angular error* Absolute twist error	0.00	-0.02	0.01	0.99	
Distance to target*Angular error* Absolute twist error	0.00	0.00	0.00	0.41	

*β = beta; CI = confidence interval; Significance codes: '***' <.001, '**' 0.01, '*' 0.05*

Table A.4.b. Results summary: impact of coil error on MEPs, random effects, session 1.

Model statistic	
AIC	3426.76
SD	0.72
ICC	0.27
groups	5
observations	1053

AIC: Akaike information criterion for quality of model fit.
SD: standard deviation of the random intercept.
ICC: Intraclass correlation describing resemblence of datapoints within participant groups

Analysis of the fixed effects showed that *distance to target* (β = -.12, p = .01; M = 6.66, SD = 4.80) and *absolute twist error (*β = -.12, p = .03; M = 4.07, SD = 3.28) significantly predicted MEP size when clustering of MEP values with participants was accounted for. To account for the log-transformed dependent variable, Beta coefficients were transformed back to raw units by exponentiating the coefficient, subtracting 1 and multiplying by 100 (Ford, 2018). This showed that when all other predictors were held constant, MEP size decreased by 11.43% when *distance to target* increased by 1mm, and MEP size decreased by 11.12% when *twist error* increased by 1 degree (Figure A.4). All other main effects and interactions were found to be non-significant.

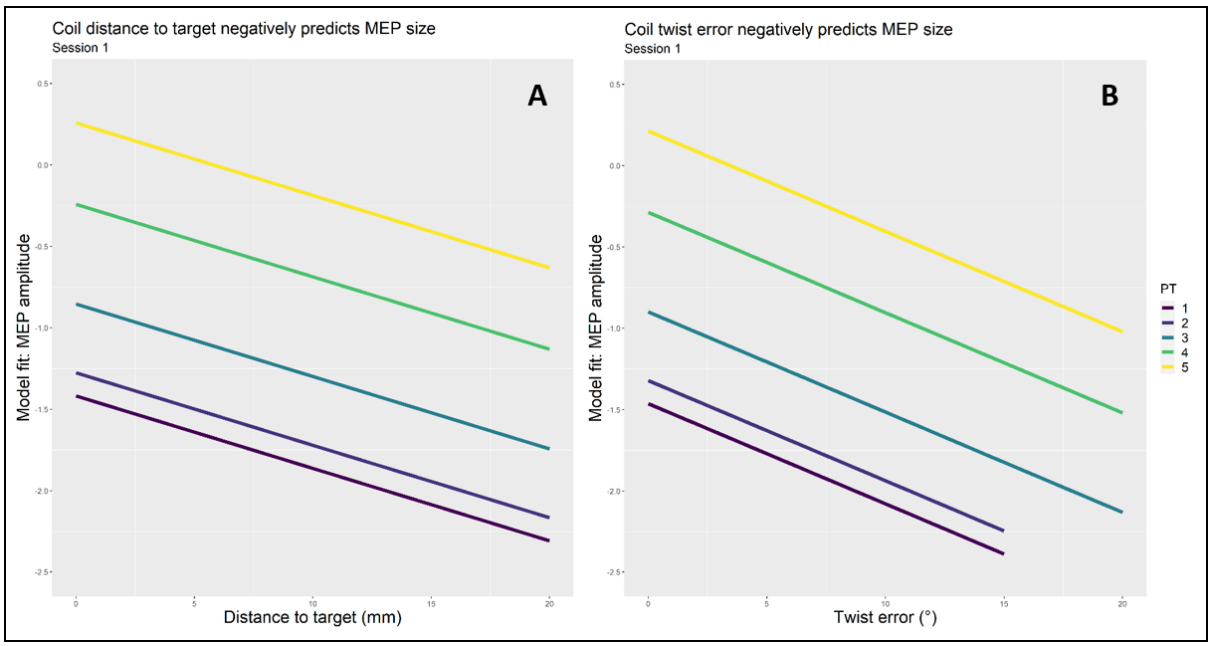

Figure A.4. TMS coil error predicts MEP amplitude, session 1. A: MEPs (mV) decrease by 11.43% when TMS coil distance to target increases by 1mm, when all other coil errors are held constant. B: MEPs (mV) decrease by 11.12% when TMS coil twist error increases by 1°, when all other coil errors are held constant.

Session 2: results

The same model selection and data-cleaning steps were repeated for session 2 data, and the same linear mixed-effects model was recommended:

$$\log MEP\ size \sim Coil\ distance\ to\ target * coil\ angular\ error * absolute\ coil\ twist\ error + (1|Participant)$$

The proportion of variance explained by fixed factors in the model alone was $R^2_{LMM(m)}$ = .05, p = .14. The proportion of variance explained by both the fixed and random factors was $R^2_{LMM(c)}$ = .17, p =.14. Table A.5.a provides results of the fixed effects of the model and

random effects are summarised in Table A.5.b. Participant accounted for 13% of variance in session 2.

Table A.5.a Results summary: impact of coil error on MEPs, Fixed effects, session 2.

	β (%)	CI (2.5-97.5%)		p	
(Intercept)	0.12	-0.49	0.74	0.70	
Distance to target	-0.09	-0.19	0.01	0.08	
Angular error	-0.10	-0.20	-0.01	0.03	*
Absolute twist error	-0.33	-0.52	-0.15	<.001	***
Distance to target*Angular error	0.02	0.00	0.03	0.03	*
Distance to target*Absolute twist error	0.03	0	0.05	0.06	
Angular error* Absolute twist error	0.06	0.02	0.09	<.001	***
Distance to target*Angular error*Absolute twist error	-0.01	-0.01	0	0.01	**

*β = beta; CI = confidence interval; Significance codes: '***' <.001, '**' 0.01, '*' 0.05*

Table A.5.b. Results summary: impact of coil error on MEPs, random effects, session 2.

Model statistic	
AIC	2938.66
SD	0.35
ICC	0.13
groups	5
observations	1079

AIC: Akaike information criterion for quality of model fit.
SD: standard deviation of the random intercept.
ICC: Intraclass correlation describing resemblence of datapoints within a participant groups

Main effects

Angular error

The model showed a significant main effect of *angular error* (β = -.10, p = .03; M = 5.91, SD = 3.56). When beta coefficients were transformed to account for log transformation of the dependent variable, the model showed that when *angular error* increased by 1mm *MEP size* decreased by -9.52% when all other predictors are held constant (~.07mV; Figure A.5.A).

Twist error

There was a highly significant main effect of *twist error* on *MEP size (*β = -.33, p <.001; M = 2.89, SD = 2.03). Transformation of the coefficient showed that when *twist error* increased by 1 degree, *MEP size* decreased by 28.11%. 28.11% of mean *MEP size* is 0.21mV (Figure A.5.B).

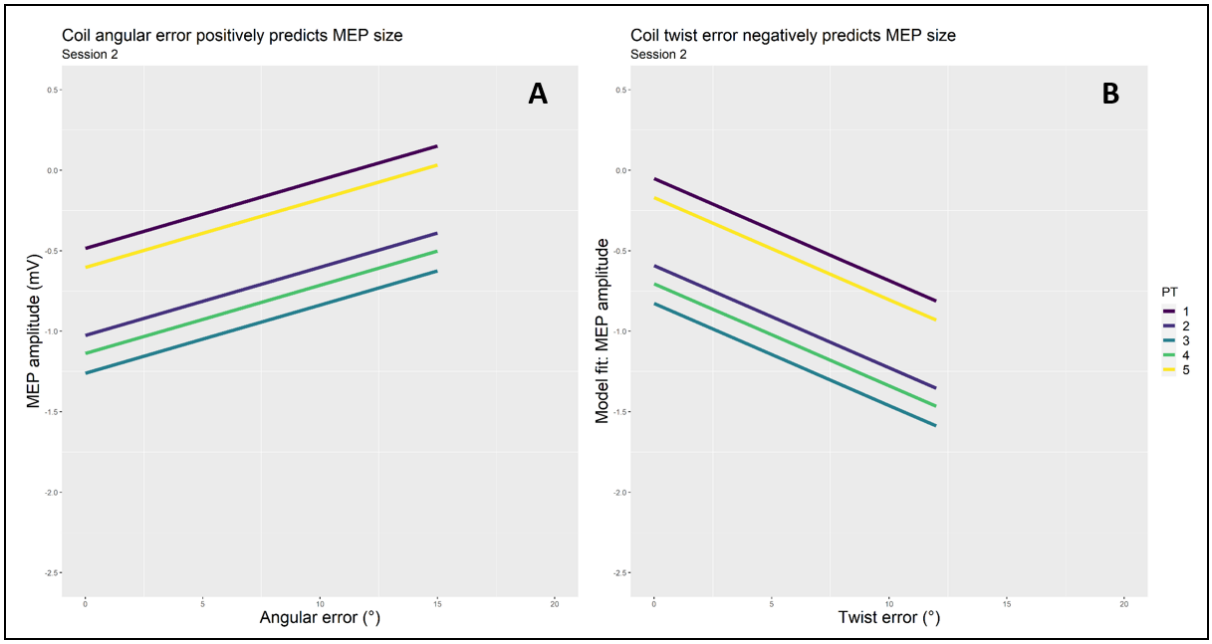

Figure A.5. TMS coil error predicts MEP amplitude, session 2. A: MEPs (mV) increased by 9.52% when TMS coil angular error increased by 1°, when all other coil errors are held constant. B: MEPs (mV) decreased by 28.11% when TMS coil twist error increased by 1°, when all other coil errors are held constant.

Two-way interactions

Distance to target*Angular error. A significant two-way interaction between the TMS coil's *distance to target* and *angular error* was detected *(*β = .02, p = .03). Angular error significantly predicted MEP size, and this effect was modulated by the coil's distance to target: when the distance to target was held constant at its mean value (M = 5.18mm, SD = 2.32), *MEP size* increased (β = .04, p <.001) when *angular error* increased by 1 degree. Transformation of the beta coefficient showed that this equated to a 4% (~0.03mV) increase in MEP size when angular error increased by 1 degree when distance to target was average. This effect diminished as the coil's distance to target increased (β = .04, p = .02) and was exacerbated as *distance to target* decreased (β = .05, p <.001). We used the *interactions* R package (Long, 2020) to visualise this interaction effect (Figure A.6). Conversely, we found that changes in the coil's *distance to target* did not significantly predict MEP amplitude when modulated by *angular error* (Figure A.6).

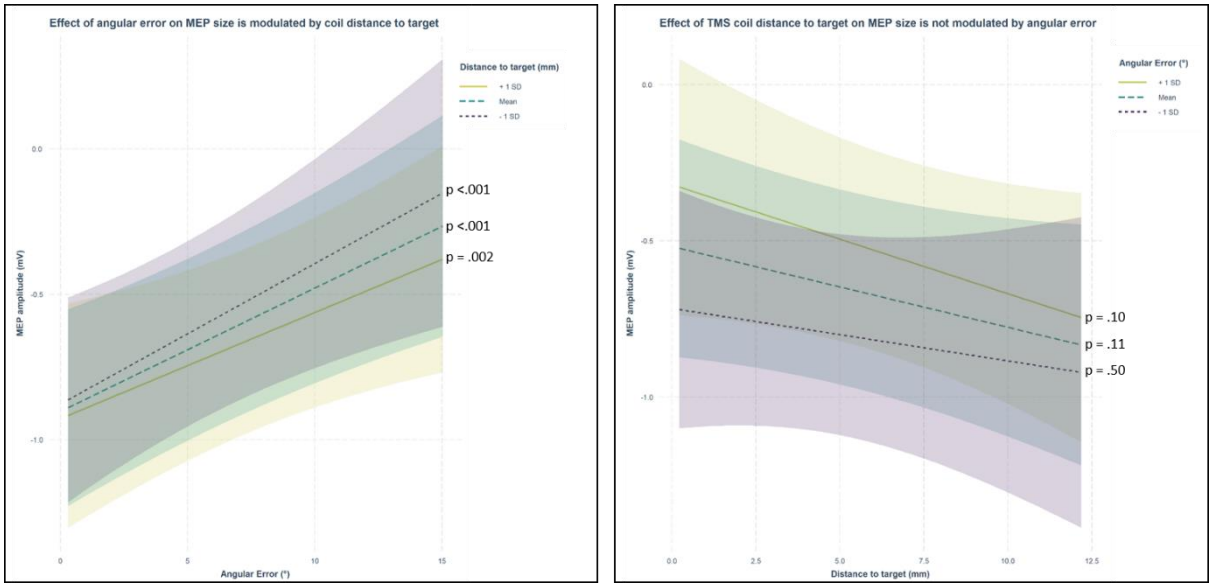

Figure A.6. interaction between angular error and coil distance to target, session 2. A: Angular error significantly predicts MEP amplitude, and this effect is modulated by the TMS coil's distance to target. B: Distance to target does not significantly predict MEP size.

Angular error*Twist error

There was a significant two-way interaction between angular and twist error in session 2 (β = .02, p < .001). Both *angular error* and *twist error* significantly predicted MEP size, and each significantly modulated the effects of the other. MEP amplitude increased with greater angular error (β = .04, p < .001), and this effect was exaggerated when twist error increased above the mean (β = .09, p < .001), whereby MEP amplitude increased by ~9% for every degree of increase in angular error, when twist error was also high (Figure A.7).

Twist error also predicted MEP amplitude, though the effect was only found to be significant when *angular error* was at or below its mean (M = 5.91, SD = 3.56; β = -.06, p<.001). Transformation of the coefficient shows this is equivalent to a 5.82% (0.05mV) decrease in *MEP size* when twist error increases by 1 degree and angular error is at or below average. (see Figure A.7).

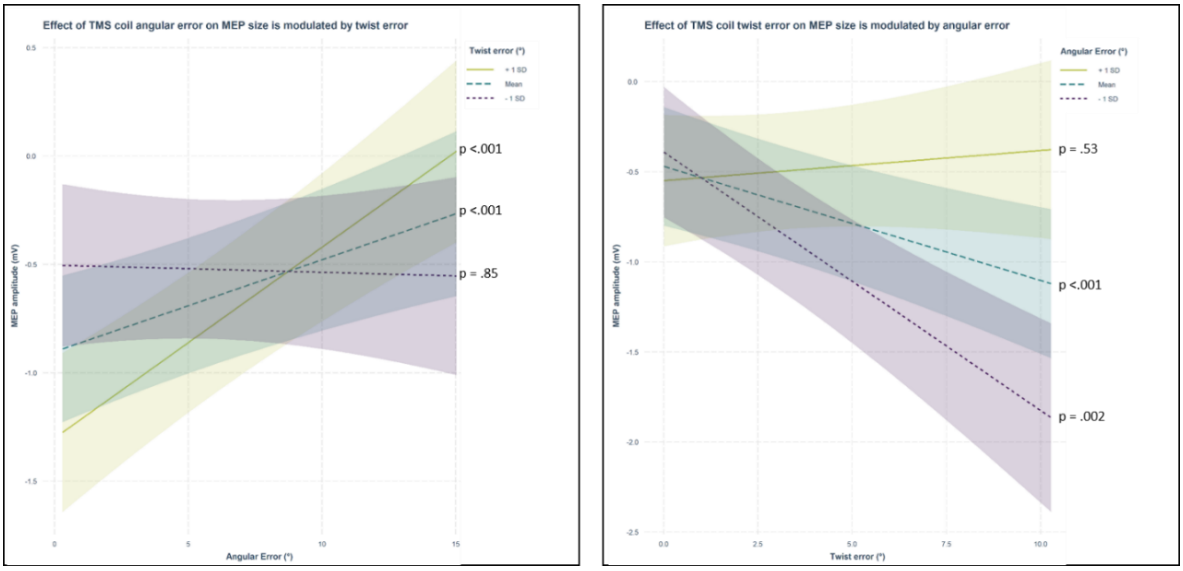

Figure A.7. Interaction between angular error and twist error, session 2. A: Angular error positively predicts MEP amplitude, and this effect is exaggerated by when twist error is high. B: Twist error negatively predicts MEP amplitude when angular error is low.

3-way interaction

Distance to target*Angular error*Absolute twist error

A significant 3-way interaction was found between the three coil error types (β = -0.01; -0.64%; ~0.005Mv, p = 0.01). *Distance to target* was found to significantly negatively predict MEP size, only when *angular error (*M = 5.91°, SD = 3.56) and *twist error (*M = 2.88°, SD = 2.03) were high (β = -.10, p<.001), this translates to a 9.52% (~.07mV) decrease in MEP size with increased distance to target.

Twist error was found to negatively predict MEP amplitude when angular error and distance to target were at or below their average values. However, this effect was found to reverse when angular error increased above its mean, whereby twist error predicted an increase in MEP amplitude when angular error was high and distance to target was small (β = .09, p < .05). The greatest moderating effect of *angular error* on *twist error* was seen when *distance to target* was low. In this case, low angular error negatively predicted MEP amplitude, such that MEPs decreased by 18% (~0.14mV) when twist error increased by 1° (β = -.17, p < .001). Conversely, high angular error positively predicted MEP size when distance to target was low, showing that MEPs increased by 9% (.07mV) when twist error increased by 1° (β = .09, p = .05).

Angular error positively predicted MEP size when distance to target was -1 standard deviation below the mean, and twist error was average (β =.05, p<.001) or +1 standard deviation above mean twist error (β =.12, p<.001). This effect was maintained at distance to target increased. For example, when distance to target was 1 standard deviation above the mean, and angular error positively predicted MEP amplitude when twist error was at (β =.04, p=.02) or above (β =.05, p<.001) average (Figure A.8).

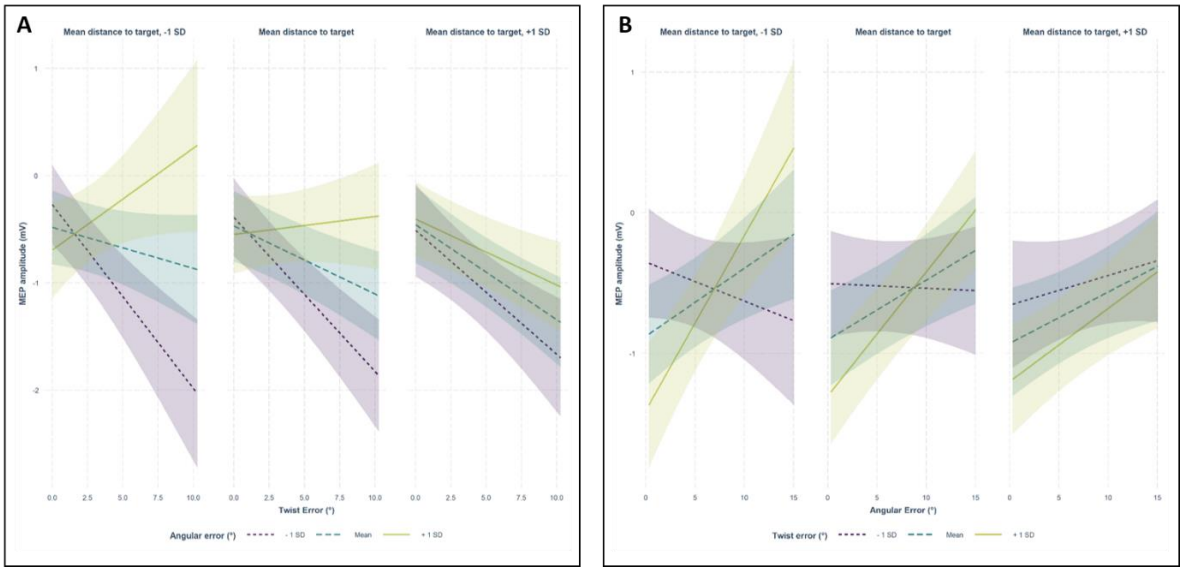

Figure A.8. Example of the 3-way interaction between coil errors in session 2. A: Twist error significantly predicts MEP size. The direction of this effect is moderated by angular error; when angular error and distance to target are low, twist error negatively predicts MEP size, but when angular error is high the relationship between twist error and MEP size is positive. As distance to target increases, this effect diminishes, and twist error significantly negatively predicts MEP size. B: Angular error significantly positively predicts MEP size such that an increase in angular error is systematically associated with larger MEPs. When distance to target is low this effect still holds; negative correlations depicted in figure B are non-significant (p>.05).

Discussion

We found that TMS coil deviation is a source of variability in TMS studies. Small movements away from the hotspot position account for some of the variance in MEP amplitude, in addition to the intrinsic variability of the MEP measure (Bestmann & Krakauer, 2015). Tools available to reduce TMS coil movement during study sessions include neuro-navigation software (Ruohonen & Karhu, 2010), which itself can be optimised by the use of individual structural MRIs, and/or the use of a mechanic coil holder (Ginhoux et al., 2013; Zorn et al., 2012). Both have been shown to improve accuracy of TMS targeting (Rossi et al., 2021), though the extent to which coil error must be minimised to avoid confounding effects is yet

to be quantified. Unfortunately, these methods rely on access to specialist equipment only available to well-funded projects and add a considerable amount of time and complexity to testing sessions.

Main effects for each coil error type and their interactions were not consistent between sessions; we did not identify a systematic effect of coil deviation on MEP amplitude across datasets. This is to be expected, since coil deviation will differ within and between subjects between sessions. Given three parameters of potential coil deviation, one single coil parameter could not be singled out, though the results show that collectively, distance to target, twist error, and angular error produce deviance in the coil's position which contributes to variance in MEP amplitude. Future studies may benefit from collection of neuro-navigation data to detect the presence of confounding coil error; if one can quantify variance explained by coil error on a case-by-case basis, it may be accounted for statistically post-hoc.

We found that a 1 mm or 1 degree change in the coil's position could predicted MEP amplitude in both sessions, though the spatial resolution of TMS is relatively large: approximately 0.5-1cm (Jp et al., 1992; Ravazzani et al., 1996; Thielscher & Kammer, 2002; Toschi et al., 2008). The effects of coil deviation on MEP amplitude are dependent on accurate identification of the hotspot position. In this study, the hotspot was identified by experienced coil operators, who employ heuristics such as angling the coil at approximately 45° relative to the medial-sagittal plane of the participant's head (Brasil-Neto et al., 1992; Mills et al., 1992). While this estimation is appropriate in the absence of computational modelling of TMS application, recent work has demonstrated that the optimal angle for a TMS coil is subject-specific, and can vary within a 45° degree window of perpendicularity to the central sulcus (Balslev et al., 2007).

Data from session 2 revealed a positive relationship between increased angular error and MEP size. Due to the manual hotspotting protocol used in this study, it is not possible to conclude if this effect, or any of those reported above, demonstrate inaccurate hotspot identification during study set-up, or more specific conclusions such as change in the coil's angle throughout a session is associated with increased MEP size. Further optimised investigation is needed to resolve the issue.

The findings of this study indicate that some variance in tDCS study outcomes might be attributed to variance in the chosen measure of physiological excitability changes: TMS-MEPs. Further investigation is needed to quantify if there is a threshold at which coil deviation affects MEP amplitude. In the meantime, and in the absence of affordable and accessible solutions to reduce TMS coil deviation, careful training of TMS coil operators should include emphasis on the importance of stable coil positioning not only concerning the coil's distance to the target, but the angle and twist of the hand-held device. A need for economically accessible accessory equipment is clear, since existing neuro-navigation and coil holding accessories are known to reduce error.

References linked to citations in this section can be found in the main References section of the thesis.

B. Example eligibility screening form

ReCAPS STUDY – PARTICIPANT SCREENING QUESTIONNAIRE (FULL)

Please note the following before completing the questionnaire.

This questionnaire:

- Contains questions about your medical history and other personal information that may be sensitive.
- The questions are necessary to make sure you are suitable for the study.

Demographic information
Name: **Date of Birth:** **Sex:** Male ☐ Female ☐ Other ☐ **Handedness** (before stroke): Left ☐ Right ☐ Both ☐
Contact Information
Telephone: **Address:** **Email:**
GP details
GP Telephone: **Address:** **Email:**
Information about your stroke

Date of stroke:

First stroke? Yes ☐ No ☐

Only stroke? Yes ☐ No ☐

Type of stroke: *(If you do not know, please leave blank)*

Ischemic (clot/blockage) ☐ (thrombolised? Yes ☐ No ☐) Haemorrhagic (bleed) ☐

Where in the brain was your stroke? *(Please provide as much detail as possible)*

Information about your motor weakness

Which arm/hand was affected by the stroke? Left ☐ Right ☐ Bilateral ☐

Is your arm/hand still weak? Yes ☐ No ☐

Are you able to extend your fingers outwards with no assistance? *(e.g. without using the unaffected hand or a surface, such as a table top, to help you)*

Not at all☐ Only very slightly☐ Somewhat☐ Yes, but with slight difficulty☐ As easily as with my other hand☐

Can you grasp objects with no assistance? *(e.g. cup or pen)*

Yes ☐ No ☐

MRI Scan

Have you previously had an MRI scan? Yes ☐ No ☐

If Yes, have you had an MRI for a research study? Yes ☐ *(please name the study / researcher involved)* No ☐

Would you be willing to have an MRI scan for this study? Yes ☐ *(please complete MRI safety form*) No ☐

TMS/tDCS Screening Questionnaire		
Please answer the following questions	**Yes**	**No**
1. Are you younger than 18 years?	☐	☐
2. Are you pregnant or do you think you are?	☐	☐
3. Have you ever had severe head trauma associated with loss of consciousness?	☐	☐
4. Have you ever had brain surgery or surgical procedures to your spinal cord?	☐	☐
5. Do you have metal in the brain, skull or elsewhere in your body? If so, please specify the type of metal and location:	☐	☐
6. Do you have a cardiac pacemaker or intracardiac lines?	☐	☐
7. Do you have an implanted neurostimulator (e.g. DBS, VNS)	☐	☐
8. Do you have a medication infusion device implant?	☐	☐
9. Do you have a skin disease or skin allergy? If so please specify:	☐	☐
10. Do you have cochlear implants?	☐	☐
11. Are you taking or did you take within the last two weeks any prescribed medications as part of treatment or research (excluding contraceptives)? If so, please specify:	☐	☐
12. Have you ever had a fainting spell or syncope? If so, please specify the occasion(s):	☐	☐
13. Do you or a close family member suffer from migraines?	☐	☐
14. Do you suffer from any neurological or psychiatric disease? If so, please specify:	☐	☐
15. Do you have epilepsy or have you ever had a convulsion or a seizure?	☐	☐
16. Do you have any hearing issues (e.g. tinnitus)?	☐	☐

NEUROIMAGING: VOLUNTEER SAFETY QUESTIONNAIRE

TO BE COMPLETED IN ALL MODALITIES OF NEUROIMAGING

The handling, processing, storage and destruction of data will be conducted in accordance with the Data Protection Act (1998).

I. The *absolute* contra-indications for MRI scanning are listed below. If you answer yes to any of the following we will *not* be able to scan you:

	Yes	No
Do you have a cardiac pacemaker or artificial heart valves?	☐	☐
Do you have cerebral aneurysm clips?	☐	☐
Have you undergone permanent eyelining as a cosmetic procedure?	☐	☐
Have you any cochlear implants (ear implants)?	☐	☐

II. Before entering the MRI scan room please inform us if any of the following apply:

	Yes	No	Unsure
Are you claustrophobic?	☐	☐	☐
Have you had any surgery?	☐	☐	☐
Are any artificial devices implanted into your body (e.g. joint replacements, coils, implants or clips)?	☐	☐	☐
Have you ever had a job in the metal-working industry or have you ever been exposed to metal dust or splinters?	☐	☐	☐
Have you ever had an injury to your eyes involving metal at high speed?	☐	☐	☐
Do you wear a hearing aid or have dentures, bridges, braces, dental or breast implants?	☐	☐	☐
Do you wear a false limb, caliper, brace, or have any artificial devices attached to your body (e. g clips or rings)?	☐	☐	☐
Have you had any neurosurgery including the insertion of clips or plates?	☐	☐	☐

Do you have any shrapnel from a war injury or explosion?	☐	☐	☐
Do you have an infusion pump or Hickman line?	☐	☐	☐
Are you diabetic, epileptic or ever had a seizure?	☐	☐	☐
Are you wearing Nicotine patches?	☐	☐	☐
Do you have one or more tattoos?	☐	☐	☐
Have you removed all loose metal objects, wallets, watches, bra and jewellery from your person?	☐	☐	☐

For female volunteers only:

	Yes	**No**
Could you be pregnant?	☐	☐
Are you wearing a diaphragm / Interuterine Device (Coil) or any other contraceptive device?	☐	☐
Are you wearing any hormone replacement contraceptive patches?	☐	☐

If you have answered Yes/Unsure to any of the previous questions, please can you provide further information that you feel may be helpful:
(e.g. if you answered yes to having surgery, please indicate what surgery you had)

C. Example participant information sheet

ReCAPS STUDY - INFORMATION SHEET (PATIENT)

Scientific Title of Research: Re-opening the critical period for plasticity after stroke with dose controlled non-invasive brain stimulation

Department: Department of Clinical and Movement Neurosciences

Name and Contact Details of the Researchers:

Dr Carys Evans ([redacted]) Tel: [redacted]

Jenny Lee ([redacted]) Tel: [redacted]

Name and Contact Details of the Chief and Principal Investigators:

Prof Nick Ward ([redacted]). Tel: [redacted]

Prof Sven Bestmann ([redacted]). Tel: [redacted]

YOU WILL BE GIVEN A COPY OF THIS INFORMATION SHEET

INTRODUCTION

We would like to invite you to take part in our research study. This study is part of a charity funded research project and will also be conducted in part fulfilment of a PhD. Before you decide whether to take part, it is important that you understand why the research is being carried out and what it will involve.

Please read and consider this information carefully. You may wish to discuss it with others. If there is anything you do not understand, or if you would like more information, please ask us. Take time to decide whether you would like to take part.

There are two parts to this information sheet:

Section 1

1.1. Study Details: describes the ReCAPS study and what will happen if you take part.

1.2. Study Techniques: describes what techniques we will be using.

Section 2

2.1. Study Impact: describes benefits and risks of taking part, and your rights to withdraw.

2.2. Data Protection: outlines how the data is used and issues of confidentiality.

You should read both sections before you make a decision.

Thank you.

Section 1

1.1. Study Details

What is the purpose of the ReCAPS study?

This study is exploring how improvements in your arm and hand after stroke are associated with changes in brain activity. We also want to see whether we can modify these changes using brain stimulation.

We know that the responsiveness, or "excitability", of the brain changes after a stroke. These changes are believed to be related to how the brain reorganises itself after a stroke, which is an important part of re-learning and rehabilitation. In the first weeks and months after a stroke the brain is very excitable, but over time this state returns back to normal levels. We want to map how excitability changes over time and explore whether brain stimulation is an effective tool to make the brain more excitable. If you decide to participate in this study it will not have an impact on your recovery, but we hope that it will increase our understanding of the post-stroke brain so that new, effective therapies can be developed in the future.

Why have I been invited?

We are approaching you because you have had a stroke a) within the last 8 weeks or b) at least 6 months ago.

Do I have to take part?

No. If you decide to take part you will be given this information sheet to keep and be asked to sign a consent form, which you will also be given to keep. Your participation in this study is entirely voluntary. Even if you decide to take part you are still free to withdraw at any time and without giving a reason. A decision to withdraw at any time, or a decision not to take part, will not affect the standard of care you receive.

Will I be paid for my participation?

Participation in this study is voluntary. However, if you are traveling from within the M25 we will be able to reimburse you for study related travel expenses.

What will the study involve?

The following flow diagram is designed to give you a quick summary of what to expect if you decide to take part. The rest of this document includes more detailed information about each aspect of the study.

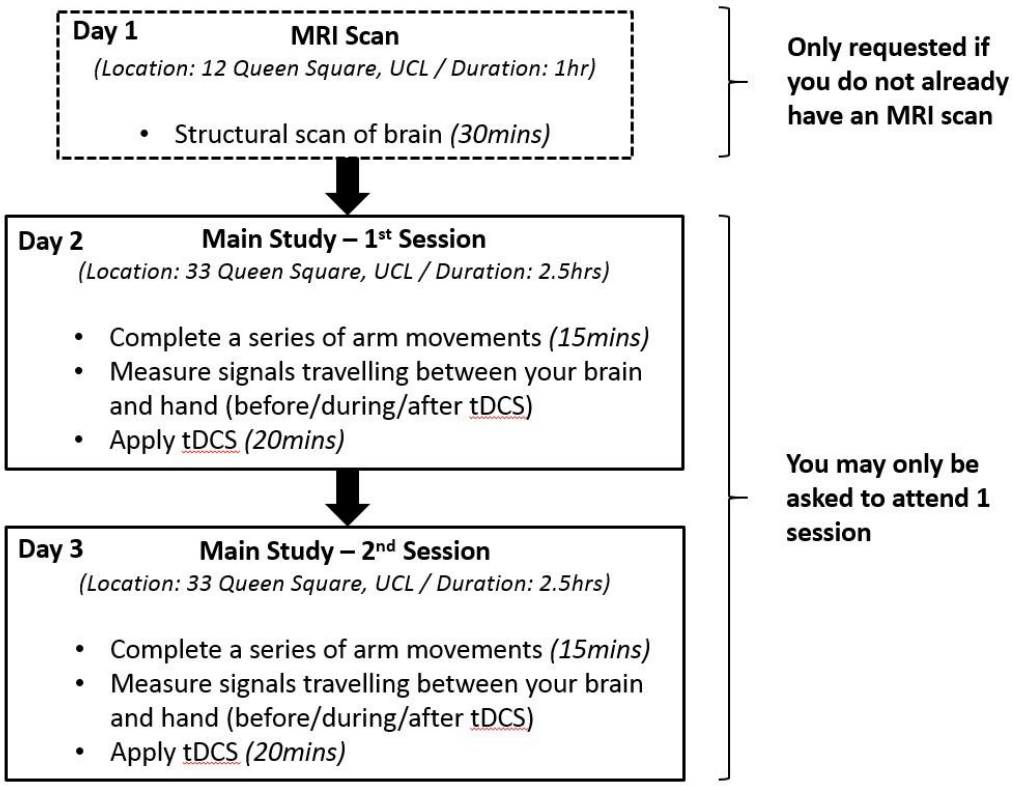

How many study sessions will I be asked to attend? *(Ticked below)*

Structural MRI Experiment, **1 session**: 1 hour. ***12 Queen Square***

Combined tDCS-TMS Experiment, **1 session**: 1.5 hours. ***33 Queen Square***

Combined tDCS-TMS Experiment, **2 sessions**: 2 x 1.5 hours. ***33 Queen Square***

If you decide to take part, you will be asked to attend one or two study sessions at the **Department of Clinical and Movement Neurosciences**, located at **33 Queen Square, 4th Floor, London WC1N 3BG**. Each session will last up to 2.5 hours and will be scheduled approximately two weeks apart.

Before you take part in the study, **we may request that you attend an additional session** if you have not already had an MRI scan of satisfactory quality for the study. If this is the case, you maybe asked to attend three sessions in total. If you are requested to have an MRI scan, this will take place at the **Wellcome Trust Centre for Human Neuroimaging**, located at **12 Queen Square, London WC1N 3AR** and will take approximately 1 hour.

What will happen during each study session?

At the start of each session we will carry out simple physical tests, including some arm and hand movements, in order to measure how well recovered you are. We will then measure the electrical activity transmitted between your brain and the finger muscles of your affected hand. This will be measured by applying transcranial magnetic stimulation (TMS) to the head. The electrical activity generated by TMS will be recorded using small electrodes attached to your fingers.

During each session we will also apply transcranial direct current stimulation (tDCS) to the head to assess whether tDCS can change the electrical activity in the brain. Any changes in activity are temporary and you will not be able to detect them. Two electrodes will be applied to the head and a weak current will run between them for up to 20 minutes.

If you are asked to attend two study sessions, they will be scheduled about 2 weeks apart. The procedure will be the same in each session. In one session you may receive “real” tDCS (the current will run for up to 20 minutes) and in the other session you may receive “sham” tDCS (the current will run for only 30 seconds). The stimulation you receive (real or sham) in each session will be chosen at random. This means that some participants will receive real tDCS first, then sham tDCS in the second session and vice versa. The order in which participants receive real or sham stimulation will be decided at random. You will not be told which stimulation you are receiving until the end of the study, when you can be informed if you wish.

The different techniques are explained in more detail below in section 1.2.

At the end of the study, if you are interested in being contacted about future research we can add you to the departmental participant database. With your consent, we will include your contact details, demographic data, and some scores from the tasks included in this study on the database.

1.2. Study Techniques

Assessment of Upper Limb impairment

During this study, we will assess the movement of your affected arm and hand. This will involve asking you to perform a range of movements, such as extending your arm or rotating your shoulder, to the best of your ability. It will take approximately 15 minutes and will be performed by a trained researcher or physiotherapist. A researcher may record a video of this assessment, so that the score given can be reviewed by a second trained researcher or physiotherapist after the day of testing.

Transcranial Magnetic Stimulation (TMS)

TMS will be used to measure the electrical activity transmitted between your brain and the finger muscles of your affected hand. You will be seated in a comfortable chair with your arm resting on a pillow in front of you. A TMS coil will be held against your head by the experimenter and brief pulses of stimulation will be applied (see picture). Small electrodes attached to your fingers with sticky tape will measure the effects of the stimulation.

We will aassess your brain excitability by stimulating the region of the brain that controls your fingers. Each magnetic pulse will feel like a tap on your head. This study includes both single-pulse TMS, and repetitive TMS (rTMS). rTMS involves pulses being delivered very quickly, while singlepulse TMS includes a distinct pause between each TMS pulse.

At high stimulation intensities there may be some incidental stimulation of the muscles in your face, which you may experience as a jaw twitch or eye blink. Similarly, the magnetic pulse in the coil makes a loud clicking noise and this becomes louder at high intensities. Earplugs are available if you would like to minimise any discomfort from noise. If you find these unpleasant, you should ask the experimenter to stop the experiment.

Transcranial direct current stimulation (tDCS)

We will be assessing whether tDCS can be used to influence brain excitability. During tDCS you will have two small electrodes applied to the head using conductive paste. This will be connected to a small box, which can produce small amounts of electricity. During 'real' stimulation, you will receive very small currents via the electrodes for up to 20 minutes. During 'sham' stimulation, the tDCS stimulator will be turned off after 30 seconds, once the target intensity has been reached. Participants can expect to feel a slight tingling sensation during the first few seconds of stimulation.

MRI Scan

(only required if you do not already have an MRI image of satisfactory quality)

Magnetic resonance imaging (MRI) provides pictures of the brain (as well as other parts of the body). It is a painless and safe technique. During the scan you will be asked to lie on a comfortable padded table inside a large tube that comprises the imaging magnet (see picture). You will be asked to remain still during this time. The scanner is loud while it is working and you will be given protective earplugs. You may also ask for an eye mask. Due to the powerful magnetic field involved, you must not bring any metal into the scanner room. **If you have any non-removable metal in or on your body, then you cannot have an MRI scan.** If you have any questions about what is allowed, we can help you to determine whether you are eligible. **Some of the exclusion criteria include the presence of: cardiac pacemaker, aneurysm clip, cochlear implants, tattoos, pregnancy, shrapnel, history of metal fragments in eyes, or neurostimulators.** Once you are inside the MRI scanner, we will ask you to stay inside for up to 30 minutes. If you suffer from claustrophobia, then being inside the tube of the magnet may be uncomfortable for you and it may not be possible for you to participate. Please discuss this with us if you are concerned about it. In the event of an unexpected finding on your scan, a radiologist will review it and contact your GP directly if further tests are advised.

Section 2

2.1. Study Impact

What happens to the results of the research project?

Once the study is complete, a summary report of the main findings will be prepared. You will be provided a copy of this report by email or post. The results will also be presented

within a PhD thesis and submitted to peer-reviewed journals. You will be able to receive a copy of any published journal articles if you wish. You will not be identified personally in any publication.

What are the possible benefits of taking part?

This study will not directly benefit your recovery, but we hope that the information obtained will improve our understanding of the relationship between brain activity and recovery, and guide future developments of treatment after a stroke.

What are the possible disadvantages and risks of taking part?

TMS uses very short magnetic fields. **Therefore, they can be harmful to people who have a pacemaker, an implanted medication pump, a metal plate in the skull or metal objects inside the eye or skull (for example after brain surgery or an accident). Please inform the investigators if you think this might apply to you.**

With TMS, it is possible to cause seizures (fits) in susceptible individuals using high intensity pulses. With the lower strength pulses that we use, following agreed safety guidelines, seizures have not occurred. In the unlikely event of a seizure, you will be given appropriate medical treatment. The DVLA have indicated that this would be regarded as a provoked seizure and would not affect the standard period of 1 month following a stroke during which driving is not permitted. The only other known side effect of TMS is headache, which goes away with simple painkillers. No long-term side effects of TMS have been described. Please tell the investigators if you have ever had a seizure, fit or epilepsy.

tDCS uses very low intensity currents to stimulate the brain. During the procedure participants will feel a slight tingling sensation at the site of stimulation. When used for prolonged periods of time there is a slight risk of burns. However, in the current protocol, low intensities for short periods of times will be used. Therefore, the risks are very minimal.

MRI uses a large imaging magnet to generate pictures of the brain. It is a painless and safe technique. At present, MRI carries no known risks of injury or discomfort in participants who answer NO to a set of specified criteria.

Will the findings affect me personally?

The tests used in this study are currently research tools only and of uncertain significance. They would therefore not affect you as an individual participant. We do hope the information obtained will guide future developments of treatment after a stroke.

In the event of an unexpected finding, a researcher will contact a radiologist who will review your scan and decide if further imaging is advisable. If further tests are required, the radiologist will contact yourGP to talk to them directly, who will in turn contact you to arrange an appointment. Please note that the scans used for this study are not diagnostic scans, and there is not a guarantee that they will pick up all pathology.

What happens if I no longer want to carry on with the research?

You can withdraw at any time without giving a reason and without it affecting any benefits that you are entitled to. If you decide to withdraw, no further data will be collected and you

will not be required to take part in any further research procedures. Any identifiable data already collected with consent will be retained and used in the study. To safeguard your rights, we will use the minimum personally-identifiable information possible.

What happens if something goes wrong?

If you have a concern about any aspect of this study, you should ask to speak to the researchers who will do their best to answer your questions. Contact details are provided at the top of this information sheet.

If you remain unhappy and wish to complain formally, please contact the chief investigator, Prof Nick Ward ([redacted] / [redacted]). All communication will be dealt in strict confidence.

If you wish to talk to someone independent of the study, please feel free to contact the Patient Advice and Liaison Service by email (PALS@uclh.nhs.uk) or post:

PALS
Ground Floor Atrium
University College Hospital
235 Euston Road
London NW1 2BU

PALS
Box 25
National Hospital for Neurology and
Neurosurgery
Queen Square
London WC1N 3BG

2.2. Data Protection

Who will have access to my data?

University College London (UCL) is the sponsor for this study based in the United Kingdom. We will be using information from you and your medical records in order to undertake this study and will act as the data controller for this study. This means that we are responsible for looking after your information and using it properly. UCL will keep identifiable information about you until project completion.

Your rights to access, change or move your information are limited, as we need to manage your information in specific ways in order for the research to be reliable and accurate. If you withdraw from the study, we will keep the information about you that we have already obtained. To safeguard your rights, we will use the minimum personally-identifiable information possible.

You can find out more about how we use your information by contacting the researchers on the project or by contacting UCL's Data Protections Office at data-protection@ucl.ac.uk**.**

What happens to the information collected in this study?

UCL will collect information about you for this research study from you and/or your medical records if you are still based at a clinic/rehabilitation unit. This information will include your name, NHS number, contact details and health information, which is regarded as a special category of information. We will use this information to confirm your eligibility to take part in the study and to contact you about the study. UCL will also make sure that relevant

information about the study is recorded for your care, and to oversee the quality of the study.

Individuals from UCL and regulatory organisations may look at your medical and research records to check the accuracy of the research study. The only people in UCL who will have access to information that identifies you will be people who need to contact you to about taking part in the study or audit the data collection process. The people who analyse the information will not be able to identify you and will not be able to find out your name, NHS number or contact details.

UCL will keep identifiable information about you from this study until project completion. Data will be kept in a secured accommodation and on secured computers in the Department of Clinical and Movement Neurosciences at UCL. The data will be used only for the purpose of informing the research questions in this study, and only accessible by the authenticated researchers on the project. After the research study has finished, all personal identifiable data will be destroyed. Data directly related to the study questions will be retained securely at UCL for 10 years in accordance with UCL Records retention schedule, and may be accessed by the research teams for comparison with future data.

Will my taking part in the study be kept confidential?

All information about your participation in this study will be kept strictly confidential, anonymised, and will be collected and stored in accordance with the General Data Protection Regulation, 2018. You will be assigned a number so that your data will be made anonymous at the point of data collection and it will not be possible to identify you from your results.

With your permission, your GP will be informed that you are taking part in this research study. The researchers may also contact your GP to request health-related information, such as details of medical procedures, scans or medications. This will only be required if the information cannot be obtained from you directly, and is necessary to confirm your eligibility to participate. All correspondence between the researcher team and your GP will be strictly confidential.

If your condition changes during the course of the study, such that you are unable to continue with the study, you will be withdrawn from the study. However, information collected up until that point may still be used.

Limits to confidentiality

Please note that assurances on confidentiality will be strictly adhered to unless evidence of wrongdoing or potential harm is uncovered. In such cases the University may be obliged to contact relevant statutory bodies/agencies.

Please note that confidentiality will be maintained as far as it is possible, unless during our conversation I hear anything which makes me worried that someone might be in danger of harm, I might have to inform relevant agencies of this.

Confidentiality will be respected subject to legal constraints and professional guidelines. Confidentiality will be respected unless there are compelling and legitimate reasons for this

to be breached. If this were the case we would inform you of any decisions that might limit your confidentiality.

Data Protection Privacy Notice

All information that is collected during the course of the research will be stored in accordance with the General Data Protection legislation – GDPR.

Notice:

The data controller for this project will be UCL. The UCL Data Protection Office provides oversight of UCL activities involving the processing of personal data, and can be contacted at data-protection@ucl.ac.uk. UCL's Data Protection Officer is Lee Shailer and he can also be contacted at data-protection@ucl.ac.uk.

Your personal data will be processed for the purposes outlined in this notice. The legal basis used to process your personal data will be performance of a task in the public interest. You can provide your consent for the use of your personal data in this project by completing the consent form that has been provided to you.

Your personal data will be processed and will be retained until the end of the study. After this date, all data will be anonymised and may be accessed by the research teams for comparison with future data. We will endeavour to minimise the processing of personal data wherever possible.

If you are concerned about how your personal data is being processed, please contact UCL in the first instance at data-protection@ucl.ac.uk. If you remain unsatisfied, you may wish to contact the Information Commissioner's Office (ICO). Contact details, and details of data subject rights, are available on the ICO website at: https://ico.org.uk/for-organisations/dataprotection-reform/overview-of-the-gdpr/individuals-rights/

Who is organising and funding the research?

This observational study is being organised by the researchers and chief investigators aforementioned in this form and is sponsored by UCL. The costs of the research are being paid for by Brain Research, UK. All research studies are reviewed by an independent group of people, called a research ethics committee to protect your safety, rights, well-being and dignity.

Who has reviewed the research?

This research project has been reviewed and approved by the XXX Research Ethics Committee**.** It has also been reviewed by the Health Research Authority.

Thank you for reading this information sheet and for considering taking part in this research study.

D. Example "what to expect" information sheet

ReCAPS Study - What to Expect

This document provides a **short summary** of what to expect if you agree to take part in the ReCAPS study. More detail is provided in the Information Sheet. Please do not hesitate to ask us questions if something is unclear, or if you would like us to explain something further.

MRI Scan (Location: 12 Queen Square, UCL / Duration: 1 hour)

Not everyone will need to have an MRI scan.

If you are unsure whether you need one, please confirm with one of the researchers.

 If we ask you to have a scan, it will involve lying in an MRI scanner for up to 30 minutes. MRI scans are painless, but some people find them claustrophobic. Please let us know if this might affect you. You will also be given headphones to wear because the scanner can be loud.

The main study (Location: 33 Queen Square, UCL)

If you choose to take part in the full experiment, you will be asked to attend 1-2 sessions that will take place approximately 2 weeks apart.

Each session will be identical apart from the application of real or sham tDCS stimulation. For example:

Session 1: "real" stimulation

Session 2: "sham" stimulation

These sessions will happen in a random order and you will not be able to tell which session is real and which one is sham.

Transport can be requested for all sessions

Sessions (Duration: 1.5 hours each)

We will ask you to **complete a series of movements** while sitting on a chair. This is to assess the level of impairment in the arm and hand affected by the stroke. *Duration: 15 minutes.*

A researcher will then **measure signals travelling between your brain and your hand** using TMS (transcranial magnetic stimulation). These signals will be measured several times throughout the session.

During the session, we will also apply a stimulation technique called tDCS (transcranial direct current stimulation). This causes a warm, tingling sensation under the electrodes, which will be placed on your head. *Duration: 20 minutes.*

You will have the opportunity to take breaks throughout the session, and you can stop the session at any time.

E. Example consent form

ReCAPS STUDY - CONSENT FORM (patients)

Scientific Title of Research:	Re-opening the critical period for plasticity after stroke with dose-controlled non-invasive brain stimulation.
Department	Department of Clinical and Movement Neurosciences.

Please complete this form after you have read the Information Sheet and/or listened to an explanation about the research.

You will be given a copy of this Consent Form to keep and refer to at any time.

Please tick:

1. I confirm that I have read the information sheet dated 20/12/18 (Version 3.0) for the above study. I have had the opportunity to consider the information, ask questions and have had these answered satisfactorily. ☐
2. I understand that my participation is voluntary and that I am free to withdraw at any time without giving any reason, without my legal rights being affected. ☐
3. I understand that relevant sections of my medical notes and data collected during the study, may be looked at by individuals from UCL, from regulatory authorities or from the NHS Trust, where it is relevant to my taking part in this research. I give permission for these individuals to have access to my records. ☐
4. I consent to members of the central research team for this study to have access to my radiological datasets and any relevant clinical information needed to confirm I meet the inclusion criteria to take part in the study. ☐
5. I understand that the information collected about me will be used to support other research in the future, and may be shared anonymously with other researchers. ☐
6. I agree to my General Practitioner being informed of my participation in the study, and exchanging any relevant clinical information needed to confirm I meet the inclusion criteria to take part in the study. ☐
7. I agree to take part in the above study. ☐

Participant Database (optional)

If you would like your contact details to be retained so that you can be contacted in the future by UCL researchers who would like to invite you to participate in follow up studies to this project, or in future studies of a similar nature, please tick the appropriate box below.

Yes, I would be happy to be contacted in this way ☐

No, I would not like to be ☐

Name of participant	Date	Signature
Researcher	Date	Signature

Contact for further information:

Researchers:

Dr Carys Evans Email: [redacted]. Tel: [redacted]

Ms. Jenny Lee Email: [redacted] Tel: [redacted]

Chief and Principal Investigators:

Prof Nick Ward Email: [redacted]. Tel: [redacted]

Prof Sven Bestmann Email: [redacted]. Tel: [redacted]

-1 copy to be kept by Participant

-1 copy to be kept as part of the study documentation